1996

Design of new anticonvulsant drugs. Part I: Synthesis and computer modeling of sodium channel-directed hydantoins. Part II: SAR studies on alpha-phenyllactams.

Milton Lang Brown
University of Alabama at Birmingham

INFORMATION TO USERS

This manuscript has been reproduced from the microfilm master. UMI films the text directly from the original or copy submitted. Thus, some thesis and dissertation copies are in typewriter face, while others may be from any type of computer printer.

The quality of this reproduction is dependent upon the quality of the copy submitted. Broken or indistinct print, colored or poor quality illustrations and photographs, print bleedthrough, substandard margins, and improper alignment can adversely affect reproduction.

In the unlikely event that the author did not send UMI a complete manuscript and there are missing pages, these will be noted. Also, if unauthorized copyright material had to be removed, a note will indicate the deletion.

Oversize materials (e.g., maps, drawings, charts) are reproduced by sectioning the original, beginning at the upper left-hand corner and continuing from left to right in equal sections with small overlaps. Each original is also photographed in one exposure and is included in reduced form at the back of the book.

Photographs included in the original manuscript have been reproduced xerographically in this copy. Higher quality 6" x 9" black and white photographic prints are available for any photographs or illustrations appearing in this copy for an additional charge. Contact UMI directly to order.

UMI

A Bell & Howell Information Company
300 North Zeeb Road, Ann Arbor MI 48106-1346 USA
313/761-4700 800/521-0600

DESIGN OF NEW ANTICONVULSANT DRUGS. PART I: SYNTHESIS AND COMPUTER MODELING OF SODIUM CHANNEL-DIRECTED HYDANTOINS. PART II: SAR STUDIES ON α-PHENYLLACTAMS

by

MILTON LANG BROWN

A DISSERTATION

Submitted in partial fulfillment of the requirements for the degree of Doctor of Philosophy in the Department of Chemistry in the Graduate School, The University of Alabama at Birmingham

BIRMINGHAM, ALABAMA

1996

ABSTRACT OF DISSERTATION
GRADUATE SCHOOL, UNIVERSITY OF ALABAMA AT BIRMINGHAM

Degree Doctor of Philosophy Major Subject Chemistry

Name of Candidate Milton Lang Brown

Title Design of New Anticonvulsant Drugs. Part I: Synthesis and Computer Modeling of Sodium Channel-Directed Hydantoins. Part II: SAR Studies on α-Phenyllactams

The anticonvulsant activity of diphenylhydantoin (DPH or phenytoin) is consistent with its actions on the neuronal voltage-dependent sodium channel (NVSC). To further elucidate the binding requirements for this site, we synthesized several hydantoin analogs and evaluated these for in vitro inhibition of ^{3}H-batrachotoxinin A 20-benzoate ([^{3}H]-BTX-B) and/or in vitro whole animal anticonvulsant assays. The results suggest that hydantoins and 2,4-oxazolidinediones bind differently to the sodium channel and that hydantoin binding may be enhanced by a free imide NH group and increased log *P*.

We also investigated the effects of log *P* and 5-phenyl ring orientation on the binding of 5-phenylhydantoins to the NVSC. Log *P* and in vitro sodium channel-binding (log (IC_{50}) for twelve analogs and DPH were correlated by linear regressions analysis ($r^2 = 0.638$). The correlation suggests that simple partitioning into the lipid phase is not sufficient to explain the effects of hydantoins on the NVSC. Comparisons of NVSC binding affinities for lipophilic isomers having varied phenyl ring orientations suggest that a preferred N1, C5, C6, C7 torsion angle range from -15 to 15° is important for hydantoin binding to the sodium channel.

Comparative molecular field analysis (CoMFA) was employed to generate a 3-D QSAR model. Correlation by partial least squares (PLS) analysis of in vitro sodium channel binding activity and the CoMFA descriptor column generated a final model with R^2 = .997 for the training set. A structurally novel α-hydroxy-α-phenylamide designed for the hydantoin CoMFA model was synthesized and evaluated for sodium channel activity. The α-hydroxy-α-phenylamide, a potent binder to the NVSC, establishes that the intact hydantoin ring is not necessary for efficient binding to this site.

Further, we investigated the hydantoin binding site for stereoselectivity by resolving the enantiomers of previously synthesized racemic hydantoins by chiral phase high pressure liquid chromatography (HPLC). Evaluation of NVSC binding for each enantiomer revealed a modest example of enantioselective binding to the hydantoin site in the NVSC.

Finally, we evaluated the effects of *ortho*, *meta* and *para* electron withdrawing (-Cl) and donating (CH_3O-) substituents on the anticonvulsant activity of α-hydroxy-α-phenyllactams. The α-hydroxy-α-(4-chlorophenyl)caprolactam administered orally in rats exhibited good anti-MES anticonvulsant activity (ED_{50} 21.8 mg/kg) and therapeutic protection (ant-MES T.I. >11.5), suggesting this compound as a new anticonvulsant with clinical potential.

Abstract Approved by: Committee Chairman Wayne J. Brouillette

Program Director

Date 5/15/96 Dean of Graduate School

DEDICATION

I humbly dedicate my life to Jesus Christ, totally devoting all that He has given me to advance His message of salvation. I lovingly dedicate the entire contents of this work in honor of my parents, Mr. and Mrs. Milton Irvin Brown, my sisters Pamela and Michelle Brown, my wife and lover Dr. Sandra R. Brown, and my sweet little daughters Tyler Noel and Jordan Nicole Brown.

ACKNOWLEDGEMENTS

I publicly acknowledge the saving grace of Jesus Christ and thus I am compelled to credit past, present and future success to Him.

To my parents, simple words cannot express my gratitude for your unending sacrifice, many prayers and undying love. I have and always will hold true to the Christian values and moral principles that you have so diligently taught me. I love and thank you.

To my highschool sweetheart, lover and soul mate, Dr. Sandra R. Brown, thank you for all the sacrifices and encouragement you have given me over the years in my efforts to achieve this milestone. I love you dearly. Thanks, also for the greatest blessings of all, Tyler Noel and Jordan Nicole. You make my life so happy and exciting.

To Mr. and Mrs. Noel Roper and family, thank you for all your kindness and prayers over the years. You have always been a pillar of support for me. Special thanks to Everett Roper, you are truly a friend and a brother.

To the Brown, Davis and Roberts families, thank you for your love, prayers and encouragement. Special thanks to Mr. and Mrs. Charles Brown and family for all of your help and advice over the years.

To Dr. Wayne Brouillette, I thank you for your instructions in chemistry, leadership in my research project and role in my development as a scientist. Thanks to my committee members, Drs. Muccio, Brown, Kiely and Christian for your contributions to my research project. Special thanks to all labmates and friends in the UAB chemistry department, especially Cecil Jones, Tracy Hutchison, David Morton and Dr. Charles Watkins--your friendship will always be cherished.

Special thanks to my friend and colleague Karl McCleary, your encouragement and conversations are deeply appreciated. I promise to see you on the other side.

I would also like to express my thanks to Dr. and Mrs. William Lusain and family, for helping me in time of need. May God richly bless you.

To the West End community, especially Mr. Myles Smith and Mr. Jerroll Richardson, your kindness, friendship, contributions and support will always be remembered.

I also gratefully acknowledge financial support from the Patricia Robert Harris Fellowship, the National Consortium for Educational Access, the UAB Comprehensive Minority Faculty Development Program and the UAB Department of Chemistry. Finally, to the numerous unmentioned individuals who have made a positive impact on my life and have helped me to complete this goal, I say thank you.

TABLE OF CONTENTS

TABLE OF CONTENTS (Continued)

LIST OF TABLES

LIST OF TABLES (Continued)

LIST OF TABLES (Continued)

LIST OF TABLES (Continued)

LIST OF FIGURES

LIST OF FIGURES (Continued)

LIST OF FIGURES (Continued)

MISCELLANEOUS STUDIES ON HYDANTOINS

Figure Page

SYNTHESIS AND ANTICONVULSANT ACTIVITIES OF PHENYL SUBSTITUTED α-HYDROXY-α-PHENYLCAPROLACTAMS AND α-ALKYL-α-HYDROXY-α-PHENYLAMIDES

LIST OF SCHEMES

INTRODUCTION

Epilepsy was recognized early in human history, as documented[1] by Hippocrates in 400 B.C. Early Greek writers notably referred to this disease as παράσσω (pronounced *sparrasò*) derived from δπαιρω (pronounced *spairò*) transliterated as "spasmatic contractions, to convulse with epilepsy, to mangle, to rend or tear."

Epilepsy is a key element in the *La Transfigurazione*, the last painting (1520 A.D.) from the artist Raphael. The portait reveals, in the upper half of the picture, Christ's transfiguration on the Mount and, in the lower half, the young epileptic boy's seizure at the foot of the mountain in the presence of the disciples. Raphael depicts both events, which are described in succession in the *9th* chapters of the Gospels of Mark and Luke, as if they took place at the same time. By synchronizing both scenes, Raphael demonstrated a remarkable correlation between Christ and the epileptic boy, portraying the epileptic seizure as a symbolic representation of the transfiguration.[2] Thus for those of us who believe in the divinity of Jesus Christ and the authenticity of the sacred scriptures, Christ's transfiguration, symbolized by (1) suffering, (2) death and (3) the resurrection, provides a significant parrallel to the experience of epilepsy vividly portrayed in three stages as: (1) the aura and cry

(Mark *IX*:18, 26 and Luke *IX*:39), (2) the spasm or convulsion (Mark *IX*:26) and (3) the post-convulsive relief (Mark *IX*: 26).

Epilepsy is defined medically as a neurological disorder of the central nervous system (CNS) characterized by recurrent seizures. A seizure thus occurs when neurons of the cerebral cortex become irritable and fire in repeated bursts. When these bursts involve a large aggregate of neurons, a clinically detectable seizure occurs.[3] Epileptic seizures can originate from either a portion of the cerebral cortex (localization related), or have widespread origin (generalized). Thus distinguishing between these two types of seizure episodes can be important for therapeutic decisions.

The most widely used classification system for seizures (Table 1) was developed in 1981 by the International League Against Epilepsy (ILAE).[4] From this classification of epileptic seizures were termed three categories: partial (focal) seizures, generalized seizures of nonfocal origin (convulsive or nonconvulsive) and unclassified seizures.

Partial seizures are classified as neuronal discharges or convulsions originating initially from a specific cortical area. Depending on the anatomical or functional system involved, several types of partial seizures can occur. The causes of partial convulsive seizures are related to a variety of brain lesions, such as post-traumatic scars, tumors, or infection. These seizure types are possible among all age groups but are most frequently presented in the elderly. Partial convulsive seizures may further develop into generalized seizures. Partial convulsive seizures

that occur with impairment of consciousness are subclassified as complex partial and those seizures that occur without impairment of consciousness are termed simple partial seizures.

Focal motor seizures with epileptic march, commonly called Jacksonian seizures, are presented with orderly movement of the hands and legs. Focal motor without march are seizures that occur with only clonic twitching and numbness. These types of seizures are usually confined to a single limb or muscle group on one side of the body.

Somatosensory seizures are characterized by feelings of numbness (pins and needles) and include visual, auditory, olfactory, gustatory, or vertiginous seizures. Seizures that occur with autonomic symptoms are expressed with repetitive attacks of abdominal pain, vomiting, palpitation, thoracic sensation, thirst, flushing, sweating, pupil dilation and tachycardia. Partial seizures may also be associated with psychic symptoms presenting signs of confusion, distorted memory, depersonalization, distorted or imagined flashbacks, sensations of unreality, sensations of extreme leisure or displeasure, fear, hallucinations and dream states.

Seizures that occur with automatism describe disorders involving involuntary motor activity are preceeded with a state of clouded consciousness, either during or after the seizure, and usually are followed by amnesia of the event. Overall, the most commonly presented partial seizures are focal motor, Jacksonian, autonomic and psychomotor seizures. These seizures generally respond fairly well to treatments with anticonvulsant drugs.

Convulsive seizures are termed generalized when it is not possible to single out one anatomic or functional system of the brain that is responsible for the clinical manifestations. With generalized seizures, consciousness is usually impaired and the specific cause of the seizure is rarely determined. Causes of this seizure type are generally attributed to metabolic disturbances, genetic factors or diffused lesions. Individuals from all ages can be affected by generalized convulsions.

Generalized convulsive seizures that bring about a loss of consciousness [(usually less than 20 seconds (s)] are classified as simple absence seizures. During an absence attack, the patient may seem to stare without any interruption of ongoing motor activity and may be unresponsive to stimulus. After this type of seizure, there is usually no loss of memory or confusion. Frequent simple absence seizures are given the status of petit mal and are most prevalent in children. Petit mal seizures can be treated with anticonvulsants but are unresponsive to hydantoins.

Another type of generalized seizure is the complex absence seizure, which presents signs such as mild clonic jerks (absences with clonic components), increases in postural tone (retropulsive absences with tonic components) and automatisms (absences with automatism or with autonomic components). Complex absence seizures respond fairly well to anticonvulsant drugs like oxazolidinediones, succinimides, barbiturates, sodium valproate, and diazepam.

Generalized seizures that occur with prolonged loss of consciousness are classified as myoclonic, clonic, tonic, and tonic-clonic. Myoclonic jerks are defined

as sudden brief muscular contractions. Generalized clonic seizures, which occur especially in children, are characterized by a mixture of fast (10 or more per s) and slow discharges, followed by a loss of consciousness and bilateral clonic contractions. Tonic seizures, which also occur mainly in children, are characterized by fast rhythmic seizures. Vocalization and autonomic changes may also accompany tonic seizures and the tonic leg flexion component of the seizure may result in injuries due to falling.

The tonic-clonic or grand mal seizures are characterized by tonic contraction of all muscle groups. Initial contractions may be flexor, rapidly followed by prolonged limb extension. During this period rapid vibratory tremors may appear. The clonic contractions spread through the body, then slow until the seizure ends. Grand mal seizures are less prevalent in children than are other forms of generalized seizures. Usually these seizure types respond well to anticonvulsant treatment with barbiturates, hydantoins or iminostilbenes, but oxazolidinediones and succinimides are ineffective.

Atonic seizures are characterized by a sudden decrease in muscle tone, consequently leading to drooping of the head and limbs. The loss of muscle tone is usually evident in posture and results in slumping of the individual to the ground.

Table 1. Classification of Epileptic Seizures[4]

I. Partial convulsive seizures

A. Simple partial seizures (consciousness not impaired)

1. With motor signs [focal motor without march, focal motor with march (Jacksonian), versive, postural, phonatory (vocalization or arrest of speech)].

2. With somatosensory or special sensor symptoms (simple hallucinations, e.g., tingling, light flashes, buzzing) somatosensory, visual, auditory, olfactory, gustatory, vertiginous).

3. With autonomic symptoms or signs (including epigastric sensation, pallor, sweating, flushing, piloerection and pupillary dilatation).

4. With psychic symptoms (disturbance of higher cerebral function). These symptoms rarely occur without impairment of consciousness and are much more commonly experienced as complex partial seizures [dysphasic, dysmnesic (e.g., deja-vu), cognitive (e.g. dreamy states distortion of time sense), affective anger, fear, etc.), illusions (e.g., macropsial), structural hallucinations (e.g., music, scenes)]

B. Complex partial seizures (with impairment of consciousness: may sometimes begin with simple symptomatology) (psychomotor seizures).

1. Simple partial onset followed by impairment of consciousness

   (a) With simple partial features (A.1-4) followed by impairment of consciousness
   (b) With automatisms

2. With impairment of consciousness

   (a) With impairment of consciousness only
   (b) With automatisms

C. Partial seizures evolving to secondarily generalized seizures. (This may be generalized tonic-clonic, tonic or clonic.)

1. Simple partial seizures (A) evolving to generalized seizures

2. Complex partial seizures (B) evolving to generalized seizures

3. Simple partial seizures evolving to complex partial seizures evolving to generalized seizures.

II. Generalized seizures (convulsive or nonconvulsive)

A. Absence seizures (petit mal seizures)
B. Myoclonic seizures
C. Clonic seizures
D. Tonic seizures
E. Tonic-clonic seizures (grand mal seizures)
F. Atonic seizures (Astatic)
(combinations of the above may occur, e.g., B and F, B and D)

III. Unclassified epileptic seizures

Includes all seizures that cannot be classified because of inadequate or incomplete data and some that defy classifications in the described categories. This includes some neonatal seizures, e.g., rhythmic eye movements, chewing and swimming movement.

IV. Addendum

Prolonged or repetitive seizures (status epilepticus). The term "status epilepticus" is used whenever a seizure persists for a sufficient length of time or is repeated frequently enough that recovery between attacks does not occur. Status epileptics may be divided into partial (e.g., Jacksonian), or generalized (e.g., absence status or tonic-clonic status). When very localized motor status occurs, it is referred to as epilepsia partialis continua.

Since seizures are the manifestations of an underlying disorder of the CNS, it is necessary to consider not only the symptom (seizure) but the underlying pathophysiology as well. In 1989, the ILAE further refined the classifications (Table 1) by organizing the causes of epilepsies into specific syndromes[5] (Table 2). The classification of syndromes include four major categories: localization-related (partial) epilepsy syndromes, generalized epilepsy syndromes, epilepsy syndromes of undetermined nature and special syndromes. Further, a distinction is made between idiopathic (no overt causes; probably genetic) and symptomatic (secondary to some CNS damage). Altogether, knowledge of syndromatic histories may permit

better identification of epilepsy diseases and thereby possibly minimizing the risk of recurrent seizures.

Table 2. International Classification of Epilepsies and Epileptic Syndromes[5]

1. Localization-related (focal, local, partial) epilepsies and syndromes

    1.1 Idiopathic, with age-related onset (e.g., benign epilepsy with centrotemporal spikes)

    1.2 Symptomatic

2. Generalized epilepsies and syndromes

    2.1 Idiopathic, with age-related onset
    •Juvenile myoclonic epilepsy (impulsive petit mal)

    2.2 Idiopathic and /or symptomatic
    •Lennox Gastaut syndrome

    2.3 Symptomatic

3. Epilepsies and syndromes undetermined as to whether they are focal or generalized

4. Special syndromes

    4.1 Situation-related seizures
    •Febrile convulsions
    •Seizures related to other identifiable situations, such as stress, hormonal changes, drugs, alcohol or sleep deprivation

    4.2 Isolated, apparently unprovoked epileptic events

One common method used in the prevention and control of recurrent seizures or epilepsy is anticonvulsant drug treatment. A fundamental concept in drug treatment of epilepsy is seizure prevention, with the aim of seizure elimination without interfering with cognitive function or inducing toxicity. Only when the risk of recurrent seizures is high should antiepileptic medications be considered.[6]

Through the years a number of anticonvulsants (Table 3) have become available since the introduction of the barbiturate phenobarbital in 1912. However the most commonly used anticonvulsants can be simplified into eight structural classes (Figure 1 and Table 4).

Table 3. Marketed Anti-Epileptic Drugs[7]

Year introduced	International nonproprietary name	U.S. trade name (company)
1912	Phenobarbital	Luminal (Winthrop)
1935	Mephobarbital	Mebaral (Winthrop)
1938	Phenytoin	Dilantin (Parke-Davis)
1946	Trimethadione	Tridione (Abbott)
1947	Mephenytoin	Mesantoin (Sandoz)
1949	Paramethadione	Paradione (Abbott)
1951	Phenacemide	Phenurone (Abbott)
1952	Metharbital	Gemonil (Abbott)
1953	Phensuximide	Milontin (Parke-Davis)
1954	Primidone	Mysoline (Ayerst)
1957	Methsuximide	Celontin (Parke-Davis)
1957	Ethotoin	Peganone (Abbott)
1960	Ethosuximide	Zarontin (Parke-Davis)
1968	Diazepam	Valium (Roche)
1974	Carbamazepine	Tregretol (Geigy)
1975	Clonazepam	Klonopin (Roche)
1978	Valproate	Depakene (Abbott)
1981	Clorazepate	Tranxene (Abbott)
1993	Felbamate	Felbatol (Wallace)
1994	Neurontin	Gabapentin (Parke-Davis)

The eight structural classes of the most commonly prescribed anticonvulsants are hydantoins, iminostilbenes, fatty acids, dicarbamates, benzodiazepines, succinimides, barbiturates, and amino acids[7-9] (Table 4 and Figure 1). The most commonly prescribed anticonvulsant is the hydantoin, 5,5-diphenylhydantoin (DPH). This compound was reported in 1938 by Meritt and Putman to have efficacy against electrically induced seizures in cats. In the same year, Merritt and Putman reported on the anticonvulsant activity of DPH in man. Since its introduction into clinical practice, DPH has become one of the most extensively used anticonvulsant drugs in the treatment of psychomotor seizures and generalized convulsions.

Even with available marketed anticonvulsants, there exists a need for new agents that extend seizure control, along with a reduction in side effects (Table 4). While the search continues for the ideal anticonvulsant[10] (Table 5), the use of animal models (Table 6) has been of major importance in identifying and developing new anticonvulsants.[7,11,12]

Unfortunately, there does not exist a single animal model that reflects all of the physiological processes and symptomatologies of all known epilepsies. Therefore, different approaches can be used when choosing an animal model for the evaluation of new pharmacological agents. In general, compounds are placed in a primary anticonvulsant screen, which includes chemical and electrically induced challenges. Once a highly active compound has been identified using the primary screen, more advanced mechanistic and seizure type models (Table 8) are needed

to establish and quantify the neuropharmacological, metabolic and toxicological profiles of the experimental compound.

The Maximal Electroshock Seizure Test (MES) and the Subcutaneous Metrazol Seizure Threshold Test (scMET) are two standard tests used to evaluate and quantitate anticonvulsant activity.[11, 12] Generally, compounds active in the scMET test are most likely to have clinical efficacy against petit mal seizures, whereas the MES test is usually selective of drugs effective against grand mal seizures. Drugs that are resistant to MES challenges are suggested to evaluate effects on threshold, while anti-scMET agents are useful against seizure spread. Threshold refers to a minimal or clonic seizure, therefore, a drug active in this mechanism could raise the threshold for seizure discharge. The ability of a drug to block the tonic extensor component of maximal seizures is reflected in the ability to block generalized seizure spread.

The MES test includes the induction of seizures with a 60 cycle alternating current of 50 mA intensity (5-7 times the intensity needed to invoke a minimal electroshock seizure) delivered for 0.2 s via corneal electrodes. A drop of 0.9% saline is instilled in the eye prior to application of the electrodes in order to prevent the death of the animal. Abolition of the hind limb tonic extension component of the seizure is defined as protection and results are expressed as the number of animals protected divided by the number of animals tested at a particular time interval.

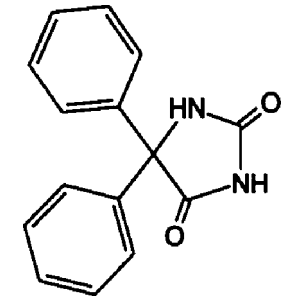

5,5-DIPHENYLHYDANTOIN

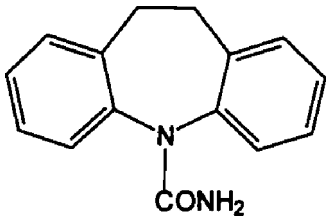

CARBAMAZEPINE

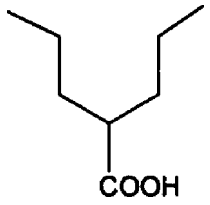

VALPROIC ACID

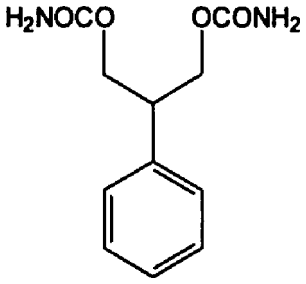

FELBAMATE

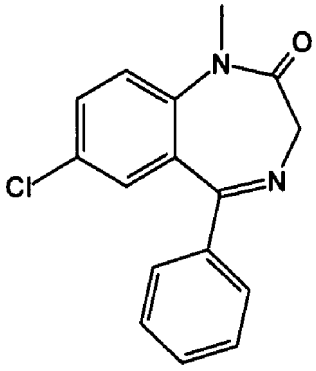

DIAZEPAM

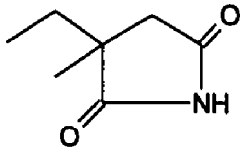

ETHOSUXIMIDE

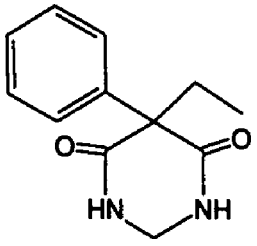

PRIMIDONE

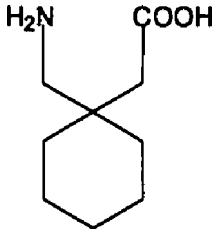

GABAPENTIN

Figure 1. Structures of the most commonly prescribed anticonvulsants.

Table 4. Most Commonly Used Anticonvulsants in the U.S.

Anticonvulsant (structural class)	% Prescribed to U.S. epileptics in 1992[a]	Seizure type effective against	Primary site of action[f]	General side effects
Phenytoin (hydantoins)	48.4	Tonic-clonic, Partial onset	NVSC[c]	gum hyperplasia, rash, gastric upset, fetal hydantoin syndrome
Carbamazepine[b] (iminostilbenes)	30.5	Tonic-clonic, Partial onset	NVSC[c]	initial sedation, gastric upsets. blurred vision
Valproate (fatty acids)	13.3	Primary generalized (Generalized absence), Partial onset	NVSC	gastric upsets, blood and liver disorders
Felbamate (dicarbamate)	.1	Primary generalized Partial onset	NVSC ? NMDA (glycine ?)	headache, nausea, vomiting, dizziness, fatigue
Diazepam (benzodiazepines)	[d]	Primary generalized (not tonic-clonic)	GABA	not administered chronically
Ethosuximide (succinimides)	[d]	Generalized absence	CC (T-type)[e]	initial sedation, photophobia, gastric upsets, blood disorders

Table 4. (Continued)

Primidone (barbiturates)	d	Partial onset Tonic-clonic	GABA	sedation, psychotic episodes
Gabapentin[e] (amino acids)		Partial onset with or without Tonic-clonic	amino acid brain levels	drowsiness, weight gain, somnolence

[a]Reference 7. [b]% includes both generic carbamazepine and tegretol. [c]Neuronal voltage-dependent sodium channel. [d]All others reported total 6.6%. [e]Calcium channels. [f]Reference 8. [g]Reference 9.

Table 5. General Properties of an Ideal Anticonvulsant [10]

Fundamental components	Ideal properties
Efficacy	Selective for seizure types Additive or synergistic with other anticonvulsants Novel mechanism of action
Adverse effects	Increased therapeutic index Devoid of serious or chronic adverse effects Lack of teratogenic potential
Pharmaceutics	Multiple dose formulations Admistration by multiple routes Water soluble
Pharmacokinetics	Simple profile Not metabolized No effect on hepatic enzymes No effect on metabolism of other drugs No interaction with other anticonvulsants or drugs

Table 6. Available Genetic, Chemical and Electrical Models Used in Primary Screen [11]

Genetic models (seizure types)	Chemical models (seizure types)	Electrical models (seizure types)
photosensitive baboon, *Papio papio*	pentetrazol, pentenyltetrazol, metrozol, leptazol (generalized tonic-clonic, tonic)	supramaximal seizure pattern or *MES* maximal electroshock 50 μA (seizure spread, generalized tonic-clonic seizures)
audiogenic seizure mice, *DBA/2J, SJL/J* (genetically determined epilepsy)	fluorothyl (generalized tonic seizures)	supramaximal seizure pattern or *MES* maximal electroshock 12 μA (seizure spread, seizure threshold)
epileptic prone rats, *GEPR-3, GEPR-9*		
mongolian gerbil, *Meriones unguiculatus* (reflex epilepsy)		
chicken		
tottering mice, *tg/tg strain*		
dogs		

The Subcutaneous Metrazol Seizure Threshold Test (scMET) is performed by the introduction of a 0.5% solution of metrazol subcutaneously in the posterior midline at a dose of 85 mg/kg, which produces seizures in greater than 95% of mice. The animal is observed for 30 min. Failure to observe a single episode of clonic spasms of at least 5 s duration is defined as protection and the results are

expressed as the number of animals protected divided by the number of animals tested at a particular time interval.

The Rotorod Toxicity Test is included as part of a standard anticonvulsant screen and is useful in evaluating neurotoxicity. In this test, the animal is placed on a one inch diameter plastic rod which is rotated at 6 revolutions per minute (rpm). Normal mice can remain on a rod rotating at this speed indefinitely. Neurotoxicity is defined as the failure of the animal to remain on the rod for 1 min and is expressed as the number of animals exhibiting toxicity divided by the number of animals tested at some time interval.

Over the years many structural classes of anticonvulsants have been discovered.[13,14] Figure 2 represents the remarkable relationship in structure between the most common anticonvulsant structural types and hydantoins.

Overall, a large number of hydantoins have been synthesized[15] and evaluated for anticonvulsant activity . Correlations of structure-activity relationships (SAR)[13, 14] using MES and scMET data have allowed for assessment of general trends.

In general, SAR suggests[13, 14] that significant MES activity is obtained when the hydantoins possess at least one phenyl substitution at C5, with optimum MES activity when a second 5-phenyl ring is attached. Replacement of one 5-phenyl ring with a methyl or ethyl group decreases MES activity, but imparts moderate MET

Table 7. Anticonvulsant Data for the Most Commonly Prescribed Anticonvulsants.

Substance	Time of test (h)	Rotorod TD_{50} (mg/kg)	MES (mg/kg)[c]	s.c.PTZ (mg/kg)	s.c.Bic (mg/kg)	s.c.Pic (mg/kg)	s.c. Strych (mg/kg)
Phenytoin	22	65.5 (52.5-72.1)	9.50 (8.13-10.4) [6.89]	no protection up to 300 [<0.22]	no protection up to 100 [<0.65]	no protection up to 100 [<0.65]	maximum 50% protection at 55-100 [<0.65]
Carbamazepine[d]	0.25	71.6 (45.9-135)	8.81 (5.54-14.1) [8.13]	no protection			
Valproate	1/4, 1/4	426 (369-450)	272 (247-338) [1.57]	149 (123-177) [2.87]	360 (294-439) [1.18]	387 (341-444) [1.10]	293 (261-323) [1.45]
Felbamate	22	816 (590-1024)	50.1 (35.6-61.7) [16.3][b]	148 (121-171) [5.51]	>300	156 (122-202) [4.93]	>700
Diazepam[d,e]	1/4, 1/2	7.3 (4.60-8.70)	19.1 (12.9-28.8)	0.165 (0.128-0.206)	1.2	1.2	13
Ethosuximide	1/2, 1/2	441 (383-485)	no protection up to 1000 [<0.44]	130 (111-150) [3.38]	459 (350-633) [0.96]	243 (228-255) [1.82]	maximum 62.5% protection at 250-1000
Primidone[d]	3, 24	680 (647-717)	11.4 (4.16-16.7)	58.6 (36.0-83.6)			

Table 7. (Continued)

Gabapentin[a]	1, 4/3	9.4	53 (30-75)	32 (13-53)	57 (36-89)	34 (1-69)

[a]Reference 16. Reference 17. [b][ ] protective index = TD_{50}/ED_{50}. [c]First number TD_{50}; second number ED_{50}. MES, maximal electroshock seizure; s.c. PTZ subcutaneous pentylenetetrazol; s.c. PTZ, subcutaneous picrotoxin; s.c. Bic, subcutaneous bicucculine; s.c. Strych, subcutaneous strychnine. ED_{50} in mg/kg p.o. mouse, (95% confidence interval). [d]Reference 12. [e]Reference 11.

Table 8. In Vivo Models Used to Determine Mechanism of Action and Seizure Type [11]

synthesis of GABA	competitive antagonist's of GABA	GABA/ benzodiazepine channel complex	benzodiazepine receptor inverse agonist	glycine antagonist
isoniazid	bicuculline	picrotoxin	β-carboline	strychnine
3-mercapto propionic acid				
allylglycine				
thiosemi carbazide				
methionine sulfoximine				

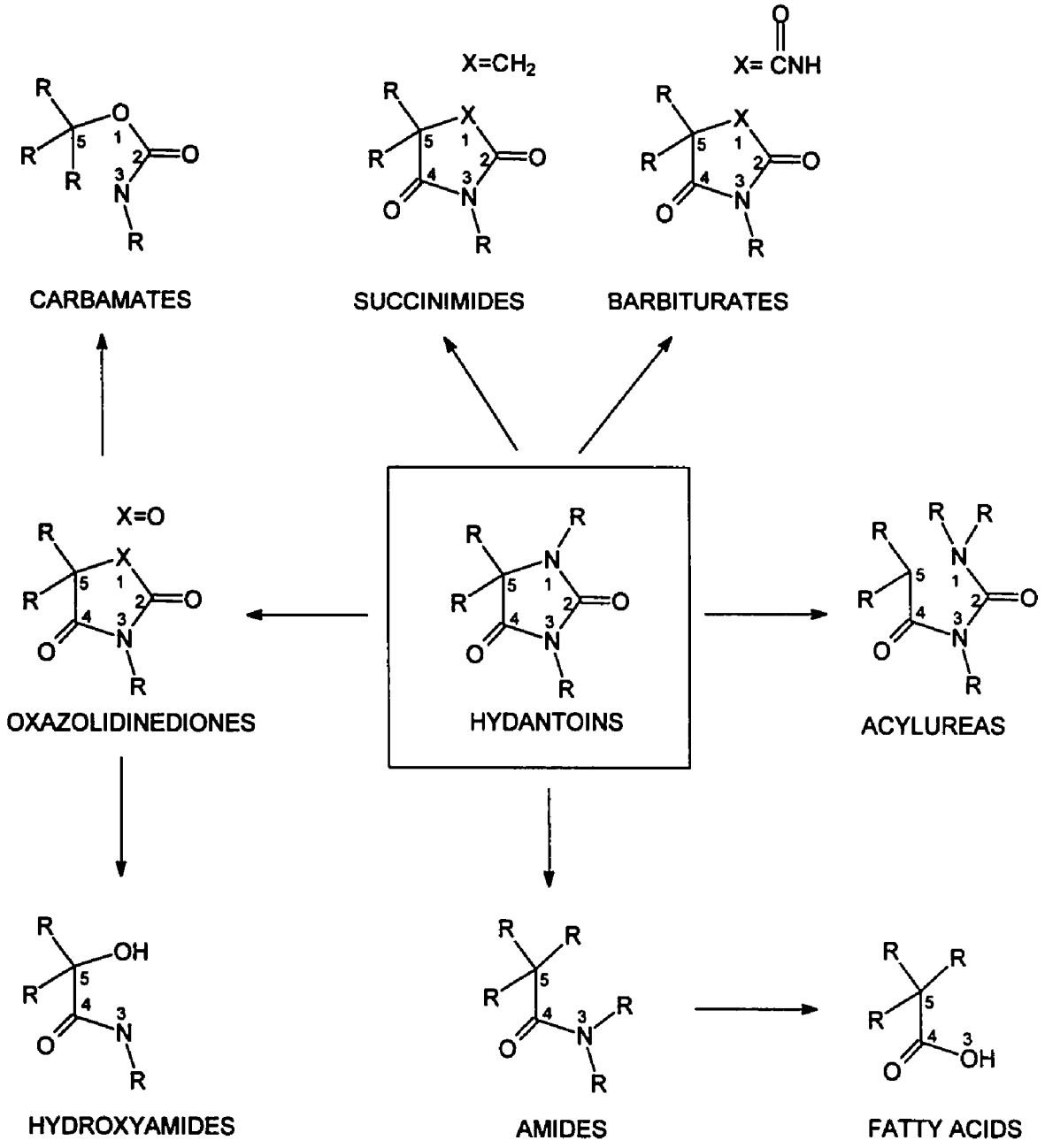

Figure 2. Relationships of common anticonvulsant structures to hydantoins.

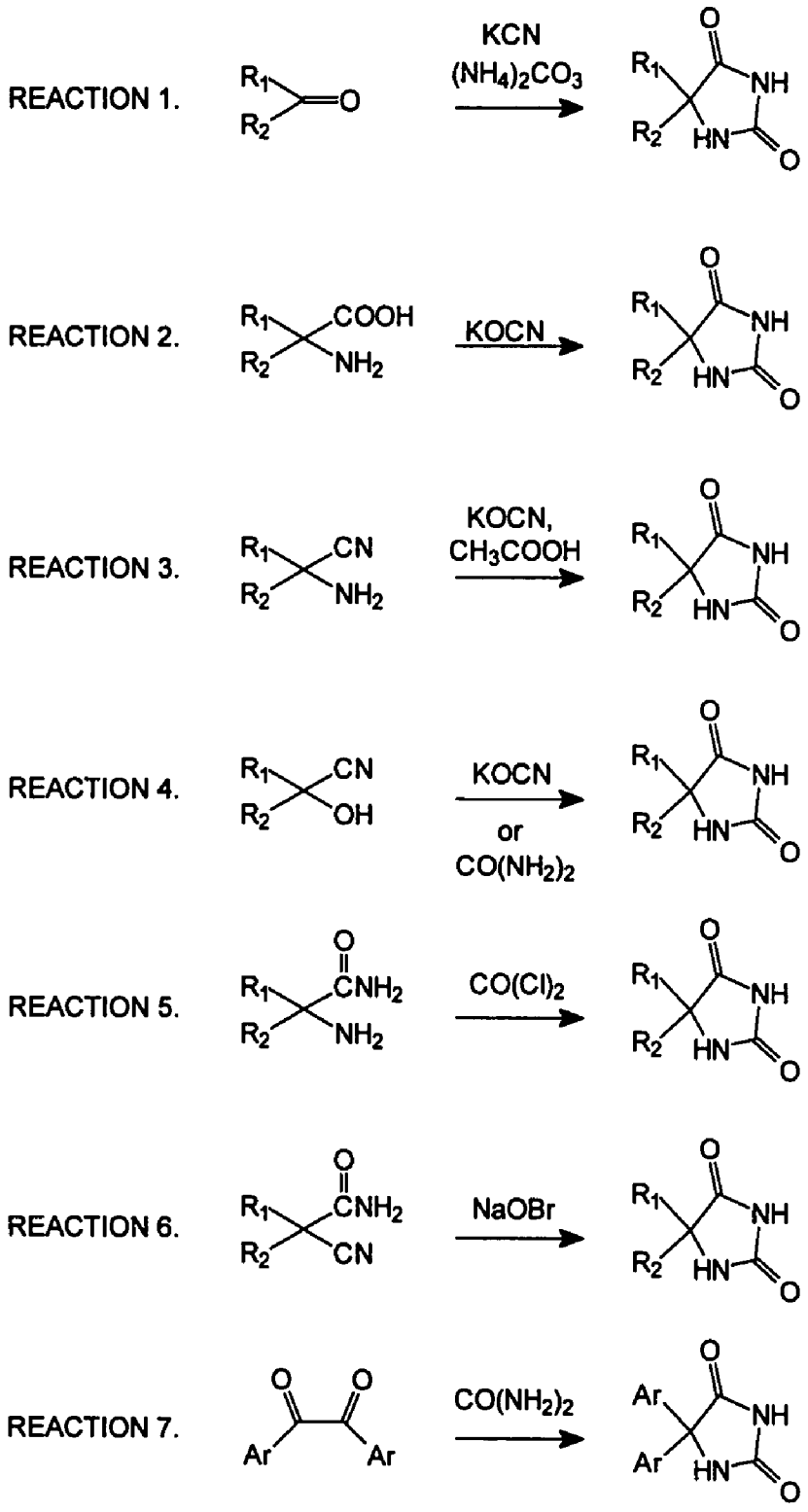

Figure 3. General methods for synthesizing 5-substituted hydantoins.

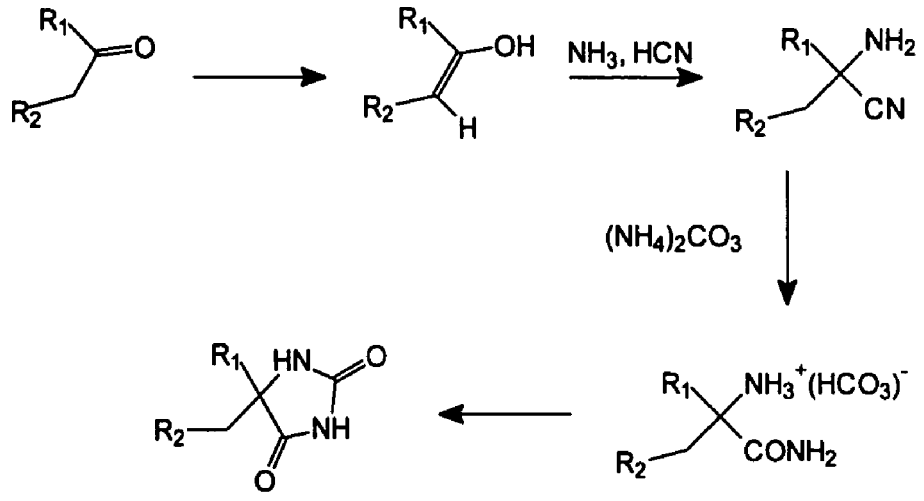

Figure 4. Proposed mechanism for Bucherer-Berg reaction.

effects. Introduction of a methyl group at N1 does not alter MET activity but decreases MES activity. Substitutions at N3 decrease MES activity. Phenyl ring substitutions suppress MES and MET activity. Replacement of oxygen in 5,5-diphenylhydantoin at C2 by sulfur reduces MES and confers small MET activity.

The synthesis of hydantoins has been throughly reviewed.[15] The Bucherer-Berg reaction[16] (Figure 3, REACTION 1) represents one of the most commonly used method for synthesizing hydantoins. This method involves the preparation of hydantoins from aldehydes or ketones using potassium cyanide (KCN) and ammonium carbonate [$(NH_4)_2CO_3$]. The general procedure is to warm 1 mole of aldehyde or ketone between 40 and 60 °C with 2 moles KCN and 4 moles of $(NH_4)_2CO_3$ in 50% alcohol for 2 hr, after which the hydantoin is usually isolated when the solution is cooled. The reaction mechanism (Figure 4) is suggested to include the formation of aminonitrile followed by conversion of aminonitrile to aminoamide, followed by ring closure to afford the hydantoin. The formation of hydantoins via amino acids has been accomplished using potassium cyanate in basic aqueous solution. The resulting hydantoin is obtained by acidifying the alkaline reaction mixture (Figure 3, REACTION 2). The mechanism involves the formation of urea acid derivative followed by ring closure to the hydantoin (Figure 5).

Cyanohydrins (Figure 3, REACTION 4) have been useful in forming hydantoins via reaction with $(NH_4)_2CO_3$ in 50% alcohol. The reaction mechanism

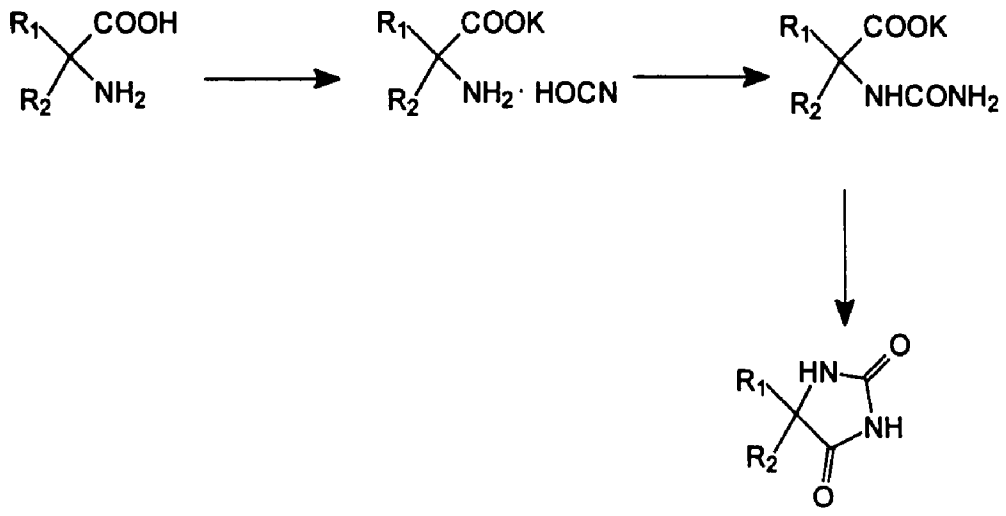

Figure 5. Reaction mechanism for converting amino acids into hydantoins.

is suggested to involve the conversion of cyanohydrin to aminonitrile followed by transformation of aminonitrile to hydantoin (Figure 6).

Diaryl ketones may be used to form hydantoins (Figure 3, REACTION 7) upon reacting with urea and an alkali hypohalite. A reaction mechanism has been proposed that implicates the pinacalone rearrangement, upon addition of urea to the diarylketone (Figure 7).

The synthesis of hydantoins from the reaction of alkali hypohalites on cyanoamides (Figure 3, REACTION 6) has been performed. The mechanism (Figure 8) proposed involves a Hofmann degradation of the amide group to an isocyanate intermediate. The isocyanate reacts with the amide followed by partial hydrolysis of the cyanide group to give the hydantoin.

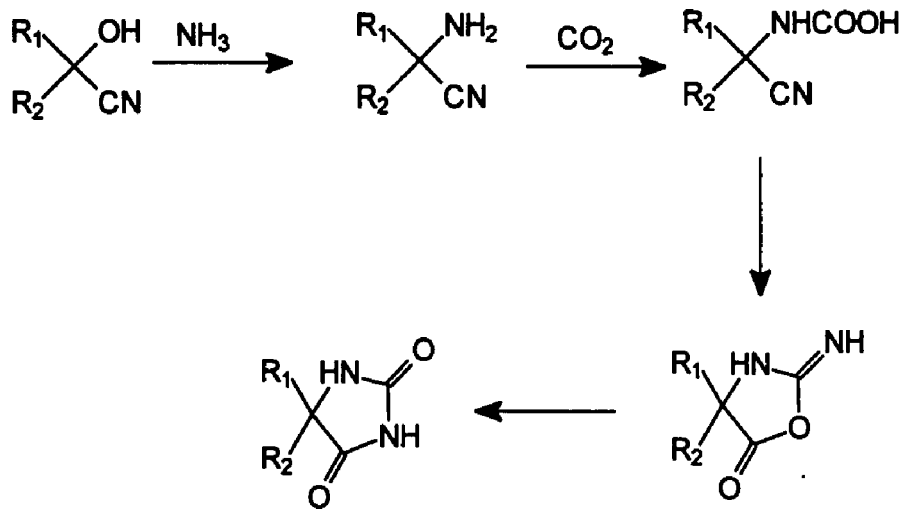

Figure 6. Reaction mechanism of converting cyanohydrins to hydantoins.

Approximately 1-3% of the U.S. population is affected by epilepsy.[19] On a larger scale, more than 50 million persons worldwide are estimated to have some type of epilepsy[20] and one out of four of these individuals suffer from seizure types

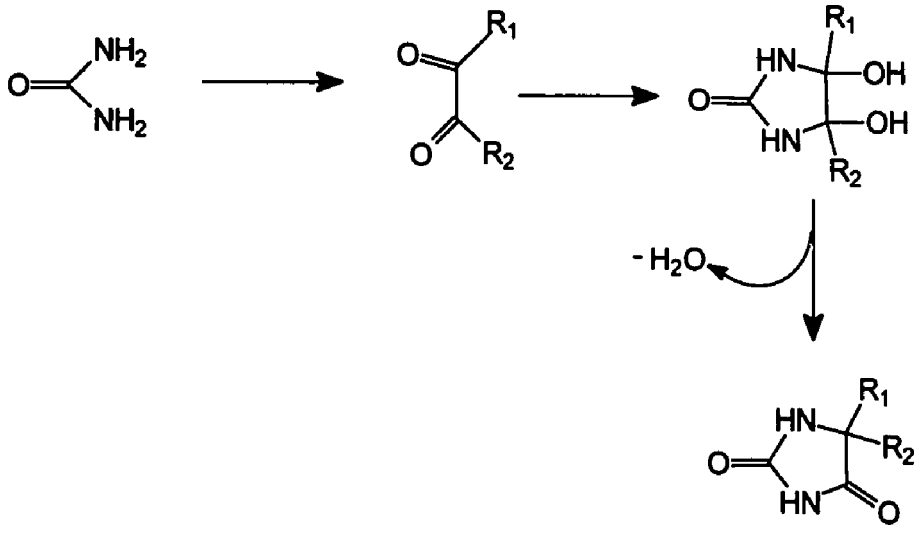

Figure 7. Reaction mechanism for converting diaryldiketones into hydantoins.

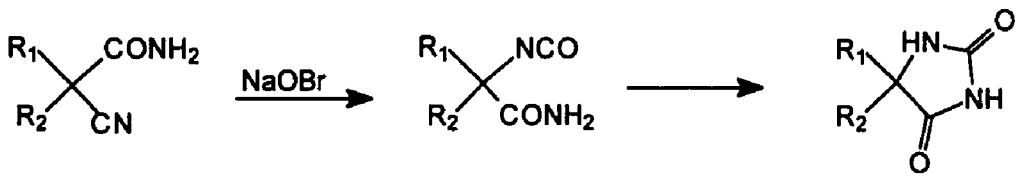

Figure 8. Reaction mechanism for the converting cyanoamides into hydantoins.

that are resistant to anticonvulsant therapy. Therefore, there is an impending need for new therapeutic treatments of epilepsy.

In recent years new anticonvulsant drugs such as felbamate and gabapentin, have demonstrated good anticonvulsant potential (Table 7) and have undergone clinical testing (Table 4). These drugs have been used most commonly as add-on medication for patients with intractable epilepsy and have demonstrated promise in reducing seizure frequency and occurrence[21].

Developmental anticonvulsants[22-24] currently under investigation are listed in Table 9 and their structures are shown in Figure 9. Studies are currently underway to ascertain seizure effectiveness and determine the primary site(s) of action for these agents. These drugs appear promising for those patients who are refractory to therapy or do not tolerate currently marketed agents. Thus these new drugs may overcome some of the recognized shortcomings of traditional anticonvulsants, offering clinicians and patients added therapeutic options.[24]

Advances in the understanding of the mechanism(s) of action for anticonvulsants have been instrumental in the development of new drugs.[9, 25-33]

Targeted mechanisms, which include receptor mediated inhibition, excitatory modulation, transmitter systems and ion channels, are presented in Table 10.

The role of ion channels has been demonstrated to be of great importance in the mechanisms of voltage conductance and anticonvulsant activity.[34-37] Thus we are interested in investigating structural requirements for ligands binding to anticonvulsant site(s) on or within the neuronal voltage-sensitive sodium channel (NVSC). Of considerable interest is a binding site in the NVSC, suggested as the likely site of action for the most commonly prescribed anticonvulsant diphenylhydantoin.[38]

The NVSC can be described as a transmembrane protein complex involved in generating electrical signals by action potentials in neurons and other excitable cells. Action potentials consist of three phases: (1) depolarization by the rapid increase (0.5 ms) of sodium entry into the cell, (2) calcium entrance into the cell and (3) potassium movement out of the cell (2.0 ms) repolarizing the cell and setting the resting membrane potential (-60 mV).[39]

The biphasic behavior of depolarization and repolarization controls sodium ion channel function and results from two separable gating processes[40, 41] termed activation and inactivation.[42] Activation controls the rate and voltage dependence of the increase in sodium concentration following depolarization. Inactivation is involved in controlling the rate and voltage dependence of positive potential returning to negative potential as the voltage-activated sodium channel restores itself to the resting level during maintained depolarization.

Voltage-activated sodium channels have three main states: resting, opened (active) and inactivated, and the distribution of channels among these states are a function of membrane potential and time.[43, 44] Interconversions between states are important in considering the modes of drug action. Compounds may, because of changes in access or interconversion rates, have different binding affinities to the resting, opened or inactivated state of the sodium channel. This provides a possible explanation for the binding differences and therapeutic effects among anticonvulsants, local anesthetics and antiarrythmics.[45-47]

Understanding channel topography begins with the knowledge of sodium channel substructure. The composition of sodium channel substructure has been found to be tissue and species dependent.[41]

Sodium channels from rat brain consist of three polypeptides, which include a 260-kilodalton (kDa) α subunit, a 36 kDa β_1 subunit and a 33 kDa β_2 subunit.[41, 48,49] Four channel isoforms (Table 11), designated types I, II, IIA and III, have been found with distinct locations.[50, 51]

Much of the information about the protein components of the NVSC has been gained through the use of neurotoxins (Table 12).[52] The inhibitors tetrodotoxin and saxitoxin modulate neurotoxin binding site 1 and are associated with the inhibition of Na^+ ion flux. Grayanotoxin and the alkaloids veratridine, batrachotoxin and aconitine inhibit receptor site 2 and cause persistent activation of the sodium channel. Sea anemone toxin and the polypetide scorpion toxin bind at receptor site 3 and slow sodium channel inactivation. Site 4 binds β-scorpion toxins, which affect

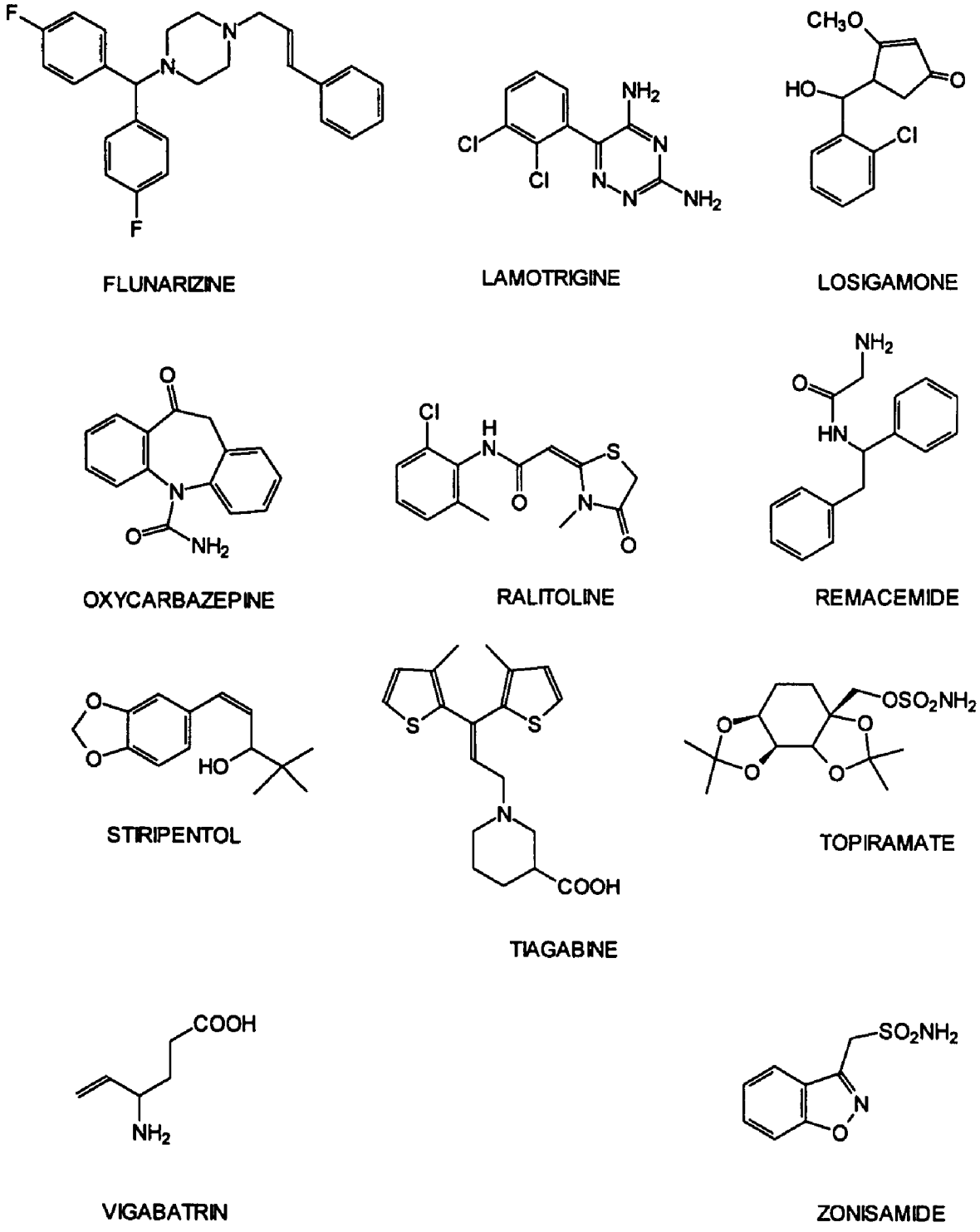

Figure 9. Structures of new developmental anticonvulsants.

Table 9. Selected Data for New Developmental Anticonvulsants

Tradename (company)[a]	Seizure effective against	Primary site of action	Side effects
Flunarizine (Jansen)	juvenile	Ca entry blocker[a]	drowsiness, headaches, vertigo
Lamotrigine (Wellcome)	partial, generalized	NVSC[h]	diplopia, drowsiness, dizziness, ataxia, headache, nausea, vomiting
Losigamone (Schwabe)	f	GABA-gated chloride channel	diplopia, dizziness, headache
Oxycarbazepine (Ciba-Geigy)	generalized tonic-clonic, partial	g	tiredness, headache, dissiness, ataxia
Ralitoline (Godecke)	f	NVSC	g
Remacemide (Fisons)	f	NMDA[b]	g
Stirpentol (Biocodex)	absence	g	gastric disturbances, insomnia, weight loss
Tiagabine (Abbott)	partial, generalized	GABA[c]	e
Topiramate (McNeil)	f	g	
Vigabatrin (Marion Merrell Dow)	refractory partial, generalized tonic-clonic	GABA-T[d]	drowsiness, ataxia, headache
Zonisamide (Dianippon)	refractory partial, secondarily generalized tonic-clonic	g	drowsiness, ataxia, anorexia, GI discomfort, decreased spontaneity, renal stones

[a]Reference 24. [b]NMDA, N-methyl-D-aspartate. [c]GABA, gamma amino butyric acid. [d]GABA-T, gamma amino butyric acid transaminase. [e]No noticable side effects. [f]Clinical efficacy not yet determined. [g]Site of action not yet determined. [h]Reference 8.

Table 10. Potential Sites for Anticonvulsant Agents.[8, 9, 26, 30]

Potential sites of anticonvulsant drugs	
1. Benzodiazepine receptor(s)	9. Adenylate cyclase
2. GABA site(s)	10. Adenosine triphosphatase
3. Chloride ion channel	11. Calcium transport
4. Adenosine receptors(s)	12. Presynaptic neurotransmitter receptor
5. Acetylcholine receptors(s)	13. Sodium ion transport
6. Sodium ion channel	14. Excitatory amino acid receptor(s), (glutamate and aspartate)
7. Norepinephrine receptor(s)	15. Kainate receptor
8. Dopamine receptors(s)	

Table 11. Neuronal Sodium Channel Types and Location in Rat Brain.

Neuronal sodium channel types	Primary location	Possible receptor
I	cell bodies	anticonvulsant
II	embryonic and neonatal axons	local anesthetics
IIA	adult axons	
III		

sodium channel activation. Brevetoxins and ciguatoxins cause persistent repetitive firing of the NVSC. Two additional toxins, *Conus striatus* and *Goniopora* coral toxin, have been found to affect sodium channel inactivation by binding at distinct site(s). Neurotoxin site 7, which binds δ-conotoxin, causes non-voltage-dependent sodium channel inactivation.

The isolation of batrachotoxinin (Figure 10) from the skin secretion of the Colombian arrow poison frog, *Phyllobates aurotaenia,*[53] and the development of [^{3}H]-batrachotoxinin A 20-α-benzoate (^{3}H-BTX-B)[54-56] as a probe have been useful in evaluating the relative potencies of compounds binding to the NVSC in vitro.

A commonly used assay for the binding of anticonvulsants to the NVSC monitors the inhibition of binding of ^{3}H-BTX-B to rat brain synaptoneurosomes in the presence of the selected compound. Evaluation of sodium channel binding thusrequires the preparation of rat synaptoneurosomes and measures the ability of the test compound to modulate ^{3}H-BTX-B binding.

Table 12. Classification of Neurotoxins and Actions on the Neuronal Sodium Channel

Site	Toxin	Sodium channel effect
1	Tetrodotoxin Saxitoxin	block Na^+ currents
2	Aconitine Batrachotoxin Grayanotoxin Veratridine	Na^+ channel activators

Table 12 (Continued)

3	Scorpion α-toxins (North American, North African) Sea Anemone toxin	slow Na^+ channel inactivation (voltage-dependent)
4	Scorpion β-toxins (Central and South American)	enhance activation
5	Brevetoxin Ciguatoxin	persistent repetitive firing activation
6	Conus Straitus Goniopora Coral toxin	slow sodium channel inactivation
7	σ-Conotoxin	allows sodium channel inactivation (non-voltage dependent)

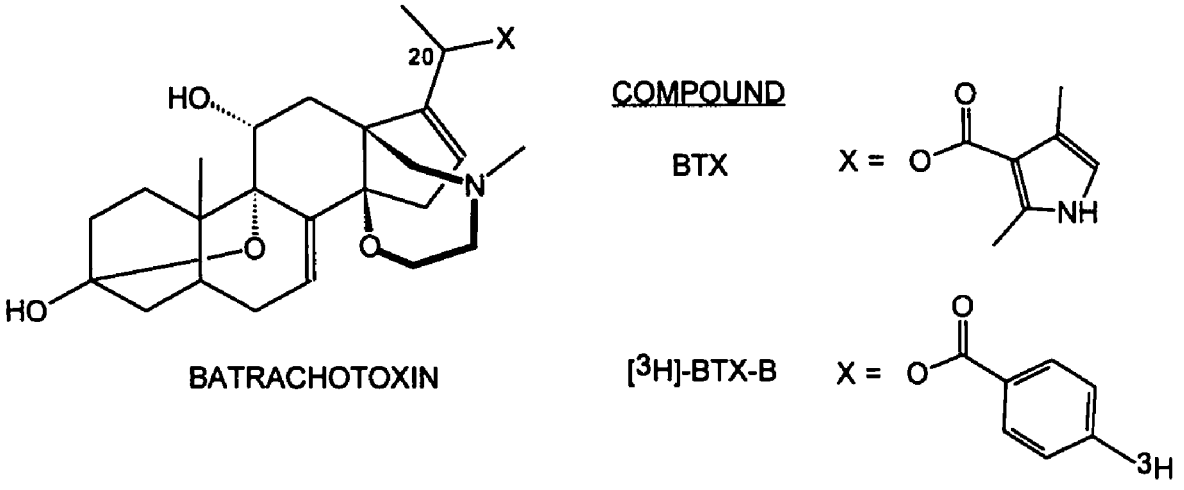

BATRACHOTOXIN

Figure 10. Structure of the lipid soluble neurotoxin batrachotoxin and analog [^{3}H]-BTX-B

The preparation of synaptoneurosomes involves the removal and dissection of cerebral cortex from freshly sacrificed Spague-Dawley rats. The brain cortex is weighed and the tissue combined and homogenized in a 1:2 weight(w) / volume (v) of cold Hepes incubation buffer. After an equal volume of cold Hepes incubation buffer is added the tissue is centrifuged at 1000 X G for 15 minutes. The pellet is resuspended in 1:20 w/v of cold Hepes incubation buffer. The tissue is passively filtered through 3 layers of 160 µM mesh nylon and a Whatman #4 filter and centrifuged at 1000 X G for 30 min. The pellet is resuspended in a cold isotonic sucrose solution (isotonic sucrose solution: 10 mM $Na_2H_2PO_4 \cdot H_2O$, 0.32 mM Sucrose, pH = 7.4 with trizma base or NaOH) starting with a 1:13 w/v dilution. An absorbance at 280 nm is obtained for 75 λ of tissue in 1.5 mL of distilled H_20. If a reading of 1.0 absorbance unit (which corresponds to 2.25 mL of tissue) is not obtained, then the volume of tissue added to the storage tube should be adjusted proportionately. The storage tubes are capped, counted and frozen on an angle at -20 °C. An example of an experimental synaptosome yield is presented in Table 13. The frozen tissue tubes can be stored at -70 °C and are viable for 3 to 4 months.

The frozen tissue can be prepared for use by allowing the tissue to thaw at room temperature. The cold tissue must be centrifuged at 1000 X G for 15 min at 0-5 °C. The resulting pellet should be resuspended in 2.25 mL of cold Hepes incubation buffer and incubated for 15 min on ice prior to usage in the assay to provide viable synaptoneurosomes.[54]

Table 13. Biological Results for a Yield of Synaptosomes Prepared from Rat Cerebral Cortex

# of rats	weight of cortex[a]	# of storage tubes
2	2.2	17

[a]Experimental results, cortex weight may vary with age and size of the rats.

The [^{3}H]-BTX-B assay[54-56] measures the relative ability of compounds to allosterically inhibit the binding of ^{3}H-BTX-B to neurotoxin site 2. ^{3}H-BTX-B, the *para*-^{3}H-benzoate C20 ester of batrachotoxin in Figure 10 was prepared by New England Nuclear with a specific activity of 30 Ci/mol.

The ^{3}H-BTX-B assay involves the incubation of the test compound (at seven different concentrations spanning the IC_{50}) with the synaptoneurosomes (~1 mg of protein) for 40 min at 25 °C. A total volume of 320 μL is contained within each test tube, consisting also of 10 nM [^{3}H]BTX-B and 50 μg/mL of scorpion venom. Incubations are terminated by dilution with ice cold buffer and filtration through a Whatman GF/C filter paper, and the filters washed four times with ice cold buffer. Filters are counted and specific binding determined by subtracting the nonspecific binding, which is measured in the presence of 300 μM veratridine, from the total binding of [^{3}H]BTX-B. All experiments are performed in triplicate and included a control tube containing 40 μM DPH. The IC_{50} values are determined from a Probit analysis of the dose-response curve and excluded doses producing less than 10% or greater than 90% inhibition.

Drugs classes reported to effect [^{3}H]-BTX binding to the synaptoneurosomal preparations are local anesthetics,[57-63] antiarrhythmics,[62] insecticides,[64] alkaloid toxins,[65-68] anticonvulsants[69-75] and sodium channel blockers (Table 14).[51, 76, 77] In

particular, we have been interested in anticonvulsant analogs that bind to the NVSC and inhibit [^{3}H]-BTX-B.

The inhibition of [^{3}H]-BTX-B by the anticonvulsant DPH at therapeutic concentrations (40 μM) implicates the NVSC as the putative site of anticonvulsant activity.[72] The anticonvulsant DPH binds to the inactivated state of the NVSC in a frequency and voltage-dependent manner.[38] Studies also indicate that sodium channel blockade by DPH is affected by changes in intracellular, but not extracellular, pH, consistent with intracellular actions.[78] Examination of membrane effects for DPH using fluorescent fatty acid probes implied that DPH may exert an inhibitory effect on the NVSC by simple partitioning of its two phenyl rings into the lipid bilayer.[79] However, DPH exhibits saturable binding to the NVSC, which is associated with properties of specific receptor-ligand interactions.[80]

Table 14. Classes of Compounds That Inhibit [^{3}H]-BTX-B

Inhibitors of [^{3}H]-BTX-B binding	Action
Insecticides	Prolong Na^+ currents
Local anesthetics, sodium channel blockers	Inhibitors of Na^+ channel inactivation
Anticonvulsants	Inhibit rapid depolarization of Na^+ channel
Antiarrhythmics	Stabilize inactivated state
Alkaloid toxins	Na^+ channel activator

Previous studies[74] by Dr. Wayne Brouillette's laboratory have investigated anticonvulsant activity of phenyl-substituted bicyclic 2,4-oxazolidinediones and α-hydroxy-α-phenylcaprolactams in mice and measured the binding of these analogs

to the NVSC using the [^{3}H]-BTX-B assay. The phenyl-substituted bicyclic 2,4-oxazolidinedione **2** (Figure 11) exhibited good anti-MES effects (ED_{50} = 66 [51-84] mg/kg, anti-MES therapeutic index = 2.23), while displaying a modest NVSC binding (IC_{50} = 160 μM for the inhibition of [^{3}H[-BTX-B binding) suggesting a likely mechanism of action. Futhermore, the result of this study indicated that moncyclic 2,4-oxazolidinediones (**3** and **4**) and α-hydroxy-α-phenylcaprolactams (**5-11**) are not effective binders to the NVSC (Table 15).

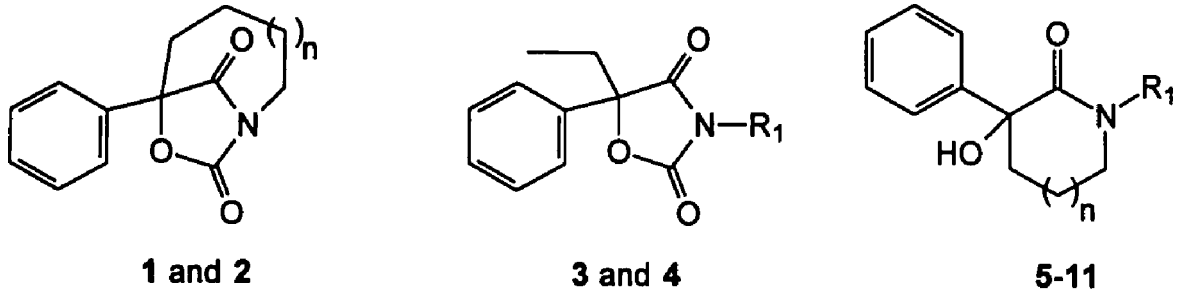

Figure 11. Structures of oxazolidinediones from a previous study **1-11**.

Table 15. Neuronal Sodium Channel Binding Potencies of Monocyclic and Bicyclic 2,4-Oxazolidinediones **1-11**

Compound	n	R_1	Na^+ channel IC_{50} (μM)
1	1		380
2	2		160
3		H	>800
4		CH_3	500
5	1	H	>800
6	1	CH_3	>800
7	1	H	>800

8	1	$CO_2C_2H_5$	590
9	2	H	>800
10	2	$CO_2C_2H_5$	640
11	3	H	>800

Subsequently, the enantioselectivity of binding to the NVSC for **2-4** was evaluated. The enantiomers of these monocyclic and bicyclic 2,4-oxazolidinediones do not enantioselectively bind to the NVSC.[75] However, (R)-(-)-**2** was 4 times more toxic than (S)-(+)-**2** in the anticonvulsant rotorod test. Thus (S)-(+)-**2** (anti-MES T.I. = 4.1) in comparison to (R)-(-)-**2** (anti-MES TI = 1.9) exhibited enantioselective therapeutic potential against MES challenges.

Early studies by Dr. Wayne Brouillette's laboratory using hydantoins containing conformationally restricted 5-phenyl substituents suggested that optimum binding to the NVSC may require a specific aromatic ring orientation (Figure 12). Compounds **15** and **17**, ring opened analogs of **16** and **18**, demonstrated drastically different binding affinities to the NVSC. As shown, no clear trend between log *P* and activity was evident (Table 16).

In contrast to inconsistent log *P* trends, the orientation of the 5-phenyl ring was suggested as important for binding of 5-phenylhydantoins to the NVSC. Thus 5-phenyl orientation and NVSC binding were examined for restricted analogs **16** and **18**. Dreiding models and *Alchemy 2* studies for low energy conformers of **16** placed the plane of the 5-phenyl group perpendicular to the plane of the hydantoin ring. However, the tricyclic hydantoin **18**, which bound with greater affinity (Table

16, IC_{50} = 250 μM), contained a phenyl ring plane held in a "coplanar" relationship. The association of increased affinity with 5-phenyl orientation was suggested as important for binding of 5-phenylhydantoins to the NVSC.

In the history of drug development, much information has been obtained from quantative structure activity relationship (QSAR) studies. A quantitative study in 1942 of *in vitro* activity for 46 sulfonamides provided a major stimulus in QSAR development and indicated potential value in considering the influences of substituents on charge distribution.[81] During this time, physical chemists were developing parameters to quantify the electronic effects of substituents in chemical reactions and ionic equilibria. Thus the Hammett relationships demonstrated that chemical reactivity of *meta*- and *para*-substituted benzene analogs could be correlated by the equation $\log (k_x/k_H) = \rho \cdot \sigma_x$, where K_x expresses the rate for the derivative and k_H is the rate constant for the unsubstituted parent molecule.

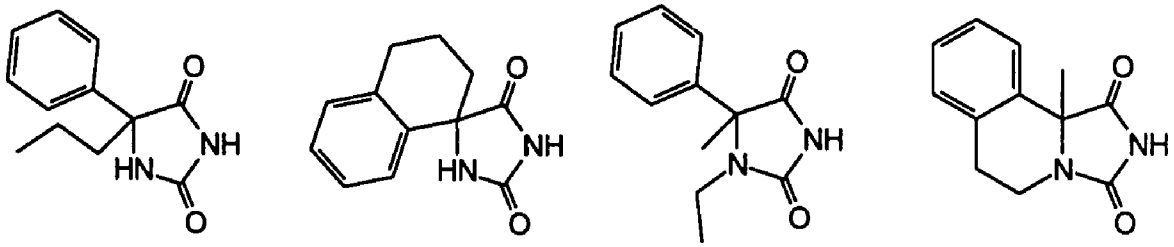

Figure 12. Structure of hydantoins with restricted 5-phenyl ring.

The constant σ_x refers to the electronic effect of the substituent in relation to hydrogen and is positive for electron-withdrawing groups and negative for electron-

Table 16. Neuronal Sodium Channel Potencies and Log *P* for Hydantoins **15-18**, Containing Conformationally Constrained 5-Phenyl Rings

compound	Na^+ channel IC_{50} (μM)	log *P*[a]
15	130	1.46
16	1600	1.96
17	720	1.52
18	250	2.02

[a]Log *P* calculated by the addition of the appropiate π value to the log *P* of the parent 5-phenylhydantoin (log *P* = 0.46) and not published in reference.

donating groups. The ρ values reflect the sensitivity of the substrate to electron release or withdrawal by the substituent (ρ is positive when electron-withdrawing groups increase the rate and negative when electron-donating groups increase the rate).[82]

In 1962, Corwin Hansch established our modern classical multi-parameter approach to QSAR.[82] Using the partition coefficient as a hydrophobic scale, a scale of hydrophobic constants was set up for benzene derivatives in an analogous fashion to a Hammett equation and expressed as the log $(P_X/P_H) = \pi$,[83] where the partition coefficient P_H, is the measure of the ratio of a drug's solubility in octanol as compared to that in water for the parent molecule and P_X refers to the partition coefficient for the substituted molecule. The parameter π is represented by the logarithm of the ratio of the partition coefficients of the substituted molecule to the parent compound.

Hansch postulated that molecules that are highly hydrophilic will not readily partition from water into the lipid membrane. If the destination of a molecule is a

receptor within or beyond that membrane, such a molecule will have a low probability of reaching that receptor. Thus the idea was born that for a particular receptor an optimum value of log *P* or π would be found to correspond to the maximum probability of reaching the receptor. The simplist way of expressing this idea mathematically would be to postulate that log (1/C) was parabolically dependent on log *P* and thus the extremely useful Hansch equation $\log(1/C) = k_1(\log P) - k_2(\log P)^2 + k_3(\sigma) + k_4$ was proposed. With this Hansch equation, a full-scale development of QSAR began.[84-88]

The objective of QSAR has been to find parameters from experiment or theory that correlate with biological activity and to represent this relationship by a simple equation, for example: biological activity = constant *p* (*p* = physicochemical and/or structural parameter). If a good model (i.e., correlation coefficent) is found, it may be used to predict other molecules having greater activity in the biological system.

Severe limitations in predicting new drugs result from the fact that a drug structure has to be optimized for many parameters involved in its pharmacological action, such as solubility, stability, absorption, metabolism, transport, steric size, and electronic distribution. A QSAR can often be developed that encompasses a prediction for some features, but never simultaneously for all.

The real value that classical QSAR development provides is the understanding of relationships between physical properties and activity. The major advantages achieved through a predictive QSAR model can be realized by (1) a

reduction in the number of synthesized compounds needed to reach a potentially enhanced analog and (2) the amount of animals used for testing.

Problems of classical QSAR are most associated with factors involved in making linear predictions. The reliable use of linear models to predict unknown biological activity from known activities of the QSAR data set relies on the degree of similarity between members of the original training set. Thus the design of new compounds from a linear model is restricted to the structural class contained within the database.[89]

It is also well recognized that linear relationships reach a maximum (or a cutoff) value and, thus, do not continue on forever.[90, 91] Therefore the properties of compounds are best predicted in regions spanned by data points and least accurate when extrapolated. Furthermore, the data within this spanned space should have a good spread between values.

Published anticonvulsant models, which include hydantoins, suggest hydrogen-bonding complexes,[92, 93] dipole moments,[94] the orientation of electron donor groups in relation to two hydrophobic regions[95-97] and lipophilicity[98, 99] as correlated properties. With the emergence of computer technology, graphical QSAR[100] researchers have gained access to 3-dimensional (3-D) relationships for hydantoin anticonvulsants,[101-103] otherwise unavailable with classical linear models.

The development of computer modeling software like SYBYL (Tripos, Inc.) and the 3D-QSAR module Comparative Molecular Field Analysis (CoMFA) has been useful in extrapolating important 3-D properties for ligands that bind to

receptor sites with unresolved crystallographic structures.[104, 105] CoMFA samples the differences in steric and electrostatic fields surrounding a set of ligands and correlates the differences with biological activity.

The most basic CoMFA consists of (1) obtaining reliable biological data for a set of at least 4 or more compounds, (2) conformational analysis and charge calculations, (3) alignment of molecules in a database, (4) calculation of CoMFA values, (5) partial least squares (PLS) correlation of CoMFA descriptors and biological data, (6) analysis of the final CoMFA model and (7) design and prediction of new analog(s).

Conformational analysis involves acquiring all of the lowest energy minimized geometries for each compound in the dataset. Methods of accessing these structures include the use of x-ray crystallographic structures,[106] nuclear magnetic resonance (NMR),[105] computational approaches (semi-empirical[107] and molecular mechanics[108, 109]) or conformational searching routines (i.e., SYBYL/GRIDSEARCH and SYSTEMATICSEARCH).[109]

Single point calculations of atomic charges for all atoms in all geometric conformers can be calculated using available modules, such as Del Re,[110] Gasteiger/Marsili,[111] Hückel,[112] Pullman[113] and MOPAC.[114] Once charges have been calculated, a monumental task for the researcher is to choose which conformation and atoms to use in the alignment of the dataset molecules. Usually this task is repeated many times until a satisfactory final model is achieved.

Calculation of the CoMFA column, which represents many columns of values describing the differences in steric and electrostatic potentials, is accomplished by encompassing all molecules within a grid box in the x, y and z directions that extend past the aligned molecules in each direction. A probe atom is used within this region to calculate the differences in steric and electrostatic potentials at each grid point.

Partial Least Squares (PLS) analysis is an iterative regression technique used to solve linear models in a stepwise fashion.[115, 116] The analysis includes two phases: (1) crossvalidation and (2) noncrossvalidation PLS. Crossvalidation accesses the probable predictive value of a particular model by a brute force method of attempting predictions of all of the input target values. The most important parameter obtained from a crossvalidative PLS is the optimum number of components. Generally, the optimum number of components is chosen by comparing analysis using increasing numbers of components and accepting the number, where the change in the correlation coefficient (R^2) is less than 5% when a component is added.

A final model with R^2 is obtained by noncrossvalidation using the optimum number of components obtained from the previous crossvalidated analysis. The relative steric and electrostatic contributions in the final model can be determined and viewed graphically as areas of space around the molecules. CoMFA theory describes areas of least overlapped steric and electrostatic at 50% contoured

contribution. Thus choosing contributions closer to 0% and 100% displays areas of greatest steric and electrostatic difference.

The results of the model are depicted by color coded regions of space around the molecules where favored and disfavored areas of steric and electrostatic differences exist. Based on the information obtained and the ability of the investigator to discern the important pharmacophore properties, analogs can be designed and predicted that best fit the model.

Utilizing diverse structural classes within the CoMFA model is of great advantage. The use of structurally diverse ligands corresponds to large differences of steric and electrostatic fields and thus CoMFA, which measures the differences of these fields, can generate better results. However the most important advantage provided by CoMFA modeling is the ability to design ligands that are structurally different from compounds in the original dataset.[89]

The CoMFA correlation technique of PLS provides another significant advantage over classical methods such as multiple regressions (MR).[115-119] This advantage is evident in the general reduction of chance correlations when using PLS versus MR.

Numerous successes have been reported for mapping properties of central nervous system (CNS) receptors by CoMFA methods.[120-136] Recently, the first CoMFA study for a NVSC site was reported for Brevetoxins (neurotoxin site 5) and resulted in the identification of a useful pharmacophore model.[120]

Table 17. Successful CNS CoMFA Studies

CNS receptor(s)
Benzodiazepine receptor(s)[a]
δ_3 receptor(s)[b]
Cannabinoid[c]
Calcium Channel[d]
Nicotinic Acetylcholine[e]
GABA[f]
Muscarinic[g]
Dopamine[h]
Serotonin (5-Hydroxytryptamine) or (5-HT)[i]

[a]Reference 121-124. [b]Reference 125 and 126. [c]Reference 127 and 128. [d]Reference 129. [e]Reference 130. [f]Reference 131. [g]Reference 132. [h]Reference 133. [i]Reference 89 and 134.

GOALS AND RATIONALE

Evaluation of neuronal voltage-sensitive sodium channel (NVSC) binding for previously synthesized smissmanones[137] suggested that N3-alkylation and the conformational constraint of a 5-alkyl substituent over one face of the oxazolidinedione ring improved activity. In order to evaluate similar structural comparisons of previously synthesized conformationally constrained bicyclic hydantoins, we propose the synthesis, sodium channel evaluation and calculation of log *P* for analogous ring opened hydantoins **1-3** and **16**.

Examination of membrane effects for diphenylhydantoin (DPH) using fluorescent fatty acid probes[138] implied that DPH may exert an inhibitory effect on the NVSC by simple partitioning of its two phenyl rings into the lipid bilayer. However, DPH exhibits saturable binding to the NVSC, which is associated with properties of specific receptor-ligand interactions.[139] We have thus been interested in investigating specific receptor properties of hydantoins that result in optimum NVSC affinity. An early study[140] from our laboratory suggested that 5-phenyl ring orientation may be important for hydantoins binding to the NVSC. However, this preliminary investigation did not consider the effects of changes in lipophilicity. In order to investigate the conformational requirement of 5-phenyl ring orientation, and to quantitate this specific interaction independent of lipophilic effects, we proposed

the design (by computer modeling), synthesis, calculation of log *P* and NVSC evaluation for hydantoins **1-12**.

Given the absence of high resolution structural data for the NVSC, we proposed the use of comparative molecular field analysis (CoMFA) to help extrapolate important 3-dimensional (3-D) properties associated with the optimum binding of hydantoins to this site. CoMFA samples the differences in steric and electrostatic fields surrounding a set of ligands and correlates these differences, by partial least squares (PLS) analysis, with biological activity.[141]

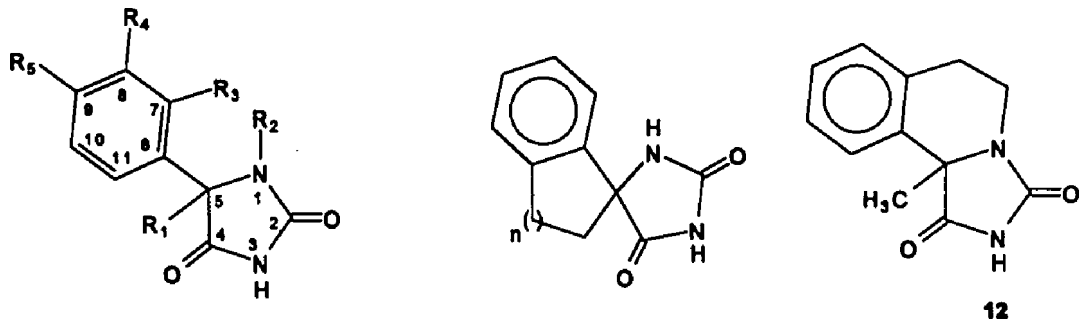

	R_1	R_2	R_3	R_4	R_5
1	n-C $_3H_7$	H	H	H	H
2	n-C $_4H_9$	H	H	H	H
3	n-C $_5H_{11}$	H	H	H	H
4	n-C $_4H_9$	H	CH_3	H	H
5	n-C $_4H_9$	H	H	CH_3	H
6	n-C $_4H_9$	H	H	H	CH_3
7	CH_3	C_2H_5	H	H	H
DPH	Ph	Ph			

	n
8	1
9	2
10	3
11	4

12

Figure 13. Structures of hydantoins **1-12** and DPH.

Thus we proposed to evaluate correlations of two models, log *P* and CoMFA, with NVSC binding and present the first 3-D pharmacophore model for the NVSC

hydantoin receptor site. To construct our models, we synthesized new compounds, calculated log *P* and evaluated the NVSC binding for 5-alkyl-5-phenylhydantoin **13-15** (which extends our series of analogs to include larger log *P* values), and we utilized previously reported NVSC data for hydantoins **1-3** and **7-11** and **16**. We tested the pharmacophore model, by predicting NVSC activities for previously reported structurally diverse hydantoin analogs not included in our model. From this tested model, we designed, synthesized and evaluated the NVSC binding for **14**, a new site-directed analog.

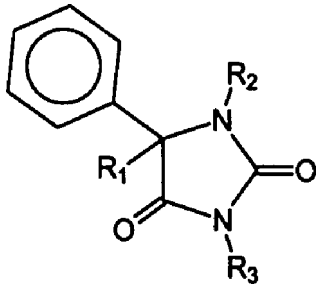

	R_1	R_2	R_3
13	C_6H_{13}	H	H
14	C_7H_{15}	H	H
15	C_9H_{17}	H	H
16	C_4H_9	H	CH_3

Figure 14. Structures of hydantoins **13-16**.

Finally, α-hydroxy-α-phenyllactams **17**, synthesized[142] by this laboratory as a precursor of anticonvulsants called "smissmanones", was previously evaluated for anticonvulsant activity[137] in mice. Compound **17** demonstrated good anticonvulsant activity (MES ED_{50} = 63 mg/kg and scMET ED_{50} = 74 mg/kg) and exhibited analogous anti-MES T.I. [anti-MES therapeutic index (T.I.) = 3.3, Table 2], as compared to phenacemide (anti-MES T.I. = 4.8, Table 2), a structurally similar prescribed anticonvulsant.

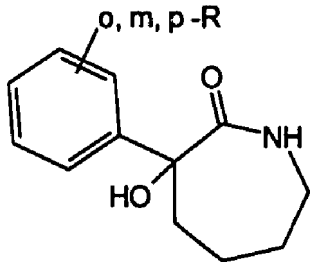

	R
17	H
18	ortho-Cl
19	meta-Cl
20	para-Cl
21	ortho-OCH_3
22	meta-OCH_3
23	para-OCH_3

Figure 15. Structures of α-hydroxy-α-phenyllactams **17-23**.

The demonstration of promising anti-MES activity and the ready availability of starting materials presented **17** as a candidate for further development. Often the substitution of electron-donators or withdrawers on benzene rings dramatically alters CNS activity, thus in this study we proposed the synthesis and anticonvulsant evaluation of lactams **18-23**, which investigated the effects of *ortho*, *meta* and *para* [electron withdrawing (-Cl) and donating (CH_3O-) groups] α-phenyl substitutions on anticonvulsant activity.

Further α-hydroxy-α-phenyllactams **24**, a potent sodium channel binder (IC_{50} = 9 μM [7-11]), was selected for anticonvulsant testing and demonstrated good preliminary anticonvulsant activity. To study effects on anticonvulsant activity of α-alkyl-α-hydroxy-α-phenylamides with increased alkyl side chains, we propose the synthesis and anticonvulsant evaluation of **25** and **26**. The results of these studies are presented in the following sections.

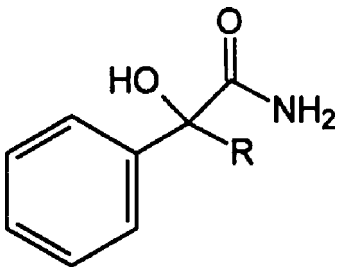

	R
24	C_7H_{15}
25	C_9H_{19}
26	$C_{13}H_{25}$

Figure 16. Structures of α-hydroxy-α-phenyllactams **24-26**.

BICYCLIC HYDANTOINS WITH BRIDGEHEAD NITROGEN. COMPARISON OF ANTICONVULSANT ACTIVITIES WITH BINDING TO THE NEURONAL VOLTAGE-DEPENDENT SODIUM CHANNEL

WAYNE J. BROUILLETTE,*[†] VLADIMIR P. JESTKOV,[†§] MILTON L. BROWN,[†] M. SHAMIM AKHTAR,[†] TIMOTHY M. DELOREY,[†‡] AND GEORGE B. BROWN[‡]

Department of Chemistry and Department of Psychiatry and Behavioral Neurobiology, University of Alabama at Birmingham, Birmingham, Alabama 35294

"Reprinted with permission from: Brouillette, W. J.; Jestkov, V. P; **Brown, M. L.**; Aktar, M. S.; Delorey, T. M.; Brown, G. B. Bicyclic Hydantoins with Bridgehead Nitrogen. Comparison of Anticonvulsant Activities with Binding to the Neuronal Voltage-Dependent Sodium Channel. *J. Med. Chem.* **1994**, *37*, 3289-3293."

---

*Address correspondence to this author.

[†]Department of Chemistry

[‡]Department of Psychiatry and Behavioral Neurobiology

[§]Dr. Jestkov was a visiting scientist from the National Research Center for Biologically Active Compounds, 23 Kirov Str., Staraya Kupavna, Moscow region, Russia.

Abstract

The anticonvulsant activity of diphenylhydantoin (DPH or phenytoin) is consistent with its actions on the neuronal voltage-dependent sodium channel. To further elucidate the binding requirements for this site, we synthesized several hydantoin analogs and evaluated these in in vitro sodium channel-binding and/or in vivo whole animal anticonvulsant assays. 5-Pentyl-5-phenylhydantoin (**8**), the most potent binder to the sodium channel in this study, had the same affinity as DPH (IC_{50} = 40 μM), revealing that one phenyl ring is sufficient for good interactions. Since our previous studies with monophenyl-substituted bicyclic 2,4-oxazolidinediones suggested that N3-alkylation and the conformational constraint of a 5-alkyl substituent over one face of the oxazolidinedione ring improved activity, we synthesized two examples of analogous bicyclic hydantoins. However, the bicyclic hydantoins were much less potent binders to the neuronal voltage-dependent sodium channel than their monocyclic counterparts. The binding activity for the more potent bicyclic hydantoin, 1,8-diaza-9,10-dioxo-7-phenylbicyclo[5.2.1]decane (**4**) (IC_{50} = 427 μM), was comparable to the ring opened, N3-methylated monocyclic hydantoin model 5-butyl-3-methyl-5-phenylhydantoin (**9**) (IC_{50} = 285 μM), and these were 8-11 times less potent than the homologous monocyclic model **8**, which contains a free imide NH. Furthermore, 5-butyl-5-phenylhydantoin (**7**, IC_{50} = 103 μM) was less potent than **8**, suggesting that increased log *P* may enhance binding. Thus, unlike 2,4-oxazolidinediones, N3-alkylation of hydantoins dramatically decreases sodium channel-binding activity.

Bicyclic hydantoin **4** was nevertheless a good anti-MES anticonvulsant in mice (ED_{50} = 86 mg/kg), although this activity likely results from mechanisms other than interactions at the neuronal voltage-dependent sodium channel. Compound **4** was also relatively neurotoxic (TD_{50} = 124 mg/kg). These results suggest that the binding of hydantoins to the sodium channel may be enhanced by (a) a free imide NH group, and (b) increased log *P*. Furthermore, 2,4-oxazolidinediones and hydantoins must either orient differently in the same binding site or interact with different sites on the neuronal voltage-dependent sodium channel.

We have been interested in the preparation of bicyclic imides with structures **1-4** as probes of cyclic imide anticonvulsant binding sites. These compounds were first proposed by Edward E. Smissman,[1] and we named them "smissmanones" upon reporting the first successful synthesis of examples from this class.[2]

The neuronal voltage-dependent sodium channel is a putative site of action for the anti-maximal electroshock (anti-MES) anticonvulsants diphenylhydantoin (DPH or phenytoin, Figure 1; a cyclic imide) and carbamazepine (which contains an acyclic urea side chain).[3,4] These agents bind to the sodium channel at therapeutically relevant concentrations. Such binding is voltage- and frequency-dependent, providing a consistent explanation for selective effects on hyperactive versus normal neurons. Unfortunately, this binding site is not well characterized, although compounds that bind with enhanced potency and selectivity may provide better anti-MES anticonvulsants.

We have utilized smissmanones as part of a study to delineate structural features on cyclic imides that result in tight binding. We previously reported the syntheses[2] and the anticonvulsant and sodium channel-binding activities[5] for bicyclic 2,4-oxazolidinediones **1** and **2** and the monocyclic model **5**. We have also reported the synthesis of bicyclic hydantoin **3**.[6] Here we describe the synthesis of bicyclic hydantoin **4**, and we present new sodium channel-binding and whole animal anticonvulsant activities for bicyclic hydantoins **3** and **4**,which permit comparisons with the bicyclic 2,4-oxazolidinediones. Additionally, trends in sodium channel-binding activities for homologous hydantoins are discussed with regard to effects of structure versus log *P* on binding.

Chemistry

The syntheses of compounds **1**,[2] **2**,[2] **3**,[6] **5**,[5] and **6**,[7] were previously described. Hydantoins **7** and **8** were prepared according to a literature method[8] from commercially available valerophenone and hexanophenone, respectively, using the Bucherer-Bergs reaction. Methylation[9] of the imide nitrogen in **7** using NaOH and dimethyl sulfate gave previously reported **9**[10] in 87% yield.

The synthesis of bicyclic hydantoin **4** was based upon the approach[6] that we developed for preparing **3** and is summarized in Scheme I. In this 8-membered ring system, experimental procedures were essentially the same as those utilized previously in the 7-membered ring system involved in the synthesis of **3**. One exception is the conversion of bromolactam **11**, prepared by the monobromination of lactam **10** in 40% yield (according to a published procedure[11]), to cyanolactam

12. During the synthesis of **3**,[6] this step was accomplished in 55% yield by treating α-bromocaprolactam with NaCN and 18-crown-6 in CH_3CN. However, the treatment of **11** under identical conditions resulted exclusively in elimination to provide the α,β-unsaturated lactam. This behavior was also observed by others who reported[12] that the treatment of **11** with cyanide in EtOH, DMF, or DMSO under a variety of conditions failed to produce any nitrile **12**. After a number of trials using differing conditions of cyanide salt, solvent, and catalyst, we found that treating **11** with NaCN and $PhCH_2NEt_3^+ Cl^-$ in CH_3CN provided **12** in 50% isolated yield. Lactam **12** then underwent α-phenylation using Ph_5Bi in essentially quantitative yield (as compared to 74% yield for the 7-membered ring procedure). The nitrile **13** was hydrolyzed to the amide **14** (91% yield), and this was cyclized upon treatment with $Pb(OAc)_4$ via an intramolecular N-alkylation of the intermediate isocyanate to provide **4** in 67% yield (as contrasted to 48% yield for the comparable cyclization that produced **3**).

Results and Discussion

While the widely prescribed cyclic imide anticonvulsant diphenylhydantoin (DPH or phenytoin; Figure 1) interacts well with the sodium channel, other common cyclic imide anticonvulsants, such as barbiturates and 2,4-oxazolidinediones (e.g., trimethadione in Figure 1), are poor binders. However, our previous biological studies[5] with 2,4-oxazolidinediones demonstrated that 5-alkyl-5-phenyl-2,4-oxazolidinediones exhibited both anti-MES and modest sodium channel-binding activities. Furthermore, the sodium channel-binding activity of this class was

moderately enhanced by methylation of the imide nitrogen to give **5** (Figure 1 and Table 2), although this activity was judged insufficient to account for the moderate anti-MES effect. As summarized in Table 2, the greatest improvement in sodium channel-binding activity for the 2,4-oxazolidinediones resulted from incorporation of the N-methyl and 5-alkyl substituents into a ring to provide **2**, which was a good anti-MES anticonvulsant (ED_{50} = 66 mg/kg) that was also a relatively good binder to the sodium channel (IC_{50} = 160 μM). Since diphenylhydantoin (phenytoin; see Table 2) is a more potent anti-MES anticonvulsant (ED_{50} = 10 mg/kg) and a better sodium channel binder (IC_{50} = 40 μM) than **2**, we proposed that bicyclic hydantoin derivatives **3** and **4**, as was found for **1** and **2**, may provide better anti-MES and sodium channel-binding activities than monocyclic hydantoins. As part of the present study on hydantoins, we also evaluated the sodium channel-binding activity of compound **7**, a monocyclic model for bicyclic hydantoin **3**. Similarly, hydantoins **8** and **9** also represent ring opened analogs of bicyclic hydantoin **4**, but each results from a different disconnection along the alkyl bridge. As shown in Table 2, the IC_{50} obtained for **8** in the sodium channel-binding assay was nearly identical to that reported for DPH, revealing that appropriately substituted 5-alkyl-5-phenylhydantoins, like DPH, may interact efficiently with the sodium channel.

We were thus encouraged by the proposition that, as observed for the 2,4-oxazolidinediones, incorporation of the 5-alkyl substituents of **7** and **8** into a bicyclic structure (**3** and **4**) might further enhance sodium channel-binding activity in the hydantoin series. However, as shown in Table 2, the opposite effect was observed.

While bicyclic hydantoin **4**, which contains the larger alkyl bridge, was a better binder than **3**, this activity remained 11-fold less potent than that seen for monocyclic model **8**.

Comparisons of the sodium channel-binding activities for homologous pairs of compounds (e.g., **1** vs **2**; **3** vs **4**; **7** vs **8**) in Table 2 revealed that the larger compounds were consistently more potent binders, suggesting that partition coefficients (*P*) may be important. We also determined in the present study the sodium channel-binding affinity for hydantoin **6**, which we evaluated previously,[7] and found that the results were consistent with the above trend. We thus estimated the log *P* values for the compounds in Table 2 using reported (experimentally measured)[13] log *P* values for the parent structures 5-phenyl-2,4-oxazolidinedione (log *P* = 1.09) and 5-phenylhydantoin (log *P* = 0.46), to which were added the appropriate π values for C5 and N3 substituents to provide the final log *P*. The π values used were 0.5 for each CH_2 or CH_3 in the alkyl chain at C5[14] and 0.56 for an N-CH_3 substituent.[14] The extra ring closure in bicyclic compounds **1**-**4** was treated as a contribution of -0.5.[13] For example, the log *P* for hydantoin **9** was calculated as log $P_{parent} + \pi_{5\text{-butyl}} + \pi_{N\text{-Me}}$ = 0.46 + 2.0 + 0.56 = 3.01. Since the ring closure of **9** provides bicyclic hydantoin **4**, the log *P* of **4** was calculated as log $P_9 + \pi_{ring\ closure}$ = 3.01 + (-0.5) = 2.51. Log *P* values for all other compounds in Table 2 were estimated in a similar fashion.

Since changes in log *P* corresponded with changes in IC_{50} in the sodium channel-binding assay, a comparison was made between different structures with

similar log *P* values to provide insight into structural requirements other than log *P* that are important for the binding of hydantoins to this site. Hydantoins **8** and **9** have essentially the same lipophilicity, but **8** is seven times more potent, revealing that a free imide NH group is necessary for optimum activity. This conclusion is further supported by the observation that hydantoin **9**, which is more lipophilic than **7** but contains an N-methyl group, is two times less potent in binding to the sodium channel. Finally, N3-alkylated monocyclic hydantoin **9** is more lipophilic and a more potent binder to the sodium channel than the analogous N3-alkylated bicyclic hydantoin **4**, revealing that, unlike 2,4-oxazolidinediones, conformational restriction of the 5-alkyl group across one face of the cyclic imide ring has little effect on sodium channel-binding potency.

Several compounds in Table 2 were also evaluated for their whole animal anticonvulsant effects in mice. Of particular relevance to this study was the observations that bicyclic hydantoins **3** and **4**, which were poor binders to the sodium channel, both possessed relatively good anti-MES anticonvulsant activities. This activity for **4** was quantitated, providing an anti-MES ED_{50} of 86 mg/kg. Unfortunately, toxicity in the rotorod assay was nearly as great (TD_{50} = 124 mg/kg), revealing a poor therapeutic ratio. Since the anti-MES activity of **4** must not result from the modest sodium channel-binding activity, other potential mechanisms of action were investigated. Phase V evaluation revealed an ED_{50} (114 mg/kg) against seizures induced by subcutaneous bicuculline (a $GABA_A$ antagonist) that was nearly as potent as the anti-MES effect, suggesting that the mechanism of action may

involve the GABA system. In vitro radioligand binding assays in Phase Va using [^{3}H]flunitrazepam (a benzodiazepine receptor agonist) and [^{3}H]GABA, as well as studies on [^{3}H]adenosine uptake, revealed no significant effects.

In summary, 5-alkyl-5-phenylsubstituted monocyclic hydantoins may bind efficiently to the sodium channel. The above studies suggest that the binding of these hydantoins to the sodium channel is enhanced by (a) increased log *P* and (b) a free imide NH group. In contrast to 5-alkyl-5-phenyl-2,4-oxazolidinediones, alkylation of the hydantoin imide nitrogen with a methyl group or the presence of a bridging 5-alkyl substituent across one face of the hydantoin ring, as in smissmanones **3** and **4**, diminishes sodium channel-binding activity. Thus 2,4-oxazolidinediones and hydantoins must either orient differently at a single site or interact with different sites on the neuronal voltage-dependent sodium channel.

Experimental Section

Hydantoins **7** and **8** were prepared from valerophenone and hexanophenone, respectively, via a Bucherer-Bergs reaction as previously described.[8] Hydantoin **7** underwent N3-methylation[9] using NaOH and Me_2SO_4 to give **9**.[10]

Except for the conversion of **11** to **12**, the synthetic procedures for preparing smissmanone **4**, as summarized in Scheme I, were essentially identical to those reported[6] for the preparation of **3**. ^{1}H and ^{13}C NMR spectra were recorded in $CDCl_3$ at ambient temperature on a GE 300 FT NMR spectrometer (300.1 MHz for ^{1}H). IR spectra were recorded on a Beckman Acculab-1 spectrometer, and elemental analyses were performed by Atlantic Microlabs of Atlanta, GA.

[^{3}H]Batrachatoxinin A 20-α-benzoate ([^{3}H]BTX-B) with a specific activity of 30 Ci/mmol was obtained from New England Nuclear (Boston, MA).

Hexahydroazocin-2(1H)-one-3-carbonitrile (12). A mixture of bromolactam **11** (2.7 g, 0.013 mol), powdered NaCN (3.0 g, 0.061 mol), and benzyltrimethylammonium chloride (3.9 g, 0.021 mol) in anhydrous acetonitrile (25 mL) was heated at reflux with stirring for 30 h. This was concentrated to dryness on a rotary evaporator, and EtOAc (50 mL) was added to the crystalline residue. The mixture was stirred and heated at reflux for 20 min, filtered, and the filter washed with additional hot EtOAc (75 mL). The filtrate was concentrated and the residue was chromatographed on a flash silica column (2.5 x 20 cm; 10:10:1 $CHCl_3$/Et_2O/EtOH). The appropriate fractions were combined and concentrated to give **12** (1.0 g, 50%) as a white solid: mp 164-166° (EtOAc).

Sodium Channel-Binding Assay. We previously reported the details of this procedure.[5] Briefly, synaptoneurosomes (~1 mg protein) from rat cerebral cortex were incubated for 40 min at 25 C° with the test compound (7 different concentrations spanning the IC_{50}) in a total volume of 320 µL containing 10 nM [^{3}H]BTX-B and 50 µg/mL of scorpion venom. Incubations were terminated by dilution with ice cold buffer and filtration through a Whatman GF/C filter paper, and the filters were washed three times with ice cold buffer. Filters were counted in a Beckman scintillation counter. Specific binding was determined by subtracting the nonspecific binding, which was measured in the presence of 300 µM veratridine, from the total binding of [^{3}H]BTX-B. All experiments were performed in triplicate and

included a control tube containing 40 μM DPH. The IC_{50} values were determined from a Probit analysis of the dose-response curve and excluded doses producing less than 10% or greater than 90% inhibition.

Anticonvulsant Assays. All whole animal anticonvulsant and neurotoxicity assays were conducted by the Antiepileptic Drug Development Program of the Epilepsy Branch, National Institute of Neurological Disorders and Stroke. A description of this testing program along with the protocols employed has been published.[15] Briefly, phases I and II employ ip administration in mice for two anticonvulsant assays, a maximal electroshock (MES) test and a subcutaneous metrazol (scMet) test, and a rotorod toxicity test. Phase I is a preliminary qualitative assay, and selected compounds from Phase I undergo quantification of activities (ED_{50} and TD_{50}) in Phase II. Phase V involves anticonvulsant drug differentiation in mice (ip) and consists of an in vitro portion and an in vivo portion. The latter evaluates activity against seizures induced by subcutaneous bicuculline, picrotoxin, and strychnine, since each of these convulsants acts by a somewhat different mechanism. Bicucculine and picrotoxin bind to different sites on the $GABA_A$ receptor, while strychnine acts at the glycine receptor. The in vitro portion consists of radioligand receptor binding assays in Phase Va using crude whole mouse brain synaptic membranes[16] for benzodiazepine receptor binding (employing [^{3}H]flunitrazepam, a benzodiazepine receptor agonist)[17] and γ-aminobutyric acid receptor binding (employing [^{3}H]GABA).[18,19] Additionally, Phase Va includes

adenosine uptake studies in mouse whole brain synaptosomes (employing [^{3}H]adenosine).[20]

Acknowledgments

We thank James Stables of the Antiepileptic Drug Development Program, Epilepsy Branch, National Institute of Neurological Disorders and Stroke for the anticonvulsant data presented in Table 2. M.L.B. was supported by a Patricia Robert Harris fellowship for predoctoral studies.

References

(1) Smissman, E. E.; Matuszack, A. J. B.; Corder, C. N. Reduction of Barbiturates Under Hydroboration Conditions. *J. Pharm. Sci.* **1964**, *53*, 1541-1542.

(2) Brouillette, W. J.; Einspahr, H. M. Bicyclic Imides with Bridgehead Nitrogen. Synthesis and X-Ray Crystal Structure of a Bicyclic 2,4-Oxazolidinedione. *J. Org. Chem.* **1984**, *49*, 5113-5116.

(3) Willow, M.; Catterall, W. A. Inhibition of Binding of [^{3}H]Batrachatoxinin A 20-α-Benzoate to Sodium Channels by the Anticonvulsant Drugs Diphenylhydantoin and Carbamazepine. *Mol. Pharmacol.* **1982**, *22*, 627-635.

(4) Willow, M.; Kuenzal, E. A.; Catterall, W. A. Inhibition of Voltage-Sensitive Sodium Channels in Neuroblastoma Cells and Synaptosomes by the Anticonvulsant Drugs Diphenylhydantoin and Carbamazepine. *Mol. Pharmacol.* **1984**, *25*, 228-234.

(5) Brouillette, W. J.; Brown, G. B.; DeLorey, T. M.; Shirali, S. S.; Grunewald, G. L. Anticonvulsant Activities of Phenyl-Substituted Bicyclic 2,4-Oxazolidinediones and Monocyclic Models. Comparison with Binding to the Neuronal Voltage-Dependent Sodium Channel. *J. Med. Chem.* **1988**, *31*, 2218-2221.

(6) Akhtar, M. S.; Brouillette, W. J.; Waterhous, D. V. Bicyclic Imides with Bridgehead Nitrogen. Synthesis of an Anti-Bredt Bicyclic Hydantoin. *J. Org. Chem.* **1990**, *55*, 5222-5225.

(7) Brouillette, W. J.; Brown, G. B.; DeLorey, T. M.; Liang, G. Sodium Channel Binding and Anticonvulsant Activities of Hydantoins Containing Conformationally Constrained 5-Phenyl Substituents. *J. Pharm. Sci.* **1990**, *79*, 871-874.

(8) Novelli, A.; Lugones, Z. M.; Velasco, P. Hydantoins III. Chemical Constitution and Hypnotic Action. *Anales Asoc. Quim Argentina* **1942**, *30*, 225-231.

(9) Oldfield, W.; Cashin, C. H. The Chemistry and Pharmacology of a Series of Cycloalkanespiro-5'-hydantoins. *J. Med. Chem.* **1965**, *8*, 239-249.

(10) Knabe, J.; Wunn, W. Racemic and Optically Active Hydantoins from Disubstituted Cyanoacetic Acids. *Arch. Pharm.* **1980**, 313, 538-543.

(11) Nagasawi, H. T.; Elberling, J. A.; Fraser, P. S. Medium Ring Homologs of Proline as Potential Amino Acid Antimetabolites. *J. Med. Chem.* **1971**, *14*, 501-508.

(12) Ridley, D. D.; Simpson, G. W. Preparations of 3-Substituted Tetra- and Hexahydroazocin-2(1H)-ones and Derivatives. *Aust. J. Chem.* **1981**, *34*, 569-581.

(13) Lipinski, C. A.; Giese, E. F.; Korst, R. J. pKa, Log P, and MedChem CLOGP Fragment Values of Acidic Heterocyclic Potential Bioisosteres. *Quant. Struct.-Act. Relat.* **1991**, *10*, 109-117.

(14) Lien, E. J. Structure-Activity Correlations for Anticonvulsant Drugs. *J. Med Chem.* **1970**, *13*, 1189-1191.

(15) Porter, R. J.; Cereghino, J. J.; Gladding, G. D.; Hessie, B. J.; Kupferberg, H. J.; Scoville, B.; White, B. G. Antiepileptic Drug Development Program. *Cleve. Clin. Q.* **1984**, *51*, 293-305.

(16) Enna, S. J.; Snyder, S. H. Influences of Ions, Enzymes, and Detergents on γ-Aminobutyric Acid Receptor Binding in Synaptic Membranes of Rat Brain. *Mol. Pharmacol.* **1977**, *13*, 442-453.

(17) Braestrap, C.; Squires, R. F. Specific Benzodiazepine Receptors in Rat Brain Characterized by High-Affinity [^{3}H]Diazepam Binding. *Proc. Natl. Acad. Sci. U.S.A.* **1977**, *74*, 3805-3809.

(18) Zukin, S. R.; Young, A. B.; Snyder, S. H. Gamma-Aminobutyric Acid Binding to Receptor Sites in the Rat Central Nervous System. *Proc. Natl. Acad. Sci. U.S.A.* **1974**, *71*, 4801-4807.

(19) Enna, S. J.; Snyder, S. H. Properties of γ-Aminobutyric Acid (GABA) Receptor Binding in Rat Brain Synaptic Membrane Fractions. *Brain Res.* **1975**, *100*, 81-97.

(20) Phillis, J. W.; Wu, P. H.; Bender, A. S. Inhibition of Adenosine Uptake in Rat Brain Synaptosomes by the Benzodiazepines. *Gen. Pharmacol.* **1981**, *12*, 67-70.

Table 1. Selected Data for Compounds **4** and **12-14** [a]

Compound	Isolated yield (%)	mp, °C (recrys. solv.)	^{1}H NMR ($CDCl_3$, δ)	^{13}C NMR ($CDCl_3$, δ)	IR[b] (C=O, cm^{-1})
4	67	151-152 (EtoAc/hexane)	7.6-7.3 (m, 5H, Ph), 6.2 (bs, 1H, NH), 4.0-3.6 (m, 2H, NCH_2), 2.6-2.5 (m, 1H, CH_2), 2.4-1.2 (m, 7H, CH_2)	24.6, 33.4, 41.5, 45.6, 67.5, 126.1, 128.4, 135.9, 159.7, 179.6	1705, 1765
12	50	164-166 (EtoAc)	7.0 (bs, 1H, NH), 3.9 (t, 1h, CHCN), 3.5-3.1 (m, 2H, NCH_2), 2.2-2.0 (m, 2H, CH_2), 1.8-1.4 (m, 6H, CH_2)	24.2, 24.3, 31.7, 33.5, 34.0, 42.3, 76.6, 77.0, 77.4, 118.0, 169.3	1670 (2270, CN)
13	100	oil[c]	7.6-7.3 (m, 5H, Ph), 6.3 (bs, 1H, NH), 3.5-3.1 (m, 2H, NCH_2), 2.9-2.3 (m, 2H, CH_2CPh), 2.2-1.4 (m, 6H, CH_2)	22.0, 23.0, 30.0, 38.9, 40.4, 54.5, 120.3, 126.5, 128.7, 129.0, 129.3, 171.4	1655 (2270, CN)
14[d]	91	121-123 (EtoAc/hexane)	7.4-7.2 (m, 6H, Ph + NH), 6.0-5.7 (m, 2H, NH_2), 3.2-2.6 (m, 2H, NCH_2), 2.6-2.4 (m, 1H, CH_2), 2.1-1.3 (m, 7H, CH_2)	23.5, 23.8, 30.0, 37.7, 62.1, 126.3, 127.1, 127.6, 140.5, 172.8, 176.3	1620-1680 (broad)

[a]All compounds were also analyzed by (1) GC/MS (EI, 70 ev), giving one peak in the GC and the expected molecular ion peak; (2) elemental analyses for C,H,N (within ± 0.3% of calculated values, except for **13**; see footnote c). [b]Compounds **12** and **14** were recorded in KBr; compound **4** was recorded in mineral oil; compound **13** was recorded as a thin film. [c]Purified by flash chromatography on silica ($CHCl_3$): R_f 0.51 (silica; 5% MeOH/$CHCl_3$). Anal. ($C_{14}H_{16}N_2O \cdot 3/4\ H_2O$) C, N; H: calc'd, 7.29; found: 6.61. [d]^{13}C NMR recorded at 100 °C in d_6-DMSO due to upfield peak broadening at room temperature.

Table 2. Sodium Channel-Binding and Anticonvulsant Activities

Compound	log P[b]	Na^+ channel IC_{50} (μM)	anticonvulsant (mice IP) phase I (Best Activity, mg/kg)[a] MES	scMet	Rotorod	phase II Time (h)	MES ED_{50} (mg/kg)	Rotorod TD_{50} (mg/kg)
1[c]	2.65	380	>300	300 (1/1)	>300			
2[c]	3.05	160	100 (3/3)[d]	100 (1/1)	100 (8/8)	0.25	66 [51-84][e]	147 [93-226]
3	2.01	700	100 (3/3)	100 (3/4)	300 (4/4)			
4	2.51	427[f] {376-484}[g]	100 (3/3)	>300	300 (4/4)	0.25	86 [68-96]	124 [107-149]
5[c]	2.65	500	300 (1/1)	30 (1/1)	300 (1/4)	0.5	124 [104-139]	504 [437-558]
6[h]	1.96	162 {136-193}	30 (1/1)	100 (4/4)	100 (4/4)	1.0	25 [22-28]	85 [80-90]
7	2.46	103 {85-124}						
8	2.96	39 {32-47}						

Table 2. (Continued)

9	3.01	285 {232-350}						
14		i	100 (1/3)	300 (4/4)	300 (4/4)			
DPH[j]	2.46[k]	40[l]				2.0	10 [8-10]	66 [52-72]
TMD[m]	-0.37[n]	>1000[l]				1.0	627 [538-705]	819 [652-1096]

[a]Concentration of test compound used in assay. All anticonvulsant and toxicity assays were performed 30 min. after test compound administration. [b]Calculated using parent structure log *P* values in ref 13 and π values for substituents in ref 14 (see Results and Discussion). [c]Data taken from ref 5.

[d]Number of animals protected or toxic / number tested. [e]Numbers in brackets are 95% confidence intervals. [f]Other in vitro mechanism-related assays were performed for **4** in phase Va: (1) benzodiazepine receptor (ligand = [^{3}H]flunitrazepam at 10 nM; tissue = mouse whole brain P_2 pellet): no inhibition up to 100 μM **4**. (2) GABA receptor (ligand = [^{3}H]GABA at 50 nM; tissue = mouse whole brain P_2 pellet): no inhibition up to 10 μM **4**. (3) adenosine uptake (ligand = [^{3}H]adenosine at 1 μM; tissue = mouse whole brain synaptosomes): no inhibition up to 100 μM **4**. [g]Range describing -1 to +1 standard deviation. [h]Anticonvulsant data taken from ref 7. The sodium channel value was determined in the present study. [i]33% inhibition at 500 μM. [j]Anticonvulsant data taken from ref 15. [k]Log *P* taken from ref 13. [l]References 3 and 4. [m]TMD = trimethadione. Anticonvulsant data taken from ref 15. [n]Log *P* taken from ref 14.

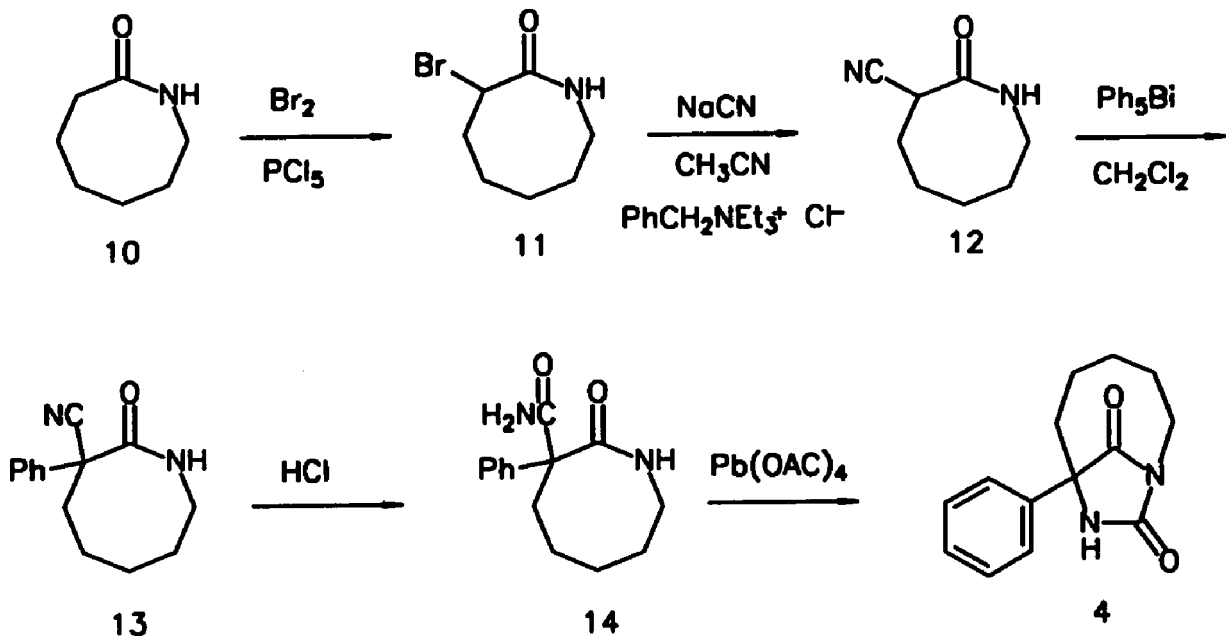

Figure 1. Structures for the cyclic imide anticonvulsants discussed in this study.

Scheme 1.

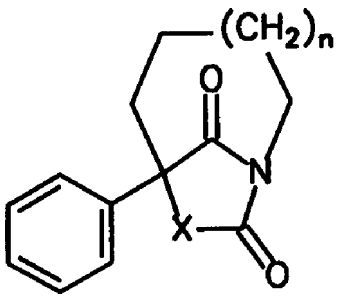

	n	X
1	1	O
2	2	O
3	1	NH
4	2	NH

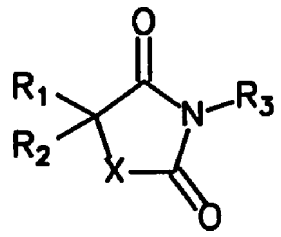

	X	R_1	R_2	R_3
trimethadione	O	CH_3	CH_3	CH_3
phenytoin	NH	Ph	Ph	H
5	O	Ph	C_2H_5	CH_3
6	NH	Ph	$n-C_3H_7$	H
7	NH	Ph	$n-C_4H_9$	H
8	NH	Ph	$n-C_5H_{11}$	H
9	NH	Ph	$n-C_4H_9$	CH_3

Table 3. Analytical Data

		calculated (%)			found (%)		
Compound	Formula	C	H	N	C	H	N
4	$C_{14}H_{16}N_2O_2$	68.83	6.60	11.47	68.75	6.61	11.52
12	$C_7H_{12}N_2O$	63.11	7.95	18.41	63.02	7.98	18.31
13[a]	$C_{14}H_{16}N_2O \cdot 3/4\ H_2O$	69.54	7.29	11.58	69.65	6.61	11.54
14	$C_{14}H_{18}N_2O_2$	68.27	7.37	11.37	68.28	7.39	11.32

[a]While intermediate **13** never provided a satisfactory elemental analysis, both the ^1H (300 MHz) and ^{13}C NMR spectra were fully assigned and revealed no impurity peaks. Compound **13** also gave only one GC peak in the GC/MS, which provided the correct molecular ion (ei, 70 ev). Intermediate **13** was successfully carried on to **14**, which yielded a satisfactory elemental analysis.

HYDANTOINS WITH CONFORMATIONALLY RESTRICTED PHENYL RINGS. EFFECTS ON SODIUM CHANNEL BINDING

MILTON L. BROWN[†], GEORGE B. BROWN[‡], AND WAYNE J. BROUILLETTE[*]

†

Department of Chemistry and Department of Psychiatry
and Behavioral Neurobiology,
University of Alabama at Birmingham, Birmingham, Alabama 35294

---

[*]Address correspondence to this author
[†]Department of Chemistry
[‡]Department of Psychiatry and Behavioral Neurobiology

Abstract

In this study, we investigated the effects of log *P* and 5-phenyl ring orientation on the binding of twelve 5-phenylhydantoins to the neuronal voltage-dependent sodium channel (NVSC). Log *P* and in vitro sodium channel-binding (log IC_{50}) for the hydantoins **1-12** and DPH were correlated by linear regressions analysis (r^2 = 0.638). The correlation, which accounts for approximately 64% of the binding effects, suggests that simple partitioning into the lipid phase is not sufficient to explain the effects hydantoins on the NVSC. NVSC binding affinities for three new hydantoins **4-6**, which are lipophilic isomers having varied phenyl ring orientations, were compared. These studies suggest that the correct 5-phenyl orientation is important for hydantoin binding to the sodium channel and the results are thus consistent with a property associated with specific ligand-receptor interactions. These studies also suggest that the preferred N1,C5,C6,C7 torsion angle range for efficient sodium channel-binding activity, given a suitable log *P* value, is from -15 to 15°.

The neuronal voltage-sensitive sodium channel (NVSC) can be described as a transmembrane protein complex[1] involved in generating electrical signals via action potentials in neurons and other excitable cells. [2, 3, 4] Action potentials consist of three phases: (1) depolarization caused by the rapid entry (0.5 ms) of sodium into the cell; (2) calcium (a secondary messenger) entrance into the cell; and (3) potassium movement out of the cell (2.0 ms), repolarizing the cell and setting the resting membrane potential (-60 mV).[5]

The biphasic behavior of depolarization and repolarization controls NVSC function and results from two separable gating processes termed activation and inactivation.[1, 6] Activation controls the rate and voltage dependence of the increase in sodium concentration following depolarization. Inactivation is involved in controlling the rate and voltage dependence of positive potential returning to negative potential as the voltage-activated sodium channel restores to the resting level during maintained depolarization.

The structural morphology of neuronal sodium channels has been found to be species and tissue dependent. For example, NVSC from eel electroplax consist of only a single α subunit.[7] However, sodium channels from rat brain contain three polypeptides; (1) a 260 kilodalton (kDa) α-subunit, (2) a 36 kDa β_1-subunit and (3) a 33 kDa β_2-subunit,[1, 5, 8] with the α subunit independently sufficient for functional expression.[5] Furthermore, sodium channels found in neurons have different pharmacological and physiological properties than those in skeletal muscle or cardiac cells.

NVSC subtypes from many species have been cloned, and amino acid sequences have been determined for examples from rat and human brain and skeletal and cardiac tissue.[4] Four NVSC isoforms from rat brain have been designated as type I, II, and IIA and III,[10] with each containing six α-helical transmembrane segments.[1] The NVSC has also demonstrated specific binding to neurotoxins, for which at least seven neurotoxin sites have been distinguished.[4, 10,11] Grayanotoxin and the alkaloids veratridine, batrachotoxin and aconitine inhibit

receptor site 2 and cause persistent activation of the sodium channel. A batrachotoxin derivative, ^{3}H-batrachotoxinin A 20-α-benzoate ([^{3}H]-BTX-B),[12-14] has been useful as a probe in evaluating the relative potencies of compounds binding to the NVSC in vitro. For example, allosteric inhibition of [^{3}H]-BTX-B binding by the anti-MES anticonvulsant diphenylhydantoin (phenytoin or DPH)[15] at therapeutic concentrations (40 μM) implicates the NVSC as an anticonvulsant target site.[16] Other classes of drugs also interact with the NVSC, including the local anesthetics and antiarrhythmics. These agents have demonstrated overlapping pharmalogical activities, illustrated by the antiarrhythmic properties exhibited by the anticonvulsant DPH and the local anesthetic lidocaine. Thus proposals for one-site[17] and two-site[18] models provide controversy concerning whether anticonvulsants, local anesthetics and antiarrhythmics act at either the same or different sites on the NVSC.

Interconversions between NVSC states may be important in considering the modes of action of these drugs. The NVSC has three main states: resting, opened and inactivated, and the distribution of channels among these states is a function of membrane potential and time.[19, 20] Compounds that bind to the NVSC may, because of changes in access or interconversion rates, have different binding affinities to the resting, opened or inactivated state of the sodium channel. This provides one possible explanation for the differences in binding and therapeutic profiles among anticonvulsants, local anesthetics and antiarrythmics.[21, 22] DPH binds to the inactivated state of the NVSC in a voltage- and frequency-dependent

manner,[23] providing an explanation for its selective effects on hyperactive versus normal neurons.

Examination of membrane effects for DPH using fluorescent fatty acid probes[24] implied that DPH may exert an inhibitory effect on the NVSC by simple partitioning of its two phenyl rings into the lipid bilayer. However, DPH exhibits saturable binding to the NVSC, which is associated with properties of specific receptor-ligand interactions.[25] Studies[18] also indicate that sodium channel blockade by DPH is affected by changes in intracellular, but not extracellular, pH, consistent with intracellular actions.

Studies have reported the effects of log *P*[26] and 5-phenyl ring orientation[27] on whole animal anticonvulsant activity. Our previous investigations demonstrated that log *P*[28] and 5-phenyl ring orientation[29] may be important for the efficient binding of hydantoins to the NVSC. Here we carefully evaluate the effects of log *P* and NVSC binding for a structurally diverse group of hydantoins **1-12** (Figure 1), which possess a range of log *P* values. Within this group, we also make comparisons between structural isomers that evaluate effects of 5-phenyl ring orientation while maintaining a constant log *P*.

Methods

Biological Data. All compounds **1-12** were evaluated for relative binding to the NVSC (Table 1) in an in vitro assay using rat cerebral cortex synaptoneurosomes. Results are expressed as log IC_{50}, where IC_{50} represents the

micromolar concentration of compound required to allosterically inhibit the specific binding of [^{3}H]-BTX-B by 50%.

Conformational Analysis. All compounds were energy minimized with the Tripos force field[30] using default bond distances and angles and neglecting electrostatics. While all compounds were synthesized and evaluated as racemic mixtures, the geometries of **1-12** were modeled in SYBYL using only the *R*-configuration at C5. Conformational searching was utilized to determine the energetically reasonable range of torsion angles (N1,C5,C6,C7) for rotation of the phenyl ring relative to the hydantoin ring. For **1-7** we performed, within the SYBYL/GRIDSEARCH routine, conformational searches of torsion angle N1,C5,C6,C7 rotated through 360° in 1° increments. For analogs **1-3**, **5** and **6**, all conformations from 0 to 180° are accessible within 2 kcal/mol from the lowest energy minimum. In contrast, GRIDSEARCHes on compounds **4** revealed higher rotational energy barriers, and a range of phenyl ring conformers within 2.0 kcal/mol of the lowest energy minimum is reported (Table 1). For example, accessible conformations of analog **4** were contained within two separate ranges and the two low energy minima positioned the ortho-methyl group either above [**4**(a)] or below [**4**(b)] the plane of the phenyl ring. Different conformations of **7** place the N-ethyl group bent above [**7**(a)] and below [**7**(b)] the plane of the hydantoin ring. For DPH the conformation of the x-ray crystal structure[31] was used.

Conformational searches on rotationally restricted 5-phenyl analogs **8-12** were performed within the SYBYL/SYSTEMATIC SEARCH routine. All local low

energy conformers within 2 kcal/mol of the lowest energy minimum are reported (Table 1). Multiple minima for each analog are listed in Table 2.

Chemistry

The syntheses of analogs **1-3**,[28] **7**,[29] **8**,[32] **9**,[29] **10-11**[33] and **12**[29] were previously described. To obtain hydantoin **11**,[33] benzocylooctenone[34] was prepared by literature methods, followed by conversion to hydantoin **11** in 30% yield via synthetic Method B (see Experimental Section). New hydantoins **4**, **5**, and **6** were also prepared by the Bucherer-Berg[35] procedure from the appropriate ketones[36] in 20%, 56% and 60% yields, respectively. The required ketones were synthesized using Grignard reactions of o, m and p-tolylnitrile and butylmagnesium bromide.

Results and Discussion

The neuronal voltage-sensitive sodium channel (NVSC) is a site of action for the anticonvulsant diphenylhydantoin (DPH), one of the most widely used agents for the treatment of generalized seizures. Unfortunately, the exact location and nature of this site has not yet been determined. We have been interested in investigating structure-activity relationships for the interactions of hydantoins with the NVSC in order to define structural features that give rise to efficient binding.[28,29] This approach may lead to new anticonvulsants with enhanced activity.

Previous investigations suggested that log *P* is important for anticonvulsant activity,[26] and our preliminary studies suggested that both log *P* and phenyl ring orientation may be important for in vitro binding to the NVSC.[28,29] In the present

study we have selected hydantoin analogs (Figure 1), which permit further evaluations for both of these properties in a relatively independent fashion.

We conveniently estimated log *P* values for new compounds, as we did in an earlier study,[28] by the addition of π values to the experimentally determined log *P* of a parent structure. We thus estimated the log *P* values in Table 1 for compounds **4-12** (the others were taken from ref 8) by adding the appropiate π values for substituents at C5 and N1 to the log P for 5-phenylhydantoin (0.46)[26] to provide the final log *P*. The π values used were 0.50 for each CH_2 or CH_3 in the alkyl chain at C5 and 0.56 for an N-CH_3 substituent.[37] For example, the log *P* for hydantoin **7** was calculated as the log $P_{parent} + \pi_{5\text{-Methyl}} + \pi_{N1\text{-Methylene}} + \pi_{Methyl}$ = 0.46 + 0.50 + 0.56 + 0.50 = 2.02. Since the ring closure of **7** provides the bicyclic hydantoin **12**, the log *P* of **12** was calculated as log $P_7 + \pi_{ring\ closure}$ = 2.02 + (-0.50) = 1.52.

We previously observed that structurally similar 5-alkyl-5-phenylhydantoin homologs **1-3** demonstrated enhanced binding to the NVSC with increases in log *P*.[28] However, as shown in Table 1, log *P* is not the only important variable. Comparisons of structurally dissimilar hydantoins with the same log *P* (e.g., **1** vs. **10**, **2** vs **11**, **9** vs **12**) demonstrate that, in addition to log *P*, structural features influence the potency of binding to the NVSC. This is further supported by the observation that compounds **2** and **11**, which have log *P* values equivalent to DPH, do not exhibit comparable binding potencies. The correlation of log *P* versus sodium channel-binding (log IC_{50}) for **1-12** and DPH (Figure 2) reveals a model that explains only about 64% of the binding effects. This result indicates that simple

nonspecific partitioning of hydantoins into the membrane lipid phase, which has been suggested by others as a possible mechanism for the effect of DPH on the NVSC,[24] is not sufficient for potent inhibition.

A preliminary study that compared the NVSC binding of **1** vs **9** and **7** vs **12** suggested that 5-phenyl orientation may be important for the in vitro binding of hydantoins to the NVSC.[29] To investigate the effects of 5-phenyl orientation, independent from the effects of log *P*, we designed, synthesized and evaluated NVSC binding for new hydantoins **4-6**, and we also prepared and evaluated known spirohydantoins **8-11** and tricyclic hydantoin **12**. Compounds **4** and **8-12** all contain phenyl rings with more restrictive energetically favorable rotameric conformations as compared to **1-3**, **5**, and **6**. Compounds **5** and **6** serve as isomeric models of **4** that do not experience significant changes in phenyl ring conformational accessibility as compared to **1-3**.

To assign limits to the 5-phenyl range important for tight binding, we measured the torsion angle N1,C5,C6,C7 for **1-12** (Table 1) using molecular modeling. The torsion angles and ranges were calculated for **1-7** using the conformational searching routine GRIDSEARCH within SYBYL (Tripos Inc., St. Louis, MO 63144). Accessible conformations for hydantoins **1-7** were reported as a range of conformers within 2 kcal/mol of the lowest energy minima. For restricted hydantoins **8-12**, torsional ranges were calculated for conformers within 2 kcal/mol of each low energy minimum. The procedure consisted of removing the bond connecting the alkyl side chain to the phenyl ring, rotating the N1,C5,C6,C7 torsion

angle by 5° and reconnecting the bond. Holding N1,C5,C6,C7 constant (by creating an aggregate of the N1, C5, C6, C7 atoms), the aggregate conformer was energy minimized. This was done in each direction (+ and - away from each local minimum) until reaching a conformation whose energy was 2 kcal/mole greater than the starting minimum. The torsion angle range was thus reported as the range (including the extreme conformers) obtained from these aggregate searches (Table 1).

As illustrated in Tables 1 and 2, compounds **8-11** represent a homologous series of spirohydantoins that contain phenyl rings that are conformationally restricted about N1, C5, C6, C7 due to a 5-alkyl side chain that is covalently bound to the *ortho* position of the 5-phenyl ring. Thus the range of accessible torsion angles defining the 5-phenyl conformations increases for larger ring sizes. One notes in Table 1 that the sodium channel-binding activity increases from **8-10**, with no further increase in activity for **11**. This trend is consistent with the inability of the 5-phenyl substituent of the smaller ring systems to adopt a preferred conformation. Unfortunately, increases in log *P* through this series also correlate with increased binding activity, with the exception that compound **11**, which exhibits a larger log *P* than **10**, does not exhibit a corresponding increase in sodium channel-binding activity. A comparison between hydantoins with identical log *P* values from the spiro series (**8-11**) and the least restricted series (**1-3**) reveals that **1** exhibits roughly the same IC_{50} as **10**, and that **2** exhibits roughly the same IC_{50} as **11**, suggesting that **10** and **11** can each adopt an optimum phenyl ring orientation.

To further pursue this question, we prepared and evaluated the constant log *P* series **4-6**. These compounds were chosen to have the same log *P* value (2.96) as the most potent compound in this study, hydantoin **3**. In this series the *o*-methyl group of **4** restricts phenyl ring orientation as compared to isomers **3**, **5**, and **6**. Interestingly, compounds **3**, **5**, and **6** all exhibit potent binding to the NVSC as compared to compound **4** (Table 1). This suggests that compound **4** can not significantly populate the phenyl ring conformation required for optimum sodium channel-binding activity.

Subtracting the N1,C5,C6,C7 torsion angle ranges of poor sodium channel binders (i.e. rigid analogs **4**, **8**, **9**) from 0 to 360°, we suggest -15 to 15° as a preferred N1,C5,C6,C7 torsion angle range for efficient sodium channel-binding activity, given a suitable log *P* value. The lowest energy conformation for active compounds **1-3, 5-6**, and **10-12** placed the N1,C5,C6,C7 torsion angle within this range and near the x-ray conformation of DPH.

In conclusion, log *P* is clearly an important parameter for the potent binding of hydantoins to the NVSC. This may result from the necessity of hydantoins to enter or cross the cell membrane prior to interaction with the channel protein. However, the above studies, which compare structurally diverse hydantoins with identical log *P*, suggest that hydantoins also bind specifically to a site on the NVSC. Furthermore, these results provide evidence for a preferred phenyl ring orientation that gives rise to the optimum binding of 5-phenylhydantoins to this site.

Experimental Section

Melting points were recorded on an Electrothermal melting point apparatus and are uncorrected. IR spectra were recorded on a Beckman Acculab 6 and Nicolet IR/42 spectrometers, and elemental analyses were performed by Atlantic Microlabs of Norcross, GA. ^{1}H NMR and ^{13}C NMR were recorded on GE (NT series) and Bruker (ARX series) NMR spectrometers operating at 300.1 MHz (for ^{1}H). The spectra were obtained in d^{6}-DMSO for hydantoins and $CDCl_3$ for all other compounds at ambient temperature and referenced internally to tetramethylsilane (TMS). The GC/MS were performed on a Hewlett Packard 5885 GC/MS. Statistics calculations and graphics drawings were performed with SigmaStat 1.02a and Sigma Plot 1.0 for Windows (Jandel, Inc.), respectively.

[^{3}H]-Batrachotoxinin A 20-α-benzoate ([^{3}H]-BTX-B) with a specific activity of 30 Ci/mol was obtained from New England Nuclear (Boston, MA).

Method A. To a stirring solution of 50% ethanol were added ketone (0.66 mol/L), KCN (1.33 mol/L) and $(NH_4)_2CO_3$ (2.66 mol/L). The solution was warmed to 50-65 °C for 12 h. After cooling to room temperature, the hydantoin precipitate was filtered and the filtrate was acidified (pH 2) by the addition of concentrated Hcl to give more precipitate, which was filtered again. The filtrate was made basic, adjusted to pH = 8 using KOH (3%), concentrated to half-volume, and the hydantion product that precipitated was filtered. The solids were combined and recrystallized from hot ethanol to give the final product.

Method B. To a solution of 50% ethanol contained in a 300 mL Parr Pressure apparatus were added ketone (0.7 mol/L), KCN (1.3 mol/L) and $(NH_4)_2CO_3$ (2.7 mol/L). The solution was heated at 125 °C for 24 h, and the apparatus cooled to room temperature. The hydantoin precipitate was filtered and the filtrate acidified (pH 2) by the addition of concentrated HCl under a hood. The filtrate was adjusted to pH 2, concentrated to half-volume, cooled and the hydantoin filtered. The crude solids were combined and recrystallized in hot ethanol to give the final hydantoin product.

Method C. Ketone and trimethylsilylcyanide (TMSCN) were combined without solvent in a 1:2 molar ratio under anhydrous conditions, and ZnI_2 (5-10 mg) was added as a catalyst. This mixture was stirred at room temperature under a nitrogen atmosphere for 12 h. The reaction was monitored by the disappearance of the C=O stretching peak (1670 cm^{-1}) in the IR spectrum of the reaction mixture. The TMS ether was not purified but was directly hydrolyzed to the cyanohydrin by dissolving the TMS ether in equal amounts of ether and 15% HCl, and stirring vigorously at room temperature for 1 h. The acidic layer was washed three times with ether. The ether extracts were combined and evaporated to give cyanohydrin in 100% yield [IR (neat) 3400 (OH), 2250 (CN) cm^{-1}]. The cyanohydrin was converted to hydantoin[35, 38] by dissolving cyanohydrin and $(NH_4)_2CO_3$ in a 1:2 molar mixture in 50% ethanol while stirring under a N_2 atmosphere. The mixture was then heated at 55-65 °C for 12 h. The reaction mixture was adjusted to pH = 8 by the addition of KOH (3%), concentrated to half-volume, and the hydantoin product was

filtered. The crude solid was recrystallized from hot ethanol to give the final hydantoin product.

5-Butyl-5-(2-methylphenyl)hydantoin (4). To a solution of 50% ethanol (80 mL) contained in a 300 mL Parr Pressure apparatus were added 1-(2-methylphenyl)pentanone (1.5 g, 8.5 mmole), KCN (1.1 g, 17.0 mmole) and $(NH_4)_2CO_3$ (3.9 g, 34.0 mmole). The solution was heated at 125 °C for 24 h, and the apparatus was cooled to room temperature. The precipitate was filtered and the filtrate was acidified (pH 2) by the addition of concentrated HCl. The filtrate was made basic (pH 8) using KOH (3%), concentrated to half-volume, cooled in an ice bath and filtered again. The combined solids were recrystallized from hot ethanol to give pure **4** (0.50 g, 20% yield): m.p. 144-145 °C; IR (KBr) 1700, 1760 (C=O), 3200 (NH) cm^{-1}.

5-Butyl-5-(3-methylphenyl)hydantoin (5). To a stirring solution of 50% ethanol (30 mL) were added 1-(3-methylphenyl)pentanone (3.2 g, 18.2 mmole), KCN (2.4 g, 36.4 mmole) and $(NH_4)_2CO_3$ (8.3 g, 73.0 mmole). The solution was warmed to 50-60 °C for 48 h. After cooling to room temperature, the precipitate was filtered and the filtrate was acidified (pH 2) by the addition of concentrated HCl. The filtrate was made basic (pH 8) by KOH (3%), concentrated to half-volume and filtered again. The combined solids were recrystallized from hot ethanol to give pure **5** (2.5 g, 56% yield): m.p. 162-164 °C; IR (KBr) 1705, 1750 (C=O), 3200 (NH) cm^{-1}.

5-Butyl-5-(4-methylphenyl)hydantoin (6). To a stirring solution of 50% ethanol (30 mL) were added 1-(4-methylphenyl)pentanone (2.6 g, 14.7 mmole), KCN (1.9 g, 29.5 mmole) and $(NH_4)_2CO_3$ (6.7 g, 59.0 mmole). The solution was warmed to 50-60 °C for 48 h. After cooling to room temperature, the precipitate was filtered and the filtrate was acidified (pH 2) by the addition of concentrated HCl. The mother liquor was made basic (pH 8) by KOH (3%), concentrated to half-volume and filtered again. The combined solids were recrystallized from hot ethanol to give pure **6** (2.1 g, 60% yield): m.p. 158-160 °C; IR (KBr) 1700, 1710 (C=O), 3200 (NH) cm^{-1}.

Sodium Channel-Binding Assay. We previously reported the details of this procedure.[39] Briefly, synaptoneurosomes (~1 mg of protein) from rat cerebral cortex were incubated for 40 min at 25 °C with the test compound (seven different concentrations spanning the IC_{50}) in a total volume of 320 μL containing 10 nM [^{3}H]BTX-B and 50 μg/mL of scorpion venom. Incubations were terminated by dilution with ice cold buffer and filtration through a Whatman GF/C filter paper, and the filters were washed four times with ice cold buffer. Filters were counted in a Beckmann scintillation counter. Specific binding was determined by subtracting the nonspecific binding, which was measured in the presence of 300 μM veratridine, from the total binding of [^{3}H]BTX-B. All experiments were performed in triplicate and included a control tube containing 40 μM DPH. The IC_{50} values were determined from a Probit analysis of the dose-response curve and excluded doses producing less than 10% or greater than 90% inhibition.

Acknowledgments

This work was taken in part from the PhD dissertation submitted in partial fulfillment of the requirements for the PhD degree in Organic Chemistry by M.L.B. M.L.B gratefully acknowledges financial support from the Patricia Robert Harris Fellowship, the National Consortium for Educational Access, the UAB Comprehensive Minority Faculty Development Program and the UAB Department of Chemistry. We also thank Ms. Bereaval Webb, a 1993 Alabama Alliance for Minority Participation (AMP) Summer Intern, for technical support.

References

(1) Catterall, W. A. Cellular and Molecular Biology of Voltage-Gated Sodium Channels. *Physiological Rev.* **1992**, *72*, S15-S48.

(2) Kirsch, G. E. Na^+ Channels: Structure, Function, and Classification. *Drug Dev. Res.* **1994**, *33*, 263-276.

(3) Catterall, W. A. Molecular Mechanisms of Inactivation and Modulation of Sodium Channels. *Renal Physiol. Biochem.* **1994**, *17*, 121-125.

(4) Kallen, R. G.; Cohen, S. A.; Barchi, R. L. Structure, Function and Expression of Voltage-Dependent Sodium Channels. *Mol. Neurobiology.* **1993**, *7*, 383-428.

(5) Catterall, W. A. Structure and Function of Voltage-Sensitive Ion Channels. *Science.* **1988**, *242*, 50-61.

(6) Armstrong, C. M. Voltage-Dependent Ion Channels and Their Gating. *Physiological Rev.* **1992**, *72*, S5-S13.

(7) Noda, M.; Shimizu, S.; Tanabe, T.; Takai, T.; Kayano, T.; Ikeda, T.; Takahashi, H.; Nakayama, H.; Kanaoka, Y.; Minamino, N.; Kangawa, K.; Matsu, H.; Raftery, M. A.; Hirose, T.; Inayama, S.; Hayashida, H.; Miyata, T.; Numa, S. Primary Structure of *Electrophorus-Electricus* Sodium Channel Deduced from Complementary DNA Sequence. *Nature.* **1984**, *312*, 121-127.

(8) Scheuer, T.; Auld, V. J.; Boyd, S.; Offord, J.; Dunn, R.; Catterall, W. A. Functional Properties of Rat Brain Sodium Channels Expressed in a Somatic Cell Line. *Science.* **1990**, *247*, 854-858.

(9) Black, J. A.; Westenbroek, R.; Ransom, B. R.; Catterall, W. A.; Waxman, S.G. Type II Sodium Channels in Spinal Cord Astrocytes In Situ: Immunocytochemical Observations. *Glia.* **1994**, *12*, 219-227.

(10) Isom, L. L.; Scheuer, T.; Brownstein, A. B.; Ragsdale, D. S.; Murphy, B. J.; Catterall, W. A. Functional Co-Expression of the β1 and Type IIA α Subunits of Sodium Channels in a Mammalian Cell Line. *J. Biol. Chem.* **1995**, *270*, 3306-3312.

(11) Fainzilber, M.; Kofman, O.; Zlotkin, E.; Gordon, D. A New Neurotoxin Receptor Site on Sodium Channels is Identified by a Conotoxin that Affects Sodium Channel Inactivation in Molluscs and Acts as an Antagonist in Rat Brain. *J. Biol. Chem.* **1994**, *269*, 2574-2580.

(12) Catterall, W. A.; Morrow, C. S.; Daly, J. W.; Brown, G. B. Binding of Batrachotoxinin A 20-α-Benzoate to a Receptor Site Associated with Sodium Channels in Synaptic Nerve Ending Particles. *J. Biol. Chem.* **1981**, *10*, 8922-8927.

(13) Brown, G. B.; Tieszen, S. C.; Daly, J. W.; Warnick, J. E.; Albuquerque, E. X. Batrachotoxin-A 20-α-Benzoate: A New Radioactive Ligand for Voltage-Sensitive Sodium Channels. *Cell Mol. Neurobiol.* **1981**, *1*, 19-40.

(14) Brown, G. B. Batrachotoxin: A Window on the Allosteric Nature of the Voltage-Sensitive Sodium Channel. *Int. Rev. Neurobiol.* **1988**, *29*, 7-116.

(15) Willow, M.; Catterall, W. A. Inhibition of Binding of [^{3}H]Batrachotoxinin A 20-α-Benzoate to Sodium Channels by the Anticonvulsant Drugs Diphenylhydantoin and Carbamazepine. *Mol. Pharmacol.* **1982**, *22*, 627-635.

(16) Catterall, W. A. Common Modes of Drug Action on Na^+ Channels: Local Anesthetics, Antiarrhythmics and Anticonvulsants. *TIPS.* **1987**, *8*, 57-65.

(17) Zimányi, I.; Weiss, S. R. B.; Lajtha, A.; Post, R. M.; Reith, M. E. A. Evidence for a Common Site of Action of Lidocaine and Carbamazepine in

Voltage-Dependent Sodium Channels. *Eur. J. Pharmacol.* **1989**, *167*, 419-422.

(18) Barber, M. J.; Starmer, C. F.; Grant, A. O. Blockade of Cardiac Sodium Channels by Amitriptyline and Diphenylhydantoin, Evidence for Two Use-Dependent Binding Sites. *Circulation Research.* **1991**, *69*, 677-696.

(19) Koumi, S.; Sato, R; Katori, R.; Hisatome, I.; Nagasawa, K.; Hayakawa, H. Sodium Channel States Control Binding and Unbinding Behavior of Antiarrhythmic Drugs in Cardiac Myocytes for the Guinea Pig. *Cardiovascular Res.* **1993**, *26*, 1199-1205.

(20) Courtney, K. R.; Etter, E. F. Modulated Anticonvulsant Block of Sodium Channels in Nerve and Muscle. *Eur. J. Pharm.* **1983**, *88*, 1-9.

(21) Catterall, W. A. Inhibition of Voltage-Sensitive Sodium Channels in Neuroblastoma Cells by Antiarryhthmics Drugs. *Mol. Pharmacol.* **1981**, *20*, 356-362.

(22) Catterall, W. A. Inhibition of Voltage-Sensitive Sodium Channels in Neuroblastoma Cells and Synaptosomes by the Anticonvulsant Drug Diphenylhydantoin and Carbamazepine. *Mol. Pharmacol.* **1984**, *25*, 228-234.

(23) Catterall, W. A. Voltage Clamp Analysis of the Inhibitory Actions of Diphenylhydantoin and Carbamazepine on Voltage-Sensitive Sodium Channels in Neuroblastoma Cells. *Mol. Pharmacol.* **1985**, *27*, 549-558.

(24) Harris, W. E.; Stahl, W. L. Interactions of Phenytoin with Rat Brain Synaptosomes Examined by Flourescent Fatty Acid Probes. *Neurochem. Int.* **1988**, *13*, 369-377.

(25) Francis, J.; Burnham, W. M. [^{3}H]Phenytoin Identifies a Novel Anticonvulsant-Binding Domain on Voltage-Dependent Sodium Channels. *Mol. Pharmacol.* **1992**, *42*, 1097-1103.

(26) Lien, E. Structure-Activity Correlations for Anticonvulsant Drugs. *J. Med. Chem.* **1970**, *13* ,1189-1191.

(27) Wong, M. G.; Defina, J. A.; Andrews, P. R. Conformational Analysis of Clinically Active Anticonvulsant Drugs. *J. Med. Chem.* **1986**, *29*, 562-572.

(28) Brouillette, W. J.; Jestkov, V. P; Brown, M. L.; Aktar, M. S.; Delorey, T. M.; Brown, G. B. Bicyclic Hydantoins with Bridgehead Nitrogen. Comparison of

Anticonvulsant Activities with Binding to the Neuronal Voltage-Dependent Sodium Channel. *J. Med. Chem.* **1994**, *37*, 3289-3293.

(29) Brouillette, W. J; Brown, G. B.; Delorey, T. M; Liang, G. Sodium Channel Binding and Anticonvulsant Activities of Hydantoins Containing Conformationally Constrained 5-Phenyl Substituents. *J. Pharm. Sci.* **1990**, *79*, 871-874.

(30) Vinter, J. G.; Davis, A.; Saunder, M. R. Strategic Approaches to Drug Design. 1. An Integrated Software Framework for Molecular Modeling. *J. Computer-Aided Molecular Design.* **1987**, *1*, 31-55.

(31) Camerman, A.; Camerman, N. The Stereochemical Basis of Anticonvulsant Drug Action. I. The Crystal and Molecular Structure of Diphenylhydantoin, a Noncentrosymmetric Structure Solved by Centric Symbolic Addition. *Acta Cryst.* **1971**, *B27*, 2205-2211.

(32) Sarges, R.; Schnur, R. C.; Belletire, J. L.; Peterson, M. J. Spiro Hydantoin Aldose Reductase Inhibitors. *J. Med. Chem.* **1988**, *31*, 230-243.

(33) Huisgen, R.; Ugi, I. Polycyclische Systeme mit Heteroatomen. *Liebigs Ann. Chem.* **1957**, *610*, 57-66.

(34) Huisgen, R; Rapp, W. I. Mitteil.: 1,2-Benzo-cycloocten-(1)-on-(3)*. *Chem. Ber.* **1952**, *85*, 826-835.

(35) Novelli, A.; Lugones, Z. M.; Velasco, P.; Hydantoins III. Chemical Constitution and Hypnotic Action. *Anales Asoc. Quim Argentina.* **1942**, *30*, 225-231.

(36) Cazes, B; Julia, S. Rèarrangements Sigmatropiques [2.3] en Sèrie Benzylique; Prèparation de Cetones Ortho-Mèthyl-Arylèes. *Tetrahedron.* **1979**, *35*, 2655-2660.

(37) Lipinski, C. A.; Giese, E. F.; Korst, R. J. pKa, Log P and MedChem CLOGP Fragment Values of Acidic Heterocyclic Potential Bioisosteres. *Quant. Struct.-Act. Relat.* **1991**, *10*, 109-117.

(38) Grunewald, G. L.; Brouillette, W. J.; Finney, J. Synthesis of α-Hydroxyamides via the Cyanosilylation of Aromatic Ketones. *Tet. Lett.* **1980**, *21*, 1219-1220.

(39) Brouillette, W. J; Brown, G. B.; Delorey, T. M; Shirali, S. S. ; Grunewald, G. L. Anticonvulsant Activities of Phenyl-Substituted Bicyclic 2,4-Oxazolidinediones and Monocyclic Models. Comparison with Binding to the

Neuronal Voltage-Dependent Sodium Channel. *J. Med. Chem.* **1988**, *31*, 2218-2221.

Table 1. Selected Properties and Sodium Channel Activities for Hydantoins in this Study

compound	%isolated yield, (method)	mp, °C	log *P*[c]	Na^+ channel IC_{50} (μM)	Torsion angle range, ° (N1,C5,C6,C7)[f]
1[a]	64 (A)	169-171 (165-166)	1.96	162 [193-136][h]	0-180[k] {4.6}
2[a]	65 (C)	204-205 (204-205)	2.46	103 [85-124]	0-180[k] {4.4}
3[a]	91 (A)	119-122 (125-127)	2.96	39 [32-47]	0-180[k] {4.4}
4	20 (A)	144-145	2.96	225 [218-233]	-108-12[l] {-37.1} 148-168[l] {159.0}
5	56 (A)	162-164	2.96	58 [57-60]	0-180[k] {3.1}
6	60 (A)	158-168	2.96	95 [86-106]	0-180[k] {3.1}
7[b]	54	173-175 (176-177)	2.02	720	0-180[k] {-42.4} {-57.1}
8	31 (A)	238-240 (238-240)	0.96	2112 [2021-2207]	-15.8- (-95.8)[i] {-35.8, -55.2, -76.4}

Table 1. (Continued)

9[b]	91	240-242 (240-242)	1.46	851[e] [953-761]	-39.6-(-84.6)[i,j] { -64.6} -22.1-(-62.1)[i] {-42.1}
10	51 (C)	250-255 (252-253)	1.96	251 [225-280]	-31.4-4.4[i] {-27.3} -50.0-(-101.0)[i] {-74.0}
11	30 (B)	201-202 (201-202)	2.46	251 [228-277]	-25.3-15.0[i] {-10.0, -25.3} -108.4-(-48.4)[i] {-73.3}
12[b]	54	154-156	1.52	250	-4.29-26.3[i] {11.6} 52.6-22.6[i] {37.6}
DPH			2.46[d]	40[f]	0-180[k] {1.5}

[a]Data taken from ref 28. [b]Data previously reported in ref 29. [c]Calculated using parent structure log *P* values in ref 28 and π values for substituents in ref 26 (see Results and Discussion). [e]The sodium channel value was determined in the present study. [f]Calculated with SYBYL 6.1 (systematic search), and represents the torsion angle range of conformations within 2 kcal/mol of the lowest energy conformer. The torsion angles were calculated in SYBYL from a coordinate system of 0 to 180° and -180 to 0°. Conformational search calculated with SYBYL 6.1 (gridsearch) Tripos, Inc. on a Silicon Graphics Indigo2 R4000 computer. [g]Torsion angle range includes degenerate conformations. [h]Range describing -1 to +1 standard deviation. [i]The number in { } represent the torsion angle of the lowest energy conformer within the range. [j]The torsion angle value was determined in the present study. [k]All conformations from 0 to 180° for this torsion angle are accessible within 2.0 kcal/mol of the lowest energy minimum. Local energy conformations are provided that are similar to the conformation of DPH. [l]The x-ray crystal structure from ref 31 was denoted as an aggregate. H atoms were added and the hydrogen bonds minimized by the Tripos Force Field to obtain the energy reported.

Table 2. Relative Energies and Phenyl Ring Orientations for the Lowest Energy Conformers of Hydantoins **4**, **5**, **7** and **9-12**[a]

Hydantoin Conformation[b]	Torsion Angle, ° C7, C6, C5, N1	Energy, kcal/mol[c]
4(a)	-37.1	10.8
4(b)	159.0	12.4
7(a)	-42.4	7.0
7(b)	-57.1	7.0
8(a)	-35.8	14.5
8(b)	-55.2	16.2
8(c)	-76.4	14.7
9(a)	-64.6	8.2
9(b)	-42.1	8.1
10(a)	-27.3	15.0
10(b)	-16.4	13.7
10(c)	-74.0	15.8
11(a)	-25.3	21.8
11(b)	-10.0	22.9
11(c)	-73.3	22.7
12(a)	37.6	10.9
12(b)	11.6	9.3

[a]Compounds **1-3**, **5** and **6** access all torsion angles from 0-180° within 2 kcal/mole of the global minimum. [b]Each conformation is a local energy minimum generated by search routines within SYBYL (see Conformational Analysis Section). [c]Calculated using the Tripos Force Field in SYBYL.

Table 3. Selected Properties for Hydantoins **4-6**

Compound	isolated yield, %	^{1}H NMR (d^6-DMSO)	^{13}C NMR (d^6-DMSO)	IR cm^{-1} (C=O), KBr
4	20	7.42-7.36 (m, 2H, Ph), 7.21-7.15 (m, 2H, Ph), 6.44-6.38 (s, 1H, NH), 2.35-2.33 (s, 3H, CH_3), 2.24-1.98 (m, 2H, CH_2), 1.41-1.19 (m, 4H, CH_2), 0.90-0.84 (m, 3H, CH_3)	177.0, 157.0, 137.0, 132.6, 128.2, 127.4, 126.1, 67.5, 36.7, 25.2, 22.3, 20.4, 14.1	1760, 1700
5	56	7.42-7.36 (m, 2H, Ph), 7.21-7.15 (m, 2H, Ph), 6.44-6.38 (s, 1H, NH), 2.35-2.33 (s, 3H, CH_3), 2.24-1.98 (m, 2H, CH_2), 1.41-1.19 (m, 4H, CH_2), 0.90-0.84 (m, 3H, CH_3)	175.9, 157.6, 138.5, 137.6, 129.1, 128.7, 125.9, 122.3, 68.9, 38.5, 25.8, 22.5, 21.6, 13.8	1750, 1705
6	60	7.42-7.36 (m, 2H, Ph), 7.21-7.15 (m, 2H, Ph), 6.44-6.38 (s, 1H, NH), 2.35-2.33 (s, 3H, CH_3), 2.24-1.98 (m, 2H, CH_2), 1.41-1.19 (m, 4H, CH_2), 0.90-0.84 (m, 3H, CH_3)	175.5, 156.7, 138.3, 134.6, 129.6, 125.1, 68.8, 38.3, 25.8, 22.5, 21.0, 13.8	1710, 1700

[a]All compounds were also analyzed by (1) GC/MS (EI, 70 eV), giving one peak in the GC and the expected molecular ion peak , and (2) elemental analysis for C, H, N (within ±0.3% of the calculated value).

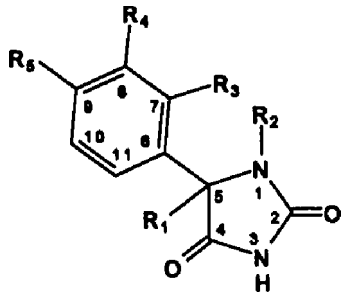

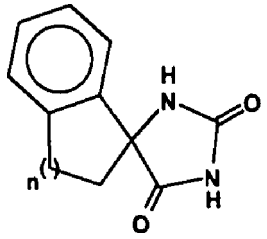

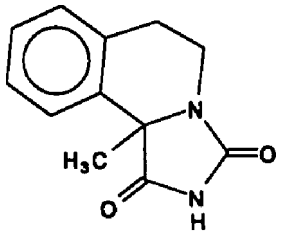

12

	R_1	R_2	R_3	R_4	R_5
1	n-C_3H_7	H	H	H	H
2	n-C_4H_9	H	H	H	H
3	n-C_5H_{11}	H	H	H	H
4	n-C_4H_9	H	CH_3	H	H
5	n-C_4H_9	H	H	CH_3	H
6	n-C_4H_9	H	H	H	CH_3
7	CH_3	C_2H_5	H	H	H
DPH	Ph	Ph			

	n
8	1
9	2
10	3
11	4

Figure 1. Structures of 5-phenylhydantoins discussed in this study.

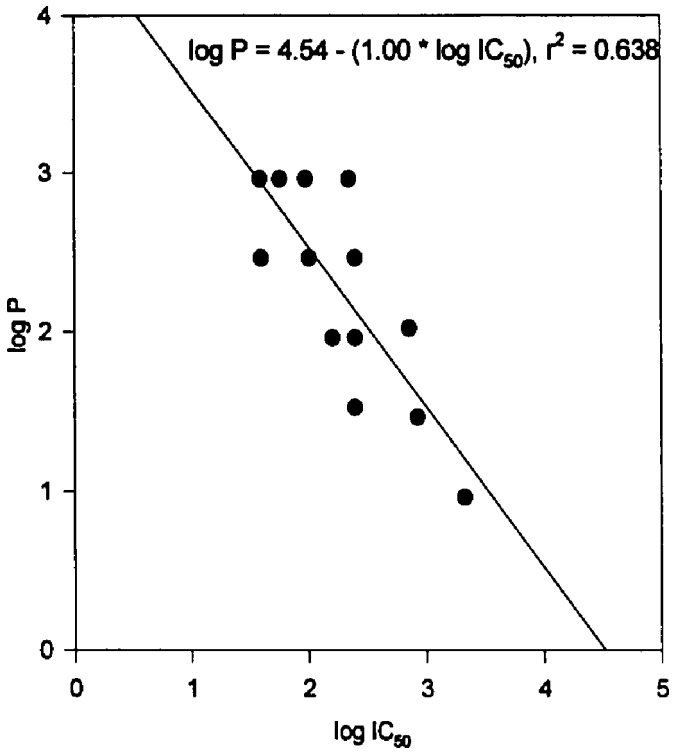

Figure 2. Log *P* versus sodium channel binding for analogs **1-12** and DPH.

Table 4. Analytical Data

Compound		%C	%H	%N
4	Theory	68.16	7.74	11.27
	Found	67.99	7.35	11.33
5	Theory	68.27	11.37	7.37
	Found	68.32	11.46	7.4
6	Theory	67.99	11.33	7.74
	Found	67.33	11.25	7.37

COMPARATIVE MOLECULAR FIELD ANALYSIS OF HYDANTOIN BINDING TO THE NEURONAL VOLTAGE-DEPENDENT SODIUM CHANNEL

MILTON L. BROWN,[†] CHRISTOPHER C. VAN DYKE,[§] GEORGE B. BROWN[‡] AND WAYNE J. BROUILLETTE[*,†]

Department of Chemistry and Department of Psychiatry and Behavioral Neurobiology,
University of Alabama at Birmingham, Birmingham, Alabama 35294
and Tripos, Inc., 1699 South Hanley Road, Suite 303, St. Louis, Missouri 63144

---

[*]Address correspondence to this author.

[†]Department of Chemistry, University of Alabama at Birmingham.

[‡]Department of Psychiatry and Behavioral Neurobiology, University of Alabama at Birmingham.

[§]Tripos, Inc.

Abstract

Comparative molecular field analysis (CoMFA), a 3-D QSAR technique, is widely used to correlate biological activity with observed differences in steric and electrostatic fields. In this study, CoMFA was employed to generate a 3-D QSAR model, based upon 14 structurally diverse 5-phenylhydantoin analogs, to help delineate structural and electrostatic features important for enhanced sodium channel binding. Correlation by partial least squares (PLS) analysis of in vitro sodium channel-binding activity (expressed as log IC_{50}) and the CoMFA descriptor column generated a final model with R^2 = .997 for the training set. The CoMFA model consisted of 73% steric and 27% electrostatic contribution and demonstrated increased predictive value as compared to a simpler correlation with log *P* (R^2 = .804) for the same training set. The CoMFA steric and electrostatic maps described two general features that result in enhanced binding to the sodium channel. These include (1) a preferred 5-phenyl ring orientation described by both the CoMFA electrostatic and steric fields and (2) a favorable steric field encapsulating the C5-alkyl chain. This model was then utilized to accurately predict literature sodium channel activities for hydantoins **14-19**, which were not included in the training set. Finally the hydantoin CoMFA model was used to design the structurally novel α-hydroxy-α-phenylamide **20**. Synthesis and subsequent sodium channel evaluation of compound **20** (predicted IC_{50} = 9 μM, actual IC_{50} = 9 μM [7-11]), a good binder to the sodium channel, establishes that the intact hydantion ring is not necessary for

efficient binding to this site. Thus α-hydroxy-α-phenylamides may represent a new class of ligands that bind with increased potency to the sodium channel.

The anticonvulsant diphenylhydantoin (DPH), or phenytoin, binds to the neuronal voltage-sensitive sodium channel (NVSC) at therapeutically relevant concentrations in a frequency and voltage-dependent manner.[1] These observations are consistent with the selective actions of DPH on hyperactive versus normal neurons.

Our earlier studies[2,3] on hydantoin analogs revealed that, when log *P* is held constant, structural variations lead to dramatic differences in sodium channel binding potency. This observation, when coupled with the reported[4] saturable effects of DPH on sodium channels, suggests that DPH undergoes interaction with a specific site on the NVSC.

Unfortunately, the exact location of this site and structural requirements for optimum binding have not yet been determined. Our previous observation of the strong influence of log *P*, given an appropriate structural type, on in vitro binding of hydantoins to the NVSC suggests that membrane entry may be required for activity. This observation, and the report that changes in intracellular pH affect the activity of DPH on sodium channels, is consistent with an intracellular binding site.[5]

Given the absence of high resolution structural data for the NVSC, in the present study we employed comparative molecular field analysis (CoMFA) to help define important 3-dimensional (3-D) properties associated with the optimum binding of hydantoins to this site. CoMFA samples the differences in steric and

electrostatic fields surrounding a set of ligands. Numerous successes have been reported using this approach for mapping receptor properties, including studies on central nervous system (CNS) active compounds[6-21] and, recently, the first CoMFA involving a NVSC site[22] that addresses binding of the brevetoxins to neurotoxin site 5.

In this study we utilized sodium channel binding data for hydantoin analogs that we previously published,[2] and we synthesized and evaluated the sodium channel binding activities for 5-alkyl-5-phenylhydantoins **5-7**, to extend the series to include larger log *P* values. Sodium channel binding data for hydantoins **1-13** and DPH (Table 1) were used to evaluate correlations with log *P* and a CoMFA model. The CoMFA model derived from the training set in Table 1 was then used to design and/or predict the sodium channel activities of hydantoin analogs **14-20** (Table 2).

Methods

Biological Data. The structures and relative sodium channel binding activities for compounds **1-13** and DPH, which form the training set, are listed in Table 1. Table 2 lists the structures and sodium channel activities of compounds **14-20**, which form the test set. In the sodium channel evaluation, the IC_{50}, which represents the micromolar concentration of compound required to displace 50% of specifically bound [^{3}H]-Batrachotoxinin A 20-α-benzoate [^{3}H]-BTX-B, was determined in an in vitro assay using rat brain cerebral cortex synaptoneurosomes.

Conformational Analysis. All compounds were energy minimized with the Tripos force field[23] using default bond distances and angles and neglecting electrostatics. While compounds were synthesized and evaluated as racemic mixtures, the geometries were modeled using only the *R*-configuration at C5. Since 5-phenyl ring orientation for hydantoin analogs has previously been suggested to be important for hydantoin binding to the NVSC,[24] we designated the C5-C6 bond, which rotates the phenyl ring, for conformational searching. Previously reported[2] low energy conformers of **1-2**, **4**, and **8-16** were used. To determine the low energy conformations for **3** and **5-7** about the C5-C6 bond, we utilized GRIDSEARCH to rotate N1, C5, C6, C7 over 360° in 1° increments as previously reported.[2] Low energy conformations of **17** were obtained by placing a cyclohexyl sidechain in a chair conformation (obtained from the SYBYL fragment library) and performing the GRIDSEARCH as described above. The lowest energy conformation for hydroxy amide **20** was obtained using GRIDSEARCH for O, C5, C6, C7 in a similar fashion. The atomic charges for all analogs were calculated using AM1 (MOPAC). Single point calculations were performed using energy-minimized geometries previously generated from the Tripos Force Field in SYBYL. Conformational searches on the rotationally restricted 5-phenyl analogs **9-13** were performed using the SYSTEMATICSEARCH routine as previously reported.[2] Likewise, conformational searches were performed on compounds **18** and **19** for which low energy conformations are listed in Table 3. In this manner, we developed a training set of 14 analogs (See Tables 1 and 3) and a test set (Table 2).

Molecular Alignment. All of the compounds in the training set have identical hydantoin ring atoms, which we used as the basis for an alignment rule (atoms N1, C2, N3, C4, C5 were fit to each other) for the CoMFA models. The n-alkyl groups at C5 for analogs **1-7**, **14-16** and **20** were placed in an extended conformation as a first approximation.

For the preliminary and final CoMFA models, the lowest energy conformer for the unrestricted analogs **1-8** was used, which in all caes contained a phenyl ring orientation similar to that found in the X-ray crystal structure[25] of DPH (see Figure 1). As a first choice in the preliminary CoMFA model, all low energy conformations for compounds **9-12** were used, and the single conformer with the smallest crossvalidated residual value was selected (Table 3). These conformers of **9-12**, were then used in the final CoMFA (Table 1).

After completing the final CoMFA, we investigated conformations and alignment for the test set analogs **14-20**. For compounds **14-20**, the global and local energy minima (within 2 kcal/mol of the global minimum) were calculated (Table 5) and the activity of each energy minimum conformer was predicted using the final CoMFA model. Consistent with our model, we aligned the hydantoin ring atoms N1, C2, N3, C4, C5 and the phenyl ring atom C6 for **14-19**. The hydroxy amide **20** was aligned in a similar fashion except that the OH group was aligned with N1 and the carboxamide was aligned with C4 and N3. This included overlapping the C4 (C=O) oxygen and the C5-alkyl side chain where appropriate.

X-ray crystal structures for carbamezapine,[33] diazepam[34] and lidocaine[35] were aligned in SYBYL (FIT routine) using the pharmacophore groupings proposed in Figure 10. For carbamazepine the amide carbonyl oxygen and both aromatic carbons attached to C6 were fit onto the amide carbonyl oxygen and both aromatic carbons attached to C6 of DPH. (An alternate alignment was not attempted.)

For diazepam (fit a), the sp^2 N, the methyl substituted N and an aromatic carbon (attached to the double bond carbon of the lactam ring) was aligned with the unsubstituted phenyl ring was aligned onto the carbonyl oxygen, the imide N and C6 of DPH, respectively. This alignment gave reasonable results. However, a second three atom alignment (fit b) was investigated, which placed diazepam's double bond carbon of the lactam ring and two aromatic carbons (attached the the double bonded lactam ring carbon) onto C5 and two aromatic carbons (attached to C5) of DPH, respectively.

For lidocaine, which contains similar pharmacophoric groups as compared to DPH, the carbonyl oxygen, an aromatic carbon (attached to the amide N) and the para aromatic carbon was fit onto the amide carbonyl oxygen, C6 and the para aromatic carbon on a phenyl ring of DPH (fit a), respectively. In an alternative alignment (fit b),lidocaine's amide N, the aromatic carbon (attached to the amide N) and the para aromatic carbon were fit onto C5 and the ring atoms (C6 and the para carbon of one ring) of DPH, respectively (Table 5).

CoMFA Calculations. CoMFA, using default parameters except where noted, was calculated in the QSAR option of SYBYL 6.0 and 6.1 on Silicon

Graphics Personal Iris and Indigo2 computers. The CoMFA grid spacing was 2.0 Å in the x, y and z directions and the grid region was automatically generated by the CoMFA routine to encompass all molecules with an extension of 4.0 Å in each direction. An sp^3 carbon and a point charge of +1.0 were used as probes to generate the interaction energies at each lattice point intersection. The default value of 30 kcal/mol was used as the maximum electrostatic and steric energy cutoff.

The preliminary CoMFA analysis was performed using the single lowest energy conformer for analogs **1-7**, which in all cases contained a phenyl ring orientation similar to that found for one phenyl ring in the x-ray crystal structure of DPH. For restricted analogs **8-13**, all local energy conformations within 5.0 kcal/mol were included in the preliminary model (Table 3). Correlation of this model allowed selection of the best fit conformer (as determined by the smallest residual in Table 3) for use in the final CoMFA. The final CoMFA analysis (Table 1) was performed with the single lowest energy conformer of analogs **1-7** (containing phenyl ring orientations similar to the x-ray crystal structure of DPH) and a single conformation for each restricted analog **8-13** (as determined from the preliminary CoMFA).

Partial Least Squares (PLS) Regression Analysis. Crossvalidated (preliminary and final models) and noncrossvalidated PLS analyses (final model) were performed within the SYBYL/QSAR routine. Crossvalidation of the dependent column (log IC_{50}) and the CoMFA column was performed with 2.0 kcal/mol column filtering. Scaled by the CoMFA standard deviation, the final crossvalidated analysis

generated an optimum number of components equal to 4 and R^2 = 0.847 (Table 4). PLS analysis with noncrossvalidation, performed with 4 components, gave a standard error of estimate of 0.051, a probability of (R^2 = 0) equal to 0.000, an F value (n_1 = 4, n_2 = 9) of 810.1 and a final R^2 = 0.997. The relative steric (0.732) and electrostatic (0.268) contributions to the final model were (Figures 6-13) contoured by contributions of the standard deviation multiplied by the coefficient at 80% for favored steric (contoured in green) and favored positive electrostatic (contoured in blue) and 20% for disfavored steric (contoured in yellow) and favored negative electrostatic (contoured in red), as shown in Figures 6-9 and 11-13 (H atoms omitted for clarity). Based on this analysis, analogs from the test set (Table 2) were predicted with no pre-existing fields and the conformations that best fit the model were selected for study (Table 5).

Chemistry

The syntheses of analogs **1-4**[3], **8**[2], **11**[29], **12**[29], **13**[2], **14-16**[2], **17**[15], and **18-19**[3] were previously described. Compounds **5**[28] (59% yield), **9**[27] (31% yield) and **17**[28] (15% yield) were prepared from commercially available hexanophenone, 1-indanone and cyclohexylphenylketone, respectively, using the Bucherer-Berg approach.[28] Hydantoins **6** and **7** each were prepared in an isolated yield of 95% from commercially available octanophenone and decanophenone, respectively, according to literature methods[26, 28] (see Scheme I).

The synthesis of the 2-hydroxy-2-phenylnonanamide **20** was accomplished using a previously reported procedure[26] for the synthesis of 2-hydroxy-2-

phenylpropanamide (Scheme I). Briefly, octanophenone (**22**) was treated under anhydrous conditions with cyanotrimethylsilane to give the cyanotrimethylsilyl ether **23**, and cleavage of the trimethylsilyl group in **23** with 5% HCl gave cyanohydrin **24** in 100% yield. The hydrolysis of **24** with cold concentrated HCl and HCl gas resulted in the precipitation of 2-hydroxy-2-phenylnonanamide **20** in 100% yield.

Results and Discussion

Our previous sodium channel SAR studies[3] suggested that log *P* was one of the parameters important for enhanced binding of hydantoins to the NVSC. We thus estimated the log *P* values for analogs **5-7** and **17-20** (Tables 1 and 2) by the approach we employed earlier, using reported experimentally measured log *P* values for the parent structures, 5-phenylhydantoin (log *P* = 0.46)[30] and 2-hydroxy-2-phenylpropanamide (log *P* = 1.2)[31] to which were added the appropiate π values for the substituents to provide the final log *P*.[32] The log *P* values for all other compounds were previously reported.[2]

Correlation of log *P* versus sodium channel binding (log IC_{50}) for **1-13** and DPH in Figure 2 had increased correlation over a previously reported[2] log *P* model, which used fewer compounds and spanned a smaller log *P* range. The log *P* correlation from the present study includes hydantoins **5-7**, which provide larger log *P* values than previously used. This correlation (Figure 2) reveals a model that explains approximately 80% of the binding effects. However, comparisons of hydantoins with the same log *P* and different structures often show very different binding affinities to the NVSC (e.g., **3** vs **4**). We thus were encouraged to use

CoMFA to investigate the differences in structural and electrostatic features of these analogs in an effort to formulate a better model.

The sodium channel binding affinities and lipophilicities for the COMFA training set are presented in Table 1. PLS correlation of in vitro sodium channel-binding, expressed as log IC_{50}, and CoMFA descriptors generated a CoMFA model with R^2 = .997 for the training set (see Table 3). Furthermore, the CoMFA model demonstrated significantly increased predictive value in comparision with the log *P* model (R^2 = .804) for the same data set.

Investigations of the CoMFA steric map revealed that an n-alkyl substitution at the C5 position appears to be required for tight binding to the hydantoin site. The contour map in Figure 7 reveals a lipophilic volume encapsulating the 5-alkyl side chain with an optimum length of 6-7 carbons (further increases gave no enhancement in binding). For phenyl ring restricted hydantoins **9-12**, the CoMFA supports the conclusion that 5-phenyl ring orientation is important for binding.[2] Compounds **9** and **10** have 5-phenyl rings restrained to spatial arrangements that occupy unfavorable electrostatic and steric regions of the model and are therefore less active sodium channel binders. Analogs **11** and **12** have greater phenyl ring flexibility and can adopt low energy conformations that allow for occupation of more favorable electrostatic and steric regions, consistent with significantly increased binding potency as compared to hydantions **9** and **10**. Figures 6 and 7, which contain highly active analog **7** (orange) and the weakly active hydantoin **9** (green)

within the electrostatic and steric CoMFA fields, respectively, illustrate the effects of proper 5-phenyl ring conformation on binding.

An important property of a QSAR model is the ability to accurately predict the relative binding potencies of new analogs. The predictive ability of the CoMFA model described here was first evaluated by calculating activities of previously published monocyclic hydantoins **14-16**,[2] hydantoin **17** and bicyclic hydantoins **18** and **19**.[3] As shown in Table 2, calculations agreed remarkably well with the experimental results.

Hydantoins **14-16** (Table 2), which have essentially identical log *P* values, were designed to confirm the importance of 5-phenyl ring orientation independent of changes in log *P*.[2] Compound **14** contains high energy phenyl ring rotamers that are significantly less populated as compared to the less restricted analogs **15** and **16**. As shown in Figure 9, the phenyl ring of the lowest energy conformer of **14**(a) does not occupy a sterically favored region of space. This is consistent with a predicted and observed binding affinity for **14**(a) that is 4 times less potent than that of **15** (for both a and b conformations of the methyl group, Table 5) and twice as inactive as **16**.

The substitution of a para methyl group in compound **16** does not appreciably alter phenyl ring orientation relative to a nonsubstituted phenyl ring. Consistently, compound **16** (IC_{50} = 95 μM) exhibited essentially the same binding potency as **2** (IC_{50} = 103 μM), which has the same size n-butyl side chain. Comparisons of analog **16** (same log *P* and phenyl ring torsion) with hydantoin **4** suggest that, given

the same log *P* and angle, longer alkyl side chains provide better sodium channel binders. Further, *m*-methyl may be favored over p-Me substitutions, as suggested by the moderately increased binding potency of **15** as compared to **16** (same log *P* and phenyl ring torsion).

Compound **17** was designed to test the influence of a more bulky, cyclic alkyl group in the 5-alkyl region. Interestingly, the sodium channel binding potency of compound **17** was correctly predicted by the CoMFA model (observed IC_{50} = 58 μM). Thus even cyclic groups in the 5-alkyl region favor sodium channel binding.

Finally, the potential utility of this CoMFA model for designing new, potent sodium channel binders was evaluated. Using the CoMFA model, the α-hydroxy-α-phenylamide **20** was designed as a new structural class that met all major requirements of the model yet did not contain the hydantoin ring. Compound **20** contains, like **1**-**7**, a relatively unrestricted phenyl ring and a seven carbon 5-alkyl side chain (Figure 9). The success of this compound as a potent sodium channel binder (IC_{50} = 9 μM) and the accuracy of prediction by the CoMFA model validates the alignment rule and reveals that the intact hydantion ring is not required for good sodium channel binding activity.

The CoMFA model and results for **20** lead to the formulation of a preliminary pharmacophore model, which includes a 5-phenyl region, a lipophilic 5-alkyl region, at least two hydrogen bond donors (NH_2 and OH) and one hydrogen bond acceptor (C=O) (Figure 10). While the hydroxyl group in **20** can be a hydrogen bond donor

or acceptor, hydrogen bond donation for this grouping is more consistent with properties of the corresponding amide nitrogen of the hydantoin ring.

Since there exists controversy over the binding of anticonvulsants, local anesthetics and antiarrhythmics to a common site[36] or different sites on the NVSC,[5] we were inclined to predict the NVSC activity for carbamazepine, lidocaine and diazepam. In this manner, we fit common functional groups contained in these molecules with important structural features derived from our pharmacophore model. The results of this study suggest that carbamazepine binds in a similar fashion as DPH. Thus the CoMFA model accurately predicts the NVSC binding for carbamazepine when it is aligned with the pharmacophore groupings found in DPH (Figure 11) (actual log IC_{50} = 2.12; predicted log IC_{50} = 2.11).

For diazepam, the alignment (Figure 12) of hydrogen bond acceptors and one phenyl ring (fit a) (predicted log IC_{50} = 2.68; actual log IC_{50} = 2.18) resulted in a relatively poor prediction. However, a simple alignment of diazepam's two phenyl rings (fit b) with those of DPH gave a more accurate prediction (predicted log IC_{50} = 2.13, actual log IC_{50} = 2.18), suggesting that properly placed phenyl and 5-alkyl substituents may be more important than hydantoin ring heteroatoms.

Similarly, hydrogen bond donors (NH) and acceptors (C=O) of lidocaine were fit with pharmacophore groupings of DPH (Table 5, fit a) (Figure 13). The poor CoMFA prediction suggests that the pharmacophoric groupings essential in predicting the sodium channel binding of DPH do not adequately explain the affinity of lidocaine for the sodium channel. However, a simple alignment (fit b), in which

the amide N, the aromatic carbon (attached to the amide N) and the para aromatic carbon of lidocaine were fit onto C5 and the ring atoms (C6 and the para carbon) of DPH, gave good results (predicted log IC_{50} = 2.60, actual log IC_{50} = 2.49). This alignment places the lidocaine phenyl ring orthoganol to the phenyl ring of DPH. These results are suggestive of a different local anesthetic receptor site, one that resembles or overlaps the phenyl ring region of the hydantoin binding site.

In conclusion, the CoMFA model in this study was predictive of sodium channel binding affinities for a number of structurally diverse hydantoins, as well as carbamazepine and diazepam, not included in the training set. Furthermore, the CoMFA model was shown to have potential utility for designing new agents in that a structurally novel α-hydroxy-α-phenylamide was also accurately predicted. Thus this CoMFA model, based only on electrostatic and steric effects, may prove useful for designing and predicting new and more potent sodium channel-directed agents.

Experimental Section

Melting points were recorded on an Electrothermal melting apparatus and are uncorrected. IR spectra were recorded on Beckman Acculab 6 and Nicolet IR/42 spectrometers, and elemental analyses were performed by Atlantic Microlabs of Norcross, GA. ^{1}H NMR and ^{13}C NMR were recorded on GE 300 MHz FT and Bruker 300 FT MHz NMR spectrometers in d^{6}-DMSO (for hydantoins) and $CDCl_3$ (for all other compounds) at ambient temperature and referenced internally to tetramethylsilane (TMS). The GC/MS were performed on a Hewlett Packard 5885 GC/MS. Statistics and graphs were completed using computer software SigmaStat

(version 1.02a) and Sigma Plot (version 1.0) for Windows from Jandel, Inc. [^{3}H]-Batrachotoxinin A 20-α-benzoate ([^{3}H]-BTX-B) with a specific activity of 30 Ci/mol was obtained from New England Nuclear (Boston, MA)

5-Heptyl-5-phenylhydantoin (6). A mixture containing octanophenone (**22**) (1.5 g, 7.5 mmol), cyanontrimethylsilane (TMSCN) (0.7 g, 7.5 mmol), and ZnI_2 (5-10 mg) were stirred at room temperature under a N_2 atmosphere. The reaction progress was monitored by the disappearance of the C=O stretching peak (1670 cm^{-1}) in the IR spectrum of the reaction mixture. After 2 h this peak was absent, indicating complete conversion to give 2-trimethylsilyloxy-2-phenylnonanecarbonitrile (**23**). The TMS ether **23** was hydrolyzed to the cyanohydrin **24** by adding ether (10 mL) and 15% HCl (10 mL), and the resulting mixture was stirred vigorously for 1 h. The acidic layer was washed with ether (3 x 20 mL). The extracts were combined and evaporated to give cyanohydrin **24** (1.8 g, 100%). IR (neat) 3400 (OH), 2250 (CN) cm^{-1}. The cyanohydrin **24** was converted to hydantoin by a previously reported literature procedure for similar compounds.[2] Using this procedure, cyanohydrin **24** (1.8 g, 9.0 mmol) and $(NH_4)_2CO_3$ (3.6 g, 3.6 mmol) were dissolved in 50% ethanol (30 mL) while stirring under a N_2 atmosphere. The mixture was heated slowly between 40-60 °C for 12 h. The basic mixture was evaporated to half-volume and cooled to room temperature. The precipitate was filtered and recrystallized from hot ethanol to give **6** (0.50 g, 21%): m.p. 124-126 °C; IR (KBr) 1710, 1755 (C=O), 3200 (NH) cm^{-1}.

5-Nonyl-5-phenylhydantoin (7). To a stirring solution of 50% ethanol (50 mL) were added decanophenone (3.0 g, 12.9 mmol), KCN (1.7 g, 25.8 mmol) and $(NH_4)_2CO_3$ (5.9 g, 51.6 mmol). The solution was warmed to 50-65 °C for 12 h. The precipitate was filtered and the filtrate was acidified (pH 2) using concentrated HCl. The resulting solid was filtered and the filtrate was made basic (pH 8) using 3% KOH. This was concentrated to half-volume and filtered again. The combined solids were recrystallized from hot ethanol to give pure **7** (3.7 g, 95% yield): m.p. 115-116 °C; IR (KBr) 1700, 1750 (C=O), 3200 (NH) cm^{-1}.

2-Hydroxy-2-phenylnonanamide (20). The cyanohydrin **24** was prepared as described in the synthesis of **6**, except that octanophenone (**22**) (4.1 g, 2.0 mmol), TMSCN (2.0 g, 2.0 mmol), ZnI_2 (5-10 mg), ether (20 mL) and 5% HCl (10 mL) were used. Cyanohydrin **24** was added to cold concentrated HCl (10 mL) and saturated with HCl gas while stirring. After 4 h a precipitate began to form, and the mixture was then allowed to stand overnight without stirring. The solid was filtered, washed on the filter with cold water (3 x 50 mL) and recrystallized from hot toluene to give pure **20** (5.3 g, 100%): m.p. 91-92 °C.

Sodium Channel Binding Assay. We previously reported the details of this procedure.[32] Briefly, synaptoneurosomes (~1 mg of protein) from rat cerebral cortex were incubated for 40 min at 25 °C with the test compound (seven different concentrations spanning the IC_{50}) in a total volume of 320 μL containing 10 nM [^{3}H]BTX-B and 50 μg/mL of scorpion venom. Incubations were terminated by dilution with ice cold buffer and filtration through a Whatman GF/C filter paper, and

the filters were washed four times with ice cold buffer. Filters were counted in a Beckmann scintillation counter. Specific binding was determined by subtracting the nonspecific binding, which was measured in the presence of 300 μM veratridine, from the total binding of [^{3}H]BTX-B. All experiments were performed in triplicate and included a control tube containing 40 μM DPH. The IC_{50} values were determined from a Probit analysis of the dose-response curve and excluded doses producing less than 10% or greater than 90% inhibition.

Acknowledgments

This work was completed in partial fulfillment of the requirements for the PhD degree in Organic Chemistry by M.L.B. M.L.B gratefully acknowledges financial support from the Patricia Robert Harris Fellowship, the National Consortium for Educational Access, the UAB Comprehensive Minority Faculty Development Program and the UAB Department of Chemistry. We also thank Ms. Bereaval Webb, a 1993 Alabama Alliance for Minority Participation Summer Intern, for technical support.

References

(1) Willow, M.; Catterall, W. A. Inhibition of Binding of [^{3}H]Batrachotoxinin A 20-α-Benzoate to Sodium Channels by the Anticonvulsant Drugs Diphenylhydantoin and Carbamazepine. *Mol. Pharmacol.* **1982**, *22*, 627-635.

(2) Brown, M. L.; Brown, G. B.; Brouillette, W. J. Hydantoins with Conformationally Restricted Phenyl Rings. Effects on Sodium Channel Binding. *PhD Dissertation of Milton Brown.*

(3) Brouillette, W. J.; Jestkov, V.P.; Brown, M. L.; Aktar, M. S.; Delorey, T. M.; Brown, G. B. Bicyclic Hydantoins with Bridgehead Nitrogen. Comparison of

Anticonvulsant Activities with Binding to the Neuronal Voltage-Dependent Sodium Channel. *J. Med. Chem.* **1994**, *37*, 3289-3293.

(4) Francis, J.; Burnham, W. M. [^{3}H]Phenytoin Identifies a Novel Anticonvulsant-Binding Domain on Voltage-Dependent Sodium Channels. *Mol. Pharmacol.* **1992**, *42*, 1097-1103.

(5) Barber, M. J.; Starmer, C.F.; Grant, A. O. Blockade of Cardiac Sodium Channels by Amitriptyline and Diphenylhydantoin. Evidence for Two Use-dependent Binding Sites. *Circulation Research.* **1991**, *69*, 677-696.

(6) Greco, G.; Novellino, C. S.; Vittora, A. Comparative Molecular Field Analysis on a Set of Muscurinic Agents. *QSAR.* **1991**, *10*, 289-299.

(7) Kim, K. H.; Greco, G.; Novellino, E.; Silipa, C.; Vittoria, A. Use of the Hydrogen Bond Potential Function in a Comparative Molecular Field Analysis (CoMFA) on a Set of Benzodiazepines. *J. Comp.-Aided Mol. Design.* **1993**, *7*, 263-280.

(8) Giovanni, G.; Ettore, N.; Fiorini, I.; Nacci, B.; Campiani, G.; Ciani, S. M.; Garofalo, A.; Bernasconii, P.; Mennini, T. Comparative Molecular Field Analysis Model for 6-Arylpyrrolo[2,1-d][1,5]Benzothiazepines Binding Selectively to the Mitochondrial Benzodiazepine Receptor. *J. Med. Chem.* **1994**, *37*, 4100-4108.

(9) Wong G.; Koehler, K. F.; Skolnick, P.; Gu, Z-Q.; Ananthan, P.; Schönholzer, W.; Hyunkeler, W.; Zhang, W.; Cook, M. Synthetic and Computer-Assisted Analysis of the Structural Requirements for Selective, High-Affinity Ligand Binding to Diazepam-Insensitive Benzodiazepine Receptors. *J. Med. Chem.* **1993**, *36*, 1820-1830.

(10) Andre, M.M.; Charifson, P. S.; Constance, E. O.; Kula, N. S.; McPhail, A. T.; Baldessarini, R. J.; Booth, R. G.; Wyrick, S. D. Conformational Analysis, Pharmacophore Identification, and Comparative Molecular Field Analysis of Ligands for the Neuromodulatory δ_3 Receptor. *J. Med. Chem.* **1994**, *37*, 4109-4117.

(11) Ablordeppy, S. Y.; El-Ashmaway, M. B.; Glennon, R. A. Analysis of the Structure Activity Relationships of Sigma Ligands. *Med. Chem. Res.* **1991**, *1*, 425-438.

(12) Thomas, B. F.; Compton, B. R. M.; Semus, S. F. Modeling the Cannabinoid Receptor: A Three-Dimensional Quantative Structure Activity Analysis. *Mol. Pharmacol.* **1991**, *40*, 656-661.

(13) Semus, S. F. A Computer Graphic Investigation into the Structural Requirements for Interaction with the Putative Cannabinoid Receptor Site. *Med. Chem. Res.* **1991**, *1*, 454-460.

(14) Chen, J. M.; Sheldon, A. Structure-Function Correlations for Calcium Binding and Calcium Channel Activities Based on 3-Dimensional Models of Human Annexins I, II, III, V, VII. *Biomol. Struct. Dynam.* **1993**, *10*, 1067-1089.

(15) Rustici, M.; Bracci, L.; Lozzi, P.; Nari, P.; Santucci, A.; Sodani, P.; Spreafico, A.; Niccolai, N. A Model of the Rabies Virus Glycoprotein Active Site. *Biopolymers* **1993**, *33*, 961-969.

(16) Nordvall, G.; Hacksell, U. Binding Site Modeling of the Muscarinic M1 Receptor: A Combination of Homology-Based and Indirect Approaches. *J. Med. Chem.* **1993**, *36*, 967-976.

(17) Caroll, F. I.; Mascrella, S. W.; Kuzemko, M. A.; Goa, Y. G.; Abraham, P.; Lewin, A. H.; Boja, J. W.; Kuhar, M. J. Synthesis, Ligand-Binding and QSAR (CoMFA and Classical) Study of 3β-(3'-Substituted Phenyl), 3β-(4'-Substituted Phenyl), 3β-(3',4'-Disubstituted Phenyl) Tropane-2β-Carboxylic Acid Methyl-Esters. *J. Med. Chem.* **1994**, *37*, 2865-2873.

(18) Agarwal, A.; Taylor, E. W. 3-D QSAR for Intrinsic Activity of 5-HT_{1A} Receptor Ligands by the Method of Comparative Molecular Field Analysis. *J. Comput. Chem.* **1993**, *14*, 237-245.

(19) Langer, T.; Wermuth, C. G. Inhibitors of Prolyl Endopeptidase: Characterization of the Pharmacophoric Pattern Using Conformational Analysis and 3D-QSAR. *J. Comp.-Aided Mol. Design.* **1993**, *7*, 253-262.

(20) Allen, M.S.; LaLoggia, A. J.; Dorn, M. J.; Constantino, G.; Hagen, T. J.; Koehler, K. F.; Skolnick, P.; Cook, J. M. Predictive Binding of β-Carboline Inverse Agonist and Antagonists via the CoMFA/GOLPE Approach. *J. Med. Chem.* **1992**, *35*, 4001-4010.

(21) Calder, J. A.; Wyatt, J. A.; Frenkel, D. A.; Casida, J. E. CoMFA Validation of the Superposition of Six Classes of Compounds Which Block GABA Receptors Non-Competitively. *J. Comp.-Aided Mol. Design* **1993**, *7*, 45-60.

(22) Rein, K. S.; Baden, D. G.; Gawley, R. E. Conformational Analysis of the Sodium Channel Modulator, Brevetoxin A. Comparison with Brevetoxin B

Conformations, and a Hypothesis About the Common Pharmacophore of the "Site 5" Toxins. *J. Org. Chem.* **1994**, *59*, 2101-2106.

(23) Clark, M. D.; Cramer III, R. D.; Opdenbosch, N. V. Validation of the General Purpose Tripos 5.2 Force Field. *J. Comput. Chem.* **1989**, *10*, 982-1012.

(24) Brouillette, W. J; Brown, G. B.; Delorey, T. M; Liang, G. Sodium Channel Binding and Anticonvulsant Activities of Hydantoins Containing Conformationally Constrained 5-Phenyl Substituents. *J. Pharm. Sci.* **1990**, *79*, 871-874.

(25) Camerman, A.; Camerman, N. The Stereochemical Basis of Anticonvulsant Drug Action. I. The Crystal and Molecular Structure of Diphenylhydantoin, a Noncentrosymmetric Structure Solved by Centric Symbolic Addition. *Acta Cryst.* **1971**, *B27*, 2205-2211.

(26) Grunewald, G. L.; Brouillette, W. J.; Finney, J. Synthesis of α-Hydroxyamides via the Cyanosilylation of Aromatic Ketones. *Tet. Lett.* **1980**, *21*, 1219-1220.

(27) Sarges, R.; Schnur, R. C.; Belletire, J. L.; Peterson, M. J. Spiro Hydantoin Aldose Reductase Inhibitors. *J. Med. Chem.* **1988**, *31*, 230-243.

(28) Novelli, A.; Lugones, Z. M.; Velasco, P.; Hydantoins III. Chemical Constitution and Hypnotic Action. *Anales Asoc. Quim Argentina.* **1942**, *30*, 225-231.

(29) Huisgen, R.; Ugi, I. Polycyclische Systeme mit Heteroatomen. *Liebigs Ann. Chem.* **1957**, *610*, 57-66.

(30) Lien, E., Structure-Activity Correlations for Anticonvulsant Drugs. *J. Med. Chem.* **1970**, *13* ,1189-1191.

(31) Hernandez-Gallegos, Z.; Lehmann, P. A. F. Partition Coefficients of Three New Anticonvulsants. *J. Pharm. Sci.* **1990**, *79*, 1032-1033.

(32) Brouillette, W. J.; Brown, G. B.; Delorey, T. M.; Shirali, S. S. ; Grunewald, G. L. Anticonvulsant Activities of Phenyl-Substituted Bicyclic 2,4-Oxazolidinediones and Monocyclic Models. Comparison with Binding to the Neuronal Voltage-Dependent Sodium Channel. *J. Med. Chem.* **1988**, *31*, 2218-2221.

(33) Lowes, M. M. J.; Caira, M. R.; Lötter, A. P.; Van Der Watt, J. G. Physicochemical Properties and X-Ray Structural Studies of the Trigonal Polymorph of Carbamazepine. *J. Pharm. Sci.* **1987**, 76, 744-752.

(34) Camerman, A.; Camerman, N. Stereochemical Basis of Anticonvulsant Drug Action II. Molecular Structure of Diazepam. *J. Am. Chem. Soc.* **1972**, *94*, 268-272.

(35) Hanson, A. W.; Röhrl, M. The Crystal Structure of Lidocaine Hydrochloride Monohydrate. *Acta Cryst.* **1972**, *B28*, 3567-3571.

(36) Zimányi, I.; Weiss, S. R. B.; Lajtha, A.; Post, R. M.; Maarten, E. A. R. Evidence for a Common Site of Action of Lidocaine and Carbamazepine in Voltage-Dependent Sodium Channels. *Eur. J. Pharmacol.* **1989**, *167*, 419-422.

(37) Postma, S. W.; Catterall, W. A. Inhibition of Binding of ^{3}H-Batrachotoxin A 20-α-Benzoate to Sodium Channels by Local Anesthetics. *Mol. Pharmacol.* **1984**, *25*, 219-227.

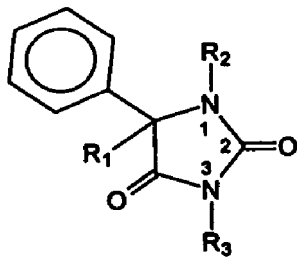

1-8, DPH

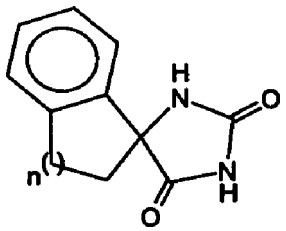

9-12

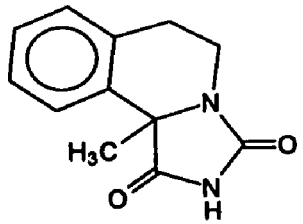

13

Table 1. Sodium Channel Binding Activities and Log *P* (Observed and Predicted) for the Training Set

Compound	R_1	R_2	R_3	n	log *P*	Na^+ channel inhibition IC_{50} μM	log IC_{50} observed	log IC_{50} predicted	log IC_{50} residual
1	C_3H_7	H	H		1.96[g]	162 [136-193][d]	2.21[a]	2.18	0.03
2	C_4H_9	H	H		2.46[g]	103 [85-124]	2.01[a]	2.04	-0.02
3	C_4H_9	H	CH_3		3.01[g]	285 [232-350]	2.45[a]	2.43	0.03
4	C_5H_{11}	H	H		2.96[g]	39 [32-47]	1.59[a]	1.59	0.00
5	C_6H_{13}	H	H		3.40	13 [9-17]	1.11[c]	1.18	-0.07

Table 1. (Continued)

6	C_7H_{15}	H	H		3.96	5 [4-6]	0.70[c]	0.77	-0.07
7	C_9H_{17}	H	H		4.96	5 [4-6]	0.7[c]	0.62	0.08
8	CH_3	C_2H_5	H		2.02[i]	720	2.86[b]	2.87	-0.01
9				1	0.96[i]	2112 [2021-2207]	3.32[j]	3.29	0.03
10				2	1.46[i]	851 [761-953]	2.93[j]	2.97	-0.04
11				3	1.96[i]	251 [225-280]	2.4[j]	2.42	-0.02
12				4	2.46[i]	251 [228-277]	2.4[j]	2.41	-0.01
13					1.52[i]	250	2.4[b]	2.38	0.02
DPH	C_6H_5	H	H		2.46[f]	40[e]	1.6	1.55	0.05

[a]Reported IC_{50} value ±1 standard deviation in ref 3. [b]Reported IC_{50} value in ref 24. [c]The sodium channel value was determined in this study. [d]Numbers in [ ] represent ±1 standard deviation. [e]Data taken from ref 1. [f]Log *P* data taken from ref 30. [g]Calculated using parent structure log *P* value in ref 3. [h]Generated from the CoMFA non-crossvalidated run (see Methods). [i]Calculated using parent structure log *P* value in ref 2. [j]Reported IC_{50} value in ref 2.

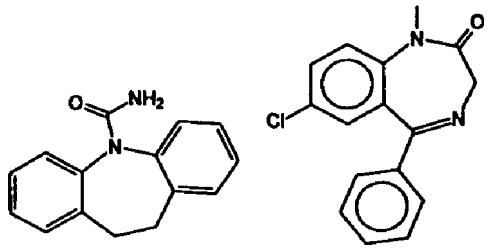

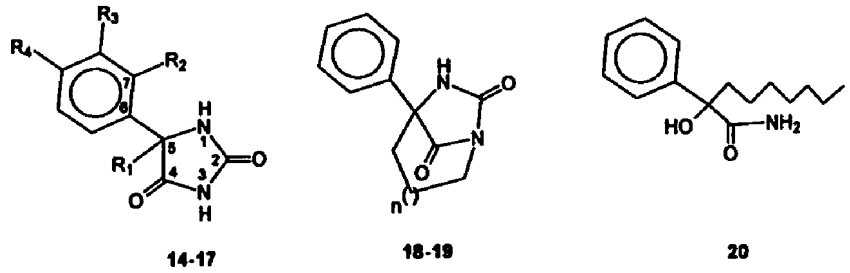

14-17 18-19 20

Table 2. Sodium Channel Inhibition for Diverse Analogs Forming the Test Set

Compound	R_1	R_2	R_3	R_4	n	log *P*	Na^+ channel inhibition[d] IC_{50} μ M	log IC_{50}[e] (μM) observed	predicted[e]	residual
14	C_4H_9	CH_3	H	H		2.96[g]	225[m] [218-233]	2.35	2.38[f]	-0.03
15	C_4H_9	H	CH_3	H		2.96[g]	58[d] [57-60]	1.76	2.07[f]	-0.31
16	C_4H_9	H	H	CH_3		2.96[g]	95[m] [86-106]	1.98	1.92	0.06

Table 2. (Continued)

17	c-C_6H_{11}	H	H	H		2.96	58 [41-82]	1.76	1.89	-0.13
18					2	2.01[b]	700[a]	2.85	3.00	-0.15
19					3	2.51[b]	427 [376-383][a]	2.63	2.45	0.18
20						3.70	9 [7-11]	0.95	0.95	0.00
CBZ[h]							131[i]	2.12	2.11	0.01
DZP[j]							152[i]	2.18	2.24	-0.40
LDC[k]							311±53[l]	2.49	3.40	-0.91

[a]Reported in ref 3. [b]Calculated using parent structure log *P* value in ref 24 and π values in ref 32. [c]log P_{20} = log $_{DPH}$ + $\pi_{N\text{-}Me}$ + $\pi_{ring\ closure}$. (see Results and Discussion). [d]Numbers in [ ] represent ±1 standard deviation. [e]Data generated from the CoMFA noncrossvalidated run (see QSAR Methods). [f]Refers to conformations **14**(a) and **15**(a) in Table 5. [g]Calculated using parent structure log *P* value in ref 2. [h]Carbamazepine (CBZ). [i]Reported in ref 1. [j]Diazepam (DZP). [k]Lidocaine (LDC). [l]Reported in ref 37. Values taken from ref 2.

Table 3. Data from PLS Crossvalidated Analysis

	Preliminary Model, log IC_{50}			Final Model, log IC_{50}		
Compound	obs[a]	pred	res	obs[a]	pred	res
1	2.21	2.17	0.04	2.21	2.11	0.10
2	2.01	2.10	-0.09	2.01	2.01	0.00
3	2.45	1.96	0.49	2.45	1.95	0.50
4	1.59	1.72	-0.13	1.59	1.74	-0.15
5	1.11	1.26	-0.15	1.11	1.31	-0.20
6	0.70	0.95	-0.25	0.70	0.95	-0.25
7	0.70	0.68	0.02	0.70	0.68	0.02
8(a)	2.86	2.98	-0.13			
8(b)	2.86	2.97	-0.11	2.86	2.89	-0.03
9(a)	3.32	3.31	0.01	3.32	2.62	0.70
9(b)	3.32	2.74	0.59			
9(c)	3.32	3.15	0.17			
10(a)	2.93	3.01	-0.08	2.93	2.85	0.08
10(b)	2.93	2.77	0.15			
11(a)	2.40	2.54	-0.14			

Table 3. (Continued)

11(b)	2.40	2.44	-0.04	2.40	2.50	-0.10
11(c)	2.40	2.72	-0.32			
12(a)	2.40	2.47	-0.07	2.40	2.53	-0.13
12(b)	2.40	2.69	-0.29			
12(c)	2.40	2.30	0.10			
12(d)	2.40	2.30	0.10			
12(e)	2.40	2.51	-0.11			
13(a)	2.40	2.52	-0.12			
13(b)	2.40	2.49	-0.09	2.4	2.58	-0.18
DPH	1.60	2.08	-0.48	1.60	2.20	-0.60

[a]refer to Table 1 for observed IC_{50} ± 1 standard deviation.

Table 4. Crossvalidated PLS Analysis

	Preliminary Model		Final Model[a]	
Components	s	R^2	s	R^2
1	0.513	0.507	0.598	0.499
2	0.391	0.726	0.486	0.696
3	0.310	0.836	0.416	0.798
4	0.258	0.891	0.381	0.847
5	0.236	0.914	0.388	0.859

[a]Optimum number of components is 4, R^2 = .847. [b]s=standard error for the estimate of log IC_{50}, R^2 = correlation coefficient or press value = 1.0 - {$\sum$(Y *predicted* - Y *actual*)^2 + (Y *actual* - Y *mean*)^2}. The preliminary model included single conformations of **1-7** and multiple conformations of **8-13** and the final model included single conformations of **1-7** and a single best fit (smallest residual as determined from the preliminary model) conformer of **8-13**.

Table 5. Conformations of the Test Compounds

Compound (conformer)	Energy, kcal/mol	Torsion Angle,° N1, C5, C6, C7	(Final Model) log IC_{50} observed	predicted	residual
14(a)	10.759	-37.5	2.35	2.69	-0.34
14(b)[a]	12.367	158.7	2.35	2.38	-0.03
15(a)	8.185	4.5	1.76	2.07	-0.31
15(b)[b]	8.153	3.8	1.76	2.15	-0.39
18(a)	40.403	-93.9	2.85	3.00	-0.15
18(b)	39.050	-1.3	2.85	2.43	0.42
19(a)	26.894	-1.1	2.63	2.45	0.18
19(b)	26.263	-53.9	2.63	3.08	-0.45
CBZ(fit a)[c,f]			2.12	2.11	0.01
DZP(fit a)[d,f]			2.18	2.68	-0.40
DZP(fit b)[d]			2.18	2.13	0.05
LDC(fit a)[e,f]			2.49	3.40	-0.91
LDC(fit b)[e]			2.49	2.60	-0.11

[a]**14**(b) was used in Table 2 and the conformation of the ortho methyl is projected over the hydantoin ring. [b]**15**(b) was used in Table 2 and the conformation projects the meta methyl towards the N1. [c]X-ray structure from ref 33 was used as the low energy conformation for CBZ. [d]X-ray structure from ref 34 was used as the low energy conformation for DZP. [e]X-ray structure from ref 35 was used as the low energy conformation for LDC. [f]Represents alignment with important pharmacophoric points in our model (see Molecular Alignment). [g]Values taken from ref 2.

Table 6. Selected Data for New Compounds

compound	isolated yield, %	m.p. °C, recryst. (solvent)	^{1}H NMR (d^6-DMSO)[b]	^{13}C NMR (d^6-DMSO)[c]	IR cm^{-1} (C=O), KBr
5	59	138-140 [lit. 140-142][d] (Ethanol)			
6	21	124-126 (Ethanol)	10.91-10.65 (s, 1H, NH), 8.79-8.56 (s, 1H, NH), 7.65-7.15 (m, 5H, Ph), 2.15-1.68 (s, 2H, CH_2), 1.45-0.98 (m, 10H, CH_2), 0.94-0.63 (m, 3H, CH_3)	176.3, 156.5, 139.3, 128.4, 127.7, 125.3, 67.5, 31.1, 28.7, 28.5, 23.3, 22.2, 13.9	1755, 1710
7	95	115-116 (Ethanol)	10.98-10.53 (s, 1H, NH), 8.70-8.44 (s, 1H, NH), 8.08-7.87 (m, 1H, Ph), 7.73-7.16 (m, 4H, Ph), 3.09-2.85 (s, 1H, CH), 2.11-1.68 (s, 2H, CH_2), 1.68-1.43 (m, 12H, CH_2), 1.40-1.04 (m, 12H, CH_2), 0.99-0.61 (m, 3H, CH_3)	176.9, 156.1, 139.8, 129.0, 128.2, 125.9, 67.1, 36.3, 28.8, 28.4, 28.4, 28.3, 28.2, 22.8, 21.7, 13.5	1750, 1700

Table 6. (Continued)

20	100	91-92 (Toluene)	7.74-7.43 (m, 2H, Ph), 7.43-7.10 (m, 3H, Ph), 6.62-6.27 (s, 1H, NH), 5.90-5.60 (s, 1H, NH), 3.54-3.17 (s, 1H, OH), 2.30-2.12 (m, 1H, CH), 2.08-1.89 (m, 1H, CH), 1.56-1.08 (m, 10H, CH_2), 0.94-0.59 (m, 3H, CH_3)	177.0, 142.4, 128.5, 127.8, 125.4, 78.8, 39.2, 31.8, 29.7, 29.2, 23.4, 22.6, 14.1	1660

[a]All compounds were also analyzed by (1) GC/MS (EI, 70 eV), giving one peak in the GC and the expected molecular ion peak, and (2) elemental analysis for C, H, N (within ±0.4% of the calculated value). [b]Compound **20** ^1H NMR taken in $CDCl_3$. [c]Compound **20** ^{13}C NMR taken in $CDCl_3$. [d]Compound reported in ref 28.

Figure 1. Lowest energy conformers similar to the x-ray structure of DPH (blue) are in red and dissimilar in green.

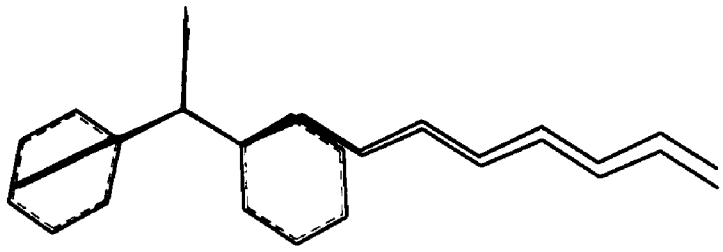

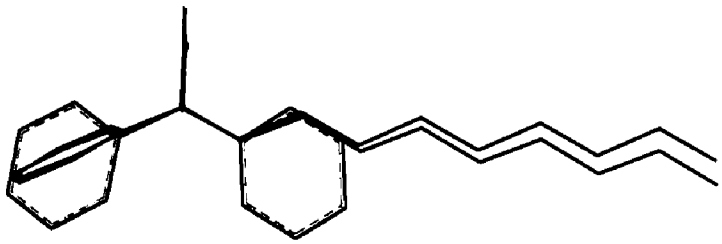

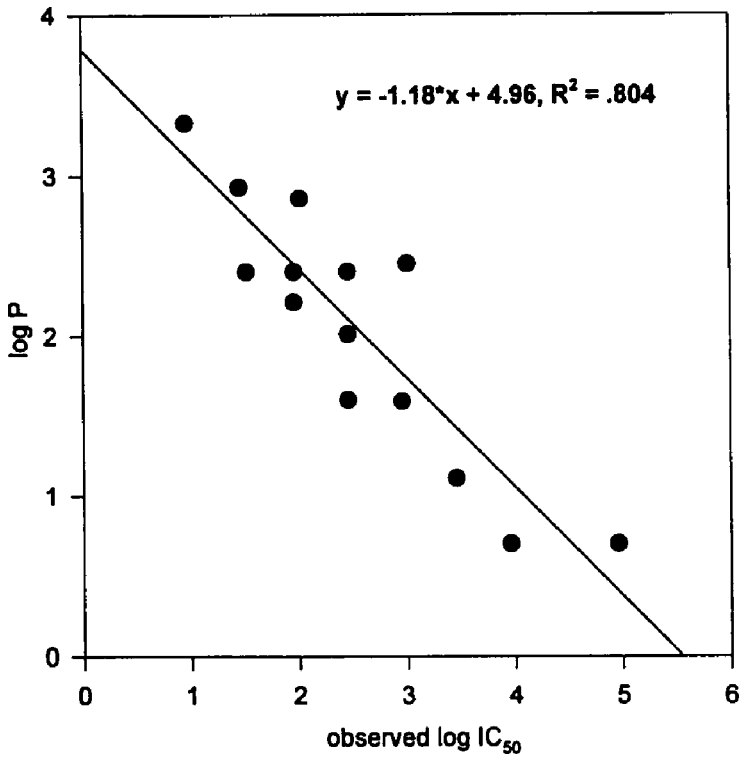

Figure 2. Plot of log *P* versus observed log IC_{50} for the training set.

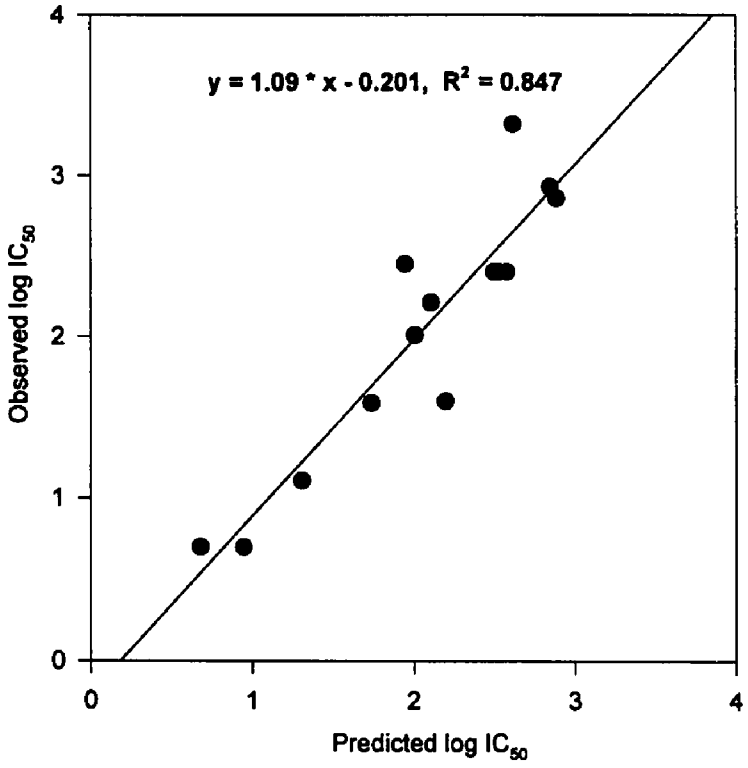

Figure 3. Plot of observed log IC_{50} versus crossvalidated predicted log IC_{50}.

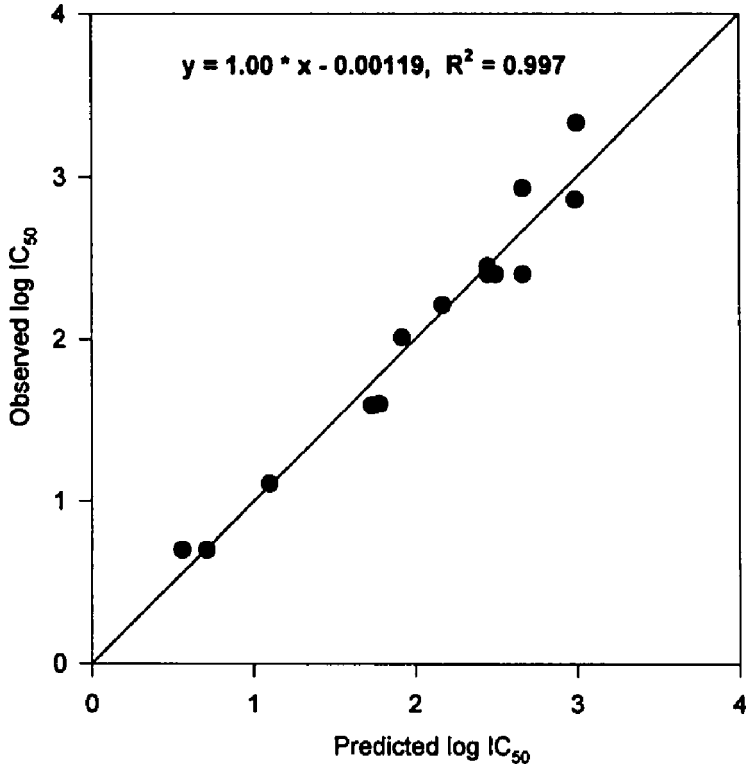

Figure 4. Plot of observed log IC_{50} versus predicted log IC_{50} values from the noncrossvalidated CoMFA model.

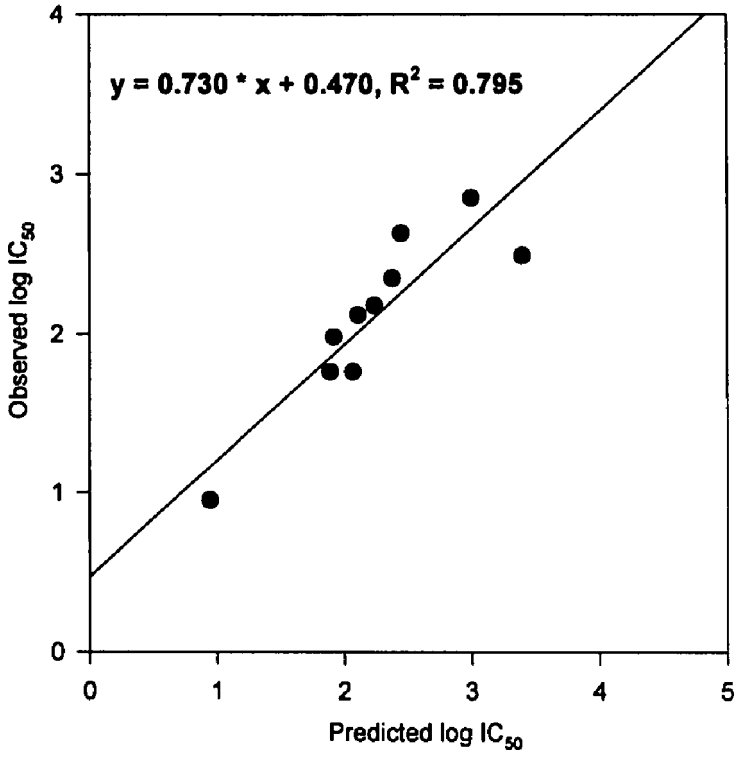

Figure 5. Plot of observed log IC_{50} versus predicted log IC_{50} values for the test set.

Figure 6. Stereoview (relaxed) of the electrostatic CoMFA field for active analog **7** (orange) and inactive analog **9** (green).Increased binding results from placing more (+) charge near blue and (-) charge near red.

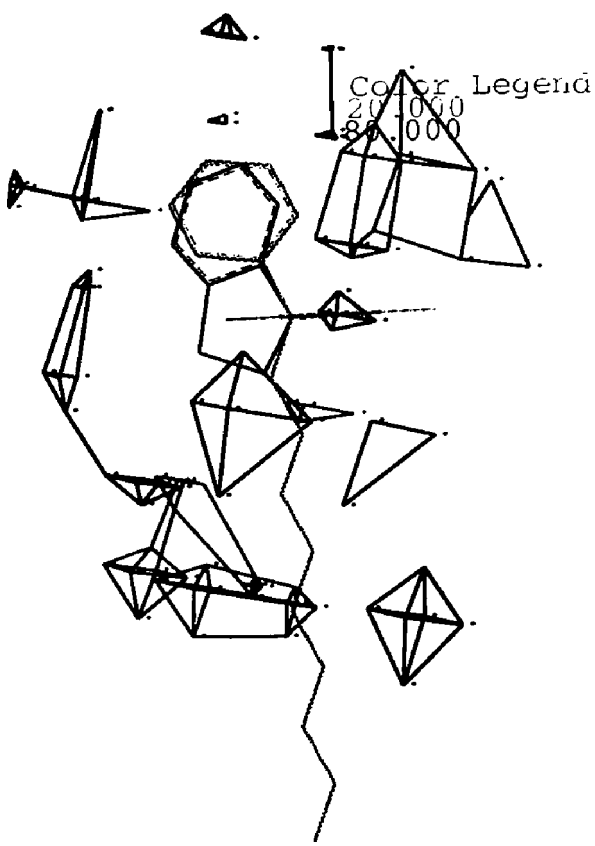
Color Legend
20.000
80.000

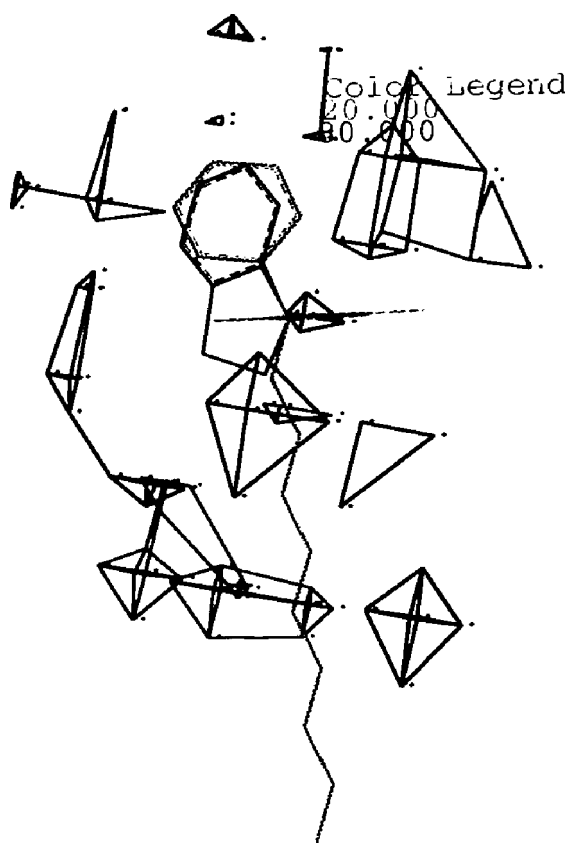
Color Legend
20.000
80.000

Figure 7. Stereoview (relaxed) of the steric CoMFA field showing highly active analog **7** (red) and weakly active **9** (blue). Increased binding results from placing more bulk near green and less bulk near yellow.

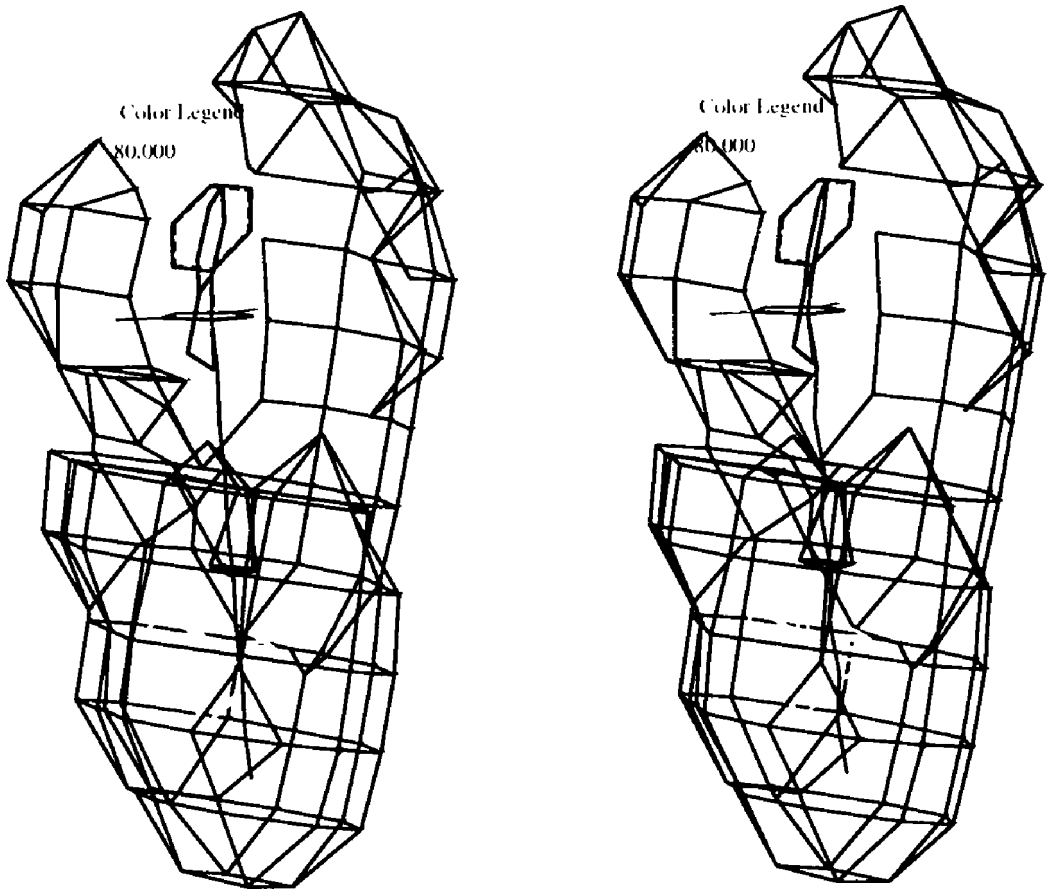
Color Legend
80.000
Color Legend
80.000

Figure 8. Stereoview (relaxed) of the steric CoMFA field showing **14** (blue) and **15** (red), more bulk is favored near green and disfavored near yellow regions.

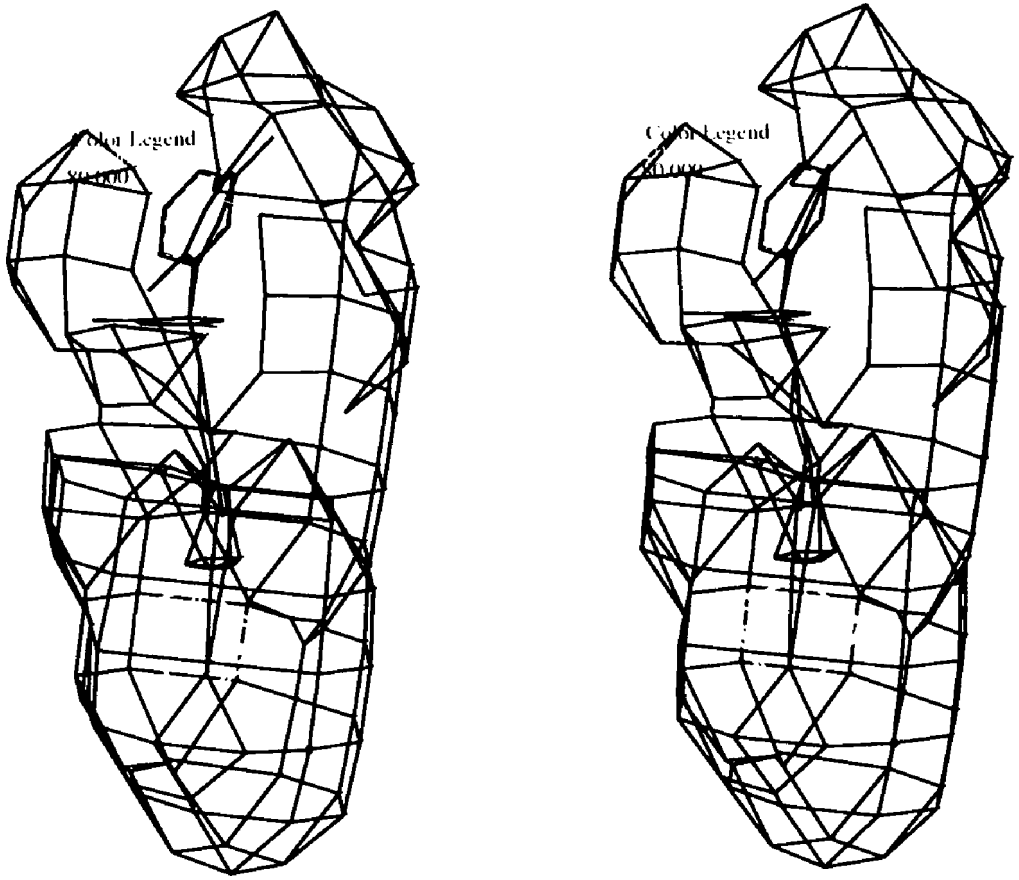

Figure 9. Stereoview (relaxed) of the steric CoMFA field showing analog **20** (red) and DPH (blue), more bulk is favored near green and disfavored near yellow regions.

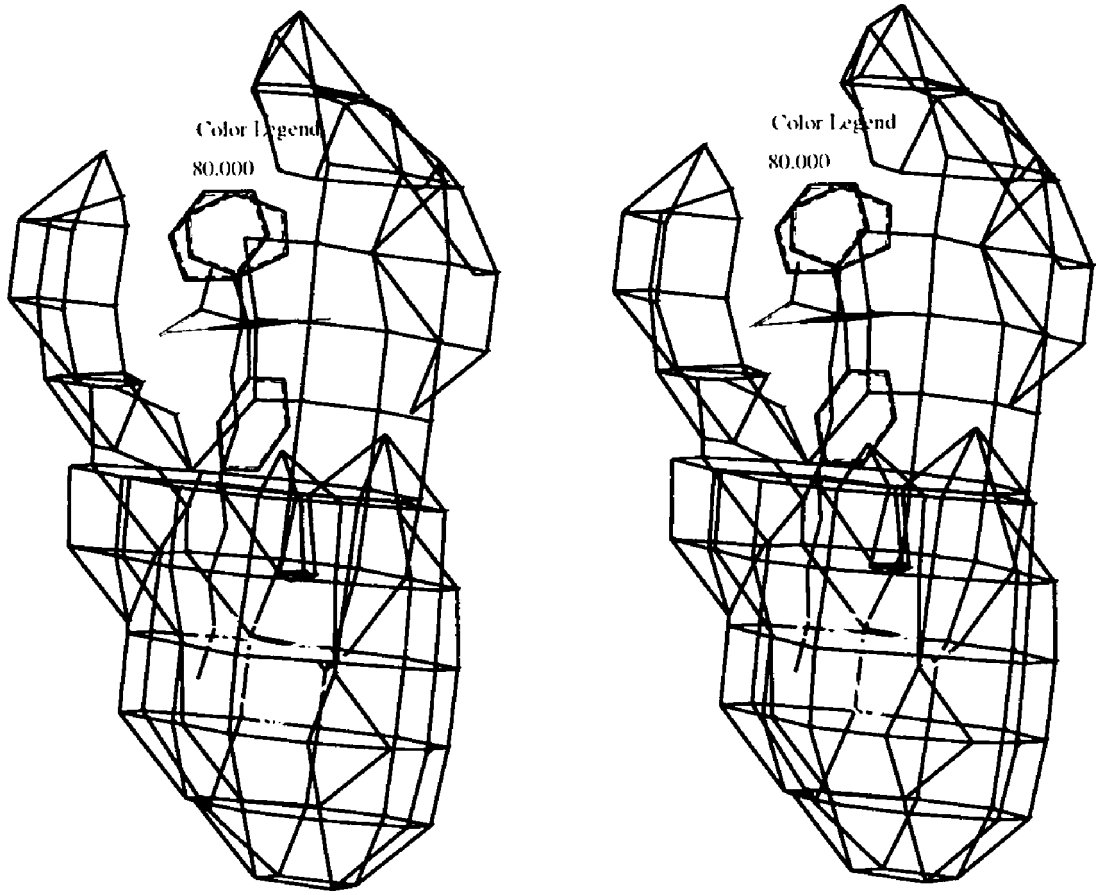
Color Legend
80.000
Color Legend
80.000

Figure 10. Fit of **20** into proposed pharmacophore model.

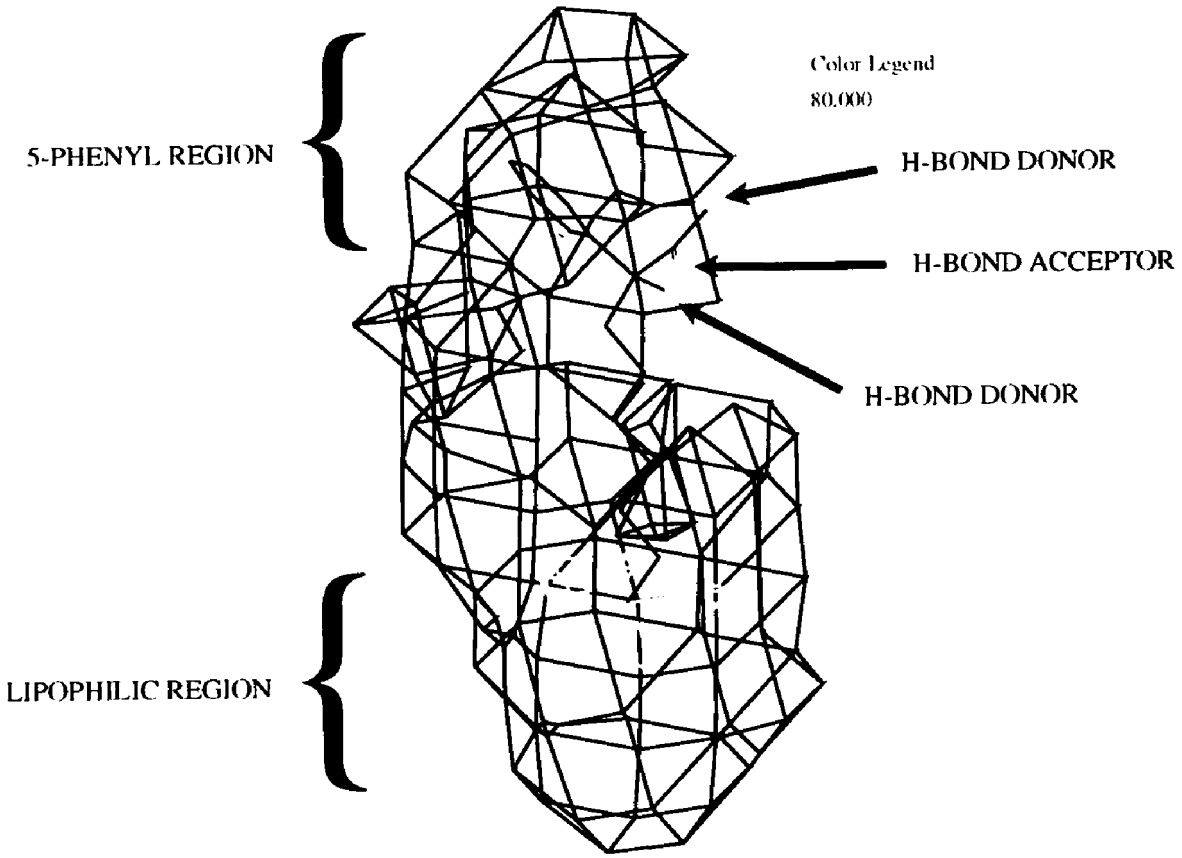
Color Legend
80.000
5-PHENYL REGION
H-BOND DONOR
H-BOND ACCEPTOR
H-BOND DONOR
LIPOPHILIC REGION

Figure 11. Stereoview (relaxed) of steric CoMFA field with CBZ (red) and DPH (blue), more bulk favored near green and disfavored near yellow regions.

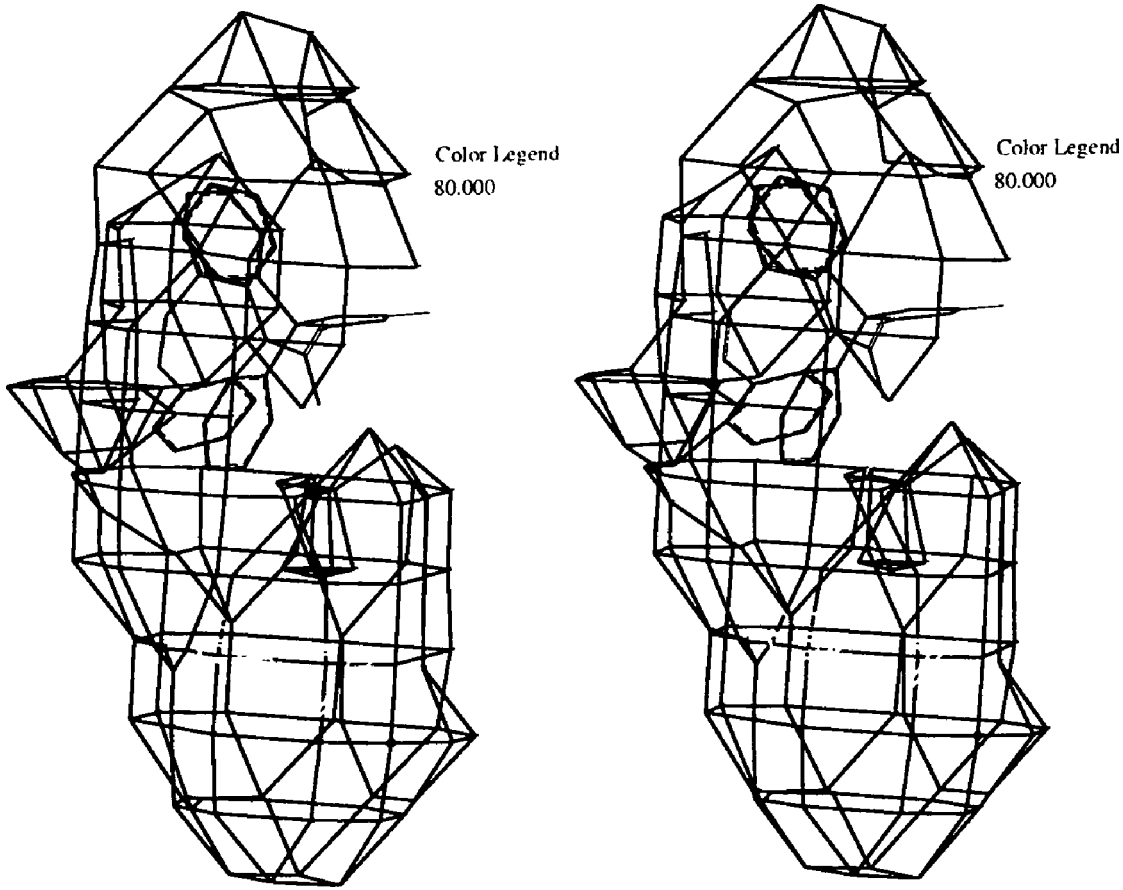
Color Legend
80.000
Color Legend
80.000

Figure 12. Stereoview (relaxed) of steric CoMFA field showing DZP (red) and DPH (blue), more bulk is favored near green and disfavored near yellow regions.

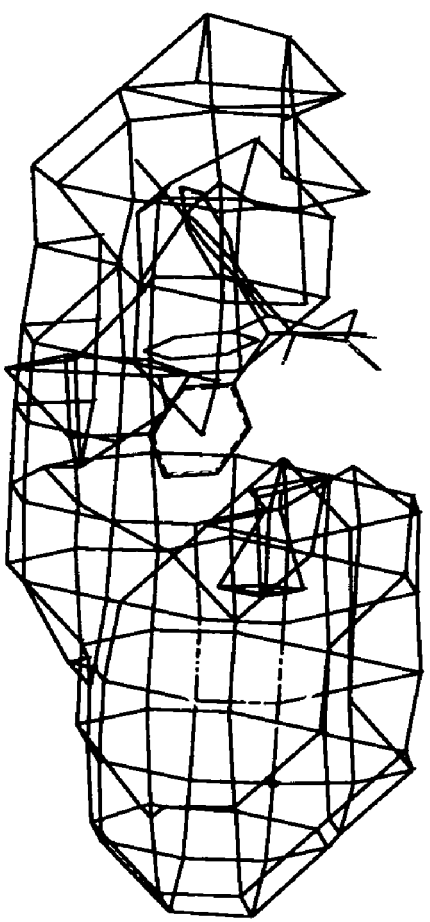
Color Legend
80.000

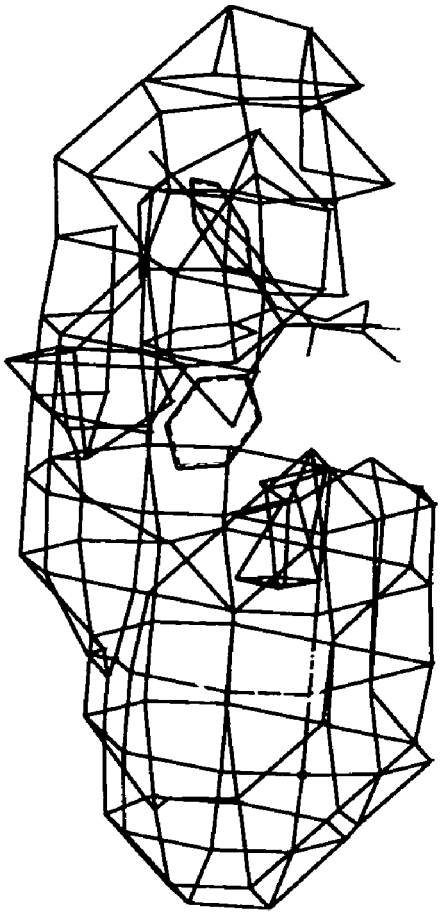
Color Legend
80.000

Figure 13. Stereoview (relaxed) of steric CoMFA showing LDC (red) and DPH (blue), more bulk is favored near green and disfavored near yellow regions.

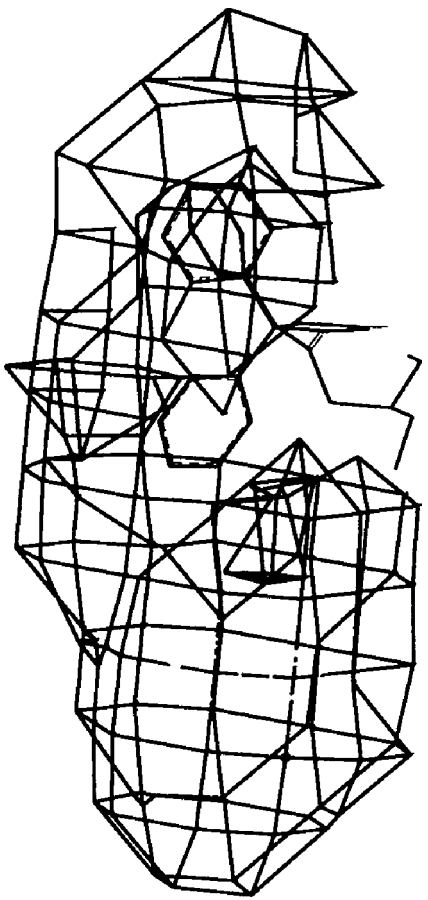

Color Legend

80.000

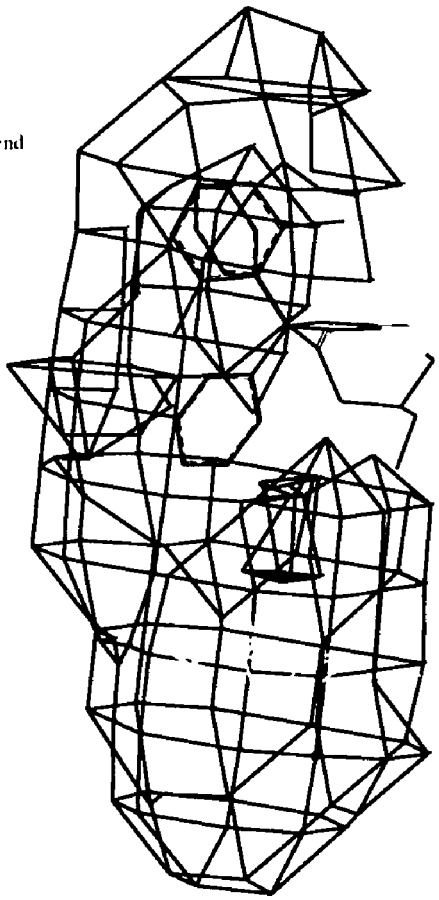

Color Legend

80.000

Scheme 1

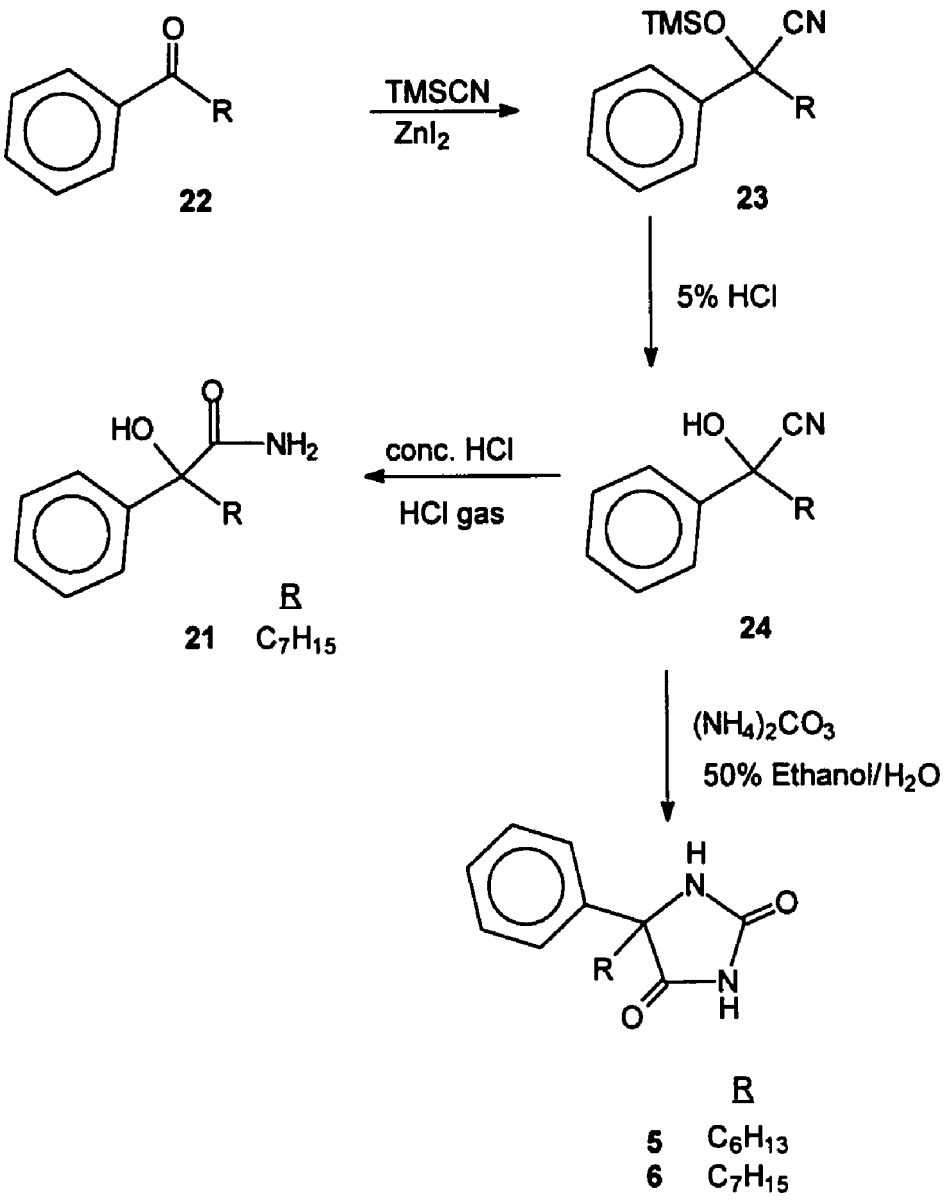
O
R
22
TMSCN
ZnI2
TMSO
CN
R
23
5% HCl
HO
CN
R
24
conc. HCl
HCl gas
HO
O
NH2
R
21
(NH4)2CO3
50% Ethanol/H2O
H
N
O
R
N
H
O
5 C6H13
6 C7H15

Table 7. Analytical Analysis

Compound		%C	%H	%N
6	Theory	68.67	8.45	10.68
	Found	68.65	8.40	10.67
7	Theory	70.30	9.02	9.65
	Found	70.29	8.97	9.64
20	Theory	72.25	9.30	5.62
	Found	72.16	9.25	5.65

MISCELLANEOUS STUDIES ON HYDANTOINS

MILTON L. BROWN,[†] AND WAYNE J. BROUILLETTE[*,†]

Department of Chemistry
University of Alabama at Birmingham, Birmingham, Alabama 35294

---

[*]Address correspondence to this author.
[†]Department of Chemistry, University of Alabama at Birmingham.

Stereochemistry has been a useful property in the development of new modern site-specific agents.[1] The resolution and physiological activities for enantiomers of central nervous system (CNS) active compounds, such as local anesthetics,[2-5] barbiturates,[6] antiarrythmics[7] and anticonvulsants,[8-22] have revealed examples where increased activity was exhibited for one optical isomer. For example, the (S)-enantiomer (ED_{50} = 8.8 mg/kg) of the anticonvulsant 3-amino-1-hydroxy-2-pyrrolidinone prevented tonic extensor seizures from low-intensity electroshock slightly better than the racemate (ED_{50} 13.2 mg/kg) and with 12 times more potency than the R-isomer (ED_{50} =105.9 mg/kg).[19]

The role of the neuronal voltage-sensitive sodium channel (NVSC) has been demonstrated to be of great importance in the mechanisms of anticonvulsant, anesthetic and antiarrhythmic action.[23-27] While local anesthetics[29-31] and antiarrhythmics are reported to bind to a saturable,[32] stereoselective[33-34] specific receptor, an examination of membrane effects for the anticonvulsant diphenylhydantoin (DPH) using fluorescent fatty acid probes[28] implied that DPH may exert an inhibitory effect on the NVSC by simple partitioning into the lipid bilayer. However, conformational preferences[35-38] for hydantoin binding and evidence of saturable[39] binding of DPH to the NVSC are suggestive of a specific hydantoin receptor-ligand interaction.

We have previously been interested in characterizing properties associated with the efficient binding of hydantoins to a specific NVSC receptor. One important stereochemical property yet to be observed for hydantions is enantioselectivity of

binding. To thoroughly investigate the property of stereoselectivity for the hydantoin binding site, we have resolved, by chiral phase high pressure liquid chromatography (HPLC), enantiomers of previously synthesized racemic hydantoins **1** and **2** and evaluated these chiral isomers for the inhibition of ^{3}H-batrachotoxinin A 20-α-benzoate ([^{3}H]-BTX-B) binding to the NVSC. In this study we report and compare the NVSC activity for each enantiomer.

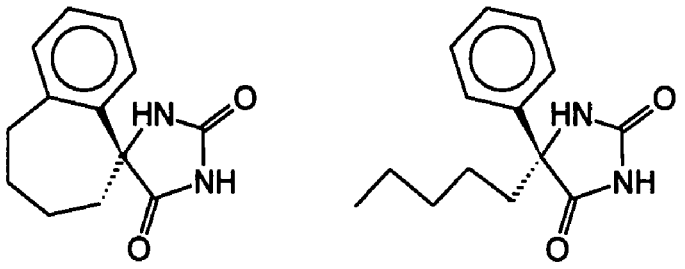

1 **2**

Figure 1. Structures of racemic hydantoin analogs in this study.

Compounds **1** and **2** were previously synthesized as racemates.[36, 37] Racemic mixtures of **1** and **2** were separated into pure enantiomers by chiral HPLC on a 21.2 x 25 cm Chiralcel OJ Column (Daicel Chemical Industries) using 10% ethanol/hexane as eluent. Table 1 lists the HPLC parameters used in this study. Optical rotations listed in Table 2 were recorded on a Perkin Elmer 141 Polarimeter and are the mean of five experiments.

The enantiomers of **1** and **2** were evaluated for relative binding to the NVSC (Table 3) in a previously described[40] in vitro assay using rat cerebral cortex synaptoneurosomes. Results are expressed as IC_{50}, which represents the

micromolar concentration of compound required to allosterically inhibit the specific binding of [^{3}H]-BTX-B by 50%.

The results of this study demonstrate that hydantoins can exhibit stereoselective binding to the NVSC. Here we report two hydantoins, chiral at C5, for which one binds with modest stereoselectivity to the hydantoin site located in the NVSC. NVSC inhibition (Table 3) for the enantiomers of spirohydantoin **1** revealed a 3-fold difference between binding potencies (the IC_{50} of (+)-**1** = 219 μM and the IC_{50} of (-)-**1** = 78 μM). However, the NVSC binding affinity for enantiomers of 5-pentyl-5-phenylhydantoin **2** (the IC_{50} of (+)-**2** = 17 μM and the IC_{50} of (-)-**2** = 38 μM) were statistically the same. These results reveal an enantioselective preference for the (-) stereoisomer of spirohydantoin **1**, revealing a property characteristic of interactions with a specific receptor.

Table 1. Chiral Separation Data

	HPLC parameters[a, b]				
compound	injection conc. (mg/mL)	flow rate (mL/ min.)	injection (μL)	wave length (nM)	retention time (min)
1	57.5	2	350	270	(+) = 33.78 (-) = 42.55
2	4	2	100	270	(+) = 33.78 (-) = 38.13

[a]Column: Chiralcel OJ (Daicel Chemical Industries). [b]Solvent: 10% ethanol/hexane; Column size: 21.2 x 25 cm

Table 2. Optical Rotation Data

compound	$[\alpha]_D^{21.5}$	cell conc. (g/mL)	solvent (temp)
(+)-**1**	+94.3	0.0082	MeOH (21.5)
(-)-**1**	-96.3	0.012	MeOH (21.5)
(+)-**2**	+31.2	0.0146	MeOH (21.5)
(-)-**2**	-32.6	0.0105	MeOH (21.5)

Table 3. Sodium Channel Binding for Enantiomers of Compounds **1** and **2**

compound	sodium channel-binding data IC_{50} (μM)
(±)-**1**	251 [225-280][a]
(+)-**1**	219 [138-347][a]
(-)-**1**	78 [53-114][a]
(±)-**2**	39 [32-47][a]
(+)-**2**	17 [14-22][b]
(-)-**2**	38 [22-65][b]

[a]Sodium channel assay performed three times, with each concentration in triplicate. [b]Sodium channel assay performed one time, with each concentration in triplicate.

A second study involved calculations of lipophilicity. Numerical descriptions of a compound's lipophilic character are much needed in assessing its biological activity. Calculations of partition coefficients (*P*), usually expressed as log *P*, represent the classical approach for assigning numerical values to a compound's lipid solubility. One very common method of calculating log *P* has been the shake-flask method, which provides the equilibrium octanol/water distribution (a measurement of the ratio of drug concentration in octanol versus water). A

problem with this common method is that some classes of compounds, especially hydantoins, are poorly soluble in the octanol/water solvent system. Low solubility renders this method inadequate in evaluating the lipophilic character of our compounds.

To overcome solubility problems, chromatographic methods can be employed, such as liquid/solid reverse phase systems. These systems generally have a chemically bonded alkylsilica (typically octadecylsilane) as a stationary phase and aqueous methanol or acetonitrile as the eluent.

Hydantoins and other classes of compounds have been assigned a numerical value describing lipophilic character through chromatographic techniques. Specifically DPH was assigned a log *P* value using a Hypersil ODS (5 μM) column. A log *P* calculation by HPLC methods[41, 42] involves the following equation: $\log P = \log k + \log (t_r + t_o)/ t_o$ where t_r is the retention time of the compound, t_o is the retention time of the unretained compound and k is the constant for the column.

Alternatively, with the increased development of computer programs, theoretical calculations of log *P* values are now possible. In particular, the Quantum Chemistry Program Exchange (QCPE) (program #608) creates tremendous advantages in that computer calculations are not limited by solubility problems or column types in determining log *P*, therefore, extending the ability of the researcher to characterize and assign numerical values to the liphilic character of endless classes of compounds.

Thus in this study we used chromatographic techniques to calculate log *P* values for hydantoins and correlated experimental data with theoretical values obtained from the QCPE #608 program (Table 4). Preliminary comparisons demonstrate reasonable correlation between the theoretical (QCPE) and experimental (HPLC) values for these hydantoin analogs.

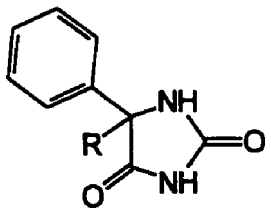

	R
1	C_2H_5
2	C_3H_7
3	C_4H_9
4	C_5H_{11}
DPH	C_6H_5

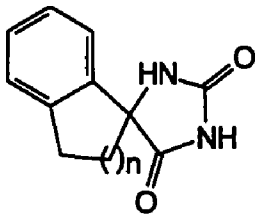

	n
5	1
6	2
7	3
8	4

Figure 2. Compounds used in log *P* calculation.

Table 4. Calculation of Log *P* by HPLC Methods and QCPE

Compound	Measured HPLC Log *P*[a]	Calculated QCPE #608 Log *P*	Measured Literature Log *P*
1	2.33	1.57	1.53[b]
2	2.36	2.11	
3	2.84	2.65	
4	3.11	3.19	
5	2.17	0.99	
6	ND[b]	1.50	

Table 4. (Continued)

7	2.63	2.05	
8	2.74	2.60	
DPH	2.68	2.64	2.47[b]

[a]The standard for k calculation was benzene (log *P* = 2.13). [b]Ref 43.
[b]ND = not determined.

Acknowledgments

This work was taken in part from the PhD dissertation submitted in partial fulfillment of the requirements for the PhD degree in Organic Chemistry by M.L.B. M.L.B gratefully acknowledges financial support from the Patricia Robert Harris Fellowship, the National Consortium for Educational Access, the UAB Comprehensive Minority Faculty Development Program and the UAB Department of Chemistry. We also thank Mr. Audray Harris, 1992 Alabama Alliance for Minority Participation (AMP) Summer Intern, for technical support.

References

(1) Gross, M. Significance of Drug Stereochemistry in Modern Pharmaceutical Research and Development. *Annual Reports in Medicinal Chemistry* **1989**, *25*, 323-331.

(2) Portig, J.; Stein, K.; Vohland, H. W. Preferential Distribution of Alpha-Hexachlorohexane in Cerebral White Matter. *Xenobiotica*. **1989**, *19*, 123-130.

(3) Hinko, C. N.; Crider, A. M.; Wood, J. D. A Comparison of Prodrug Esters of Nipecotic Acid. *Neuropharmacology*. **1988**, **27**, 475-483.

(4) Fischer, W.; Lasek, R.; Muller, M. Anticonvulsant Effects of Propranolol and Their Pharmacological Modulation. *Polish Journal of Pharmacol. and Pharm.* **1985**, *37*, 883-896.

(5) Sheldon, R. S.; Cannon, N. J.; Nies, A. S.; Duff, H. J. Stereospecific Interaction of Tocainide with the Cardiac Sodium Channel. *Mol. Pharmacol.* **1988**, *33*, 327-331.

(6) Andrews, P. R.; Mark, L. C. Structural Specificity of Barbituates and Related Drugs. *Anesthesiology*. **1982**, *57*, 314-320.

(7) Tricarico, D.; Fakler, B.; Spittelmeister, W.; Ruppersberg, J. P.; Stützel, R.; Franchini, C.; Tortorella, V.; Conte-Camerino, D.; Rüdel, R. Stereoselective Interaction of Tocainide and its Chiral Analogs with the Sodium Channels in Human Myoballs. *Pflügers Arch.* **1991**, *418*, 234-237.

(8) Küpfer, A.; Patwardhan, R.; Ward, S.; Schenker, S.; Preisig, R.; Branch, R. A. Stereoselective Metabolism and Pharmacokinetic Control of 5-Phenyl-5-Ethylhydantoin (Nirvanol) in Humans. *J. Pharmacol. Exp. Ther.* **1984**, *230,* 28-33.

(9) Arnoldi, A.; Bonsignori, A.; Melloni, P.; Merlini, L.; Quadri, M. L.; Rossi, A. C.; Valsecchi, M. Synthesis and Anticonvulsant and Sedative-Hypnotic Activity of 4-(Alkylimino)-2,3-dihydro-4H-1-Benzopyrans and -Benzothiopyrans. *J. Med. Chem.* **1990**, *33*, 2865-2869.

(10) Rey, E.; Pons, G.; Olive, G. Vigabatrin. Clinical Pharmacokinetics. *Clinical Pharmacokinetics.* **1992**, *23*, 267-278.

(11) Dudley, K. H.; Butler, T.C. ; Buis, D. L. The Role of Dihydropyrimidinase in the Metabolism of Some Hydantoin and Succinimide Drugs. *Drug Metabolism and Disposition.* **1974**, *2*, 103-112.

(12) Küpfer, A.; Lawson, J.; Branch, R. A. Steroselectivity of the Arene Epoxide Pathway of Mephenytoin Hydroxylation in Man. *Epilepsia.* **1984**, *25*, 1-7.

(13) Kwon, C-H.; Iqbal, M. T.; Wurpel, J. N. D. Synthesis and Anticonvulsant Activity of 2-Iminohydantoins. *J. Med. Chem.* **1991**, 34, 1845-1849.

(14) Conley, J. D.; Kohn, H. Functionalized D,L-Amino Acid Derivatives. Potent New Agents for the Treatment of Epilepsy. *J. Med. Chem.* **1987**, *30*, 567-574.

(15) Garske, G. E.; Palmer, G. C.; Napie, J. J.; Griffith, R. C.; Freedman, L. R.; Harris, E. W.; Ray, R.; McCreedy, S. A.; Blosser, J. C.; Woodhead, J. H. *Epilepsy Res.* **1991**, *9*, 161-174.

(16) Kohn, H.; Conley, J. D.; Leander, J. D. Marked Stereospecificity in a New Class of Anticonvulsants. *Brain Res.* **1988**, *457*, 371-375.

(17) Shen, D. D.; Levy, R. H.; Savatch, J. L.; Boddy, A. V.; Tombret, F.; Lepage, F. Comparative Anticonvulsant Potency and Pharmacokinetics of (+)- and (-) Enantiomers of Stiripentol. *Epilepsy Res.* **1992**, *12*, 29-36.

(18) Knabe, J. Untersuchungen zur Enantioselektivität von Wirkstoffen. *Arzeim. Forsch./Drug Res.* **1989**, *39*, 1379-1384.

(19) Vartanian, M. G.; Taylor, C. P. Different Stereoselectivity of the Enantiomers of HA-966 (3-Amino-1-Hydroxy-2-Pyrrolidinone) for Neuroprotective and Anticonvulsant Actions In Vivo. *Neuroscience Lett.* **1991**, *133*, 109-112.

(20) Kohn, H.; Sawley, K. N.; Legall, P.; Conley, J. D.; Robertson, D. W.; Leander, J. D. Preparation and Anticonvulsant Activity of a Series of Functionalized Alpha-Aromatic and Alpha-Heteroaromatic Amino Acids. *J. Med. Chem.* **1990**, *33*, 919-926.

(21) Chatterjie, N.; Alexander, G. J. Anticonvulsant Properties of Spirohydantoins Derived from Optical Isomers of Camphor. *Neurochemical Res.* **1986**, *12*, 1669-1676.

(22) Brouillette, W. J.; Grunewald, G. L.; Brown, G. B.; Delorey, T. M.; Akhtar, M. S.; Liang, G. Sodium Channel Binding and Anticonvulsant Activities for the Enantiomers of a Bicyclic 2,4-Oxazolidinedione and Monocyclic Models. *J. Pharm. Sci.* **1989**, *32*, 1577-1580.

(23) Jan, L. Y.; Jan, Y. N. Voltage-Sensitive Ion Channels. *Cell.* **1989**, *56*, 13-25.

(24) Triggle, D. J.; Langs, D. A. Ligand Gated and Voltage-Gated Ion Channels. *Ann. Reports in Med. Chem.* **1989**, *25*, 225-234.

(25) Kallen, R. G.; Cohen, S. A.; Barchi, R. L. Structure, Function and Expression of Voltage-Dependent Sodium Channels. *Mol. Neurobiology.* **1994**, *7*, 383-428.

(26) Trimmer, J. S.; Agnew, W. S. Molecular Diversity of Voltage-Sensitive Na Channels. *Annu. Rev. Physiol.* **1989**, *51*, 401-18.

(27) Catterall, W. A. Common Modes of Drug Action on Na^+ Channels: Local Anesthetics, Antiarrhythmics and Anticonvulsants. *TIPS.* **1987**, *8*, 57-65.

(28) Harris, W. E.; Stahl, W. L. Interactions of Phenytoin with Rat Brain Synaptosomes Examined by Flourescent Fatty Acid Probes. *Neurochem. Int.* **1988**, *13*, 369-377.

(29) Sheldon, R. S.; Hill, R. J.; Taouis, M.; Wilson, L. M. Aminoalkyl Structural Requirements for Interaction of Lidocaine with the Class I Antiarrhythmic Drug Receptor on Rat Cadiac Myocytes. *Mol. Pharmacol.* **1991**, *39*, 609-614.

(30) Hill, R. J.; Thakore, E.; Taouis, M.; Duff, H. J.; Sheldon, R. S. Transcainide: Biochemical Evidence for State-Dependent Interaction with the Class I Antiarrhythmic Drug Receptor. *Eur. J. Pharm.* **1991**, *203*, 51-58.

(31) Rock, D. M.; McLean, M. J.; Macdonald, R. L.; Catterall, W. A.; Taylor, C. P. Ralitoline (CI-946) and CI-953 Block Sustained Repetitive Sodium Action Potentials in Cultured Mouse Spinal Cord Neurons and Displace Batrachotoxinin-A 20-α-Benzoate Binding In Vitro. *Epilepsy Res.* **1991**, *8*, 197-203.

(32) Thomsen, W.; Hays, S. J.; Hicks, J. L.; Schwarz, R. D.; Catterall, W. A. Specific Binding of the Novel Na+ Channel Blocker PD85,639 to the α-Subunit of Rat Brain Na^+ Channels. *Mol. Pharmacol.* **1993**, *43*, 955-64.

(33) Wang, G. K. Binding Affinity and Stereoselectivity of Local Anesthetics in Single Batrachotoxin-Activated Na^+ Channels. *J. Gen. Physiol.* **1990**, *96*, 1105-1127.

(34) Wang, G. K.; Wang, S. Y. Altered Stereoselectivity of Cocaine and Bupivacaine Isomers in Normal and Batrachotoxin-Modified Na^+ Channels. *J. Gen. Physiol.* **1992**, *100*, 1003-1020.

(35) Brouillette, W. J.; Brown, G. B.; Delorey, T. M.; Liang, G. Sodium Channel Binding and Anticonvulsant Activities of Hydantoins Containing Conformationally Constrained 5-Phenyl Substituents. *J. Pharm. Sci.* **1990**, *79*, 871-874.

(36) Brouillette, W. J.; Jestkov, V.P.; Brown, M. L.; Aktar, M. S.; Delorey, T. M.; Brown, G. B. Bicyclic Hydantoins with Bridgehead Nitrogen. Comparison of Anticonvulsant Activities with Binding to the Neuronal Voltage-Dependent Sodium Channel. *J. Med. Chem.* **1994**, *37*, 3289-3293.

(37) Brown, M. L.; Brouillette, W. J.; Brown, G. B. Hydantoins with Conformationally Restricted Phenyl Rings. Effects on Sodium Channel Binding. *PhD Dissertation of Milton Brown.*

(38) Brown, M. L.; Van Dyke, C. C.; Brown, G. B.; Brouillette, W. J. Comparative Molecular Field Analysis of Hydantoin Binding to the Neuronal Voltage-Dependent Sodium Channel. *PhD Dissertation of Milton Brown.*

(39) Francis, J.; Burnham, W. M. [^{3}H]Phenytoin Identifies a Novel Anticonvulsant-Binding Domain on Voltage-Dependent Sodium Channels. *Mol. Pharmacol.* **1992**, *42*, 1097-1103.

(40) Brouillette, W. J.; Brown, G. B.; Delorey, T. M.; Shirali, S. S. ; Grunewald, G. L. Anticonvulsant Activities of Phenyl-Substituted Bicyclic 2,4-Oxazolidinediones and Monocyclic Models. Comparison with Binding to the Neuronal Voltage-Dependent Sodium Channel. *J. Med. Chem.* **1988**, *31*, 2218-2221.

(41) McCall, J. M. Liquid-Liquid Partition Coefficients by High-Pressure Liquid Chromatography. *J. Med. Chem.* **1975**, *18*, 549-552.

(42) Mirrlees, M. S.; Moulton, S. J.; Murphy, C. T.; Taylor, P. J. Direct Measurement of Octanol-Water Partition Coefficients by High-Pressure Liquid Chromatography. *J. Med. Chem.* **1976**, *19*, 615-618.

(43) Lien, E. Structure-Activity Correlations for Anticonvulsant Drugs. *J. Med. Chem.* **1970**, *13* ,1189-1191.

SYNTHESIS AND ANTICONVULSANT ACTIVITIES OF PHENYL-SUBSTITUTED α-HYDROXY-α-PHENYLCAPROLACTAMS AND α-ALKYL-α-HYDROXY-α-PHENYLAMIDES

MILTON L. BROWN, GANG LIANG AND WAYNE J. BROUILLETTE*

Department of Chemistry,
University of Alabama at Birmingham, Birmingham, AL 35209.

* Address correspondence to this author.

Abstract

This study investigated the effects of *ortho*, *meta* and *para* electron withdrawing (-Cl) and donating (CH_3O-) substituents on the anticonvulsant activity of α-hydroxy-α-phenyllactams. α-Hydroxy-α-(4-chloropheny)caprolactam (**7**), administered orally in rats, exhibited good anti-MES anticonvulsant activity (ED_{50} 21.8 mg/kg) and therapeutic protection (anti-MES T. I. >11.5), suggesting this compound as a new anticonvulsant with clinical potential. Preliminary anticonvulsant data for several α-alkyl-α-hydroxy-α-phenylamides suggested that a seven carbon side chain may be the optimum alkyl length for anticonvulsant activity within this class. Unlike α-alkyl-α-hydroxy-α-phenylamides, which act at the neuronal voltage-sensitive sodium channel (class I mechanism), a mechanism of anticonvulsant activity for α-hydroxy-α-phenyllactams not yet to been determined. A variety of receptor binding studies for α-hydroxy-α-phenyllactams were explored in an effort to identify a mechanism of action, but none of these revealed significant activity. α-Hydroxy-α-phenyllactams **1-4**, synthesized[1] by this laboratory as precursors of anticonvulsants called "smissmanones", were previously evaluated for anticonvulsant activity[2] in mice. Compound **1** demonstrated good anticonvulsant activity (MES ED_{50} = 63 mg/kg and scMET ED_{50} = 74 mg/kg) and exhibited a favorable anti-MES T.I. (anti-MES therapeutic index (T.I.) = 3.3, Table 2), as compared to phenacemide (anti-MES T.I. = 4.8, Table 2), a structurally similar prescribed anticonvulsant. Thus the demonstration of promising anti-MES activity

and the ready availability of starting materials suggested **1** as a candidate for further development.

Structure-activity relationship (SAR) data for lactam analogs of **1** (**2**, **3** and **4**, Table 2) revealed increased anti-MES activity for ring sizes greater than 6 carbons. With limited SAR for parent **1**, a preliminary investigation into the effects of α-phenyl substitutions (-Cl and $-OCH_3$) on anticonvulsant activity was undertaken for the 2-oxo-3-phenyl-3-oxyhexahydroazepine **1**. A comparison of anticonvulsant activities for chlorophenyl and methoxyphenyl analogs **5-10** in relation to substituent and log *P* effects will be discussed.

A preliminary investigation[2] into a mechanism of action for **1** evaluated binding to the neuronal voltage-dependent sodium channel (NVSC), but only weak binding affinity was observed. In order to investigate other potential mechanism(s) of action, compound **1** was submitted to the Novascreen/National Institutes of Mental Health Psychotherapeutic Drug Discovery and Development Program to ascertain binding affinity for the 4-aminobutyric acid ($GABA_A$ and $GABA_B$), N-methyl-D-aspartate (NMDA), glycine (inhibitory and excitatory) and benzodiazepine receptors.

Similar in structure to cyclic α-hydroxy-α-phenyllactams are the lactam-ring opened analogs α-alkyl-α-hydroxy-α-phenylamides. α-Alkyl-α-hydroxy-α-phenylamides like atrolactamide, a clinically prescribed anticonvulsant, have displayed significant anticonvulsant activity. Atrolactamide exhibited anticonvulsant action against both electrical and leptazol challenges[3] and was clinically effective in

treating grand mal seizures. However, significant side effects[3] limited the therapeutic use of this anticonvulsant.

α-Hydroxy-α-phenylnonanamide (**11**), designed from a previously reported NVSC CoMFA model,[4] exhibited good preliminary anti-MES activity in mice (Table 2). This compound also exhibited potent binding to the NVSC (Table 4), thus providing a potential mechanism of anticonvulsant action for this structural class.[4] To further investigate anticonvulsant trends for this structural class, compounds **12** and **13**, which have increased log *P*, were synthesized and screened for anticonvulsant activity in mice. Comparisons of preliminary anticonvulsant data for **11-13** will also be discussed.

Chemistry

Figure 1 provides the structures of analogs evaluated in this study. Compounds **5-10** were synthesized[1] from caprolactam using procedures previously reported for **1**. The synthesis of **11** was previously reported.[4] New analogs **12** and **13** were prepared by reacting cyanotrimethylsilane with the corresponding phenylalkylketone, followed by acid hydrolysis of the cyanohydrin to yield the α-hydroxyamide.[5] Table 1 provides selected data for newly synthesized targets.

Biology. Compounds **5-10** and **11-13** were evaluated as anticonvulsants in mice by the Anticonvulsant Drug Development Program, which was conducted by the Epilepsy Branch of the National Institutes of Neurological and Communicative Disorders and Stroke. In this screening procedure, which has been described in detail,[6] candidate compounds are first subjected to a qualitative screen (phase I) in

a small number of mice (1-4) at dose levels of 30, 100 and 300 mg/kg. The ED_{50} and TD_{50} values are obtained for active compounds in Phase II.

Phase I, employs the use of two anticonvulsant models that measure activity against subcutaneous metrazol-induced (scMET) and maximal electroshock-induced (MES) seizures, as well as a rotorod toxicity assay. Protection from these challenges was recorded as an ED_{50} (the effective dose of compound needed to protect 50% of the mice) for scMET and MES activities and a TD_{50} (the dose of compound needed to express toxicity in 50% of the mice) for rotorod toxicity.

In order to investigate possible mechanisms of action, we have evaluated compounds **1** and **11** as inhibitors of binding of ^{3}H-batrachotoxinin A 20-α-benzoate (^{3}H-BTX-B) to the NVSC. ^{3}H-BTX-B binds to neurotoxin site 2 in the NVSC. The inhibition of binding to this site is expressed as sodium channel IC_{50} values listed in Table 4 (IC_{50} represents the concentration of compound required to displace specifically bound [^{3}H]-BTX-B by 50%).

Further in vitro investigations into potential mechanism(s) of action for the anticonvulsant **1** were conducted by the Novascreen/National Institutes of Mental Health Psychotherapeutic Drug Discovery and Development program. In this manner, relative binding activities for **1** to the 4-aminobutyric acid ($GABA_A$ and $GABA_B$), the N-methyl-D-aspartate (NMDA), the glycine (inhibitory), the glycine (excitatory) and the benzodiazepine binding sites in rat or bovine brain were measured. The binding value for each assay is reported as the percent inhibition of specific binding of a radioligand by compound **1** at a 10^{-5} M concentration.

Results and Discussion

Phase I data (Table 2) for **5-7** suggest that compounds with electron withdrawing groups (Cl) in the *ortho, meta* and *para* positions are roughly equipotent against MES challenges. But only the *ortho* or *para* substituted compounds, **5** and **7**, showed separation between toxicity and anti-MES activity. Compounds **5-7** demonstrated similar preliminary potency against scMET activity compared to parent lactam **1**, but little separation between anti-scMET and toxicity was observed. Due to only moderate activity in Phase I and indications of little separation between activity and toxicity, these compounds were not further pursued in mice.

Analog **7** was further screened for oral anticonvulsant activity in rat model (Table 3). The ED_{50} from this assay was 21.8 mg/kg. Compound **7** also exhibited significant separation between toxicity and anti-MES activity in the rat, and a T.I. greater than 11.5 suggested that **7** may have clinical potential as an anticonvulsant agent.

Preliminary anticonvulsant data in mice (Table 2) for analogs **8-10**, which contain electron donating (OCH_3) substituents, implicated only the *para* substituted analog **10**, as providing anti-MES activity at 100 mg/kg or less. Separation of anticonvulsant activity from toxicity was exhibited by **10** for only anti-MES activity. Furthermore, **8-10** did not demonstrate scMET potency at concentrations of 100 mg/kg or less. Thus these compounds were not further pursued.

For the α-alkyl-α-hydroxy-α-phenylamides **12** and **13**, MES and scMET activity appeared to be less than that for **11** (Table 2), suggesting that the shorter

seven carbon side chain may be the optimum alkyl length for anticonvulsant activity. Compound **12** demonstrated toxicity at the same concentration for which it protected against scMET and MES activity (Table 2). Compound **13** was less toxic but only marginally active in the anticonvulsant screens. Since amide **11** was the most promising in this series, it was selected for Phase II quantification in mice. While possessing moderately good anticonvulsant activities in MES and scMet assays, the T.I. was nearly 1 in both cases.

As of yet, a mechanism of action for α-hydroxy-α-phenyllactams has not been determined. In vitro binding data (Table 4) suggest that α-hydroxy-α-phenyllactams do not exert anticonvulsant effects by class I (neuronal voltage-dependent sodium channel) or class II ($GABA_A$ and $GABA_B$) mechanisms. Furthermore, α-hydroxy-α-phenyllactams do not exhibit any activity at the NMDA, the glycine (inhibitory and excitatory) and the benzodiazepine receptors (Table 4). Further studies into the mechanism of action are underway.

The α-alkyl-α-hydroxy-α-phenylamide **11** binds potently to the NVSC (Table 4).[4] This suggests a class I mechanism of action for this structural type.

Finally, differences in lipophilicity between Cl- and CH_3O-substituted phenyllactam analogs **5-10** and α-alkyl substituents for amides **11-13** were considered as a possible rationale for variations in binding potency within each series of analogs. Thus we estimated the log *P* values in Table 2 using reported experimentally measured log *P* values for the parent structure 2-hydroxy-2-phenylbutanamide (log *P* = 1.20),[14] to which were added the appropriate π values

to provide the final log *P*. The π values used were 0.50 for each CH_2 or CH_3 in the alkyl chain, -0.50 for ring closure, 0.56 for N-CH_3[15] and 2.13 for phenyl rings.[16] For *ortho*, *meta* or *para* Cl or OCH_3 phenyl substitutions (*ortho*-OCH_3 = 0.84, *meta*-OCH_3 = 0.85, *para*-OCH_3 = 0.00), the appropiate literature value[16] was added. For example, the log *P* of 2-hydroxy-2-phenylnonanamide **11** was calculated as log P_{parent} + 4 x ($\pi_{Methylene}$) + π_{Methyl} + = 1.20 + 4 x (0.50) + 0.50 = 3.70. Likewise, the α-hydroxy-α-phenyllactam **5** was calculated as the log $_{parent}$ + $\pi_{Methylene}$ + $\pi_{N\text{-}Methyl}$ + $\pi_{ring\ closure}$ + $\pi_{ortho\text{-}Cl}$ = 1.20 + 0.50 + 0.56 + (-0.50) + 0.84 = 2.60. The results suggest that log *P* and anticonvulsant activity did not correlate for α-hydroxy-α-phenyllactams. For α-alkyl-α-hydroxy-α-phenylamides in this study, preliminary anticonvulsant activity did not increase with enhanced log *P*.

In conclusion, good anti-MES anticonvulsant activity and therapeutic protection demonstrated by the α-hydroxy-α-phenyllactam **7**, suggest this compound as a potential clinical anticonvulsant agent. Unlike α-alkyl-α-hydroxy-α-phenylamides, which act at the NVSC (class I mechanism), a mechanism of anticonvulsant activity for α-hydroxy-α-phenyllactams has yet to be determined. Thus the results of mechanistic binding studies for α-hydroxy-α-phenyllactams may be suggestive of a novel mechanism of action.

Experimental Section

Melting points were recorded on an Electrothermal melting apparatus and are uncorrected. IR spectra were recorded on a Beckman Acculab 6 and Nicolet IR/42 spectrometers, and elemental analyses were performed by Atlantic Microlabs of

Norcross, GA. ^{1}H NMR and ^{13}C NMR were recorded on GE 300 MHz and Bruker 400 MHz NMR spectrometers in $CDCl_3$ at ambient temperature and referenced internally to tetramethylsilane (TMS). The GC/MS were performed on a Hewlett Packard 5885 GC/MS.

2-Oxo-3-(2-chlorophenyl)-3-oxyhexahydroazepine (5). Into a dry 100 mL 3-neck roundbottom flask were added crushed Mg turnings (1.2 g, 50.0 mmoles), one crystal of I_2, and a portion of 2-chlorobromobenzene (0.5 mL, 4.6 mmol). The mixture was slowly stirred until the Grignard reaction began to occur. The remaining 2-chlorobromobenzene (3.8 mL, 35.4 mmol) in anhydrous ether (20 mL) was added dropwise. After addition the reaction was allowed to cool to room temperature and stirred for 1 h. The mixture was cooled in an ice bath and α-oxocaprolactam (**16**, 1.4 g, 12.0 mmol) in freshly distilled THF (20 mL) (over $LiAlH_4$) was added dropwise over 1 h. The reaction was allowed to warm to room temperature and stirred for 72 h. The reaction was cooled in an ice bath and 10% NH_4Cl (70 mL) was added slowly. After the reaction was quenched, the mixture was extracted with EtOAc (3 X 50 mL), dried (over anhydrous Na_2SO_4), and the solvent evaporated to give crude **5** (2.8 g, 100%). The crude product was recrystallized from hot EtOAc to give pure **5** (0.9 g, 38% yield): m.p. 122-123 °C.

2-Oxo-3-(3-chlorophenyl)-3-oxyhexahydroazepine (6). Into a dry 100 mL 3-neck roundbottom flask were added crushed Mg turnings (1.2 g, 50.0 mmol), one crystal of I_2 and a portion of 3-chlorobromobenzene (0.5 mL, 4.5 mmol). The mixture was slowly stirred until Grignard formation began to occur. The remaining

3-chlorobromobenzene (5.1 mL, 45.5 mmol) in anhydrous ether (20 mL) was added dropwise. After addition the reaction was allowed to cool to room temperature and stirred for 1 h. The mixture was cooled in an ice bath and α-oxocaprolactam (**16**, 2.0 g, 15.7 mmol) in freshly distilled THF (25 mL) was added dropwise over 1 h. The reaction was allowed to warm to room temperature and stirred for 72 h. The reaction was cooled in an ice bath and 5% H_2SO_4 (50 mL) was added slowly. After the reaction was quenched, the mixture was extracted with EtOAc (3 X 30 mL), dried (anhydrous Na_2SO_4) and the solvent evaporated to give crude **6** (3.8 g, 100% yield). Flash chromatography of **6** dissolved in chloroform (10 mL) and eluted with EtOAc (1 L) gave pure **6** (1.0 g, 27% yield): m.p. 113-115 °C.

2-Oxo-3-(4-chlorophenyl)-3-oxyhexahydroazepine (7). Into a dry 100 mL 3-neck roundbottom flask was placed an ether solution of 1M 4-chlorophenylmagnesiumbromide (53.5 mL, 53.5 mmol) which was cooled to 0 °C in an ice bath. The α-oxo-caprolactam (**16**, 1.7 g, 13.3 mmol), in freshly distilled THF (200 mL) was added dropwise over 8 h onto the cold Grignard reagent. The reaction was allowed to warm to room temperature and stirred for 24 h. The reaction was cooled in an ice bath and slowly quenched with 5% HCl (100 mL). After the reaction was quenched, the mixture was extracted in ether (3 x 200 mL), dried (anhydrous Na_2SO_4) and the solvent evaporated to give crude **7** (3.8 g, 100%). The crude **7** was washed in cold ether (20 mL) and recrystallized in EtOAc to give pure **7** (2.0 g, 63% yield): m.p. 154-155 °C.

2-Oxo-3-(2-methoxyphenyl)-3-oxyhexahydroazepine (8). Into a dry 100 mL 3-neck roundbottom flask were added crushed Mg turnings (0.7 g, 30.0 mmol), one crystal of I_2 and a portion of 2-bromoanisole (0.5 mL, 4.0 mmol). The mixture was slowly stirred until the Grignard reaction began to occur. The remaining 2-bromoanisole (2.0 mL, 19.0 mmol) in anhydrous ether (10 mL) was added dropwise. After addition the reaction was allowed to cool to room temperature and stirred for 1 h. The mixture was cooled in an ice bath and α-oxo-caprolactam (**16**, 1.0 g, 7.8 mmol) in freshly distilled THF (65 mL) (from $LiAlH_4$) was added dropwise over 1 h. The reaction was allowed to warm to room temperature and stirred for 72 h. The reaction was cooled in an ice bath and 5% H_2SO_4 (50 mL) was added slowly. After the reaction was quenched, the mixture was extracted in EtOAc (3 x 30 mL), dried (anhydrous Na_2SO_4) and the solvent evaporated to give crude **8** (1.8 g, 98%). Crude **8** was recrystallized from hot EthoAc to give pure **8** (0.8 g, 45% yield): m.p. 140-141 °C.

2-Oxo-3-(3-methoxyphenyl)-3-oxyhexahydroazepine (9). Into a dry 100 mL 3-neck roundbottom flask were added crushed Mg turnings (0.57 g, 20.0 mmol), one crystal of I_2 and a portion of 3-bromoanisole (0.5 mL, 3.3 mmol). The mixture was slowly stirred until Grignard formation began to occur. The remaining 3-bromoanisole (2.04 g, 16.7 mmol) in anhydrous ether (10 mL) was added dropwise. After addition the reaction was allowed to cool to room temperature and stirred for 1 h. The mixture was cooled in an ice bath and α-oxocaprolactam (**16**, 0.8 g, 7.0 mmol) in freshly distilled THF (65 mL) was added dropwise over 1 h. The reaction

was allowed to warm to room temperature and stirred for 72 h. The reaction was cooled in an ice bath and 5% H_2SO_4 (50 mL) was added slowly. After the reaction was quenched, the mixture was extracted with EtOAc (3 x 30 mL), dried (anhydrous Na_2SO_4) and the solvent evaporated to give crude **9** (1.2 g, 100 %). Flash chromatography of **9** dissolved in chloroform (10 mL) and eluted with EtOAc (1 L) gave pure **9** (0.3 g, 28% yield): m.p. 114-118 °C.

2-Oxo-3-(4-methoxyphenyl)-3-oxyhexahydroazepine (10). Into a dry 100 mL 3-neck roundbottom flask were added crushed Mg turnings (0.5 g, 0.02 mmol), one crystal of I_2 and a portion of 4-bromoanisole (0.5 mL, 3.8 mmol). The mixture was slowly stirred until Grignard formation began to occur. The remaining 4-bromoanisole (2.1 mL, 16.2 mmol) in anhydrous ether (10 mL) was added dropwise. After addition the reaction was allowed to cool to room temperature and stirred for 1 h. The mixture was cooled in an ice bath and α-oxocaprolactam (**16**, 1.0 g, 7.8 mmol) in freshly distilled THF (65 mL) was added dropwise over 1 h. The reaction was allowed to warm to room temperature and stirred for 72 h. The reaction was cooled in an ice bath and 5% H_2SO_4 (50 mL) was added slowly. After the reaction was quenched, the mixture was extracted with EtOAc (3 x 30 mL), dried (anhydrous Na_2SO_4) and the solvent evaporated to give crude **10** (1.8 g, 100 %). The crude was recrystallized from hot EtOAc to give pure **10** (0.30 g, 28% yield): m.p. 70-72 °C.

2-Hydroxy-2-phenylundecanamide (12). A mixture containing decanophenone (**20**) (4.0 g, 17.2 mmol), cyanontrimethylsilane (TMSCN) (1.7 g,

17.2 mmol), and ZnI_2 (5-10 mg) was stirred at room temperature under an N_2 atmosphere. The reaction progress was monitored by the disappearance of the C=O stretching peak (1670 cm^{-1}) in the IR spectrum of the reaction mixture. After 2 h this peak was absent, indicating complete conversion to give 2-trimethylsilyloxy-2-phenyldecanenitrile (**21**). The TMS ether **21** was hydrolyzed to the cyanohydrin **23** by adding ether (20 mL) and 15% HCl (10 mL), and the resulting mixture was stirred vigorously for 1 h. The acidic layer was washed with ether (3 x 20 mL). The extracts were combined and evaporated to give cyanohydrin **23** (3.90 g, 87%). IR (neat) 3400 (OH), 2250 cm^{-1}. Cyanohydrin **23** was added to cold concentrated HCl (10 mL) and saturated with HCl gas. After 4 h a precipitate began to form, which was allowed to sit overnight. The solid was filtered, washed on filter with cold water (3 x 50 mL), and recrystallized from hot toluene to give pure **12** (0.6 g, 14% yield); m.p. 81-83 °C.

2-Hydroxy-2-phenypentadecanamide (**13**). A mixture containing tetradecanophenone (**24**) (2.5 g, 8.6 mmol), cyanontrimethylsilane (TMSCN) (0.9 g, 8.6 mmol), and ZnI_2 (5-10 mg) was stirred at room temperature under an N_2 atmosphere. The reaction progress was monitored by the disappearance of the C=O stretching peak (1670 cm^{-1}) in the IR spectrum of the reaction mixture. After 2 h this peak was absent, indicating complete conversion to give 2-trimethylsilyloxy-2-phenylpentadecanenitrile (**25**). The TMS ether **25** was hydrolyzed to the cyanohydrin **26** by adding ether (20 mL) and 15% HCl (10 mL), and the resulting mixture was stirred vigorously for 1 h. The acidic layer was washed with ether (3

x 20 mL). The extracts were combined and evaporated to give cyanohydrin **26** (2.7 g, 87%). IR (neat) 3400 (OH), 2250 cm^{-1}. Cyanohydrin **26** was added to cold concentrated Hcl (10 mL) and saturated with HCl gas. After stirring for 4 h a precipitate began to form, which was allowed to sit overnight without stirring. The solid was filtered, washed on the filter with cold water (3 x 50 mL), and recrystallized in hot toluene to give pure **13** (0.6 g, 58% yield); m.p. 75-76 °C.

Anticonvulsant Assays. All anticonvulsant and neurotoxicity assays were conducted by the Anticonvulsant Drug Development Program of the Epilepsy Branch, National Institute of Neurological and Communicative Disorders and Stroke, National Institutes of Health. Compounds were injected intraperitoneally into mice as suspensions in either methylcellulose or 30% polyethylene glycol 400. After the time indicated in Table 3, the animal was subjected to either a subcutaneaous Metrazol (scMET) challenge (85 mg/kg), a maximal electroshock (MES) challenge (produced with 60 cycle AC at 50 mA for 0.2 s via corneal electrodes), or a rotorod toxicity test. The details of these procedures have been published.[6]

Sodium Channel-Binding Assay. We previously reported the details of this procedure.[13] Briefly, synaptoneurosomes (~1 mg of protein) from rat cerebral cortex were incubated for 40 min at 25 °C with the test compound (seven different concentrations spanning the IC_{50}) in a total volume of 320 μL containing 10 nM [^{3}H]BTX-B and 50 μg/mL of scorpion venom. Incubations were terminated by dilution with ice cold buffer and filtration through a Whatman GF/C filter paper, and the filters were washed four times with ice cold buffer. Filters were counted in a

Beckmann scintillation counter. Specific binding was determined by subtracting the nonspecific binding, which was measured in the presence of 300 μM veratridine, from the total binding of [^{3}H]BTX-B. All experiments were performed in triplicate and included a control tube containing 40 μM DPH. The IC_{50} values were determined from a Probit analysis of the dose-response curve and excluded doses producing less than 10% or greater than 90% inhibition.

$GABA_A$ Binding Assay. The details of this procedure were previously reported.[7] Briefly, bovine cerebellar membranes (receptor concentration 0.7 pmol/mg of protein) were incubated in 50 mM TRIS-HCl buffer at pH 7.4 for 15 min at 0 °C with a 10^{-5} M concentration of the test compound. Incubations were terminated by rapid vacuum filtration on glass fiber filters. Radioactivity trapped on the filters was determined and compared to control values. Specific binding was determined by subtracting the nonspecific binding, which was measured in the presence of 10 μM GABA, from the total binding of [^{3}H]GABA. All experiments were performed in duplicate and compared to control values of muscimol (IC_{50} = 2.6 nM).

$GABA_B$ Binding Assay. The details of this procedure were previously reported.[8] Briefly, rat forebrain membranes (receptor concentration 222 fmol/mg of protein) were incubated in 50 mM TRIS-HCl buffer at pH 7.4 containing 2.5 mM of $CaCl_2$ for 15 min at 25 °C with a 10^{-5} M concentration of the test compound. Incubations were terminated by rapid vacuum filtration on glass fiber filters. Radioactivity trapped on the filters was determined and compared to control values. Specific binding was determined by subtracting the nonspecific binding, which was

measured in the presence of 100 μM baclofen, from the total binding of [^{3}H]GABA (50 μM of isoguvacine was used to block GABA sites). All experiments were performed in duplicate tubes and compared to control values of GABA (IC_{50} = 13.0 nM).

***N*-Methyl-D-aspartate Binding Assay**. The details of this literature procedure were previously reported.[9] Briefly, rat forebrain membranes (receptor concentration 6.4 pmol/mg of protein) were incubated in 50 mM TRIS-HCl buffer at pH 7.4 for 45 min at 0 °C with a 10^{-5} M concentration of the test compound. Incubations were terminated by rapid vacuum filtration on glass fiber filters. Radioactivity trapped on the filters was determined and compared to control values. Specific binding was determined by subtracting the nonspecific binding, which was measured in the presence of 1 mM NMDA, from the total binding of [^{3}H]CGS 19755. All experiments were performed in duplicate and compared to control values of NMDA (IC_{50} = 5,896 nM).

Glycine Inhibitory Binding Assay (Strychnine-Sensitive). The details of this literature procedure were previously reported.[11] Briefly, rat spinal cord membranes (receptor concentration 3.8 pmol/mg of protein) were incubated in 50 mM $NaKPO_4$ containing 200 mM NaCl at pH 7.1 for 10 min at 4 °C with a 10^{-5} M concentration of the test compound. Incubations were terminated by rapid vacuum filtration on glass fiber filters. Radioactivity trapped on the filters was determined and compared to control values. Specific binding was determined by subtracting the nonspecific binding, which was measured in the presence of 1.0 mM strychnine

nitrate, from the total binding of [^{3}H]strychnine. All experiments were performed in duplicate and compared to control values of strychnine nitrate (IC_{50} = 47.6 nM).

Glycine Excitatory Binding Assay (Strychnine-Insensitive). The details of this literature procedure were previously reported.[10] Briefly, rat cortical membranes (receptor concentration1772 fmol/mg of protein) were incubated in 50 mM HEPES at pH 7.1 for 30 min at 4 °C with a 10^{-5} M concentration of the test compound. Incubations were terminated by rapid vacuum filtration on glass fiber filters. Radioactivity trapped on the filters was determined and compared to control values. Specific binding was determined by subtracting the nonspecific binding, which was measured in the presence of 1.0 mM glycine, from the total binding of [^{3}H]glycine. All experiments were performed in duplicate and compared to control values of glycine (IC_{50} = 304 nM).

Benzodiazepine Binding Assay. The details of this literature procedure were previously reported.[12] Briefly, bovine cortical membranes (receptor concentration 2 pmol/mg of protein) were incubated in 10 mM $NaKPO_4$ at pH 7.7 for 45 min at 0 °C with a 10^{-5} M concentration of the test compound. Incubations were terminated by rapid vacuum filtration on glass fiber filters. Radioactivity trapped on the filters was determined and compared to control values. Specific binding was determined by subtracting the nonspecific binding, which was measured in the presence of 10 μM RO-15-1788, from the total binding of [^{3}H]flunitrazepam. All experiments were performed in duplicate and compared to control values of diazepam (IC_{50} =18 nM).

Acknowledgments

We thank James Stables of the Antiepileptic Drug Development Program, Epilepsy Branch, National Institute of Neurological Disorders and Stroke, for the whole animal anticonvulsant data. We also would like to thank Charles W. Bauer at NovaScreen and Jerry Cott at the National Institutes of Mental Health for in vitro assays performed through the Nova/NIMH Psychotherapeutic Drug Discovery and Development program. M.L.B. would like to thank the National Consortium for Educational Access, the Patricia Roberts Harris Fellowship, the UAB Comprehensive Minority Faculty Development Fellowship and the UAB Department of Chemistry for financial support. These studies were taken from the PhD dissertation of M.L.B, which was submitted in partial fulfillment of the requirements for the PhD degree.

References.

(1) Brouillette, W. J.; Einspahr, H. M. Bicyclic Imides with Bridgehead Nitrogen. Synthesis and X-Ray Crystal Structure of a Bicyclic 2,4-Oxazolidinedione. *J. Org. Chem.* **1984**, *49*, 5113-5116.

(2) Brouillette, W. J.; Brown, G. B.; Delorey, T. M.; Shirali, S. S. ; Grunewald, G. L. Anticonvulsant Activities of Phenyl-Substituted Bicyclic 2,4-Oxazolidinediones and Monocyclic Models. Comparison with Binding to the Neuronal Voltage-Dependent Sodium Channel. *J. Med. Chem.* **1988**, *31*, 2218-2221.

(3) Jenney, E. H.; Lee, L. D.; Williams, H. L.; Pfeiffer, C. C. Pharmacology and Anticonvulsant Spectrum of Atrolactamide (M-144) (Themisone). *J. Pharmacol. Exp. Ther.* **1952**, *106*,

(4) Brown, M. L.; Van Dyke, C. C.; Brown, G. B.; Brouillette, W. J. Comparative Molecular Field Analysis of a Hydantoin Binding Site in the Neuronal Voltage-Dependent Sodium Channel. *PhD Dissertation.*

(5) Grunewald, G. L.; Brouillette, W.J.; Finney, J. Synthesis of α-Hydroxyamides via the Cyanosilylation of Aromatic Ketones. *Tet. Lett.* **1980**, *21*, 1219-1220.

(6) Krall, R. L.; Penry, J. K.; White, B.G.; Kupferburg, H. J.; Swinyard, E. A. Anticonvulsant Drug Development: II. Anticonvulsant Drug Screening. *Epilepsia*. **1978**, *19*, 409-428.

(7) Enna, S. J.; Collins, J. F.; Synder, S. H. Stereospecificity and Structure Activity Requirements of GABA Receptor Binding in Rat Brain. *Brain Research*. **1977**, *124*, 185-190.

(8) Bowery, N. $GABA_B$ Receptors and Their Significance in Mammalian Pharmacology. *TIPS*. **1989**, *10*, 401-407.

(9) Murphy, D. E.; Schneider, J.; Boehm, C.; Lehmann, J.; Williams, M. Binding of [^{3}H]-3-(2-Carboxypiperazin-4-yl)propyl-1-Phosphonic Acid to Rat Brain Membranes: A Selective, High Affinity Ligand for N-Methyl-D-Aspartate Receptors. *J. Pharmacol. Exp. Ther.* **1987**, *240*, 778-784.

(10) Snell, L. D.; Morter, R. S.; Johnson, K. M. Structural Requirements for Activation of the Glycine Receptor that Modulates the N-Methyl-D-Aspatate Operated Channel. *Eur. J. Pharmacol.* **1988**, *156*, 105-110.

(11) Young, A. B.; Snyder, S. H. Strychnine Binding in Rat Spinal Cord Membranes Associated with the Synaptic Glycine Receptors: Cooperativity of Glycine Interactions. *Mol. Pharmacol.* **1974**, *10*, 790-809.

(12) Sweetnam, P. M.; Tallman, J. F. Regional Difference in Brain Benzodiazepine Receptor Carbohydrates. *Mol. Pharmacol.* **1986**, *29*, 299-306.

(13) Brown, G. B.; Tieszen, S. C.; Daly, J. W.; Warnick, J. E.; Albuquerque, E. X. Batrachotoxinin-A 20-α-Benzoate: A New Radioactive Ligand for Voltage-Sensitive Sodium Channels. *Cell Mol. Neurobiol.* **1981**, *1*, 19-40.

(14) Hernandez-Gallegos, Z.; Lehmann, P. A . F. Partition Coefficients of Three New Anticonvulsants. *J. Pharm. Sci.* **1990**, *79*, 1032-1033.

(15) Lipinski, C. A.; Giese, E. F.; Korst, R. J. pKa, Log P and MedChem CLOGP Fragment Values of Acidic Heterocyclic Potential Bioisosteres. *Quant. Struct.-Act. Relat.* **1991**, *10*, 109-117.

(16) Fujita, T.; Iwasa, J.; Hansch, C. A New Substituent Constant, π, Derived from Partition Coefficients. *J. Am. Chem. Soc.* **1964**, *86*, 5175-5179.

(17) Toledo-Meza, S. E.; Zenteno-Garcia, M. T.; Juárez-Carvajal, C.; Martinez-Muñoz, D.; Carvajal-Dandoval, G. A New Homologous Series of Anticonvulsant: Phenyl Alcohol Amides. *Arzeim.-Forsh./Drug Res.* **1990**, *40*, 1289-1291.

(18) Albert, J. R.; Boxill, G. C.; Weikel, Jr., J. H. Anticonvulsant and Toxicologic Properties of Some Benzilic Amides and the Physiological Disposition of the N-Ethyl Derivative. *J. Pharmacol. Exp. Ther.* **1961**, *131*, 85-90.

Figure 1. Structures of analogs in this study.

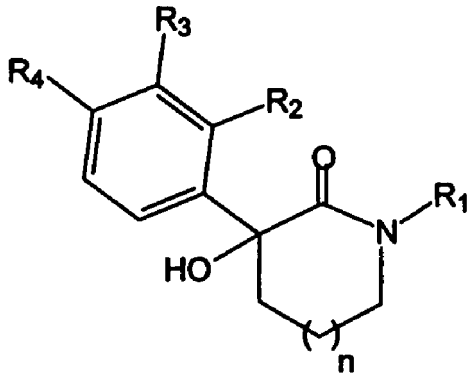

	n	R_1	R_2	R_3	R_4
1	2	H	H	H	H
2	2	$CH_2C_6H_5$	H	H	H
3	1	H	H	H	H
4	3	H	H	H	H
5	2	H	Cl	H	H
6	2	H	H	Cl	H
7	2	H	H	H	Cl
8	2	H	OCH_3	H	H
9	2	H	H	OCH_3	H
10	2	H	H	H	OCH_3

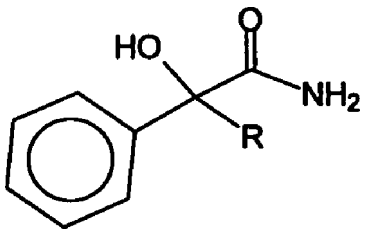

	R
11	C_7H_{15}
12	C_9H_{19}
13	$C_{13}H_{25}$
14	C_2H_5
15	C_6H_5
atrolactamide	CH_3

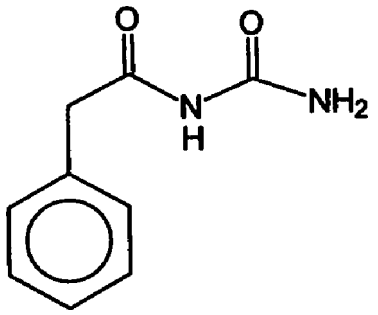

phenacemide

Scheme I.

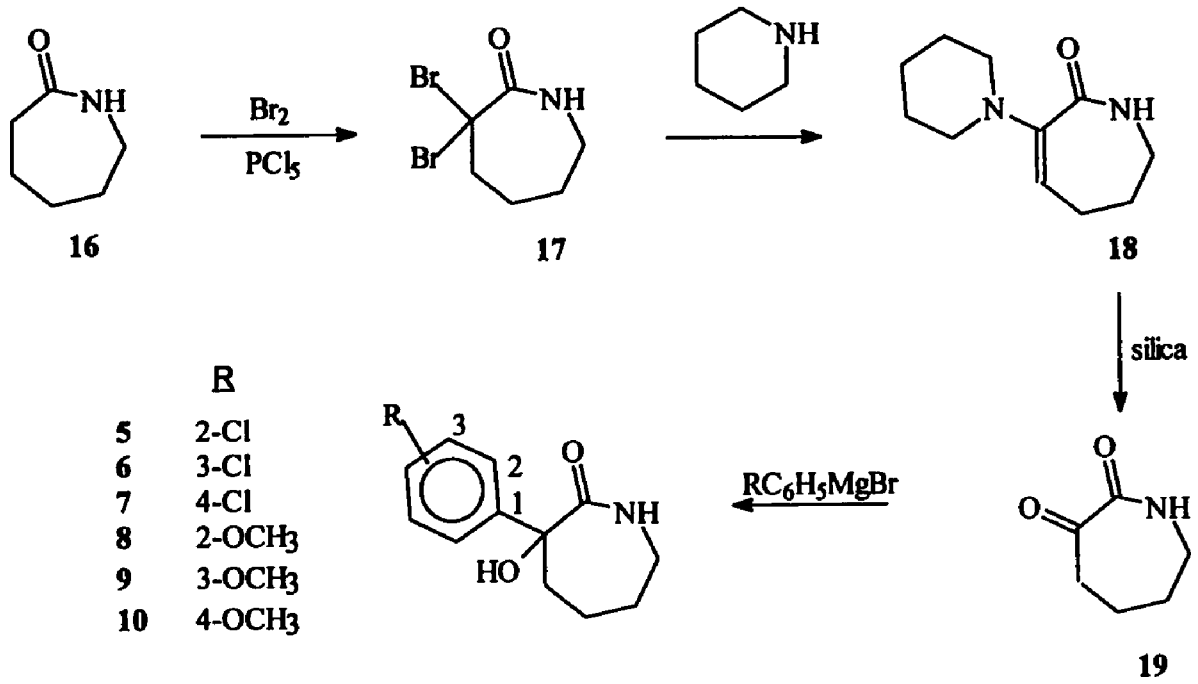
16
Br_2
PCl_5
17
18
silica
19
RC_6H_5MgBr
R
5 2-Cl
6 3-Cl
7 4-Cl
8 2-OCH_3
9 3-OCH_3
10 4-OCH_3

Scheme 2

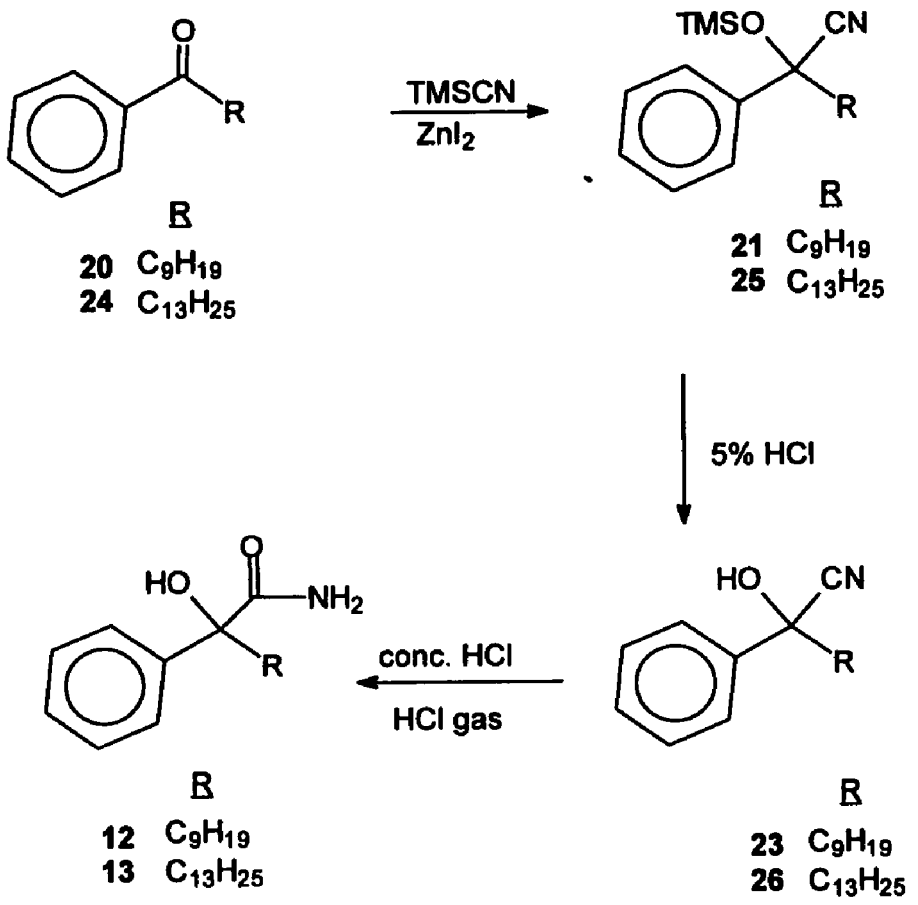
O
R
TMSCN
ZnI2
TMSO
CN
R
R
20 C9H19
24 C13H25
21 C9H19
25 C13H25
5% HCl
HO
CN
R
HO
O
NH2
R
conc. HCl
HCl gas
R
R
12 C9H19
13 C13H25
23 C9H19
26 C13H25

Table 1. Selected Data for α-Hydroxy-α-Phenylcaprolactams and Amides

Compound	Isolated yield (%)	m.p. °C (recryst. solvent)	^{1}H NMR ($CDCl_3$, δ)	^{13}C NMR ($CDCl_3$, δ)	IR, C=O stretch (KBr cm^{-1})
5	33	122-123 (EtOAc)	7.44-7.22 (m, 4H, Ph), 6.75 (s, 1H, NH), 5.12 (s, 1H, OH), 3.16-2.91 (m, 3H, CH), 2.00-1.84 (m, 2H, CH_2), 1.69-1.47 (m, 3H, CH)	25.0, 28.9, 36.0, 42.6, 127.7, 127.4, 129.4, 129.7, 132.6, 134.0, 137.2, 179.0	1613
6	27	113-115 (EtOAc)	7.44-7.22 (m, 4H, Ph), 6.50 (s, 1H, NH), 5.10 (s, 1H, OH), 3.16-2.82 (m, 3H, CH), 2.04-1.85 (m, 2H, CH_2), 1.69-1.44 (m, 3H, CH)	24.6, 28.5, 35.6, 42.2, 126.3, 127.0, 129.0, 129.3, 132.2, 133.7, 136.8, 178.6	1600
7	68	154-155 (EtOAc)	7.39-7.11 (m, 4H, Ph), 6.64 (s, 1H, NH), 5.01 (s, 1H, OH), 3.11-3.06 (m, 1H, CH), 2.87-2.79 (m, 1H, CH), 2.62-2.57 (m, 1H, CH), 2.0-1.91 (m, 1H, CH), 1.67-1.45 (m, 3H, CH)	25.4, 28.9, 35.8, 42.8, 128.2, 129.6, 129.7, 133.7, 138.5, 178.6	1650
8	45	140-141 (EtOAc)	7.51-7.19 (m, 2H, Ph), 7.14-6.78 (m, 2H, Ph), 6.42 (s, 1H, NH), 5.12 (s, 1H, OH), 3.87 (s, 3H, OCH_3), 3.25-2.73 (m, 3H, CH_2), 2.17-1.37 (m, 6H, CH_2)	25.4, 29.2, 36.1, 42.4, 56.1, 112.8, 121.4, 128.7, 129.8, 158.1, 179.9	1650

Table 1. (Continued)

9	28	114-118 (EtOAc)	7.55-7.21 (m, 1H, Ph), 7.05-6.78 (m, 3H, Ph), 6.78-6.38 (m, 1H, Ph), 6.61 (s, 1H, NH), 5.05 (s, 1H, OH), 3.84 (s, 3H, OCH_3), 3.15-2.76 (m, 2H, CH_2), 2.67-2.48 (m, 1H, CH_2), 2.12-1.11 (m, 6H, CH_2)	245.5, 29.0, 35.8, 42.8, 55.7, 78.4, 112.8, 113.6, 118.9, 130.4, 141.5, 160.5, 178.9	1650
10	28	70-72 (EtOAc)	7.29-7.26 (m, 3H, Ph), 6.93-6.90 (m, 2H, Ph), 6.34 (bs, 1H, NH), 4.96 (s, 1H, OH), 3.81 (s, 3H, OCH_3), 2.94-2.75 (m, 1H, CH), 2.71-2.48 (m, 1H, CH), 2.08-1.83 (m, 2H, CH_2), 1.83-1.34 (m, 5H, CH_2)	23.4, 25.6, 28.0, 29.0, 35.9, 39.8, 41.0, 42.7, 55.6, 114.7, 128.0, 132.14, 159.6, 179.3	1650
12	14	81-83 (Toluene)	7.74-7.50 (m, 2H, Ph), 7.45-7.19 (m, 3H, Ph) 6.57-6.30 (s, 1H, NH), 5.85-5.58 (s, 1H, NH), 3.44-3.21 (s, 1H, OH), 2.33-2.17 (m, 1H, CH), 2.13-1.92 (m, 1H, CH), 1.51-1.11 (m, 14H, CH_2), 1.05-0.71, 3H, CH_3)	13.3, 21.9, 22.6, 28.5, 28.7, 28.7, 29.0, 31.1, 38.4, 78.0, 124.1, 121.0, 127.7, 141.6, 176.1	1660

Table 1. (Continued)

13	58	75-76 (Toluene)	7.67-7.48 (m, 2H, Ph), 7.42-7.14 (m, 3H, Ph) 6.51-6.23 (s, 1H, NH), 5.70-5.38 (s, 1H, NH), 3.29-3.01 (s, 1H, OH), 2.37-2.14 (m, 1H, CH), 2.14-1.88 (m, 1H, CH), 1.73-1.52 (m, 22H, CH_2), 0.96-0.64, 3H, CH_3)	14.5, 23.0, 23.6, 29.7, 29.8,29.9, 30.0, 30.02, 32.3, 39.3, 78.8, 125.8, 128.7, 129.0, 141.2, 179.0	1675

[a]All compounds were also analyzed by (1) GC/MS (EI, 70 eV), giving one peak in the GC and the expected molecular ion peak , and (2) elemental analysis for C, H, N (within ±0.4% of the calculated value).

Table 2. Anticonvulsant and Log *P* Data for α-Hydroxy-α-Phenylamides and Lactams in Mice.

		Phase I			Phase II			
		Best Activity, mg/kg[a, h]			mg/kg[a, c]			
Compound	log *P*	MES	scMet	Rotorod	Time (h)	MES ED_{50}	scMET ED_{50}	Rotorod TD_{50}
1[b, d]	1.76	100	300	300	0.3	63 [52-72] (3.3)[m]	74 [49-105] (2.8)[n]	210 [162-234]
2[b, d]	3.43	100	100	300	0.25	84 [63-106] (2.6)	[J]	216 [182-234]
3[b, d]	1.26	>300	>300	>300				
4[b, d]	2.26	100	300	300	0.25	80 [58-98] (2.5)	108 [69-148] (1.8)	199 [160-241]
5	2.60	100 {1/3}	300 {1/1}	300 {4/4}				
6	2.62	100 {2/3}	>100 {0/1}	100 {2/8}				
7	2.62	100 {2/3}	300 {1/1}	300 {4/4}				

Table 2. (Continued)

8	1.76	300 {1/1}	300 {1/1}	300 {4/4}				
9	1.76	>100	>100	>100				
10	1.76	100 {1/3}	>100 {0/1}	>100 {0/8}	0.25	94 [77-116] (1.26)	99 [79-118] (1.19)	118 [94-142]
11	3.70	100 {1/3}	>300 {0/3}	300 {3/8}				
12	4.70	300 {1/1}		300 {4/4}				
13	6.70	300 {1/1}	300 {1/1}	>300 {0/3}				
14[f]	1.20					126 [119-133] (1.04)	67 [58-77] (1.97)	132 [119-146]
15[g]	2.33					61.8 [52.1-73] (1.4)	93.5 [71-112] (0.9)	86.5 [69-109.0]
phenacemide[k]						87 [74-100] (4.8)	116 [71-150] (3.6)	421 [337-549]

Table 2. (Continued)

atrolactamide[e,l]	0.7

[a]Unless otherwise noted, all compounds were administered intraperitoneally in mice as suspensions in 30% polyethylene glycol 400. [b]All tests were performed 30 min after compound administration. [c]Numbers in [ ] refer to 95% confidence intervals. [d]Anticonvulsant data taken from ref 2. [e]Anticonvulsant data taken from ref 3. [f]Anticonvulsant data taken from ref 17. [g]Values taken from ref 18. [h]Numbers in { } refer to number of mice protected / number of mice tested. [i]Insufficient compound to complete testing. [j]Mice died at 100 mg/kg. [k]Ref 6. [l]Anticonvulsant data not acquired using NIH methods. [m]Numbers in ( ) represents the therapeutic index and refers to the TD_{50}/MES ED_{50}. [j]Mice died at 100 mg/kg. [k]Ref 6. [l]Anticonvulsant data not acquired using NIH methods. [j]Mice died at 100 mg/kg. [l]Anticonvulsant data not acquired using NIH methods. [m]Numbers in ( ) represents the therapeutic index (T. I.) and refers to the TD_{50} / MES ED_{50}. [n]Numbers in ( ) represents the therapeutic index (T. I.) and refers to the TD_{50} / scMET ED_{50}.

Table 3. Anticonvulsant Data for Orally Administered Analog **7** in Rats.

Anticonvulsant Data							
phase I best activity, mg/kg[a, b]				phase II, mg/kg[a]			
compound	Time (hr)	MES	Rotorod	Time (hr)	MES ED_{50}	scMET ED_{50}	Rotorod ED_{50}
7	2	30 {4/4}[b]	30 {0/4}	2	21.8 (16.5-26.7)[c] [> 11.5][d]	>250[e]	>250[f]

[a]Administered *p.o* in rats. [b]{ } refers to the number of rats protected / the number of rats tested. [c]( ) 95% confidence interval. [d][ ] T.I = therapeutic index. [e]0/2 animals were protected. [f]0/2 animals showed toxicity at 250 mg/kg; 2/2 animals showed toxicity at 500 mg/kg.

Table 4. In vitro Binding Data for Analogs 1 and 11

Compound	Na^+ channel IC_{50} μ M	$GABA_a$ % inhibition at 10^{-5} M	$GABA_b$ % inhibition at 10^{-5} M	NMDA % inhibition at 10^{-5} M	Glycine (excitatory) % inhibition at 10^{-5} M	Glycine (inhibitory) % inhibition at 10^{-5} M	Benzo diazapine % inhibition at 10^{-5} M
1	>800 (40)[a]	-8.8 (28,000)[b]	-0.8 (1,760,000)[c]	8.0 (3,590,000)[d]	0.1 (3,000,000)[e]	0.6 (335,000)[f]	14.8 (34,000)[g]
11	9 [7-11][h,i] (40)[a]						

[a]The Na^+ channel IC_{50} in ( ) for diphenylhydantoin reported in ref 13. [b]The K_i in ( ) for the reference compound 4-aminobutyric acid (GABA) reported in ref 7. [c]The K_i for the reference compound 4-amino-m-butyric acid (GABA) reported in ref 9. [d]The K_i for the reference compound N-methyl-d-aspartate (NMDA) reported in ref 8. [e]The K_i for the ref compound glycine reported in ref 10. [f]The K_i for the reference compound strychinine nitrate reported in ref 11. [g]The K_i for the ref compound clonazepam reported in ref 12. [h]The [ ] represents ±1 standard deviation generated by probit analysis. [i]Compound reported in ref 4.

Table 5. Analytical Analysis

Compound	Theoretical	Found
5	C 60.13	60.06
	H 5.89	6.02
	N 5.84	5.68
6	C 60.13	60.09
	H 5.89	5.86
	N 5.84	5.74
7	C 60.13	60.07
	H 5.89	5.87
	N 5.84	5.76
8	C 66.36	66.35
	H 7.36	7.36
	N 5.87	5.84
9	C 66.36	66.35
	H 7.56	7.56
	N 5.87	5.84
10	C 66.36	66.35
	H 7.36	7.36
	N 5.87	5.84
12	C 73.61	73.72

Table 5. (Continued)

	H 9.81	9.83
	N 5.05	5.02
13	C 75.63	75.66
	H 10.58	10.65
	N 4.20	4.25

LIST OF REFERENCES

(1) Sakel, M. *Epilepsy*; Philosophical Library: New York: 1958; pp 1-204.

(2) Janz, D. Epilepsy, Viewed Metaphysically: An Interpretation of the Biblical Story of the Epileptic Boy and of Raphael's Transfiguration. *Epilepsia*. **1986**, *27*, 316-322.

(3) Locharernkul, C.; Primrose, D.; Pilcher, W. H.; Ojemann, L. M.; Ojemann, G. A. Update in Epilepsy, Part I: Diagnosis and Treatment of Epilepsy. *New York State J. of Med.* **1992**, *92*, 14-16.

(4) Bancaud, J.; Henriksen, O.; Rubio-Donnadieu, F.; Seino, M.; Dreifuss, F. E.; Penry, J. K. Proposal for Revised Clinical and Electroencephalographic Classification of Epileptic Seizures. *Epilepsia*. **1981**, *22*, 489-501.

(5) Dreifuss, F. E.; Martinez-Lage, M.; Roger, J.; Seino, M.; Wolf, P.; Dam, M.; Proposal for the Classification of Epilepsies and Epileptic Syndromes. *Epilepsia*. **1985**, *26*, 268-278.

(6) Locharernkul, C.; Primrose, D.; Pilcher, W. H.; Ojemann, L. M.; Ojemann, G. A. Update in Epilepsy, Part I: Diagnosis and Treatment of Epilepsy. *New York State J. of Med.* **1992**, *92*, 14-16.

(7) Pellock, J. M. Standard Approach to Antiepileptic Drug Teatment in the United States. *Epilepsia*. **1994**, *35 (suppl. 4)*, S11-S18.

(8) MacDonald, R. L.; Kelly, K. M. Mechanisms of Action of Currently Prescribed and Newly Developed Antiepileptic Drugs. *Epilepsia*. **1994**, *35 (suppl. 4)*, S41-S50.

(9) Taylor, C. P. Emerging Perspectives on the Mechanism of Action of Gabapentin. *Neurology*. **1994**, *44 (suppl. 5)*, S10-S15.

(10) Mattson, R. H. Current Challenges in the Treatment of Epilepsy. *Neurology*. **1994**, *44 (suppl. 5)*, S4-S9.

(11) Kupferburg, H. J. Strategies for Identifying and Developing New Anticonvulsant Drugs. *Pharm. Weekblad Sci. Edi.* **1992**, *14*, 132-138.

(12) Krall, R. L.; Penry, J. K.; White, B. G.; Kupferberg, H. J.; Swinyard, E. A. Anticonvulsant Drug Development: II. Anticonvulsant Drug Screening. *Epilepsia*. **1978**, *19*, 409-428.

(13) Ellis, G. P.; West, G. B. Anticonvulsant Drugs. *Progress in Medicinal Chemistry*. **1963**, *3*, 261-331.

(14) Vida, J. A., Anticonvulsants. *Medicinal Chemistry, A Series of Monographs-Volume 15*. Academic Press: New York; **1977**.

(15) Ware, E. The Chemistry of the Hydantoins. *Chem. Rev.* **1950**, *46*, 403-470.

(16) Satzinger, G. Antiepileptics for Gamma-Aminobutyric Acid. *Arzeim-Forsh/ Drug Res.* **1994**, *4*, 261-266.

(17) Foot, M.; Wallace, J. Gabapentin. *Epilepsy Res. Suppl.* **1991**, *3*, 109-114.

(18) Novelli, A.; Lugones, Z. M.; Velasco, P.; Hydantoins III. Chemical Constitution and Hypnotic Action. *Anales Asoc. Quim. Arg.* **1942**, *30*, 225-231.

(19) Parks, Jr, B. R.; Dostrow, V. G.; Noble, S. L. Drug Therapy for Epilepsy. *American Family Physician*. **1994**, *50*, 639-648.

(20) Pellock, J. M. Standard Approaches to Antiepileptic Drug Treatment in the United States. *Epilepsia*. **1994**, *35 (suppl. 4)*, s11-s18.

(21) Fisher, R. S. Emerging Antiepileptic Drugs. *Neurology*. **1993**, *43 (suppl. 5)*, s12-20.

(22) Graves, N. M.; Leppik, I. E. Advances in Pharmacotherapy: Recent Developments in the Treatment of Epilepsy. *J. Clin. Pharm. and Therap.* **1993**, *18*, 227-242.

(23) Swinyard, W. A.; Sofia, R. D.; Kupferberg, H. J. Comparative Anticonvulsant Activity and Neurotoxicity of Felbamate and Four Prototype Antiepileptic Drugs in Mice and Rats. *Epilepsia*. **1986**, *27*, 27-34.

(24) Leppik, I. E. Antiepileptic Drugs in Development: Prospects for the Near Future. *Epilepsia*. **1994**, *35 (suppl. 4)*, S29-S40.

(25) Porter, R. Mechanisms of Action of New Antiepileptic Drugs. *Epilepsia*. **1992**, *30 (suppl. 1)*, S29-S34.

(26) Dichter, M. A. Emerging Insights into Mechanisms of Epilepsy: Implications for New Antiepileptic Drug Development. *Epilepsia*. **1994**, *35 (suppl. 4)*, S51-S57.

(27) Brodie, M. J. Drug Interactions in Epilepsy. *Epilepsia*. **1992**, *33 (suppl. 1)*, S13-S22.

(28) MacDonald, R. L. Antiepileptic Drug Actions. *Epilepsia*. **1989**, *30 (suppl. 1)*, S19-S28.

(29) Haines, J. L.; Rich, S. S.; Tsai, M. Y.; Anderson, V. E. Altered Amino Acid Levels in Multiple Affected Sibships with Seizures. *Epilepsia*. **1985**, *26* ,641-648.

(30) Faingold, C. L.; Browning, R. A. Mechanisms of Anticonvulsant Drug Actions. *Eur. J. Pediatr.* **1987**, *146*, 8-14.

(31) Stone, W. E.; Javid, M. J. Anticonvulsive and Convulsive Effects of Lidocaine: Comparison with those of Phenytoin, and Implications for Mechanism of Action Concepts. *Neurological Res.* **1988**, *10*, 161-168.

(32) Ramsay, R. E. Advances in the Pharmacotherapy of Epilepsy. *Epilepsia*. **1993**, *34 (suppl. 5)*, S9-S16.

(33) Cramer, C. L.; Stagnitto, M. A.; Knowles, M. A.; Palmer, G. C. Kianic Acid and 4-Aminopyridine Seizure Models in Mice: Evaluation of Efficacy of Anti-Epileptic Agents and Calcium Antagonists. *Life Sciences*. **1994**, *54*, 271-275.

(34) Jan, L. Y.; Jan, Y. N. Voltage-Sensitive Ion Channels. *Cell*. **1989**, *56*, 13-25.

(35) Triggle, D. J.; Langs, D. A. Ligand Gated and Voltage-Gated Ion channels. *Ann. Reports in Med. Chem.* **1989**, *25*, 225-234.

(36) Kallen, R. G.; Cohen, S. A.; Barchi, R. L. Structure, Function and Expression of Voltage-Dependent Sodium Channels. *Mol. Neurobiology*. **1994**, *7*, 383-428.

(37) Trimmer, J. S.; Agnew, W. S. Molecular Diversity of Voltage-Sensitive Na Channels. *Annu. Rev. Physiol.* **1989**, *51*, 401-18.

(38) Catterall, W. A. Common Modes of Drug Action on Na+ Channels: Local Anesthetics, Antiarrhythmics and Anticonvulsants. *TIPS*. **1987**, *8*, 57-65.

(39) Catterall, Structure and Function of Voltage-Sensitive Ion Channels. *Science*. **1988**, *242*, 50-61.

(40) Armstrong, C. M. Voltage-Dependent Ion Channels and Their Gating. *Physiological Rev.* **1992**, *72*, S5-S13.

(41) Catterall, W. A. Cellular and Molecular Biology of Voltage-Gated Sodium Channels. *Physiological Rev.* **1992**, *72*, S15-S48.

(42) Catterall, W. A. Molecular Mechanisms of Inactivation and Modulation of Sodium Channels. *Renal Physiol. Biochem.* **1994**, *17*, 121-125.

(43) Koumi, S.; Sato, R; Katori, R.; Hisatome, I.; Nagasawa, K.; Hayakawa, H. Sodium Channel States Control Binding and Unbinding Behavior of Antiarrhythmic Drugs in Cardiac Myocytes for the Guinea Pig. *Cardiovascular Res.* **1993**, *26*, 1199-1205.

(44) Courtney, K. R.; Etter, E. F. Modulated Anticonvulsant Block of Sodium Channels in Nerve and Muscle. *Eur. J. Pharm.* **1983**, *88*, 1-9.

(45) Catterall, W. A. Inhibition of Voltage-Sensitive Sodium Channels in Neuroblastoma Cells by Antiarryhthmics Drugs. *Mol. Pharmacol.* **1981**, *20*, 356-362.

(46) Catterall, W. A. Inhibition of Voltage-Sensitive Sodium Channels in Neuroblastoma Cells and Synaptosomes by the Anticonvulsant Drug Diphenylhydantoin and Carbamazepine. *Mol. Pharmacol.* **1984**, *25*, 228-234.

(47) Catterall, W. A. Voltage Clamp Analysis of the Inhibitory Actions of Diphenylhydantoin and Carbamazepine on Voltage-Sensitive Sodium Channels in Neuroblastoma Cells. *Mol. Pharmacol.* **1985**, *27*, 549-558.

(48) Scheuer, T. Auld, V. J.; Boyd, S.; Offord, J.; Dunn, R.; Catterall, W. A. Funtional Properties of Rat Brain Sodium Channels Expressed in a Somatic Cell Line. *Science*. **1990**, *247*, 854-858.

(49) Isom, L. L.; Scheuer, T.; Brownstein, A. B.; Ragsdale, D. S.; Murphy, B. J.; Catterall, W. A. Functional Co-Expression of the β1 and Type IIA α Subunits

of Sodium Channels in a Mammalian Cell Line. *J. Biol. Chem.* **1995**, *270*, 3306-3312.

(50) Black, J. A.; Westenbroek, R.; Ransom, B. R.; Catterall, W. A.; Waxman, S.G. Type II Sodium Channels in Spinal Cord Astrocytes In Situ: Immunocytochemical Observations. *Glia.* **1994**, *12*, 219-227.

(51) Roufos, I.; Hays, S. J.; Dooley, D. J.; Schwarz, R. D.; Campbell, G. W.; Probert Jr., A. W. Synthesis and Pharmacological Evaluation of Phenylactamides as Sodium-Channel Blockers. *J. Med Chem.* **1994**, *37*, 268-274.

(52) Fainzilber, M.; Kofman, O.; Zlotkin, E.; Gordon, D. A New Neurotoxin Receptor Site on Sodium Channels is Identified by a Conotoxin that Affects Sodium Channel Inactivation in Molluscs and Acts as an Antagonist in Rat Brain. *J. Biol. Chem.* **1994**, *269*, 2574-2580.

(53) Myers, H.; Daly, J.; Malkin, B. A Dangerously Toxic New Frog (Phyllobates) Used by Embera Indians of Western Colombia. *Bull. American Museum of Natural History.* **1978**, *161*, 311-365.

(54) Catterall, W. A.; Morrow, C. S.; Dally, J. W.; Brown, G. B. Binding of Batrachotoxinin A 20-α-Benxoate to a Receptor Site Associated with Sodium Channels in Synaptic Nerve Ending Particles. *J. Biol. Chem.* **1981**, *10*, 8922-8927.

(55) Brown, G. B.; Tieszen, S. C.; Daly, J. W.; Warnick, J. E.; Albuquerque, E. X. Batrachotoxin-A 20-α-Benzoate: A New Radioactive Ligand for Voltage-Sensitive Sodium Channels. *Cell Mol. Neurobiol.* **1981**, *1*, 19-40.

(56) Brown, G. B. Batrachotoxin: A Window on the Allosteric Nature of the Voltage-Sensitive Sodium Channel. *Int. Rev. Neurobiol.* **1988**, *29*, 7-116.

(57) Creveling, C. R.; Bell, M. E.; Burke Jr., T. R.; Chaneg, E.; Lewandowski-Lovenberg, G. A.; Kim, C. H.; Rice, K. C.; Daly, J. W. Procaine Isothiocyanate: An Irreversible Inhibitor of the Specific Binding of [^{3}H]Batrachotoxin-A Benzoate to Sodium Channels. *Neurochemical Res.* **1990**, *15*, 441-448.

(58) Nettleton, J.; Wang, G. K. pH-Dependent Binding of Local Anesthetics in Single Batrachotoxin-Activated Na^+ Channels. Cocaine vs. Quaternary Compounds. *Biophysical Journal.* **1990**, *58*, 95-106.

(59) Gusovsky, F.; Nishaizawa, Y.; Padgett, W.; McNeal, E. T.; Rice, K.; Kim, C. H.; Creveling, C. R.; Daly, J. W. Voltage-Dependent Sodium Channels in Synaptoneurosomes: Studies with $^{22}Na^{+}$ influx and [^{3}H]Saxitoxin and [^{3}H]Batrachotoxin-A 20-α-Benzoate Binding. Effects of Proparacaine Isothiocyanate. *Brain Res.* **1990**, *518*, 101-106.

(60) Wang, G. K. Binding Affinity and Stereoselectivity of Local Anesthetics in Single Batrachotoxin-Activated Na^{+}Channels. *J. Gen. Physiology.* **1990**, *96*, 1105-27.

(61) Sheldon, R. S.; Hill, R. J.; Taouis, M.; Wilson, L. M. Aminoalkyl Structural Requirements for Interaction of Lidocaine with the Class I Antiarrhythmic Drug Receptor on Rat Cadiac Myocytes. *Mol. Pharmacol.* **1991**, *39*, 609-614.

(62) Hill, R. J.; Thakore, E.; Taouis, M.; Duff, H. J.; Sheldon, R. S. Transcainide: Biochemical Evidence for State-Dependent Interaction with the Class I Antiarrhythmic Drug Receptor. *Eur. J. Pharm.* **1991**, *203*, 51-58.

(63) Wang, G. K.; Wang, S. Y. Altered Stereoselectivity of Cocaine and Bupivacaine Isomers in Normal and Batrachotoxin-Modified Na^{+} Channels. *J. of Gen. Physiol.* **1992**, *100*, 1003-1020.

(64) Brown, G. B.; Guapp, J. E.; Olsen, R. W. Pyrethroid Insecticides: Stereospecific, Allosteric Interactions with the Batrachotoxinin-A Benzoate Binding Site of Mammalian Voltage-Sensitive Sodium Channels. *Mol. Pharmacol.* **1988**, *34*, 54-59.

(65) Trainer, V. L.; Moreau, E.; Guedin, D.; Baden, D. G.; Catterall, W. A. Neurotoxin Binding and Allosteric Modulation at Receptor Sites 2 and 5 on Purified and Reconstituted Rat Brain Sodium Channels. *J. Biol. Chem.* **1993**, *268*, 17114-17119.

(66) Khodorov, B. I.; Yelin, E. A.; Zaborovskaya, L. D.; Maksudov, M. Z.; Tikhomirova, O. B.; Leonov, V. N. Comparative Analysis of the Effects of Synthetic Derivatives of Batrachotoxin on Sodium Currents in Frog Node of Ranvier. *Cellular and Mol. Neuro.* **1992**, *12*, 59-81.

(67) Casebolt, T. L.; Brown, G. B. Batrachotoxin-A-Ortho-Azidobenzoate: A Photoaffinity Probe of the Batrachotoxin Binding Site of Voltage-Sensitive Sodium Channel. *Toxicon.* **1993**, *31*, 1113-1122.

(68) Brown, G. B. [^{3}H]Batrachotoxinin-A Benzoate Binding to Voltage-Sensitive Sodium Channels: Inhibition by the Channel Blockers Tetrodotoxin and Saxitoxin. *J. Neurosci.* **1986**, *6*, 2064-2070.

(69) Rock, D. M.; McLean, M. J.; Macdonald, R. L.; Catterall, W. A.; Taylor, C. P. Ralitoline (CI-946) and CI-953 Block Sustained Repetitive Sodium Action Potentials in Cultured Mouse Spinal Cord Neurons and Displace Batrachotoxin-A 20-α-Benzoate Binding In Vitro. *Epilepsy Res.* **1991**, *8*, 197-203.

(70) Garty, H. Molecular Properties of Epithelial, Amiloride-Blockable Na+ Channels. *FESEB Journal.* **1994**, *8*, 522-8.

(71) Willow, M.; Catterall, W. A. Inhibition of Binding of [^{3}H]Batrachotoxinin A 20-α- Benzoate to Sodium Channels by the Anticonvulsant Drugs Diphenylhydantoin and Carbamazepine. *Mol. Pharmacol.* **1982**, *22*, 627-635.

(72) Brouillette, W. J.; Brown, G. B.; Delorey, T. M.; Liang, G. Sodium Channel Binding and Anticonvulsant Activities of Hydantoins Containing Conformationally Constrained 5-Phenyl Substituents. *J. Pharm. Sci.* **1990**, *79*, 871-874.

(73) Brouillette, W. J.; Jestkov, V.P.; Brown, M. L.; Aktar, M. S.; Delorey, T. M.; Brown, G. B. Bicyclic Hydantoins with Bridgehead Nitrogen. Comparison of Anticonvulsant Activities with Binding to the Neuronal Voltage-Dependent Sodium Channel. *J. Med. Chem.* **1994**, *37*, 3289-3293.

(74) Brouillette, W. J.; Brown, G. B.; Delorey, T. M.; Shirali, S. S. ; Grunewald, G. L. Anticonvulsant Activities of Phenyl-Substituted Bicyclic 2,4-Oxazolidinediones and Monocyclic Models. Comparison with Binding to the Neuronal Voltage-Dependent Sodium Channel. *J. Med. Chem.* **1988**, *31*, 2218-2221.

(75) Brouillette, W. J.; Grunewald, G. L.; Brown, G. B.; Delorey, T. M; Akhtar, M. S.; Liang, G. Sodium Channel Binding and Anticonvulsant Activities for Enantiomers of a Bicyclic 2,4-Oxazolidinedione and Monocyclic Models. *J. Pharm. Sci.* **1989**, *32*, 1577-1580.

(76) Thomsen, W.; Hays, S. J.; Hicks, J. L.; Schwarz, R. D.; Catterall, W. A. Specific Binding of the Novel Na+ Channel Blocker PD85,639 to the α-Subunit of Rat Brain Na^+ Channels. *Mol. Pharmacol.* **1993**, *43*, 955-64.

(77) Zhu, Y.; Im, W.; Lewis, R. A.; Althaus, J. S.; Cazers, A. K.; Nielson, J. W.; Palmer, J. R.; Von Voigtlander, P. F. Two Metabolites of Anticonvulsant U-54494A: Their Anticonvulsant Activity and Interaction with Sodium Channel. *Brain Res.* **1993**, *606*, 50-55.

(78) Barber, M. J.; Starmer, C.F.; Grant, A. O. Blockade of Cardiac Sodium Channels by Amitriptyline and Diphenylhydantoin, Evidence for Two Use-Dependent Binding Sites. *Circulation Research.* **1991**, *69*, 677-696.

(79) Harris, W. E.; Stahl, W. L. Interactions of Phenytoin with Rat Brain Synaptosomes Examined by Flourescent Fatty Acid Probes. *Neurochem. Int.* **1988**, *13*, 369-377.

(80) Francis, J.; Burnham, W. M. [^{3}H]Phenytoin Identifies a Novel Anticonvulsant-Binding Domain on Voltage-Dependent Sodium Channels. *Mol. Pharmacol.* **1992**, *42*, 1097-1103.

(81) Bell, P. H.; Roblin, R. O. Studies in Chemotherapy: VII. A Theory of the Relationship of Structure to Activity of Sulfanil Amide Type Compounds. *J. Am. Chem. Soc.* **1942**, *64*, 2905-2917.

(82) Hammet, L. P. *Physical Organic Chemistry*; McGraw-Hill: New York, **1940**.

(83) Hansch, C.; Fujita, T.; Maloney, P. P. Correlation of Biological Activity of Phenoxyacetic Acids with Hammet Substituent Constants and Partition Coefficients. *Nature*. **1962**, *194*, 178-180.

(84) Fujita, T.; Iwasa, J.; Hansch, C. A New Substituent Constant, π, Derived from Partition Coefficients. *J. Med Chem.* **1964**, *86*, 5175-5180.

(85) Hansch, C.; Steward, A. R.; Iwasa, J.; Deutsch, E. W. The Use of Hydrophobic Bonding Constant for Structure-Activity Correlations. *Mol. Pharmacol.* **1965**, *1*, 205-213.

(86) Iwasa, J.; Fujita, T.; Hansch, C. Substituent Constants for Aliphatic Functions Obtained from Partition Coefficients. *J. Med Chem.* **1965**, *8*, 150-153.

(87) Leo, A. ; Jow, P. Y. C.; Hansch, C. Calculation of Hydrophobic Constant (Log P) from π and *f* Constants. *J. Med. Chem.* **1975**, *18*, 865-868.

(88) Leo, A.; Hansch, C.; Church, C. Comparison of Parameters Currently Used in the Study of Structure-Activity Relationships. *J. Med. Chem.* **1969**, *12*, 766-771.

(89) Agrawal, A.; Pearson, P. P.; Taylor, E. W.; Li, H. B.; Dahlgren, T.; Herslöf, M.; Yang, Y.; Lambert, G.; Nelson, D. L.; Regan, J. W.; Martin, A. R. Three-Dimensional Quantitative Structure-Activity Relationships of 5-HT Receptor Binding Data for Tetrahydropyridinylindole Derivatives: A Comparison of the Hansch and CoMFA Methods. *J. Med. Chem.* **1993**, *36*, 4006-4014.

(90) Hansch, C.; Steward, A. R.; Anderson, S. M.; Bentley, D. The Parabolic Dependence of Drug Action Upon Lipophilic Character as Revealed by the Study of Hypnotics. *J. Med. Chem.* **1967**, *11*, 1-11.

(91) McFarland. J. W. On the Parabolic Relationship Between Drug Potency and Hydrophobicity. *J. Med. Chem.* **1970**, *13*, 1192-1196.

(92) Andrews, P. R. Molecular Orbital Calculations on Anticonvulsant Drugs. *J. Med. Chem.* **1969**, *12*, 761-764.

(93) Poupaert, J. H.; Vandervorst, D.; Guoit, P.; Moustafa, M. M. M.; Drumont, P. Structure-Activity Relationships of Phenytoin-Like Anticonvulsant Drugs. *J. Med. Chem.* **1984**, *27*, 76-78.

(94) Lien, E. J.; Liao, R. C. H; Shinouda, H. G. Quantitative Structure-Activity Relationships and Dipole Moments of Anticonvulsants and CNS Depressants. *J. Pharm. Sci.* **1979**, *68*, 463-465.

(95) Andrews, P. R.; Lloyd, E. J. Molecular conformation and Biological Activity of Central Nervous System Active Drugs. *Med. Res. Rev.* **1982**, *2*, 355-393.

(96) Camerman A.; Camerman, N. Ethylphenacemide and Phenacemide: Conformational Similarities to Diphenylhydantoin and Stereochemical Basis of Anticonvulsant Activity. *Proc. Natl. Acad. Sci. USA.*. **1977**, *74*, 1264-1266.

(97) Jones, P. J.; Kennard, O. Common Stereochemical Features in Anti-Epileptic Drugs: A Reinvestigation. *J. Pharm. Pharmac.* **1978**, *30*, 815-817.

(98) Jones, G. L.; Amato, R. J.; Wimbish, G. H.; Peyton, G. A. Comparison of Anticonvulsant Potencies of Cyheptamide, Carbamazepine, and Phenytoin. *J. Pharm. Sci.* **1981**, *70*, 618-620.

(99) Lien, E., Structure-Activity Correlations for Anticonvulsant Drugs. *J. Med. Chem.* **1970**, *13* ,1189-1191.

(100) Hancsh, C.; Klein, T. E. Molecular Graphics and QSAR in the Study of Enzyme-Ligand Iteractions. On the Definition of Bioreceptors. *Acc. Chem. Res.* **1986**, *19*, 392-400.

(101) Weaver, D. Applications of Molecular Physics 'Biotechnology' to the Rational Design of an Improved Phenytoin Analogue. *Seizure*. **1992**, *1*, 223-246.

(102) Codding, P. W.; Lee, T. L. ; Richardson, J. F. Cyheptamide and 3-Hydroxy-3-Phenacyloxindole: Structural Similarity to Diphenylhydantoin as the Basis for Anticonvulsant Activity. *J. Med. Chem.* **1984**, *27*, 649-654.

(103) Andrews, P. R.; Mark, L. C.; Winkler, D. A.; Jones, G. P. Structure-Activity Relationships of Convulsant and Anticonvulsant Barbiturates: A Computer-Graphic-Based-Pattern-Recognition Analysis. *J. Med. Chem.* **1983**, *26*, 1223-1229.

(104) Cramer III, R. D.; Clark, M.; Simeroth, P.; Patterson, D. E. Recent Developments in Comparative Molecular Field Analysis (CoMFA). *QSAR: Rational Approaches to the Design of Bioactive Compounds*. **1991**, 239-242.

(105) Cramer III, R. D.; Patterson, D. E.; Bunce, J. D. Comparative Molecular Field Analysis (CoMFA). 1. Effect of Shape on Binding of Steriods to Carrier Proteins, *J. Am. Chem. Soc.* **1988**, *110*, 5959-5967.

(106) Duchamp, D. J. Molecular Mechanics and Crystal Structure Analysis in Drug Design. *Computer-Assisted Drug Design*. **1979**, *3*, 79-102.

(107) Richards, W. G. *Quantum Pharmacology*; Butterworths: London; **1977**.

(108) Allinger, N. L. Conformational Analysis. 130. MM2. A Hydrocarbon Force Field Utilizing V_1 and V_2 Torsional Terms. *J. Am. Chem. Soc.* **1977**, *87*, 8127-8134.

(109) Clark, M.; Cramer III, R. D.; Opdenbosch, N. V. Validation of the General Purpose Tripos 5.2 Force Field. *J. Comp. Chem.* **1989**, *10*, 982-1012.

(110) Del Re, G. A Single MO-LCAO Method for the Calculation of Charge Distribution in Saturated Organic Molecules. *J. Chem. Soc.* **1958**, 4031-4040.

(111) Gasteiger, J.; Marsili, M. Interative Partial Equalization of Orbital Electronegativity--A Rapid Access to Atomic Charges. *Tetrahedron*. **1980**, *36*, 3219-3228.

(112) Kier, L. B. Molecular Orbital Theory in Drug Research. *Medicinal Chemistry, A Series of Monographs-Volume 10*; Academic Press: New York; **1971**.

(113) Berthod, H.; Pullman, A. Role of the δ-Framework in the Properties of the Biological Purines and Pyrimidines: Dipole Moments and Tautermeric Equilibria. *Biopolymers*. **1964**, *2*, 438-488.

(114) Stewart, J. J. P. MOPAC: A Semi-Emperical Molecular Orbital Program. *J. Comp.-Aided Mol. Design*. **1990**, *4* , 1-105.

(115) Cramer III, R. D. Partial Least Squares (PLS): Its Strengths and Limitations. *Perspectives in Drug Discovery and Design*. **1993**, *1*, 269-278.

(116) Cramer III, R. D.; Bunce, J. D.; Patterson, D. E.; Frank, I. E. Crossvalidation, Bootstrapping, and Partial Least Squares Compared with Multiple Regression in Conventional QSAR Studies. *Quant. Struct.-Act. Relat.* **1988**, *7*, 18-25.

(117) Kim, K. H.; Martin, Y. C. Evaluation of Electrostatic and Steric Descriptors for 3D-QSAR: The H^+ and CH_3 Probes Using Comparative Molecular Field Analysis (CoMFA) and the Modified Partial Least Squares Method. *QSAR: Rational Approaches to the Design of Bioactive Compounds*. **1991**, 151-154.

(118) Kim, K. H. Nonlinear Dependence in Comparative Molecular Field Analysis. *J. Comp.-Aided Mol. Design*. **1993**, *7*, 71-82.

(119) Kim, K. H. 3D-Quantitative Structure-Activity Relationships: Nonlinear Dependence Decribed Directly from 3D Structures Using a Comparative Molecular Field Analysis (CoMFA) Approach. *Quant. Struct.-Act. Relat.* **1992**, *11*, 309-317.

(120) Rein, K. S.; Baden, D. G.; Gawley, R. E. Conformational Analysis of the Sodium Channel Modulator, Brevetoxin A, Comparison with Brevetoxin B Conformatons, and a Hypothesis About the Commmon Pharmacophore of the "Site 5" Toxins. *J. Org. Chem.* **1994**, *50*, 2101-2106.

(121) Greco, G.; Novellino, C. S.; Vittora, A. Comparative Molecular Field Analysis on a Set of Muscurinic Agents. *QSAR*. **1991**, *10*, 289-299.

(122) Kim, K. H.; Greco, G.; Novellino, E.; Silipa, C.; Vittoria, A. Use of the Hydrogen Bond Potential Function in a Comparative Molecular Field Analysis (CoMFA) on a Set of Benzodiazepines. *J. Comp.-Aided Mol. Design*. **1993**, *7*, 263-280.

(123) Giovanni, G.; Ettore, N.; Fiorini, I.; Nacci, B.; Campiani, G.; Ciani, S. M.; Garofalo, A.; Bernasconii, P.; Mennini, T. Comparative Molecular Field Analysis Model for 6-Arylpyrrolo[2,1-d][1,5]Benzothiazepines Binding Selectively to the Mitochondrial Benzodiazepine Receptor. *J. Med. Chem.* **1994**, *37*, 4100-4108.

(124) Wong G.; Koehler, K. F.; Skolnick, P.; Gu, Z-Q.; Ananthan, P.; Schönholzer, W.; Hyunkeler, W.; Zhang, W.; Cook, W. Synthetic and Computer-Assisted Analysis of the Structural Requirements for Selective, High-Affinity Ligand Binding to Diazepam-Insensitive Benzodiazepine Receptors. *J. Med. Chem.* **1993**, *36*, 1820-1830.

(125) Andre, M.M.; Charifson, P. S. Constance, E. O.; Kula, N. S.; McPhail, A. T.; Baldessarini, R. J.; Booth, R. G.; Wyrick, S. D. Conformational Analysis, Pharmacophore Identification, and Comparative Molecular Field Analysis of Ligands for the Neuromodulatory σ_3 Receptor. *J. Med. Chem.* **1994**, *37*, 4109-4117.

(126) Ablordeppy, S. Y.; El-Ashmaway, M. B.; Glennon, R. A. Analysis of the Structure Activity Relationships of Sigma Ligands. *Med. Chem. Res.* **1991**, *1*, 425-438.

(127) Thomas, B. F.; Compton, B.R.M.; Semus, S.F. Modeling the Cannabinoid Receptor: A Three-Dimensional Quantative Structure Activity Analysis. *Mol. Pharmacol.* **1991**, *40*, 656.

(128) Semus, S. F. A Computer Graphic Investigation into the Structural Requirements for Interaction with the Putative Cannabinoid Receptor Site. *Med. Chem. Res.* **1991**, *1*, 454-460.

(129) Chen, J. M.; Sheldon, A. Structure-Function Correlations for Calcium Binding and Calcium Channel Activities Based on 3-Dimensional Models of Human Annexins I, II, III, V, VII. *Biomol. Struct. Dynam.* **1993**, *10*, 1067-1089.

(130) Rustici, M.; Bracci, L.; Lozzi, P.; Nari, P.; Santucci, A.; Sodani, P.; Spreafico, A.; Niccolai, N. A Model of the Rabies Virus Glycoprotein Active Site. *Biopolymers.* **1993**, *33*, 961-969.

(131) Calder, J. A.; Wyatt, J. A.; Frenkel, D. A.; Casida, J.E. CoMFA Validation of the Superposition of Six Classes of Compounds which Block GABA Receptors Non-Competitively. *J. Comp.-Aided Mol. Design.* **1993**, *7*, 45-60.

(132) Nordvall, G.; Hacksell, U. Binding Site Modeling of the Muscarinic M1 Receptor: A Combination of Homology-Based and Indirect Approaches. *J. Med. Chem.* **1993**, *36*, 967-976.

(133) Caroll, F. I.; Mascrella, S. W.; Kuzemko, M. A.; Goa, Y. G.; Abraham, P.; Lewin, A. H.; Boja, J. W.; Kuhar, M. J. Synthesis, Ligand-Binding and QSAR (CoMFA and Classical) Study of 3β-(3'-Substituted Phenyl), 3β-(4'-Substituted Phenyl), 3β-(3',4'-Disubstituted Phenyl) Tropane-2β-Carboxcylic Acid Methyl-Esters. *J. Med. Chem.* **1994**, *37*, 2865-2873.

(134) Agarwal, A.; Taylor, E. W. 3-D QSAR for Intrinsic Activity of 5-HT_{1A} Receptor Ligands by the Method of Comparative Molecular Field Analysis. *J. Comput. Chem.* **1993**, *14*, 237-245.

(135) Langer, T.; Wermuth, C. G. Inhibitors of Prolyl Endopeptidase: Characterization of the Pharmacophoric Pattern Using Conformational Analysis and 3D-QSAR. *J. Comp.-Aided Mol. Design.* **1993**, *7*, 253-262.

(136) Allen, M.S.; LaLoggia, A. J.; Dorn, M. J.; Constantino, G.; Hagen, T.J.; Koehler, K. F.; Skolnick, P.; Cook, J. M. Predictive Binding of β-Carboline Inverse Agonist and Antagonists via the CoMFA/GOLPE Approach. *J. Med Chem.* **1992**, *35*, 4001-4010.

(137) Brouillette, W. J.; Brown, G. B.; Delorey, T. M.; Shirali, S. S. ; Grunewald, G. L. Anticonvulsant Activities of Phenyl-Substituted Bicyclic 2,4-Oxazolidinediones and Monocyclic Models. Comparison with Binding to the Neuronal Voltage-Dependent Sodium Channel. *J. Med. Chem.* **1988**, *31*, 2218-2221.

(138) Harris, W. E.; Stahl, W. L. Interactions of Phenytoin with Rat Brain Synaptosomes Examined by Flourescent Fatty Acid Probes. *Neurochem. Int.* **1988**, *13*, 369-377.

(139) Francis, J.; Burnham, W. M. [^{3}H]Phenytoin Identifies a Novel Anticonvulsant-Binding Domain on Voltage-Dependent Sodium Channels. *Mol. Pharmacol.* **1992**, *42*, 1097-1103.

(140) Brouillette, W. J.; Brown, G. B.; Delorey, T. M.; Liang, G. Sodium Channel Binding and Anticonvulsant Activities of Hydantoins Containing Conformationally Constrained 5-Phenyl Substituents. *J. Pharm. Sci.* **1990**, *79*, 871-874.

(141) Crammer III, R. D.; M. Clark, M.; Simeroth, P.; Patterson, D. E. Developments in Comparative Molecular Field Analysis (CoMFA). *QSAR: Rational Approaches to the Design of Bioactive Compounds*. **1991**, 239-242.

(142) Brouillette, W. J.; Einspahr, H. M. Bicyclic Imides with Bridgehead Nitrogen. Synthesis and X-Ray Crystal Structure of a Bicyclic 2,4-Oxazolidinedione. *J. Org. Chem*. **1984**, *49*, 5113-5116.

APPENDIX A.

Spectroscopic Data for Compounds in "Hydantoins with Conformationally Restricted Phenyl Rings. Effects on Sodium Channel Binding"

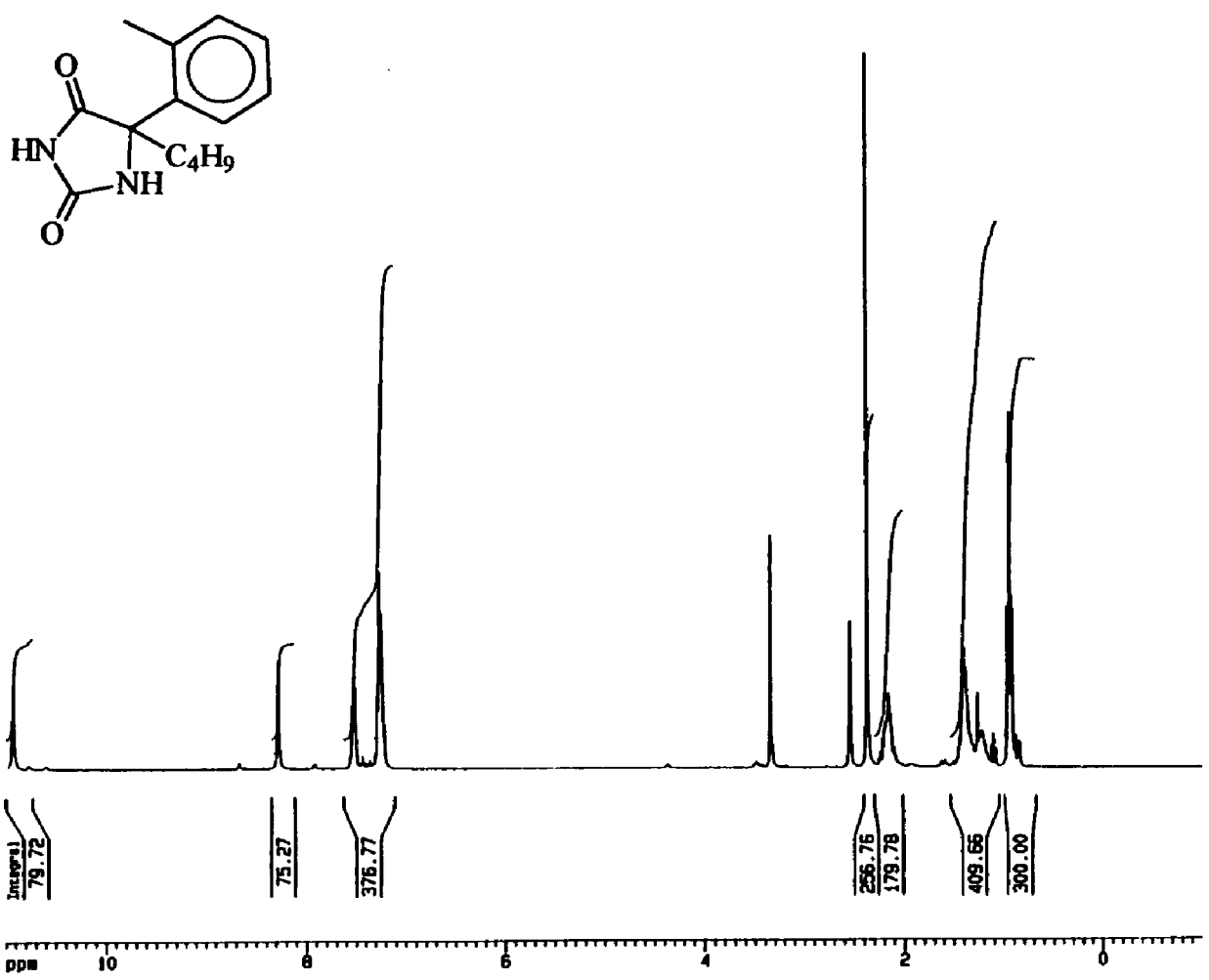


```
Current Data Parameters
NAME          mib-ometh1
EXPNO               20
PROCNO               1

F2 - Acquisition Parameters
Date            950520
Time             14.01
PULPROG          zg30
SOLVENT          DMSO
AQ          2.8542280 sec
FIDRES      0.188380 Hz
DW             81.0 usec
RG              1430
NUCLEUS           1H
D1          1.0000000 sec
P1              8.8 usec
DE             115.7 usec
SFO1        300.1365877 MHz
SWH         5172.84 Hz
TD              32768
NS                32
DS                 2

F2 - Processing parameters
SI              16384
SF          300.1347759 MHz
WDW               EM
SSB                0
LB              0.30 Hz
GB                 0
PC              1.00

1D NMR plot parameters
CX             20.00 cm
F1P            11.000 ppm
F1             3301.48 Hz
F2P            -1.000 ppm
F2             -300.13 Hz
PPMCM          0.60000 ppm/cm
HZCM           180.08088 Hz/cm
```

Figure 1. ^{1}H NMR Spectrum (300 MHz) of Compound 4 (d^{6}-DMSO).

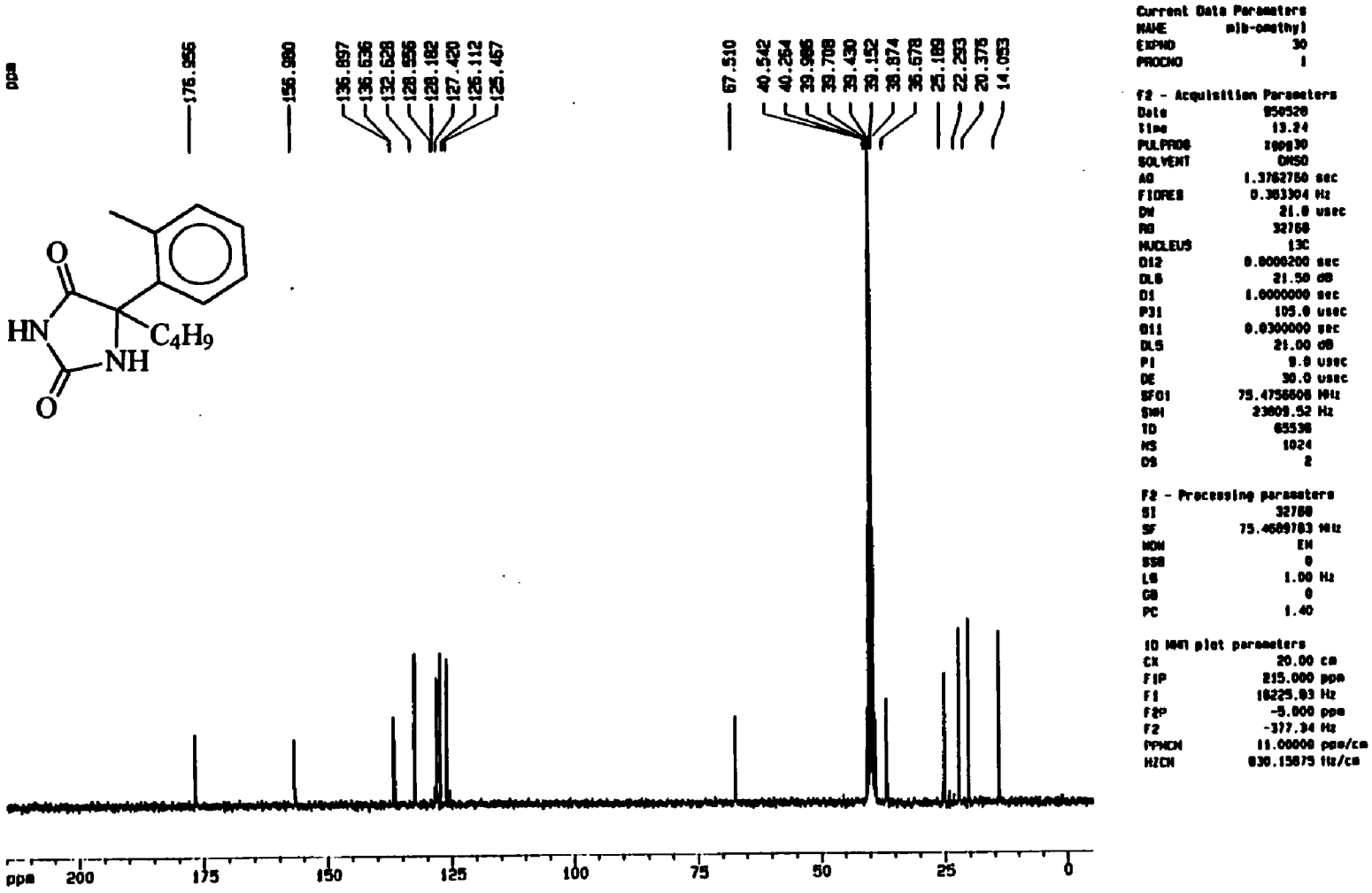

Current Data Parameters
NAME mib-omethyl
EXPNO 30
PROCNO 1

F2 - Acquisition Parameters
Date 950520
Time 13.24
PULPROG zgpg30
SOLVENT DMSO
AQ 1.3762750 sec
FIDRES 0.363304 Hz
DW 21.0 usec
RG 32768
NUCLEUS 13C
D12 0.0000200 sec
DL6 21.50 dB
D1 1.0000000 sec
P31 105.0 usec
D11 0.0300000 sec
DL5 21.00 dB
PI 9.0 usec
DE 30.0 usec
SFO1 75.4756806 MHz
SWH 23809.52 Hz
TD 65536
NS 1024
DS 2

F2 - Processing parameters
SI 32768
SF 75.4689783 MHz
WDW EM
SSB 0
LB 1.00 Hz
GB 0
PC 1.40

1D NMR plot parameters
CX 20.00 cm
F1P 215.000 ppm
F1 16225.93 Hz
F2P -5.000 ppm
F2 -377.34 Hz
PPMCM 11.00000 ppm/cm
HZCM 830.13875 Hz/cm

Figure 2. ^{13}C Spectrum (75 Mhz) of Compound **4** (d^6-DMSO).

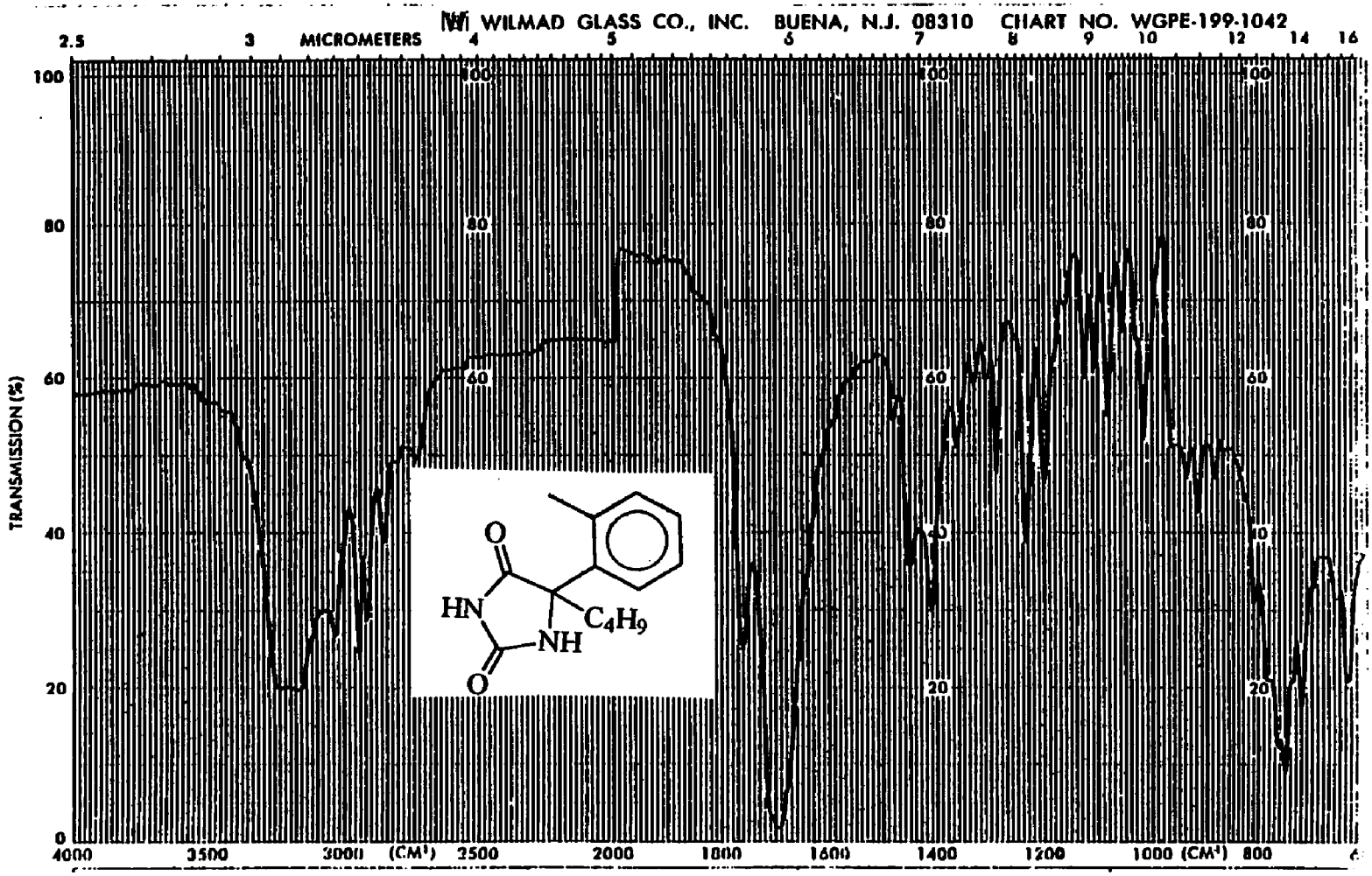

Figure 3. IR Spectrum of Compound 4 (KBr).

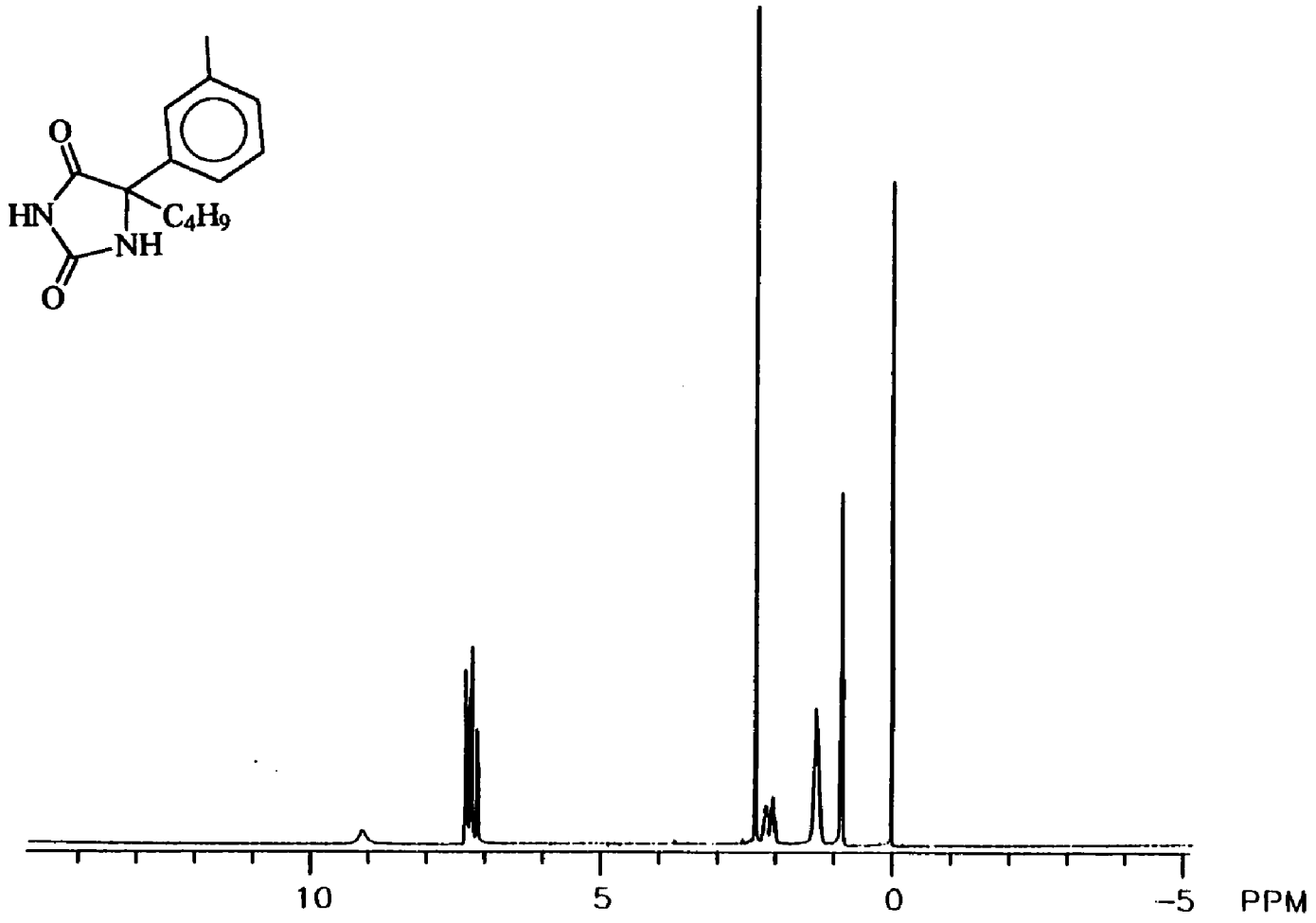

Figure 4. ^{1}H NMR Spectrum (300 MHz) of Compound 5 (d^{6}-DMSO).

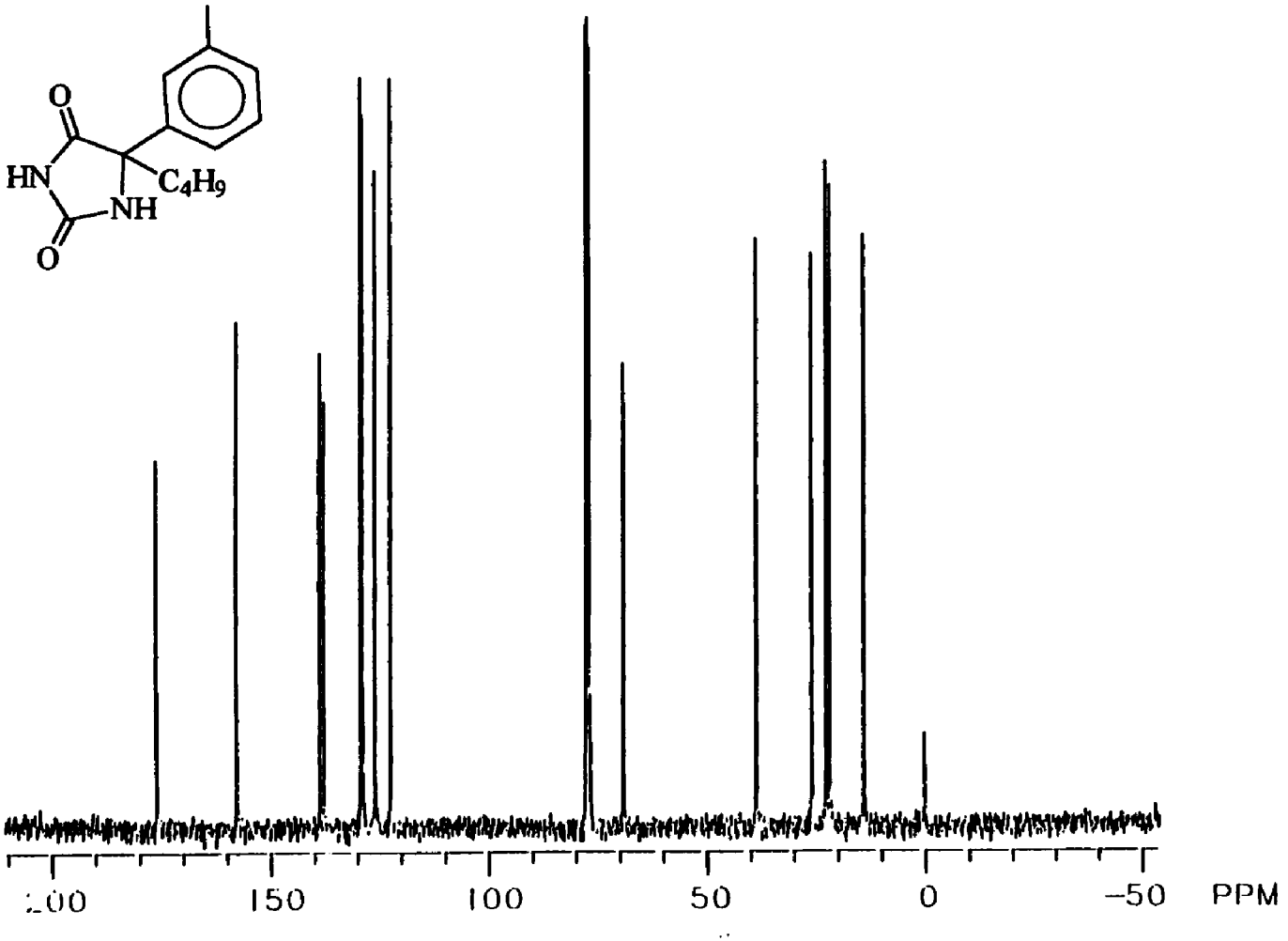

Figure 5. ^{13}C Spectrum (75 Mhz) of Compound **5** (d^6-DMSO).

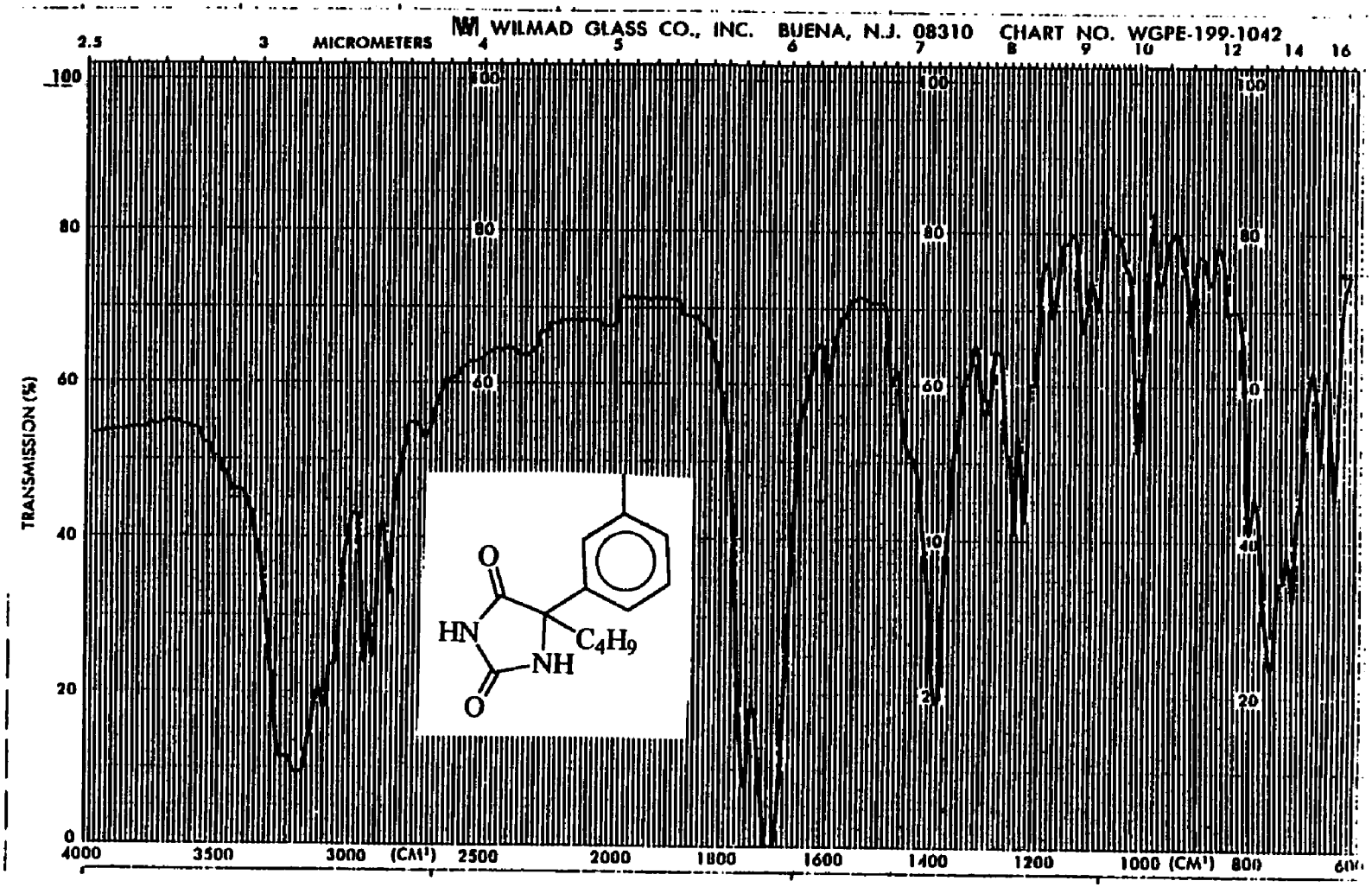

Figure 6. IR Spectrum of Compound 5 (KBr).

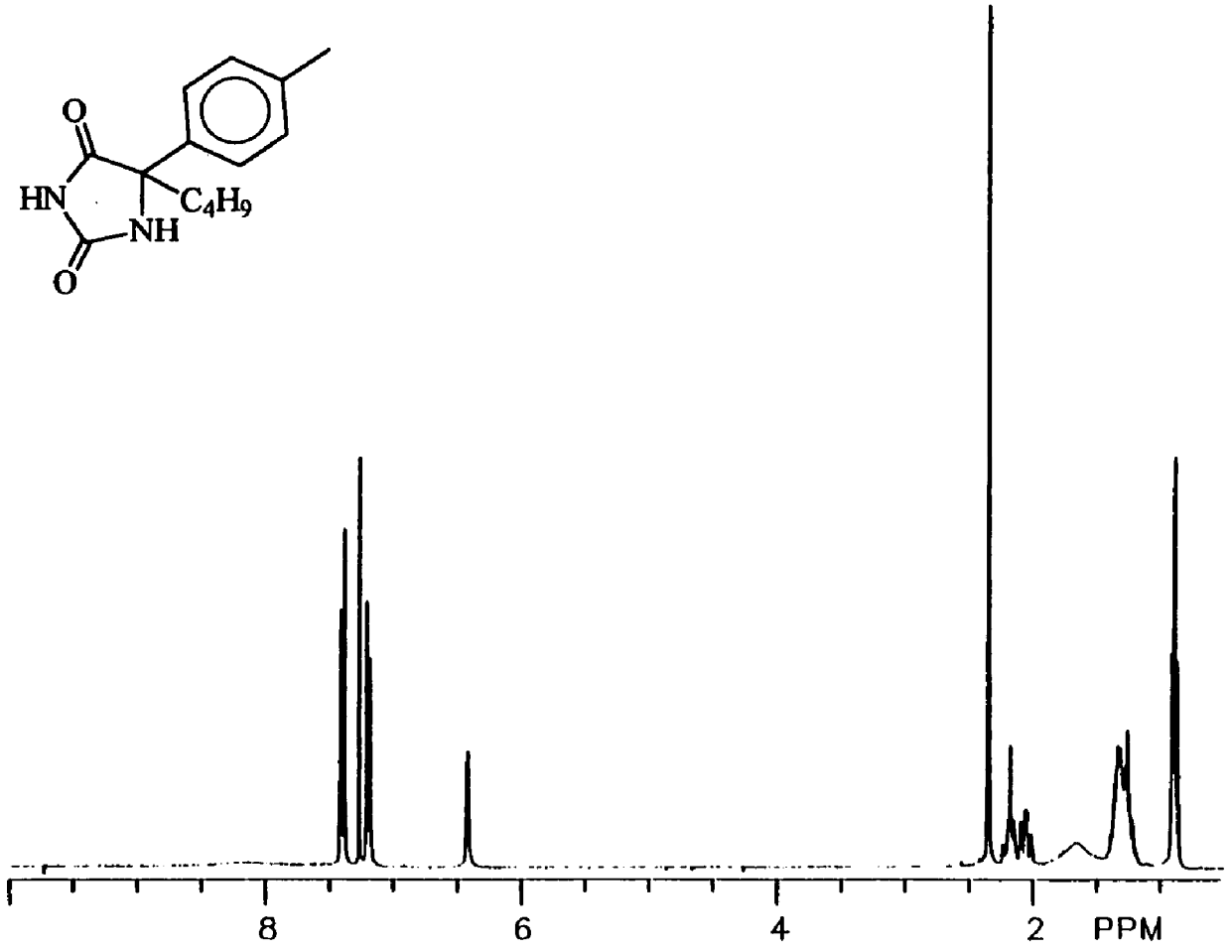

Figure 7. ^{1}H NMR Spectrum (300 MHz) of Compound 6 (d^6-DMSO).

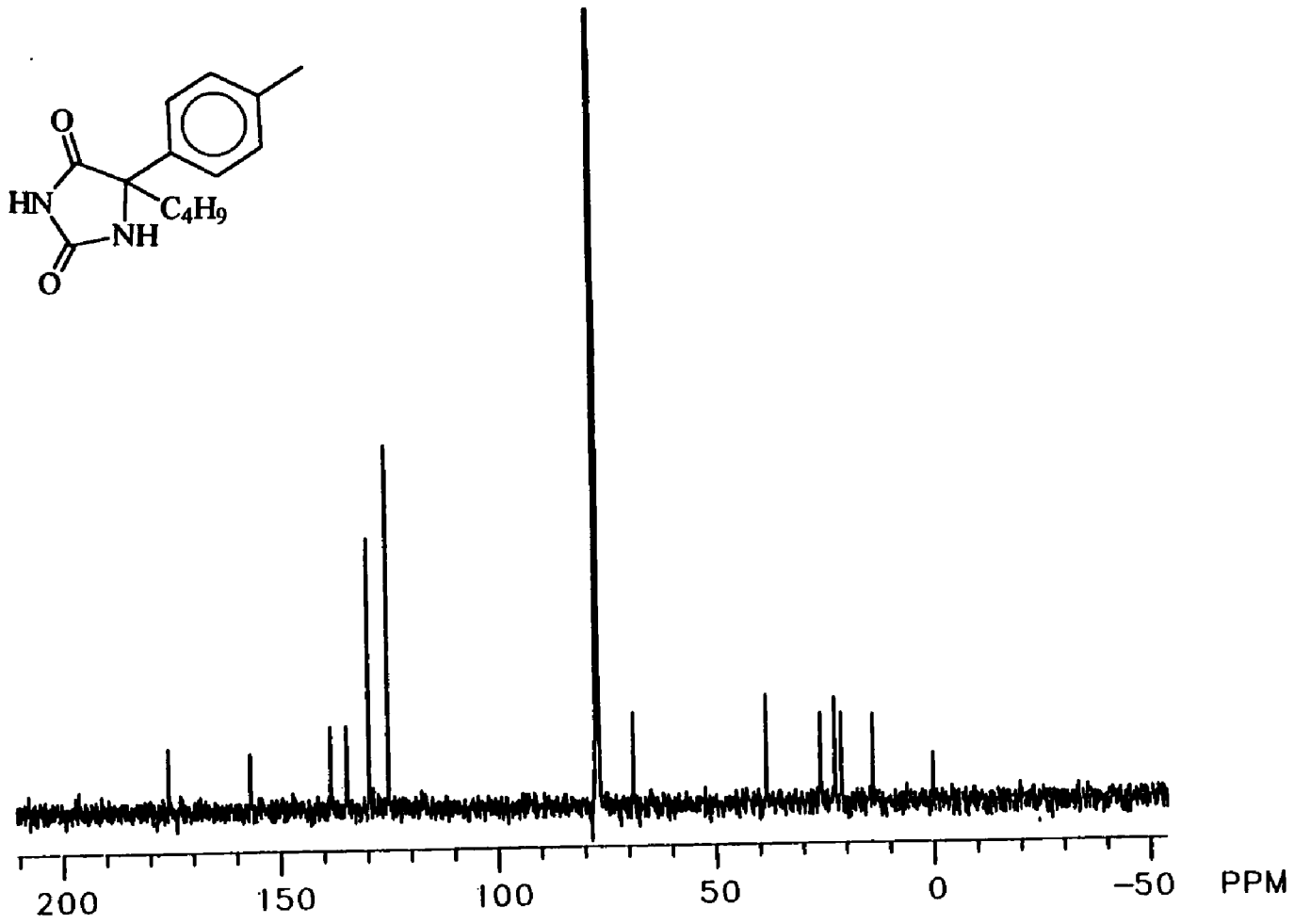

Figure 8. ^{13}C Spectrum (75 Mhz) of Compound **6** (d^6-DMSO).

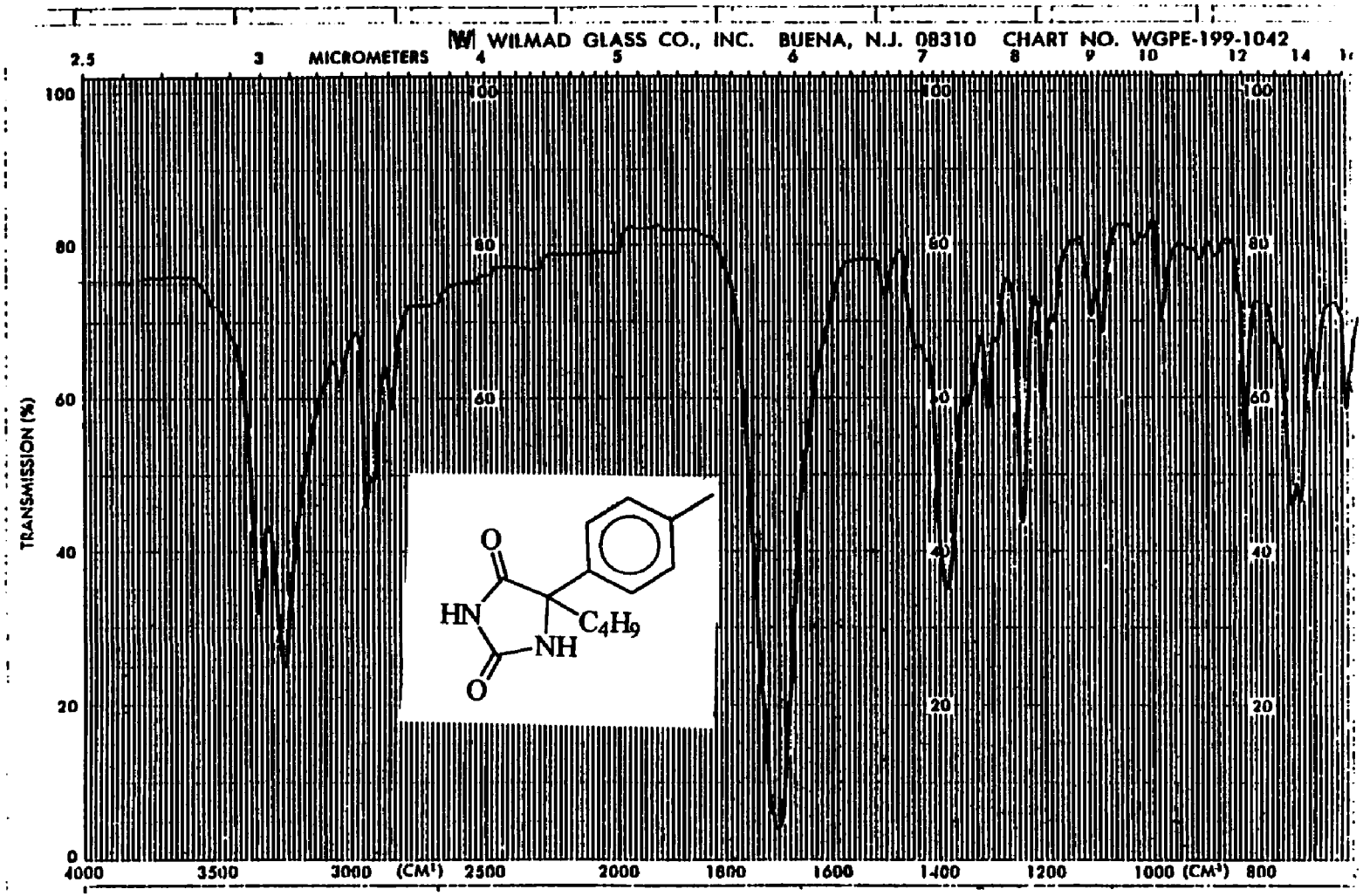

Figure 9. IR Spectrum of Compound 6 (KBr).

APPENDIX B.

Spectroscopic Data for Compounds in "Comparative Molecular Field Analysis of Hydantoin Binding to the Neuronal Voltage-Dependent Sodium Channel"

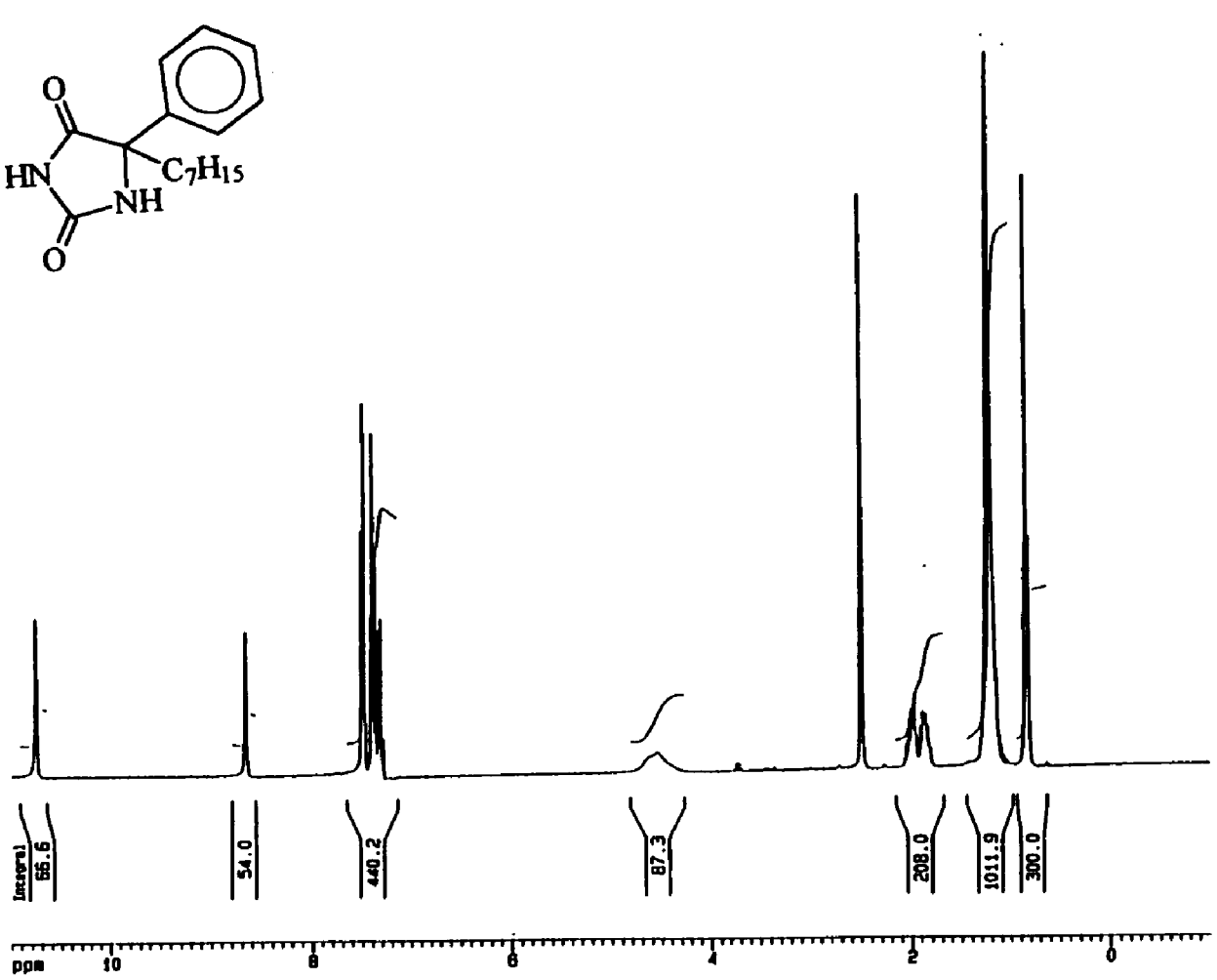


```
Current Data Parameters
NAME            ajb-II-42
EXPNO                   10
PROCNO                   1

F2 - Acquisition Parameters
Date                950228
Time                 14.52
PULPROG              zg30
SOLVENT              DMSO
AQ            2.6542208 sec
FIDRES        0.188300 Hz
DW                 81.0 usec
RG                 2050
NUCLEUS              1H
D1            1.0000000 sec
P1                  8.0 usec
DE                115.7 usec
SFO1        300.1365877 MHz
SWH            6172.84 Hz
TD                 32768
NS                    32
DS                     2

F2 - Processing parameters
SI                 16384
SF          300.1347884 MHz
WDW                   EM
SSB                    0
LB                  0.30 Hz
GB                     0
PC                  1.00

1D NMR plot parameters
CX                 20.00 cm
F1P               11.000 ppm
F1                3301.48 Hz
F2P               -1.000 ppm
F2                -300.13 Hz
PPMCM              8.60000 ppm/cm
HZCM             180.00097 Hz/cm
```

Figure 1. ^{1}H NMR Spectrum (300 MHz) of Compound 6 (d^6-DMSO).

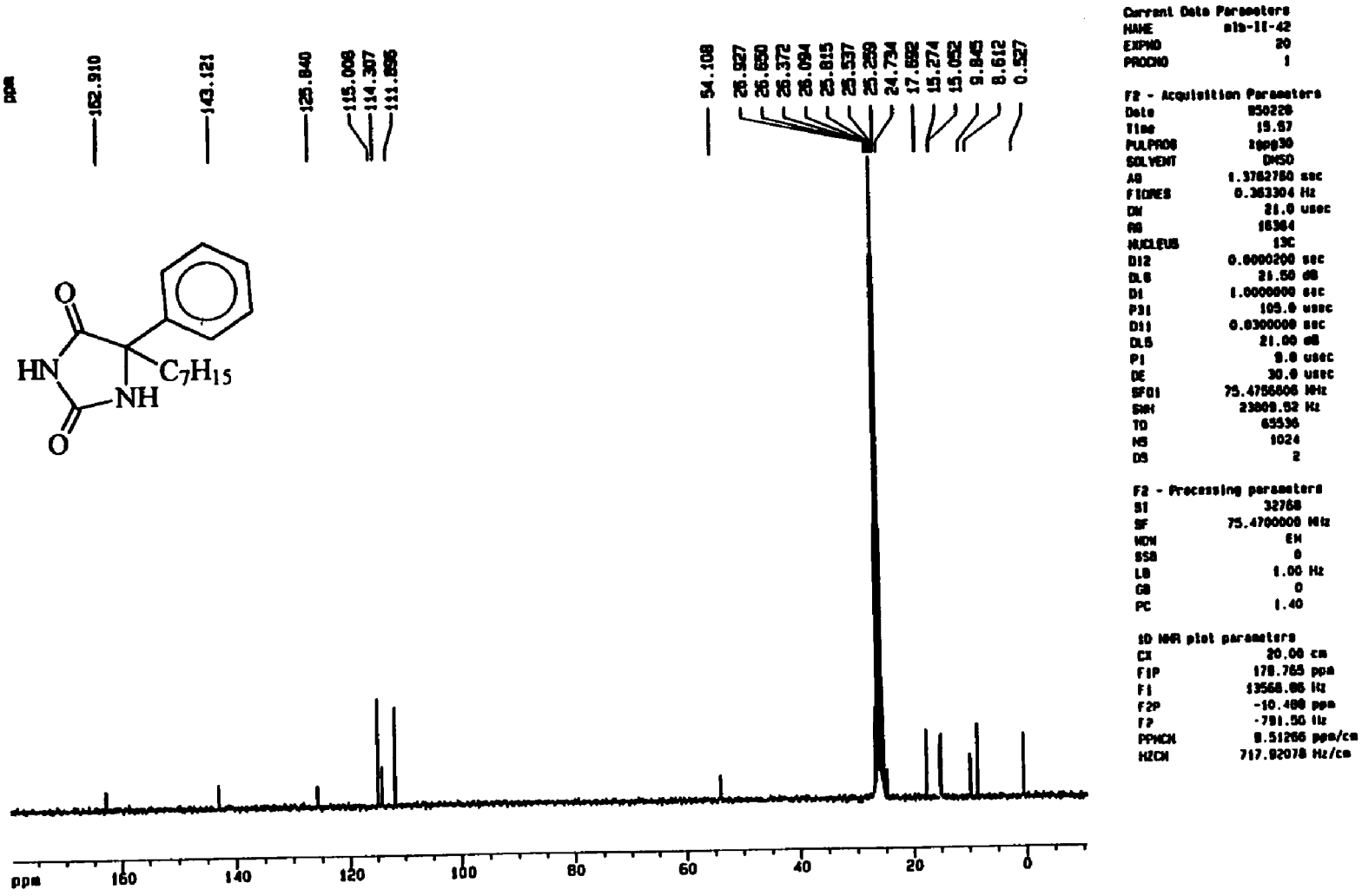

Current Data Parameters
NAME sih-II-42
EXPNO 20
PROCNO 1

F2 - Acquisition Parameters
Date 950228
Time 15.57
PULPROG zgpg30
SOLVENT DMSO
AQ 1.3762560 sec
FIDRES 0.363304 Hz
DW 21.0 usec
RG 16384
NUCLEUS 13C
D12 0.0000200 sec
DL0 21.50 dB
D1 1.0000000 sec
P31 105.0 usec
D11 0.0300000 sec
DL5 21.00 dB
P1 9.0 usec
DE 30.0 usec
SFO1 75.4756606 MHz
SWH 23809.52 Hz
TD 65536
NS 1024
DS 2

F2 - Processing parameters
SI 32768
SF 75.4700000 MHz
WDW EM
SSB 0
LB 1.00 Hz
GB 0
PC 1.40

1D NMR plot parameters
CX 20.00 cm
F1P 178.765 ppm
F1 13568.86 Hz
F2P -10.400 ppm
F2 -791.50 Hz
PPMCM 8.51266 ppm/cm
HZCM 717.92078 Hz/cm

Figure 2. ^{13}C Spectrum (75 MHz) of Compound **6** (d^6-DMSO).

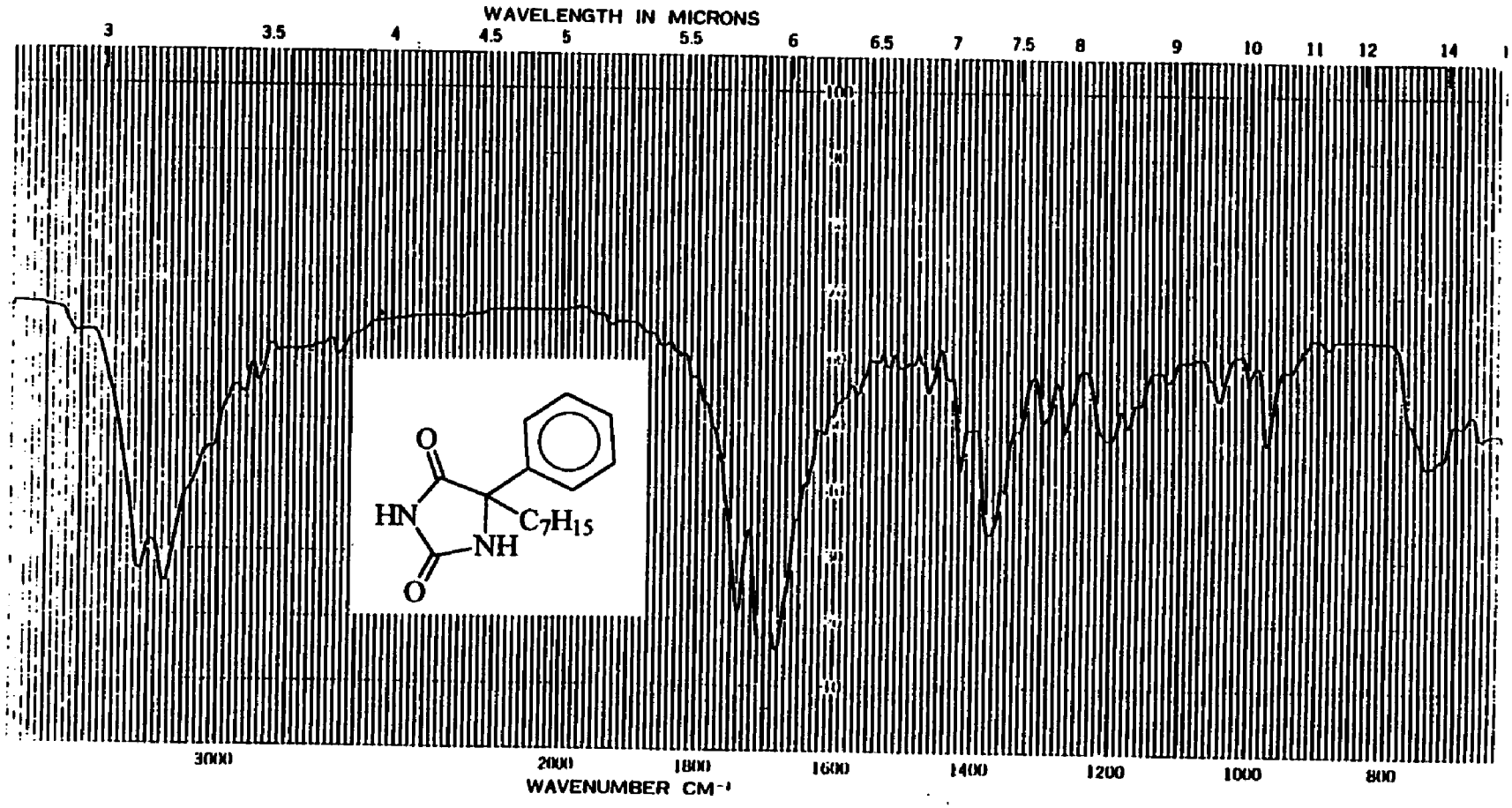

Figure 3. IR Spectrum of Compound 6 (KBr).

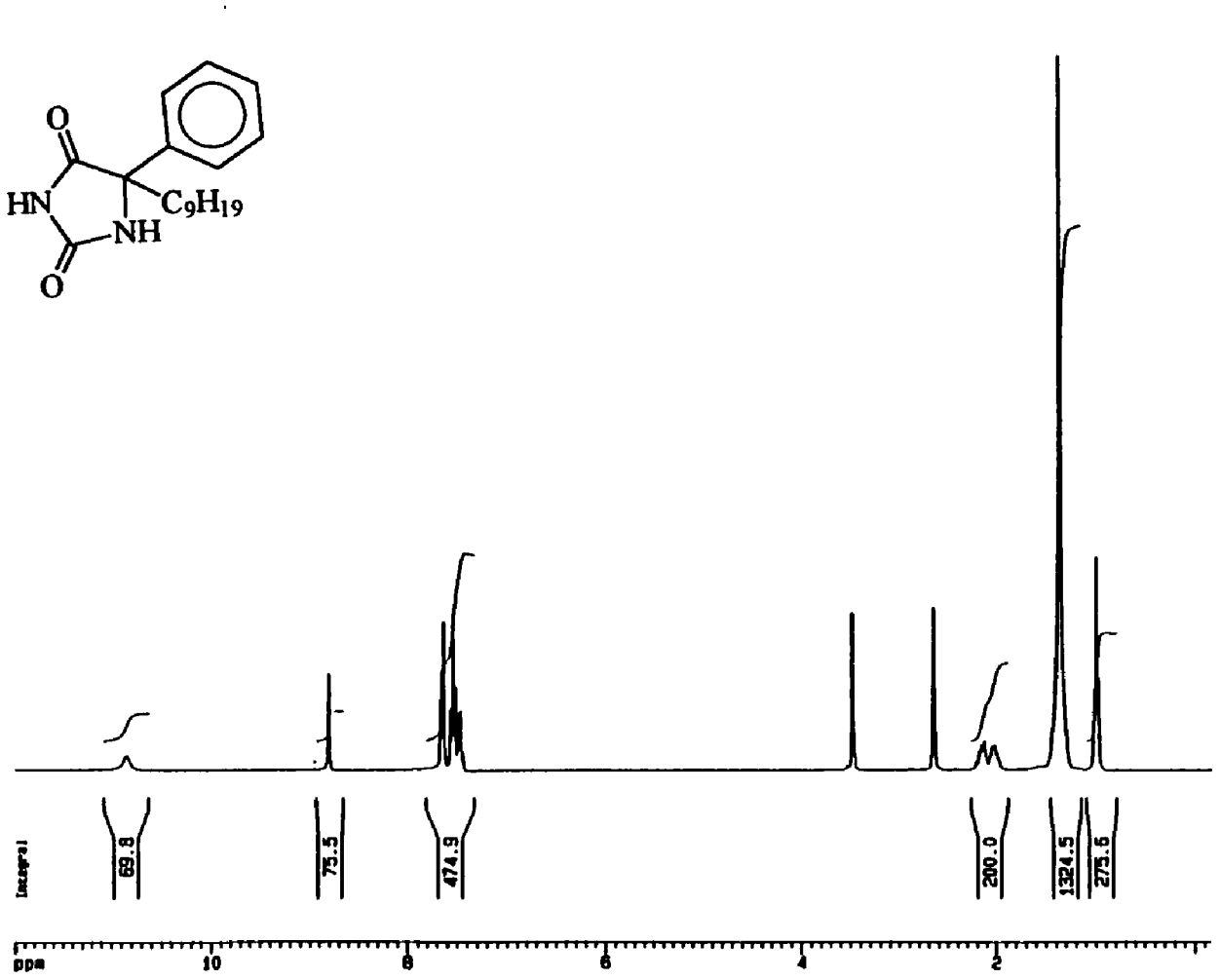


```
Current Data Parameters
NAME            mlb-hyde8
EXPNO                  12
PROCNO                  1

F2 - Acquisition Parameters
Date               950510
Time                16.14
PULPROG             zg30
SOLVENT             DMSO
AQ            2.6542288 sec
FIDRES        0.188380 Hz
DW                 81.0 usec
RG                 1430
NUCLEUS              1H
D1            1.0000000 sec
P1                  8.0 usec
DE                 15.7 usec
SFO1        300.1365077 MHz
SWH           6172.84 Hz
TD                 32768
NS                    32
DS                     2

F2 - Processing parameters
SI                 16384
SF          300.1347378 MHz
WDW                   EM
SSB                    0
LB                  0.30 Hz
GB                     0
PC                  1.00

1D NMR plot parameters
CX                 20.00 cm
F1P               12.009 ppm
F1                3604.21 Hz
F2P               -0.183 ppm
F2                -49.86 Hz
PPMCM          0.60057 ppm/cm
HZCM          180.05335 Hz/cm
```

Figure 4. ^{1}H NMR Spectrum (300 MHz) of Compound 7 (d^6-DMSO).

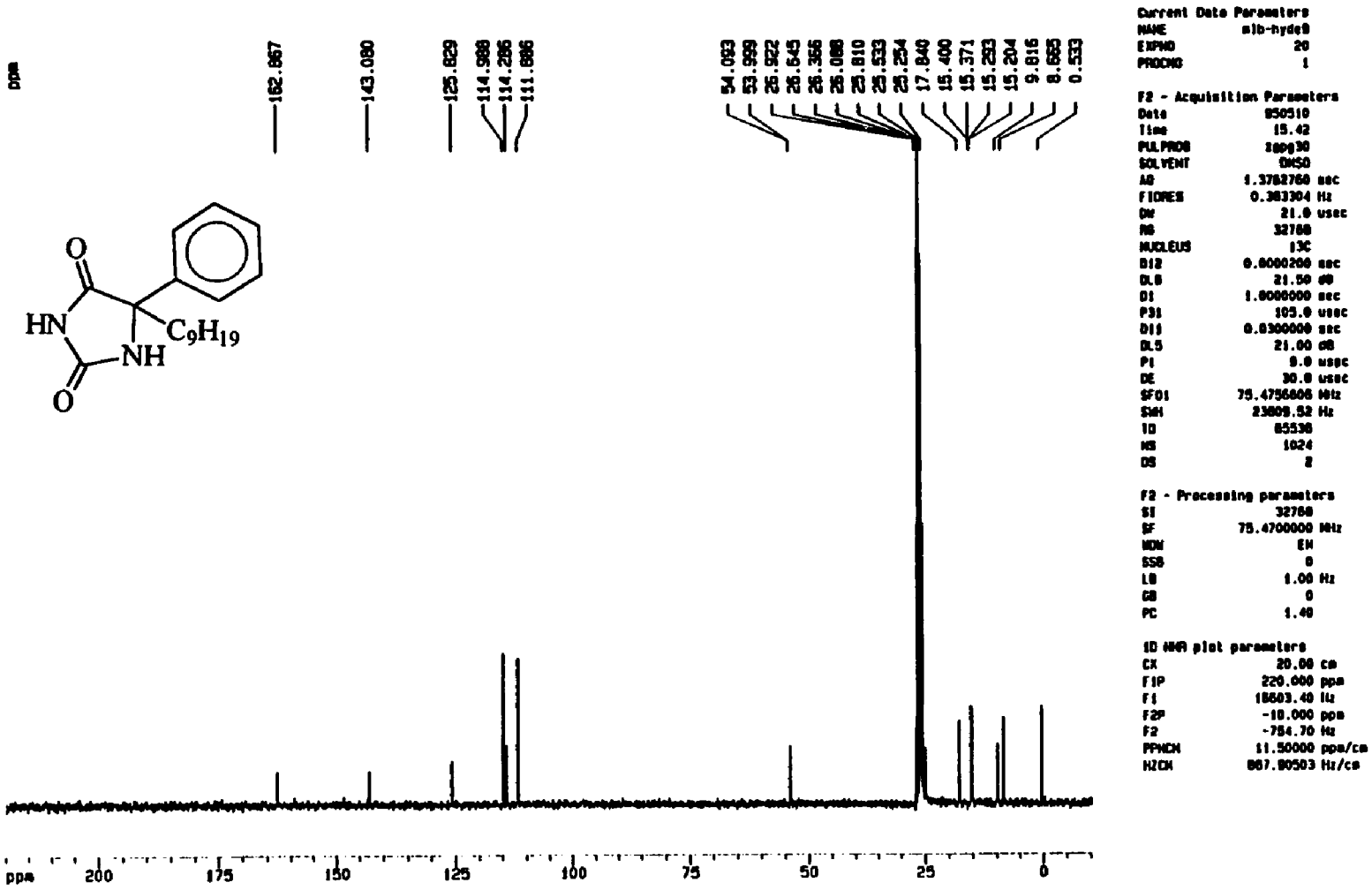

Current Data Parameters
NAME nib-hyde8
EXPNO 20
PROCNO 1

F2 - Acquisition Parameters
Date 950510
Time 15.42
PULPROG zgpg30
SOLVENT DMSO
AQ 1.3762760 sec
FIDRES 0.363304 Hz
DW 21.0 usec
RG 32768
NUCLEUS 13C
D12 0.0000200 sec
DL0 21.50 dB
D1 1.0000000 sec
P31 103.0 usec
D11 0.0300000 sec
DL5 21.00 dB
PI 9.0 usec
DE 30.0 usec
SFO1 75.4756806 MHz
SWH 23809.52 Hz
TD 65536
NS 1024
DS 2

F2 - Processing parameters
SI 32768
SF 75.4700000 MHz
WDW EM
SSB 0
LB 1.00 Hz
GB 0
PC 1.40

1D NMR plot parameters
CX 20.00 cm
F1P 220.000 ppm
F1 16603.40 Hz
F2P -10.000 ppm
F2 -754.70 Hz
PPMCM 11.50000 ppm/cm
HZCM 867.80503 Hz/cm

Figure 5. ^{13}C Spectrum (75 MHz) of Compound **7** (d^6-DMSO).

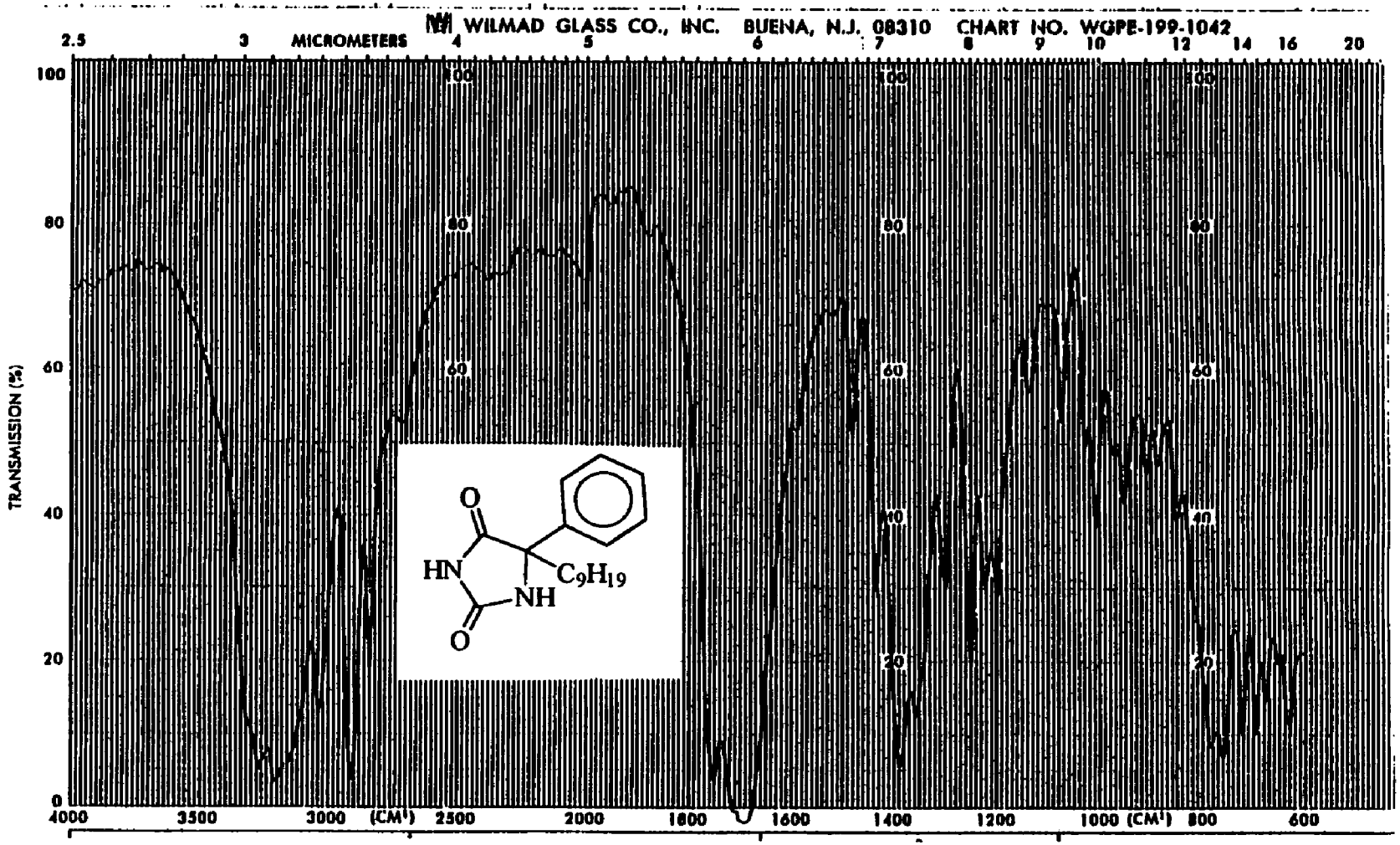

Figure 6. IR Spectrum of Compound 7 (KBr).

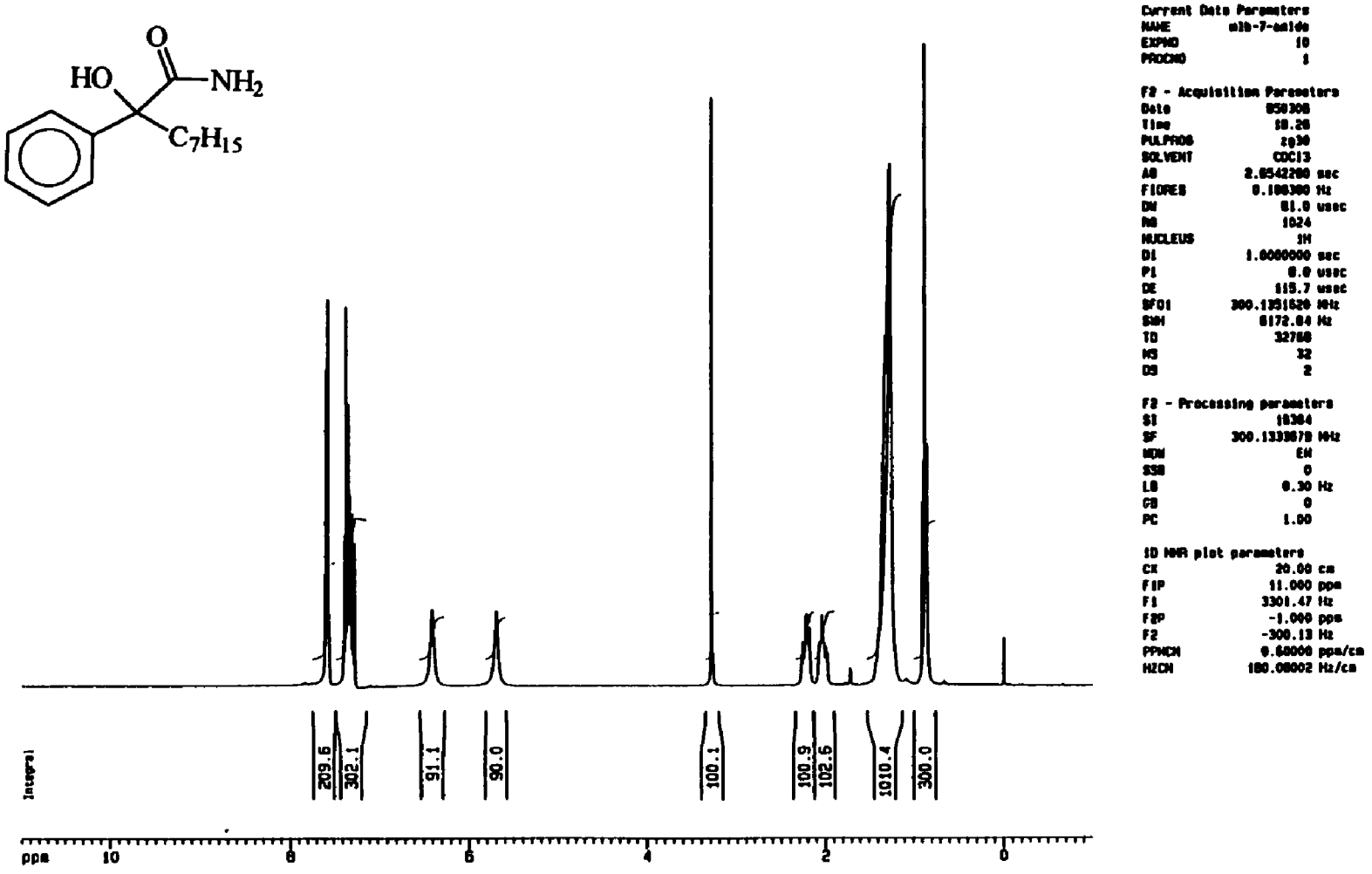

Figure 7. ^{1}H NMR Spectrum (300 MHz) of Compound **20** ($CDCl_3$).

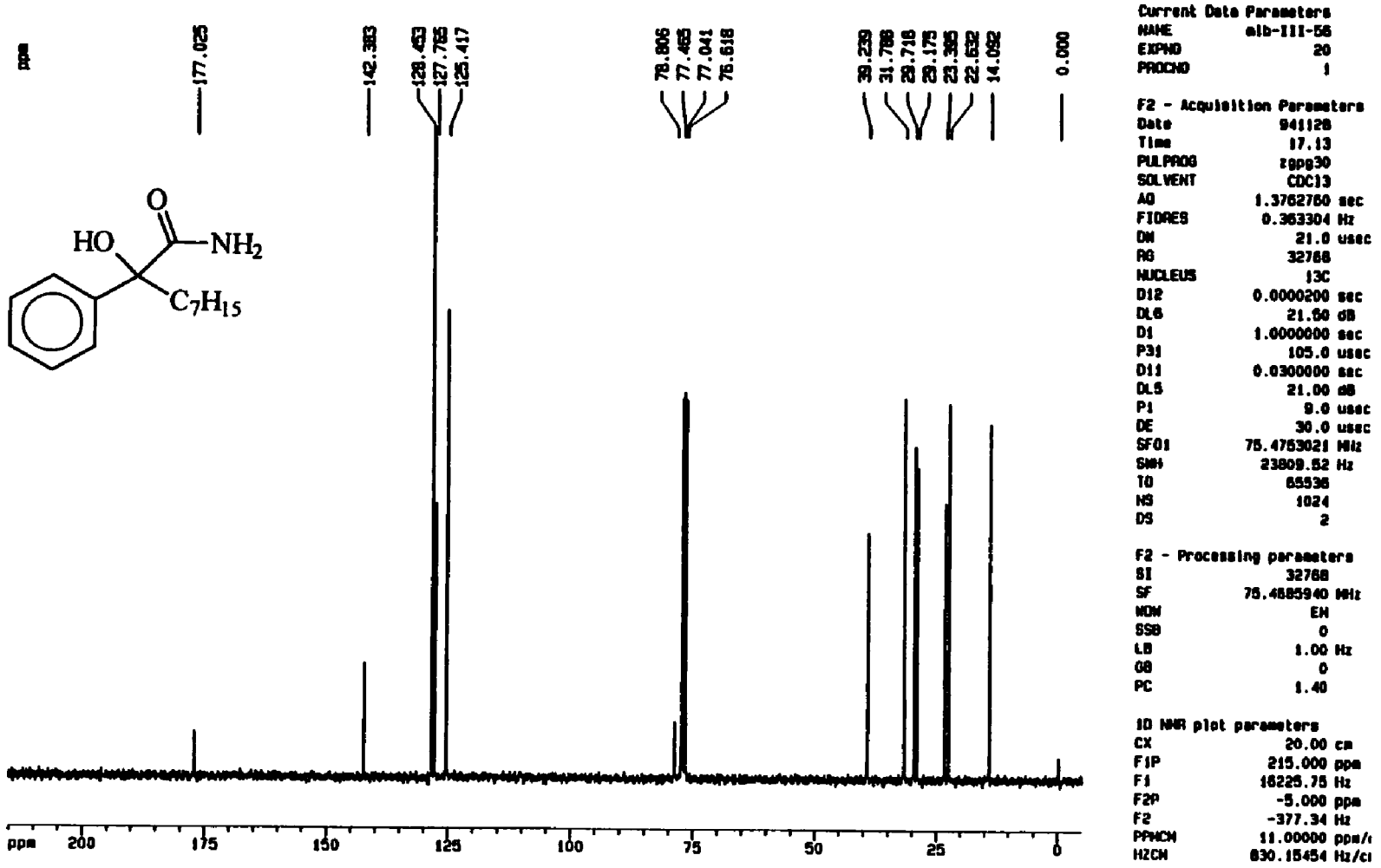

Figure 8. ^{13}C Spectrum (75 MHz) of Compound **20** ($CDCl_3$).

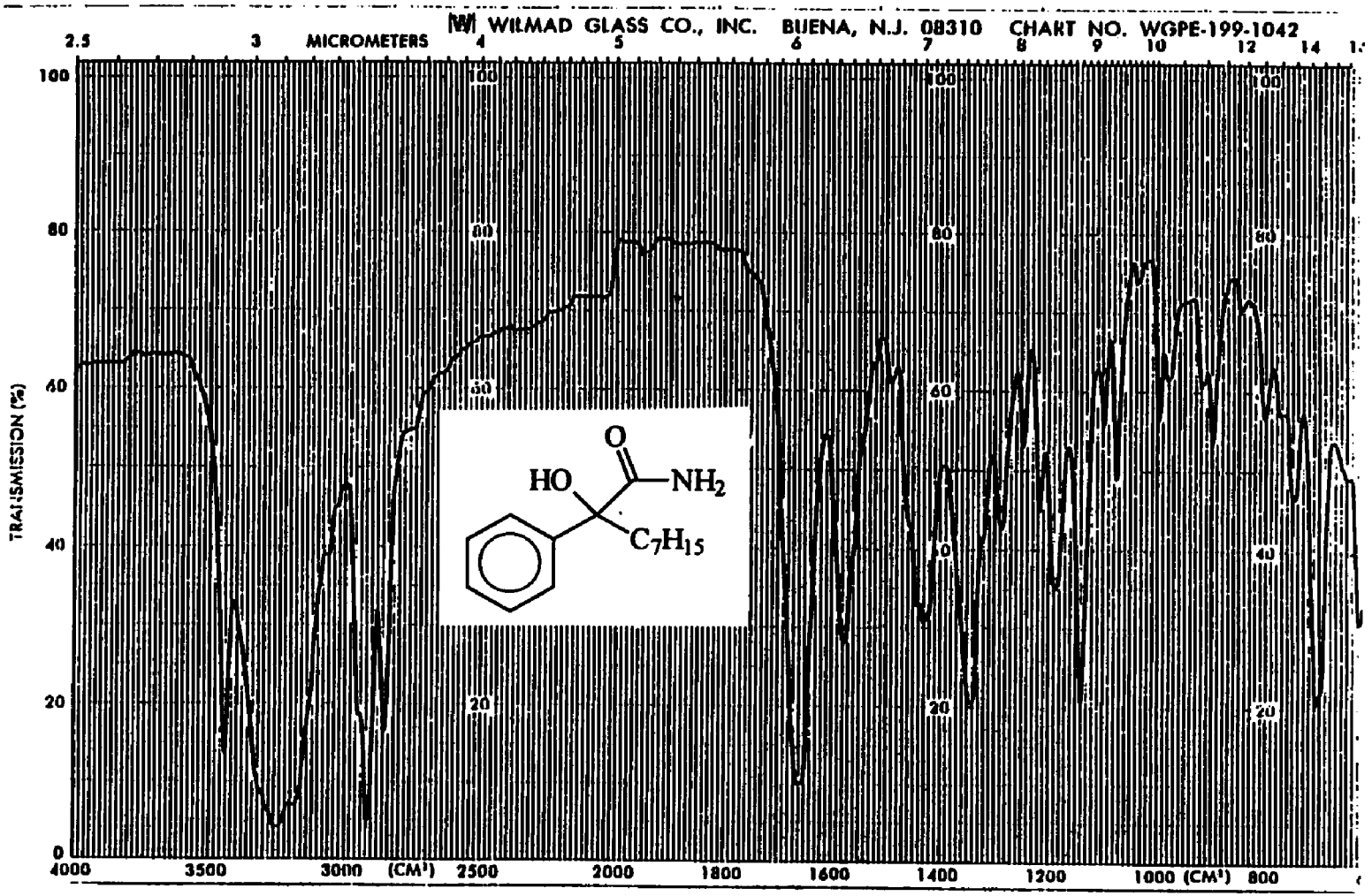

Figure 9. IR Spectrum of Compound 20 (KBr).

APPENDIX C.

Spectroscopic Data for Compounds in "Synthesis and Anticonvulsant Activities of Phenyl Substituted α-Hydroxy-α-Phenylcaprolactams and α-Alkyl-α-Hydroxy-α-Phenylamides"

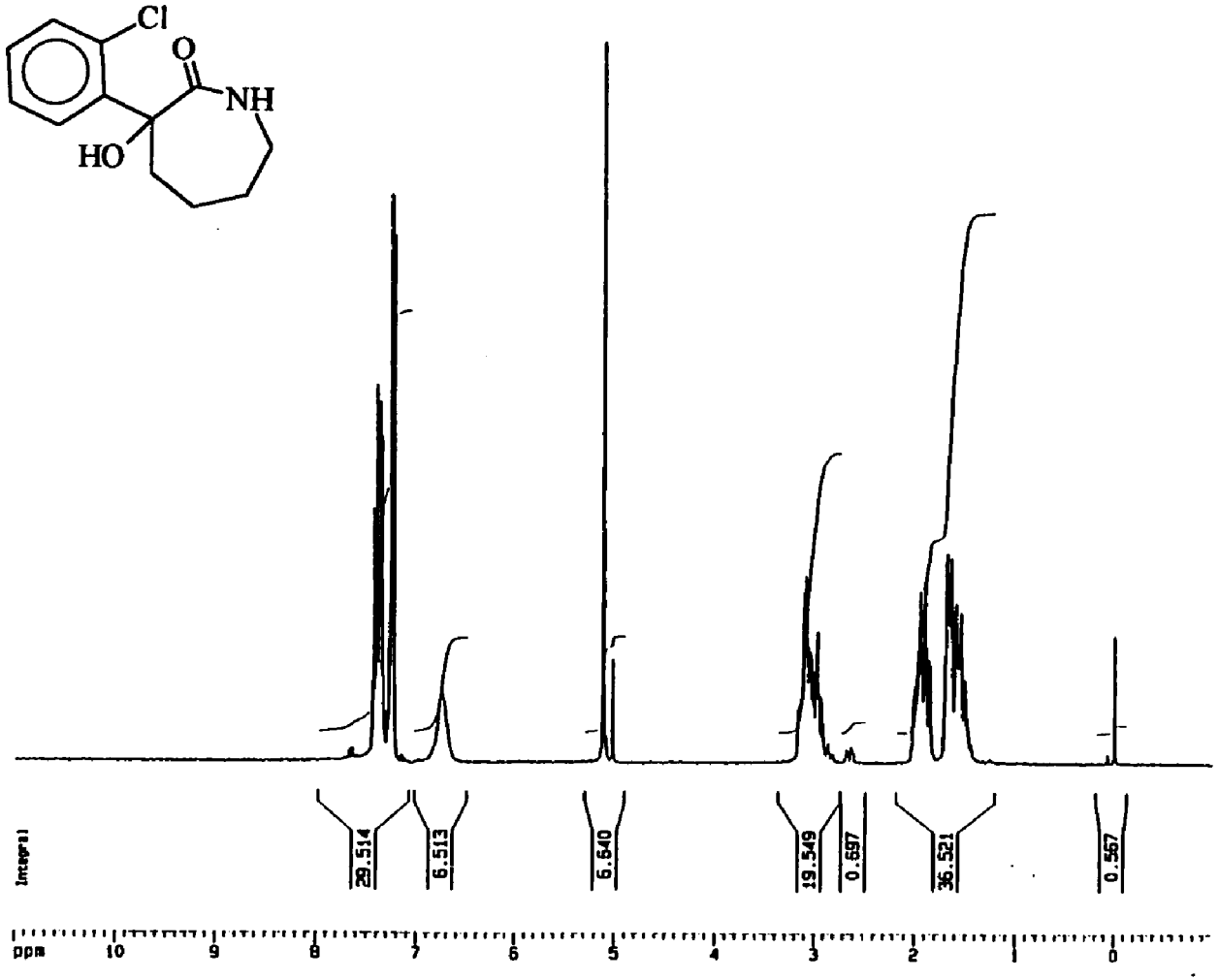


```
Current Data Parameters
NAME                  mlb-II-71
EXPNO                        20
PROCNO                        1

F2 - Acquisition Parameters
Date                    940821
Time                     16.24
PULPROG                  zg30
SOLVENT                  CDCl3
AQ                  2.6542280 sec
FIDRES              0.188380 Hz
DW                      81.0 usec
RG                      2850
NUCLEUS                  1H
D1                  1.0000000 sec
P1                       8.0 usec
DE                      115.7 usec
SFO1              300.1351620 MHz
SWH                 6172.84 Hz
TD                      32768
NS                         16
DS                          2

F2 - Processing parameters
SI                      16384
SF                300.1333664 MHz
WDW                        EM
SSB                         0
LB                   0.30 Hz
GB                          0
PC                       1.00

1D NMR plot parameters
CX                   20.00 cm
F1P                  11.000 ppm
F1                  3301.47 Hz
F2P                 -1.000 ppm
F2                  -300.13 Hz
PPMCM                0.60000 ppm
HZCM                180.08002 Hz/
```

Figure 1. ^{1}H NMR Spectrum (300 MHz) of Compound **5** ($CDCl_3$).

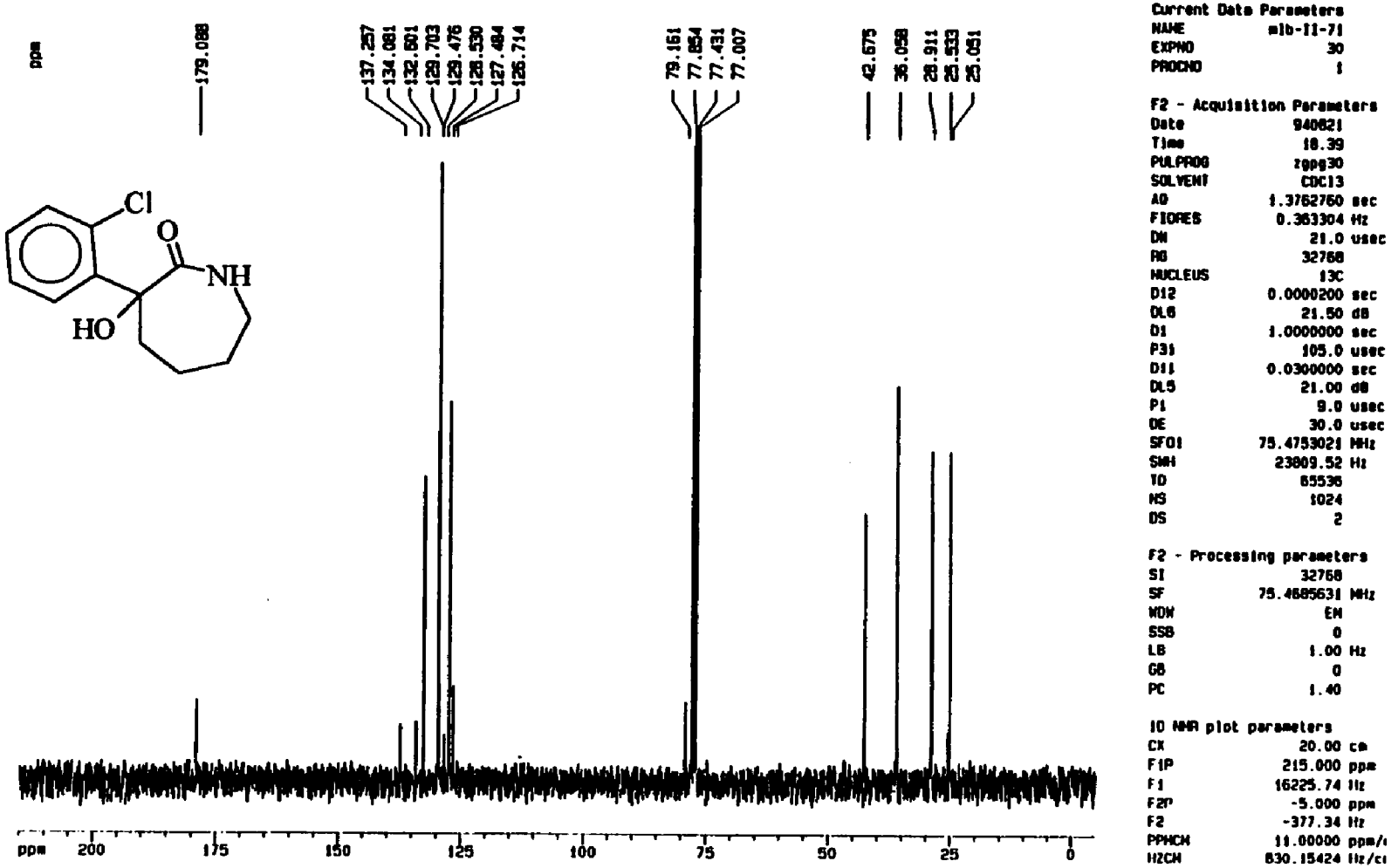

Figure 2. ^{13}C Spectrum (75 MHz) of Compound **5** ($CDCl_3$).

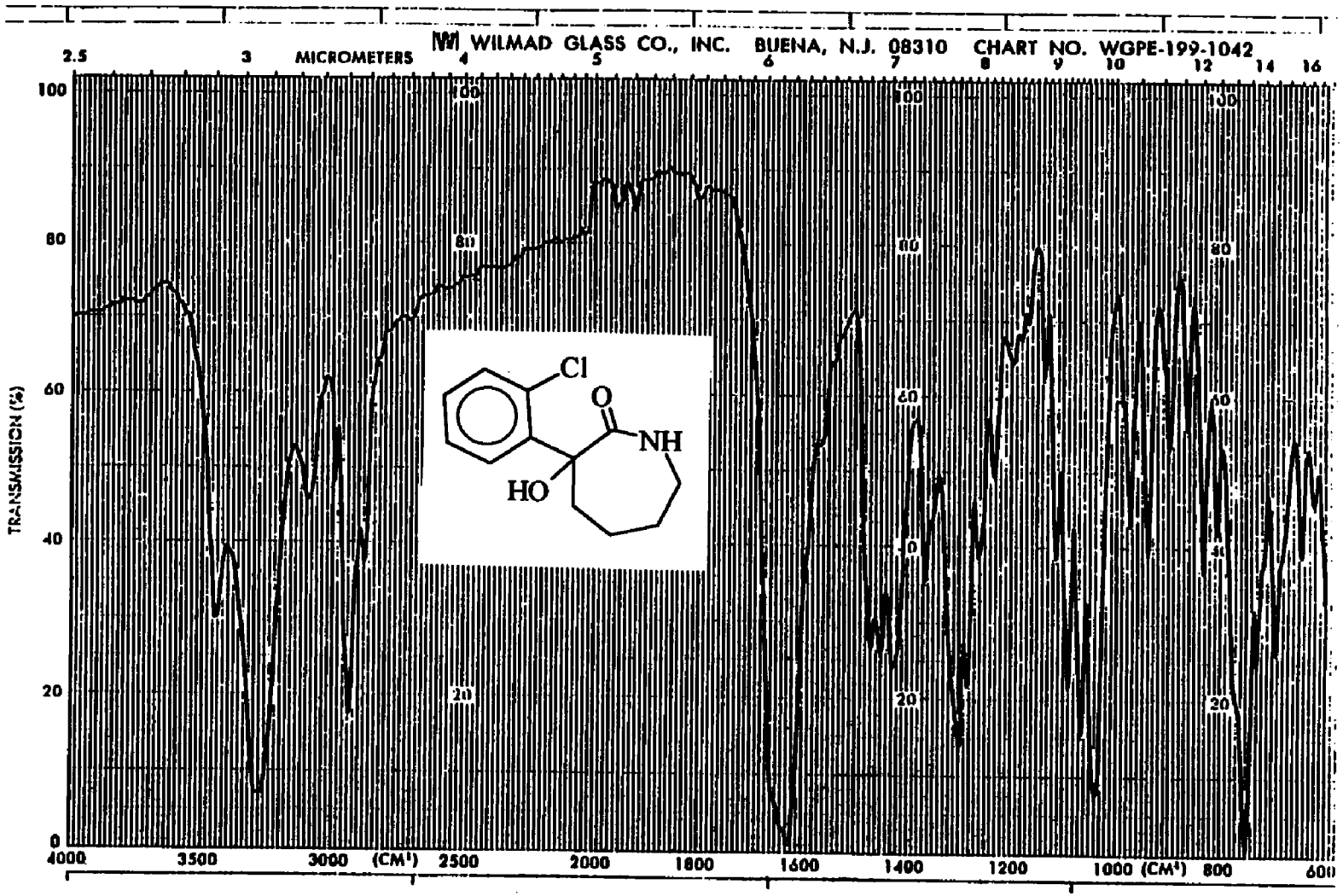

Figure 3. IR Spectrum of Compound 5 (KBr).

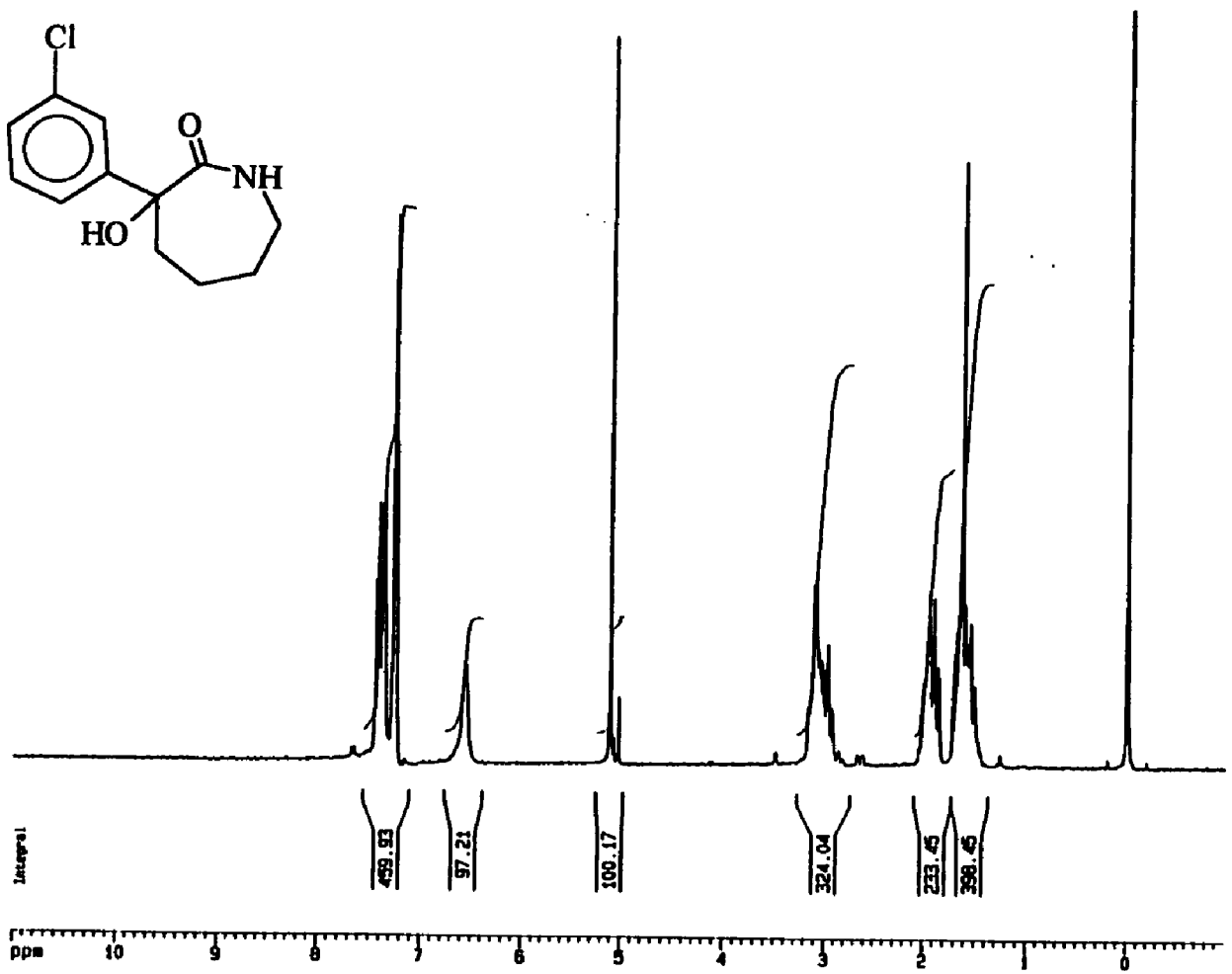

Current Data Parameters
NAME mlb-III-37
EXPNO 10
PROCNO 1

F2 - Acquisition Parameters
Date 940819
Time 13.39
PULPROG zg30
SOLVENT CDCl3
AQ 2.6542280 sec
FIDRES 0.188380 Hz
DW 81.0 use
RG 2860
NUCLEUS 1H
D1 1.0000000 sec
P1 8.0 use
DE 115.7 use
SFO1 300.1351620 MHz
SWH 6172.84 Hz
TD 32768
NS 16
DS 2

F2 - Processing parameters
SI 16384
SF 300.1333660 MHz
WDW EM
SSB 0
LB 0.30 Hz
GB 0
PC 1.00

1D NMR plot parameters
CX 20.00 cm
F1P 11.000 ppm
F1 3301.47 Hz
F2P -1.000 ppm
F2 -300.13 Hz
PPMCM 0.60000 ppm
HZCM 180.08002 Hz/

Figure 4. ^{1}H NMR Spectrum (300 MHz) of Compound 6 ($CDCl_3$).

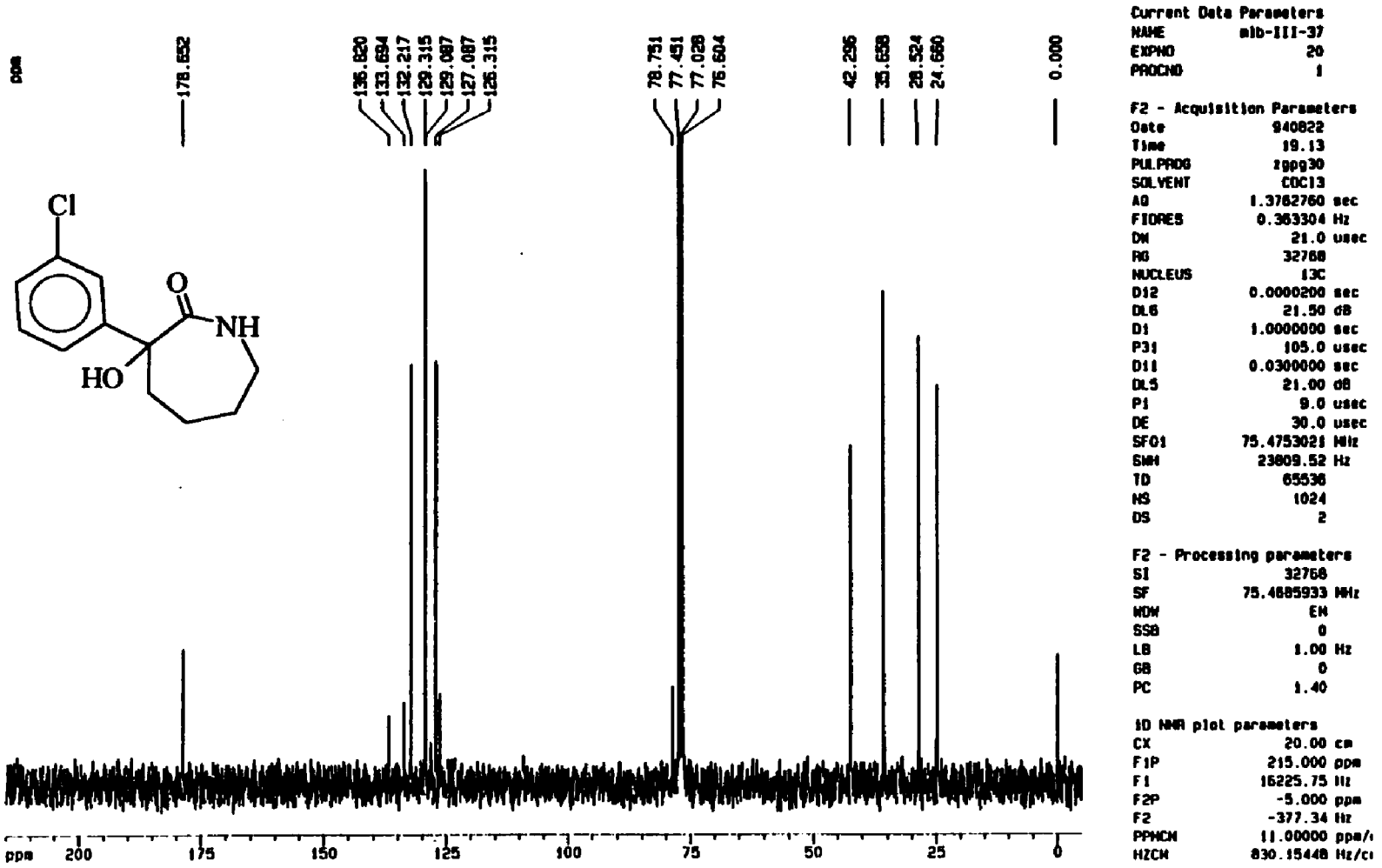

Figure 5. ^{13}C Spectrum (75 MHz) of Compound **6** ($CDCl_3$).

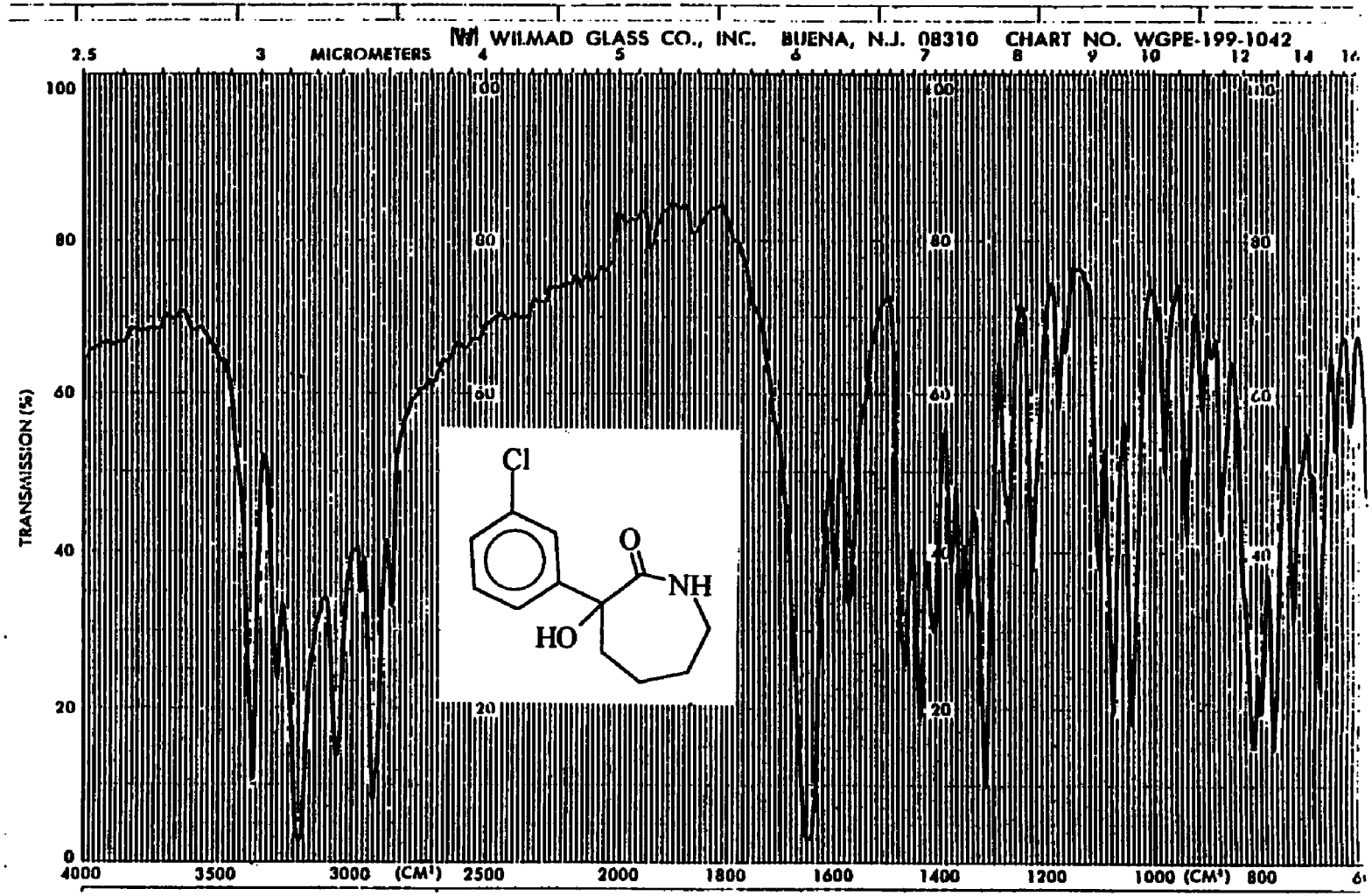

Figure 6. IR Spectrum of Compound 6 (KBr).

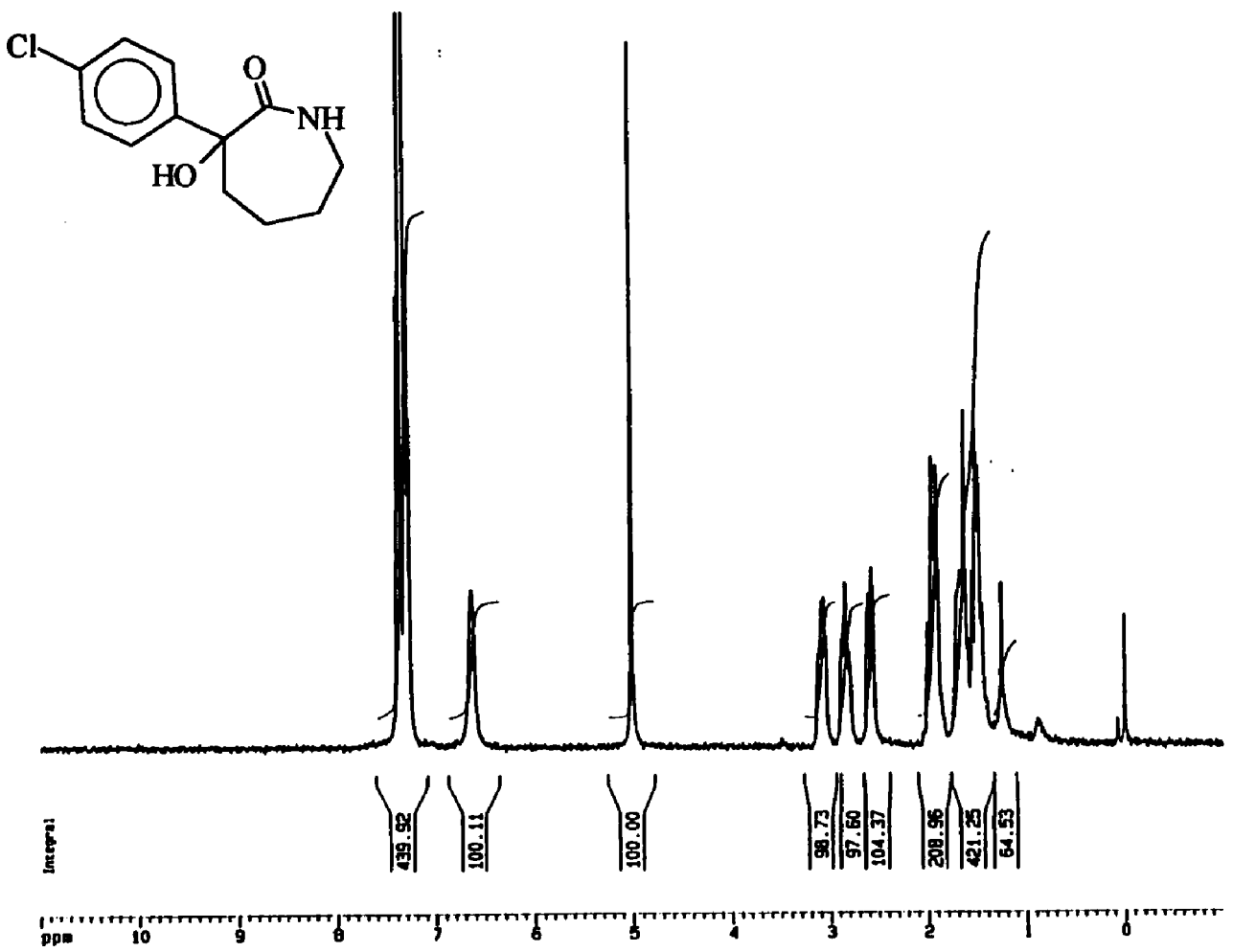

Current Data Parameters
NAME alb-II-69
EXPNO 30
PROCNO 1

F2 - Acquisition Parameters
Date 940821
Time 19.32
PULPROG zg30
SOLVENT CDCl3
AQ 2.6542280 sec
FIDRES 0.188380 Hz
DW 81.0 use
RG 4096
NUCLEUS 1H
D1 1.0000000 sec
P1 8.0 use
DE 115.7 use
SFO1 300.1351620 MHz
SWH 6172.84 Hz
TD 32768
NS 16
DS 2

F2 - Processing parameters
SI 16384
SF 300.1333653 MHz
WDW EM
SSB 0
LB 0.30 Hz
GB 0
PC 1.00

1D NMR plot parameters
CX 20.00 cm
F1P 11.000 ppm
F1 3301.47 Hz
F2P -1.000 ppm
F2 -300.13 Hz
PPMCM 0.60000 ppm
HZCM 180.09002 Hz

Figure 7. ^{1}H NMR Spectrum (300 MHz) of Compound 7 ($CDCl_3$).

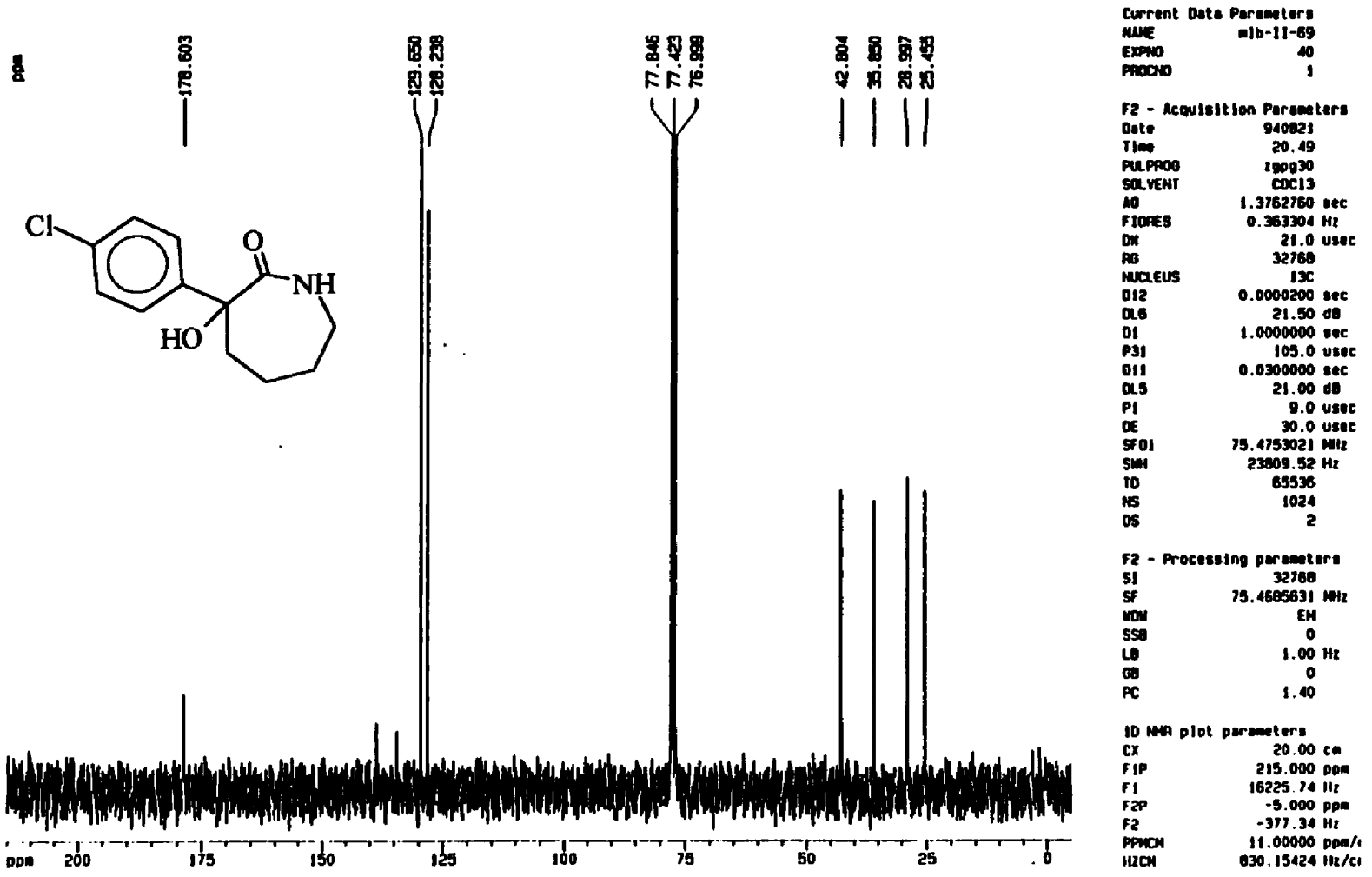

Figure 8. ^{13}C Spectrum (75 MHz) of Compound **7** ($CDCl_3$).

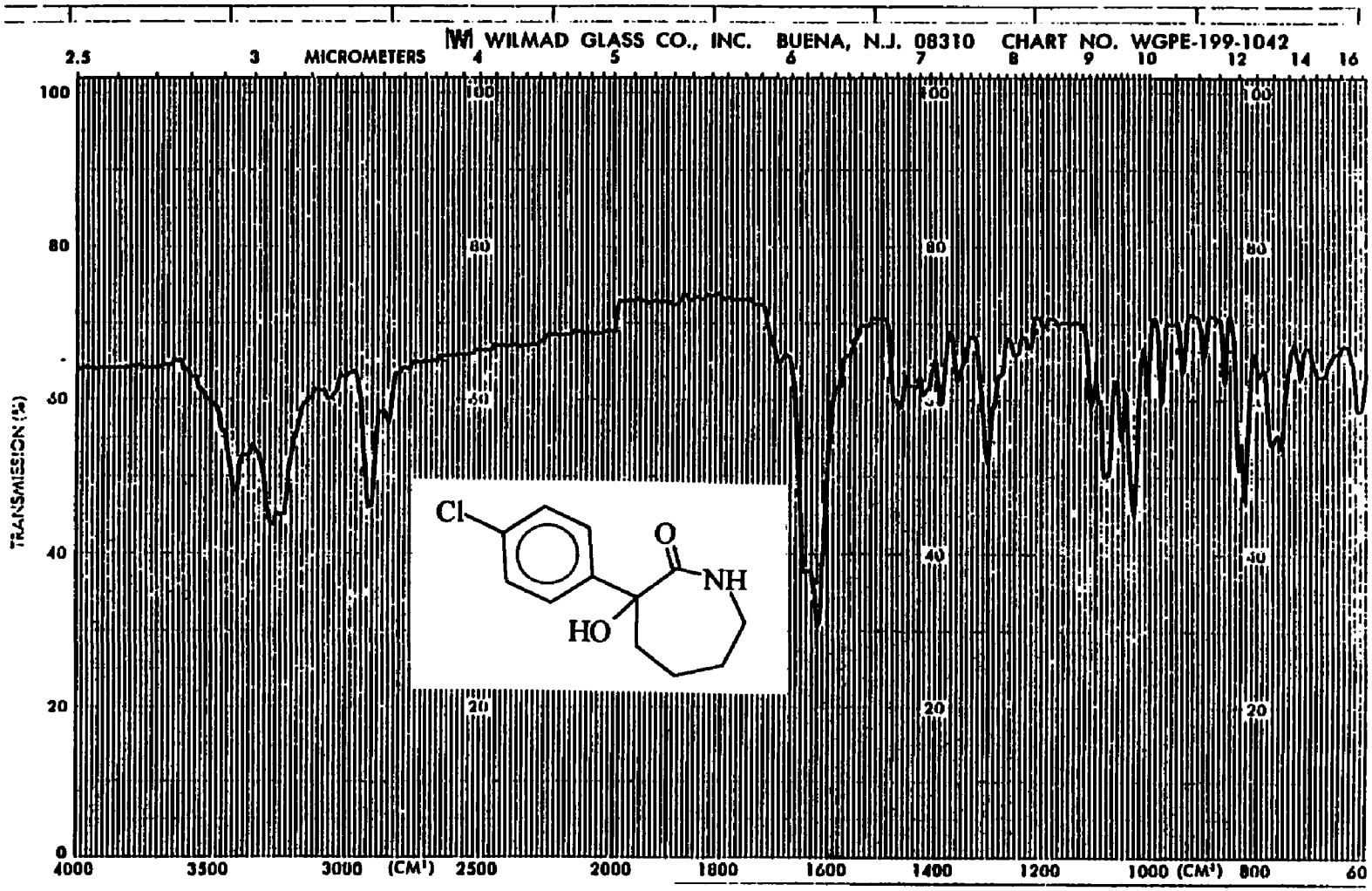

Figure 9. IR Spectrum of Compound 7 (KBr).

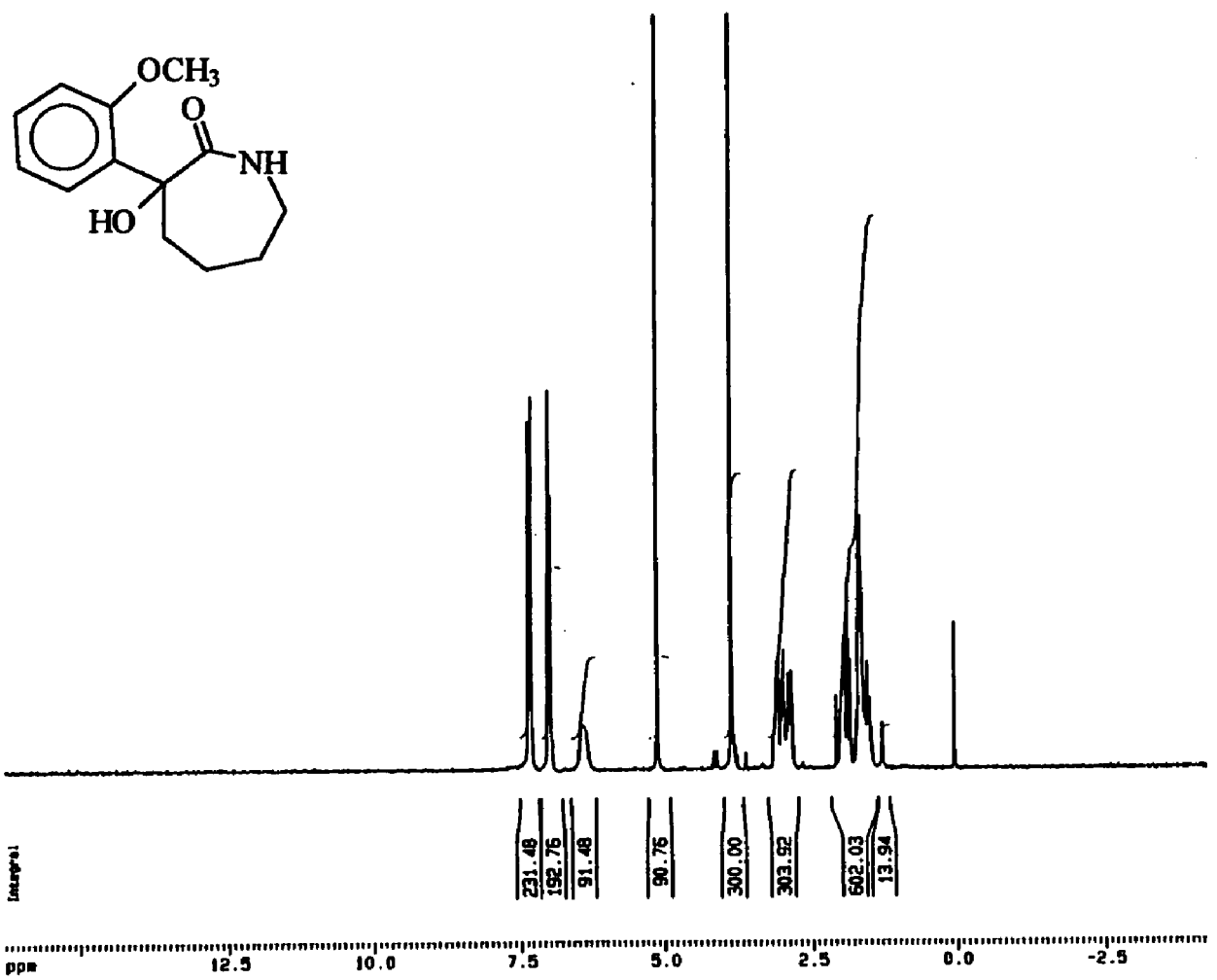

Current Data Parameters
NAME alb-III-49
EXPNO 10
PROCNO 1

F2 - Acquisition Parameters
Date 940830
Time 17.55
PULPROG zg30
SOLVENT CDCl3
AQ 2.6542280 sec
FIDRES 0.188380 Hz
DW 81.0 usec
RG 4096
NUCLEUS 1H
D1 1.0000000 sec
P1 8.0 usec
DE 115.7 usec
SFO1 300.1351620 MHz
SWH 6172.84 Hz
TD 32768
NS 16
DS 2

F2 - Processing parameters
SI 16384
SF 300.1333547 MHz
WDW EM
SSB 0
LB 0.30 Hz
GB 0
PC 1.00

1D NMR plot parameters
CX 20.00 cm
F1P 16.305 ppm
F1 4893.74 Hz
F2P -4.262 ppm
F2 -1279.10 Hz
PPMCM 1.02835 ppm
HZCM 308.64197 Hz

Figure 10. ^{1}H NMR Spectrum (300 MHz) of Compound 8 ($CDCl_3$).

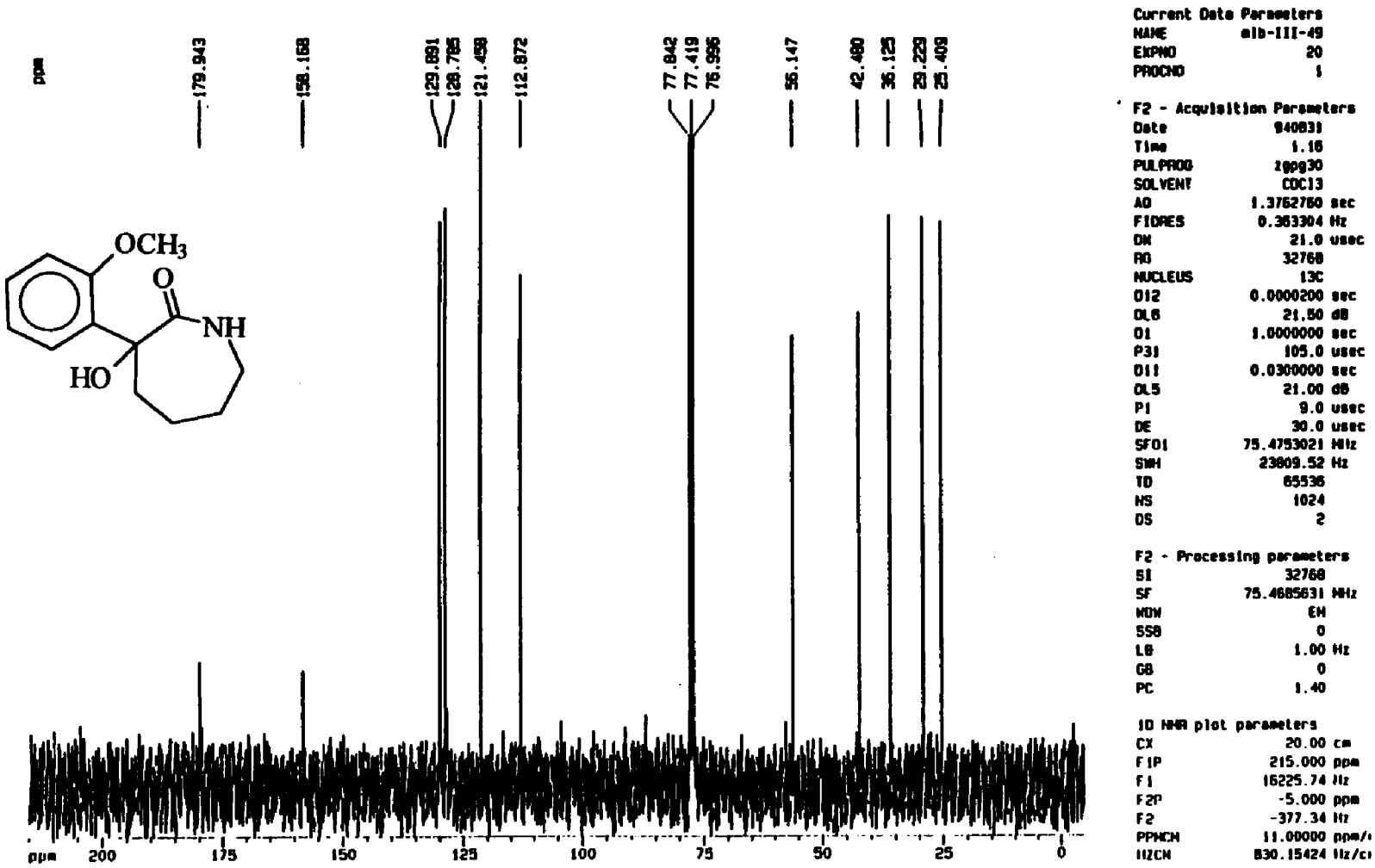

Figure 11. ^{13}C Spectrum (75 MHz) of Compound **8** ($CDCl_3$).

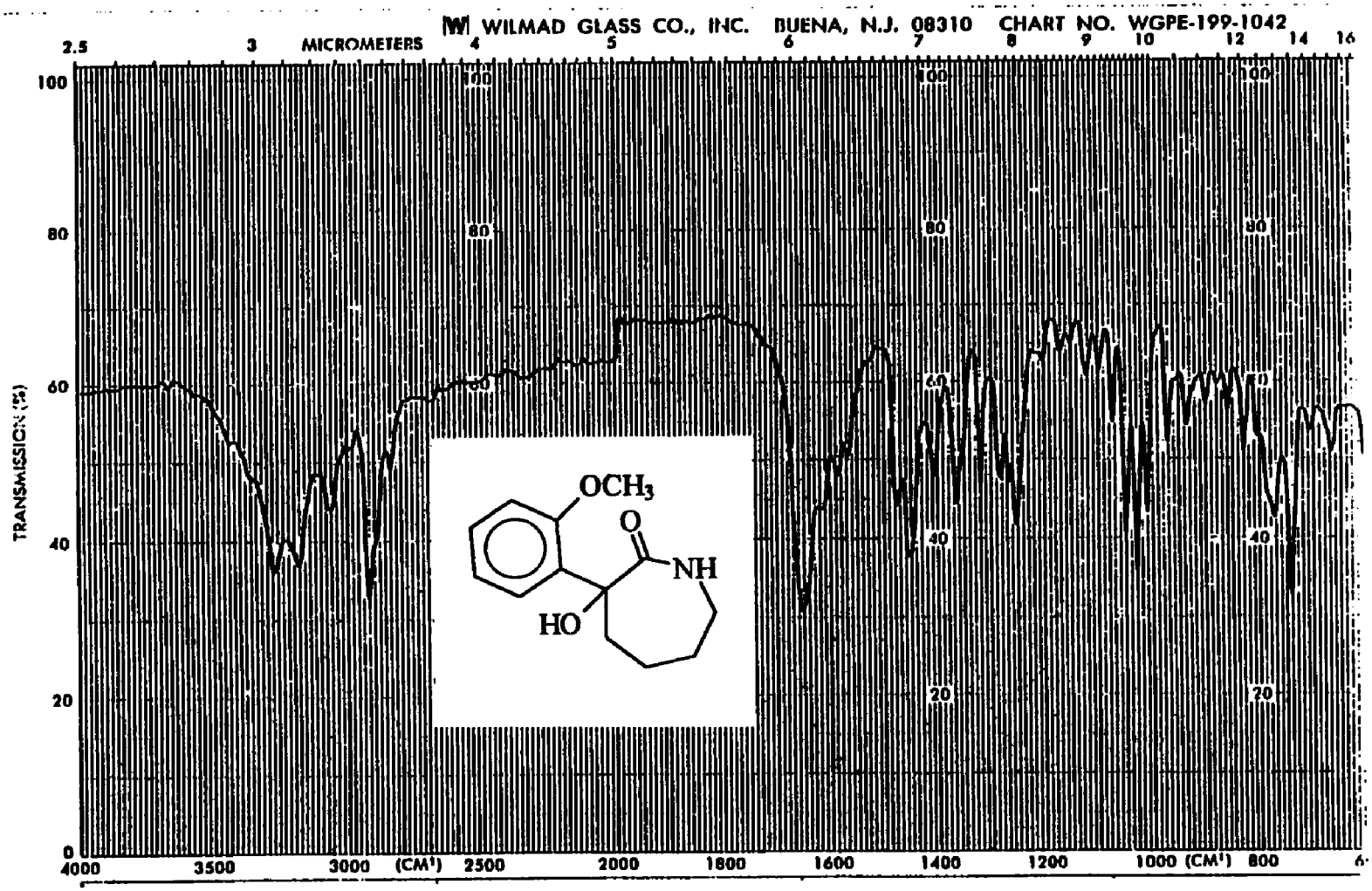

Figure 12. IR Spectrum of Compound 8 (KBr).

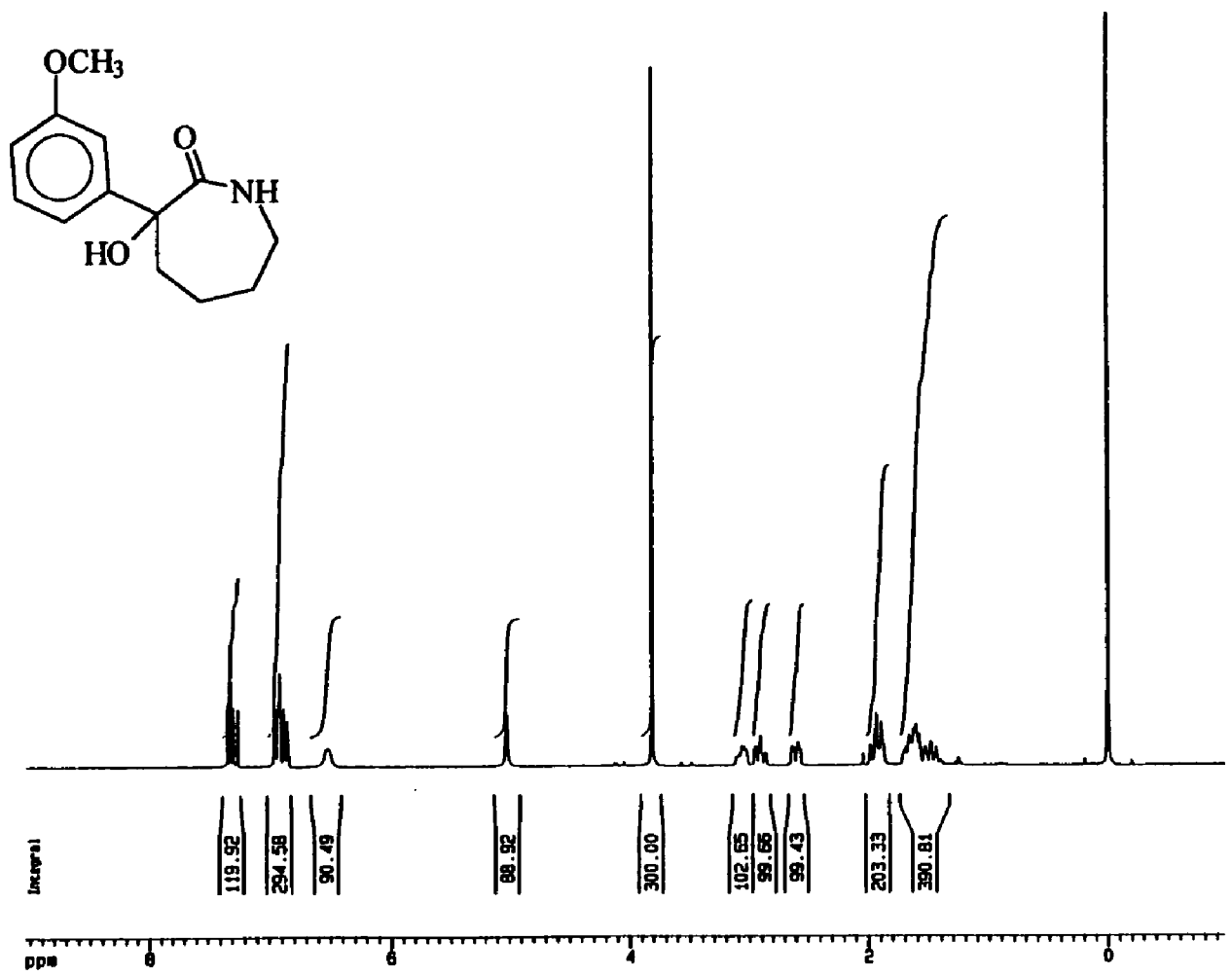


```
Current Data Parameters
NAME          alb-III-45
EXPNO                  4
PROCNO                 1

F2 - Acquisition Parameters
Date              941026
Time               18.49
PULPROG            zg30
SOLVENT            CDCl3
AQ          2.6542280 sec
FIDRES      0.188380 Hz
DW             81.0 use
RG                 2860
NUCLEUS              1H
D1          1.0000000 sec
P1             8.0 use
DE             115.7 use
SFO1      300.1351620 MHz
SWH         6172.84 Hz
TD                32768
NS                   16
DS                    2

F2 - Processing parameters
SI                16384
SF        300.1333858 MHz
WDW                  EM
SSB                   0
LB             0.30 Hz
GB                    0
PC                 1.00

1D NMR plot parameters
CX               20.00 cm
F1P               9.038 ppm
F1             2712.67 Hz
F2P              -0.964 ppm
F2             -289.35 Hz
PPMCM          0.50012 ppm
HZCM          150.10127 Hz/
```

Figure 13. ^{1}H NMR Spectrum (300 MHz) of Compound 9 ($CDCl_3$).

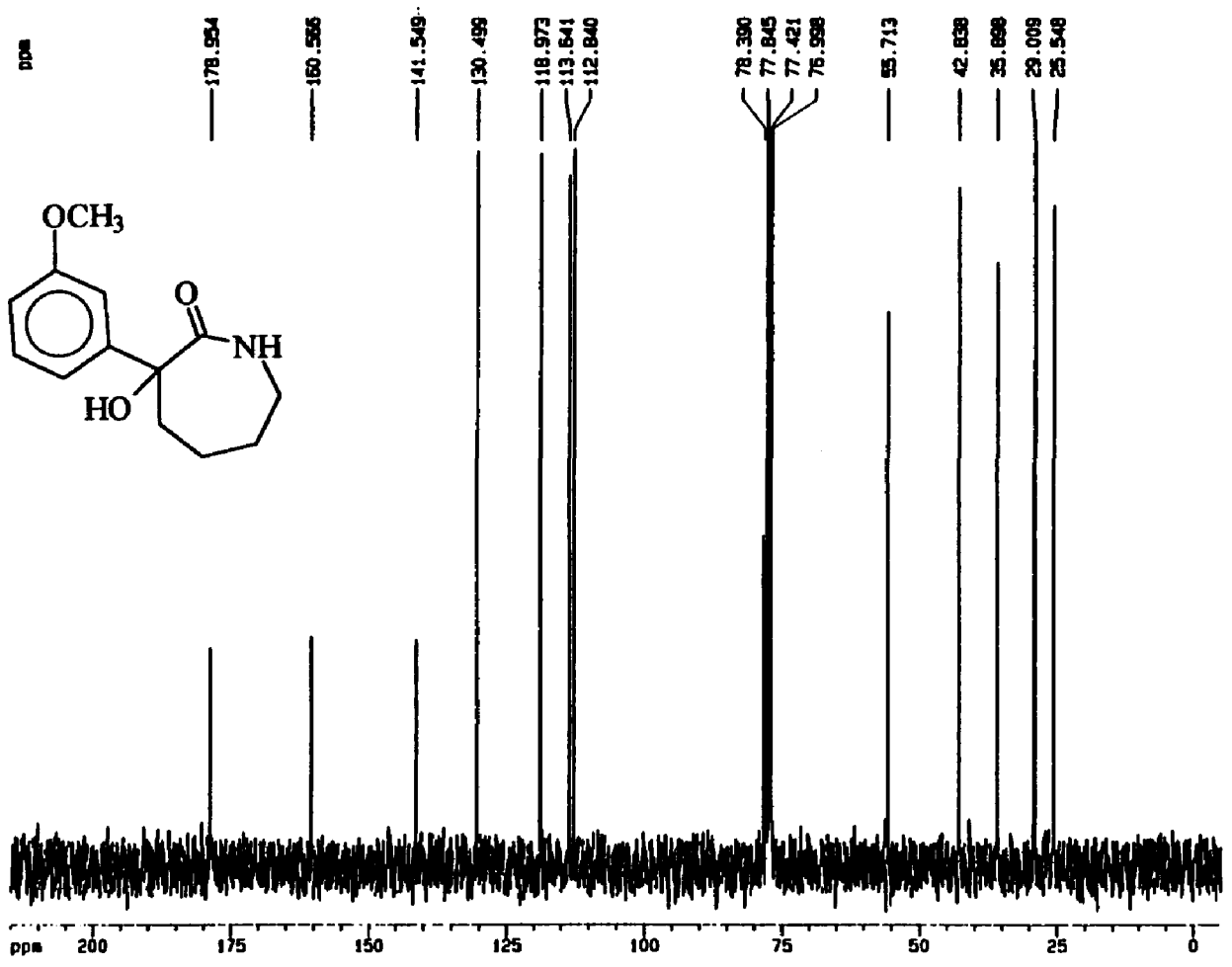

Current Data Parameters
NAME alb-III-45
EXPNO 30
PROCNO 1

F2 - Acquisition Parameters
Date 940819
Time 17.10
PULPROG zgpg30
SOLVENT CDCl3
AQ 1.3762760 sec
FIDRES 0.363304 Hz
DW 21.0 usec
RG 32768
NUCLEUS 13C
D12 0.0000200 sec
DL6 21.50 dB
D1 1.0000000 sec
P31 105.0 usec
D11 0.0300000 sec
DL5 21.00 dB
P1 9.0 usec
DE 30.0 usec
SFO1 75.4753021 MHz
SWH 23809.52 Hz
TD 65536
NS 1024
DS 2

F2 - Processing parameters
SI 32768
SF 75.4685631 MHz
WDW EM
SSB 0
LB 1.00 Hz
GB 0
PC 1.40

1D NMR plot parameters
CX 20.00 cm
F1P 215.000 ppm
F1 16225.74 Hz
F2P -5.000 ppm
F2 -377.34 Hz
PPMCM 11.00000 ppm/
HZCM 830.15424 Hz/c

Figure 14. ^{13}C Spectrum (75 MHz) of Compound **10** ($CDCl_3$).

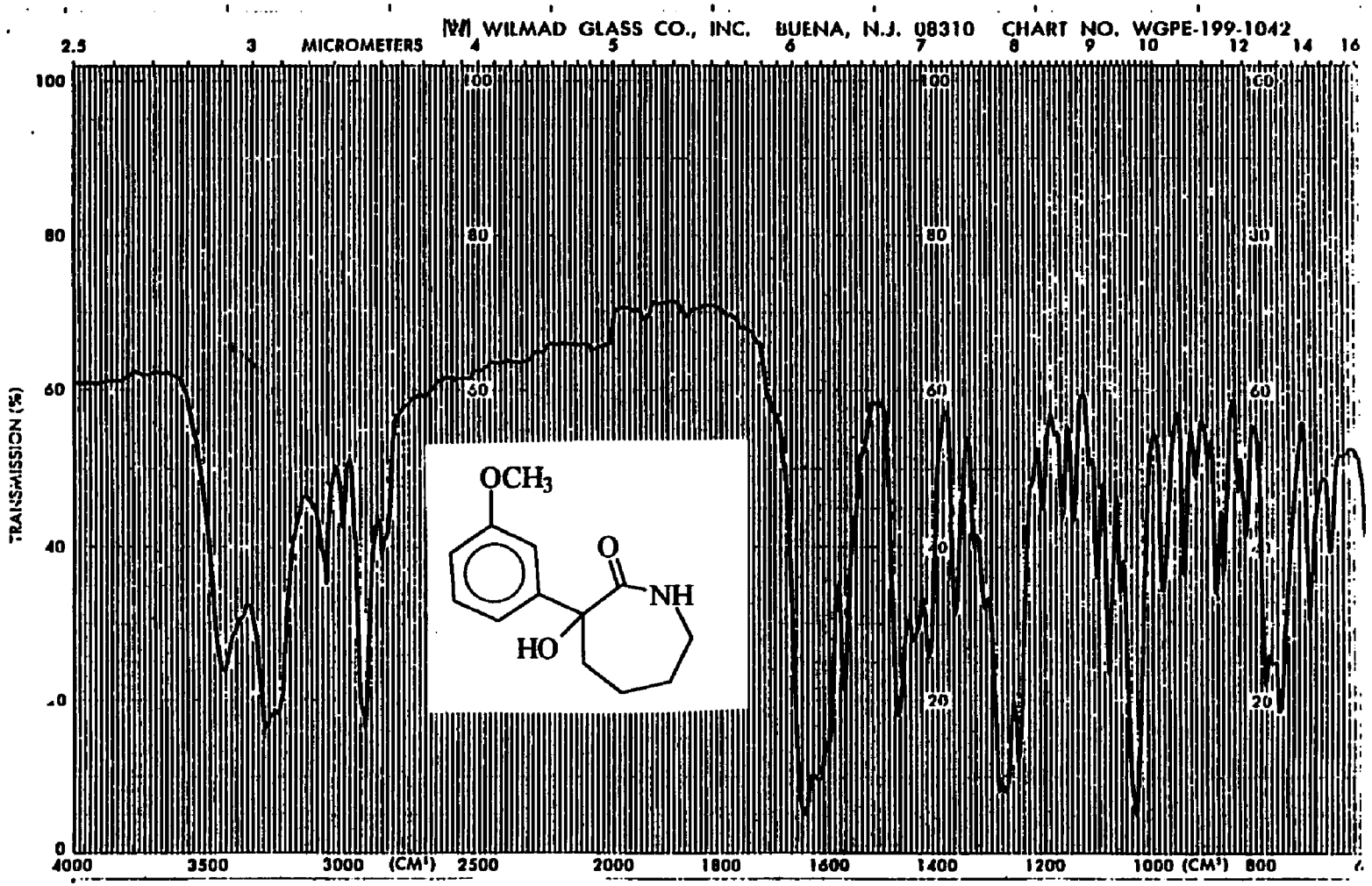

Figure 15. IR Spectrum of Compound 9 (KBr).

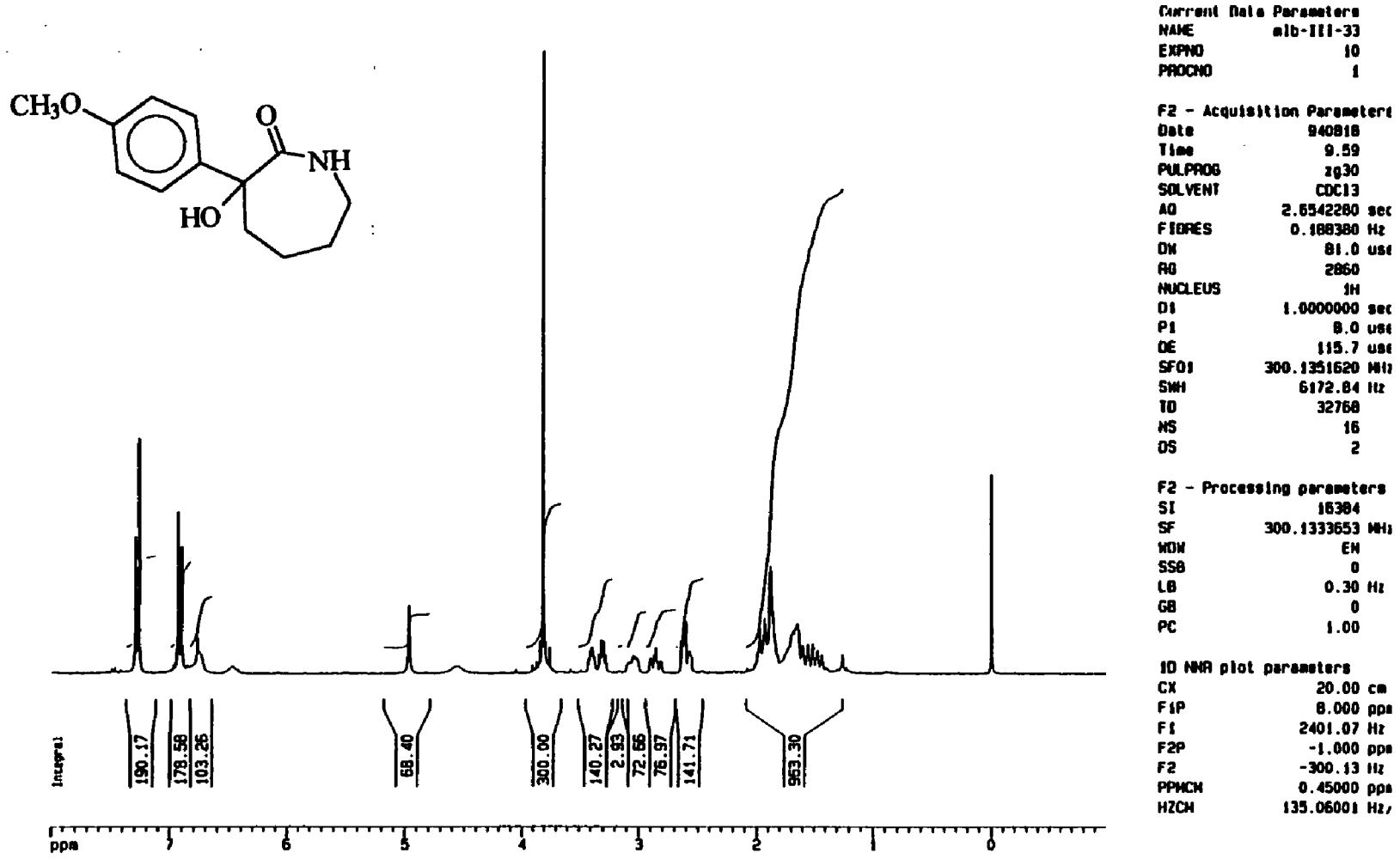


```
Current Data Parameters
NAME          alb-III-33
EXPNO                 10
PROCNO                 1

F2 - Acquisition Parameters
Date              940818
Time                9.59
PULPROG             zg30
SOLVENT             CDCl3
AQ           2.6542280 sec
FIDRES       0.188380 Hz
DW                 81.0 use
RG                 2860
NUCLEUS              1H
D1           1.0000000 sec
P1                 8.0 use
DE                115.7 use
SFO1       300.1351620 MHz
SWH           6172.84 Hz
TD                32768
NS                   16
DS                    2

F2 - Processing parameters
SI                16384
SF         300.1333653 MHz
WDW                  EM
SSB                   0
LB                 0.30 Hz
GB                    0
PC                 1.00

1D NMR plot parameters
CX                20.00 cm
F1P                8.000 ppm
F1            2401.07 Hz
F2P               -1.000 ppm
F2             -300.13 Hz
PPMCM             0.45000 ppm
HZCM          135.06001 Hz/
```

Figure 16. ^{1}H NMR Spectrum (300 MHz) of Compound 10 ($CDCl_3$).

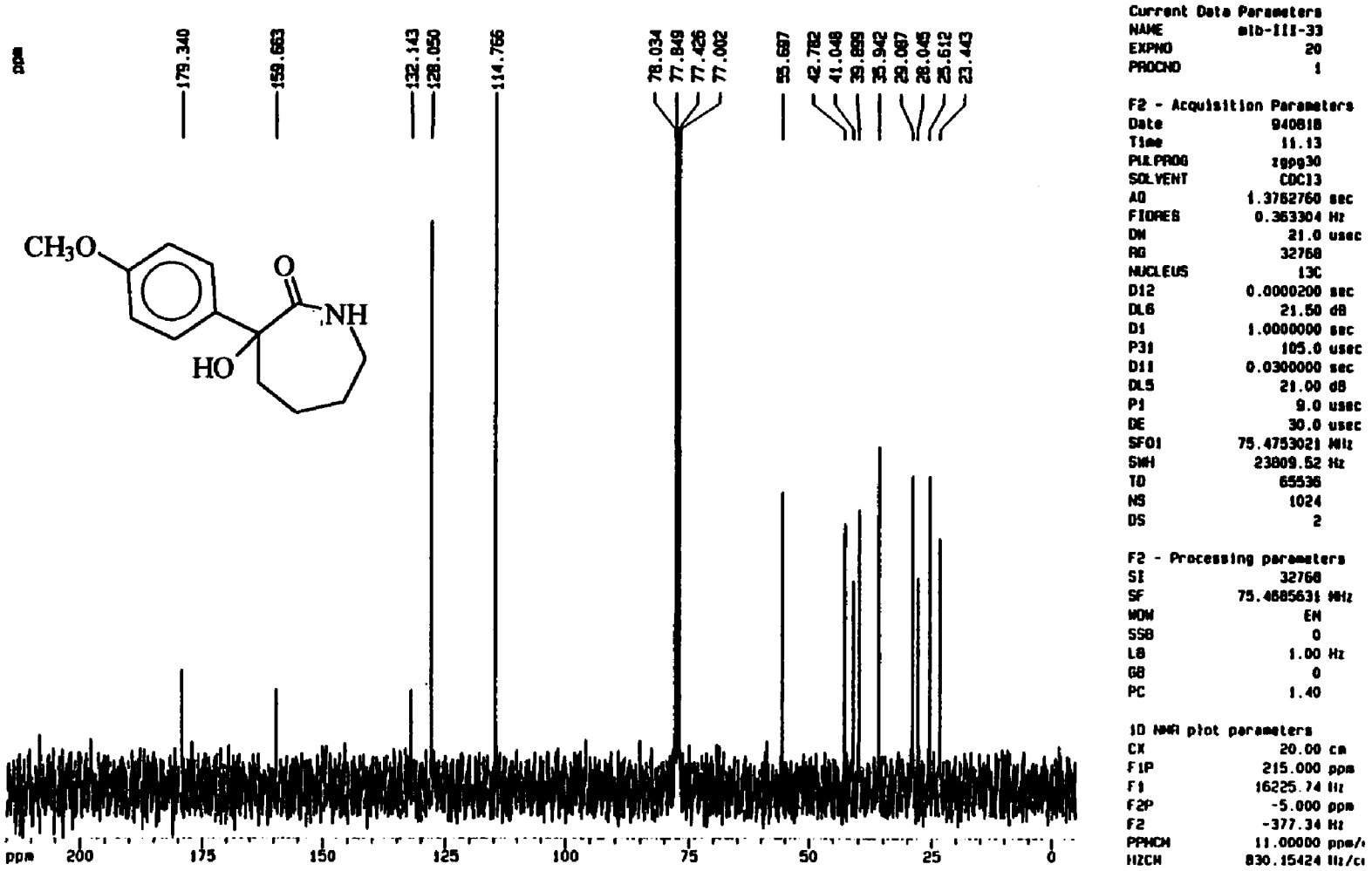

Figure 17. ^{13}C Spectrum (75 MHz) of Compound **10** ($CDCl_3$).

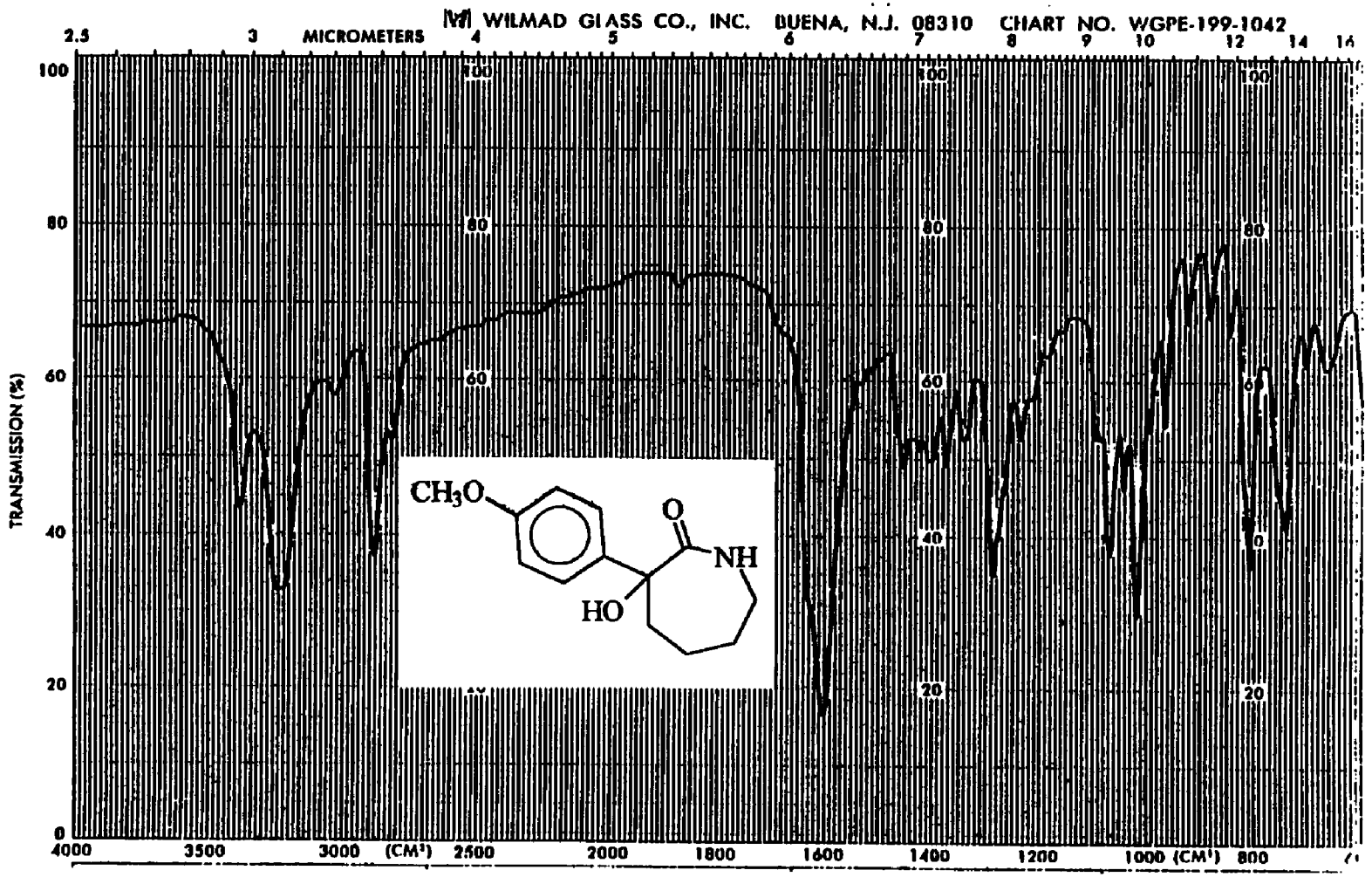

Figure 18. IR Spectrum of Compound 10 (KBr).

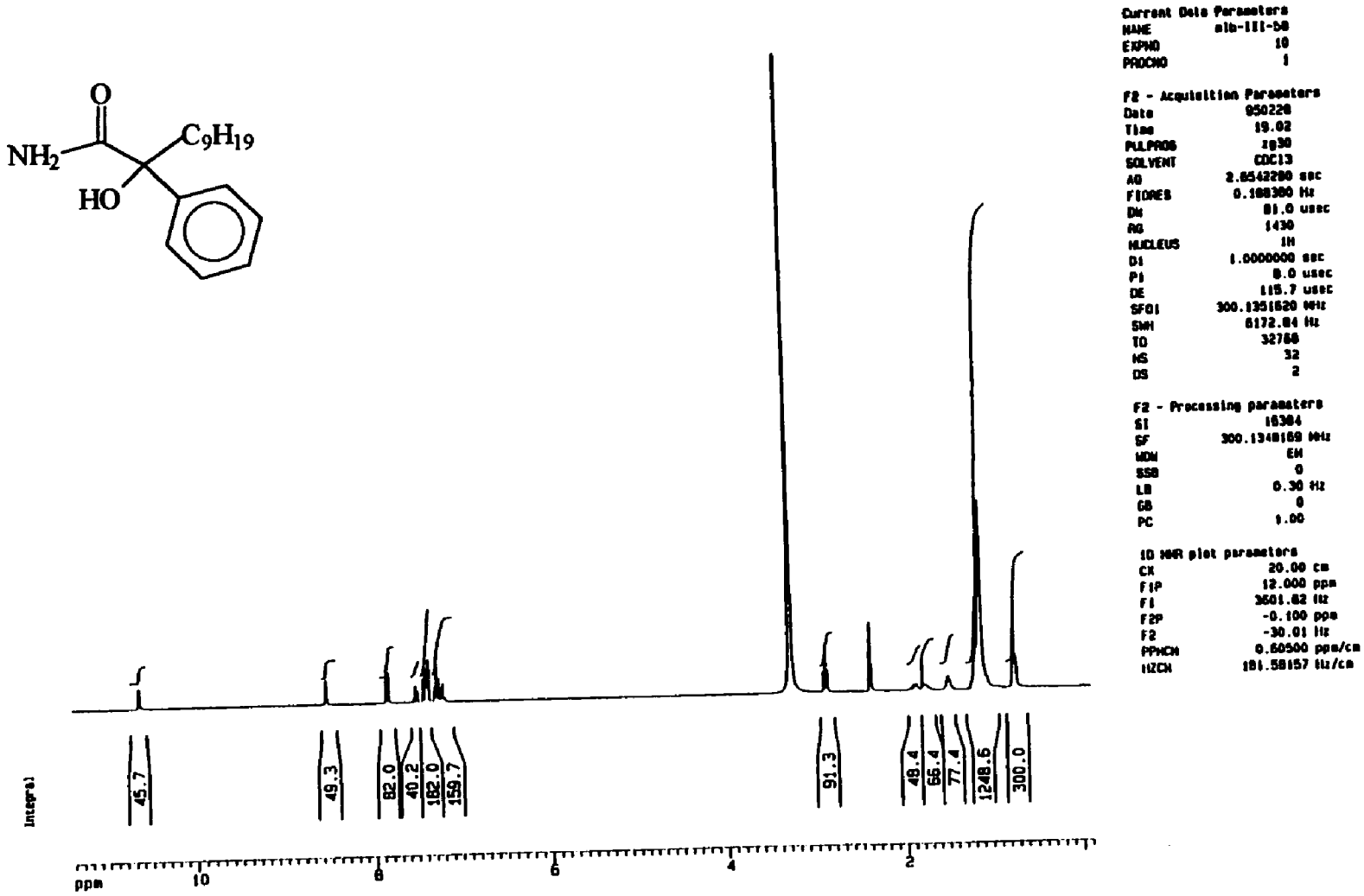

Figure 19. ^{1}H NMR Spectrum (300 MHz) of Compound 12 ($CDCl_3$).

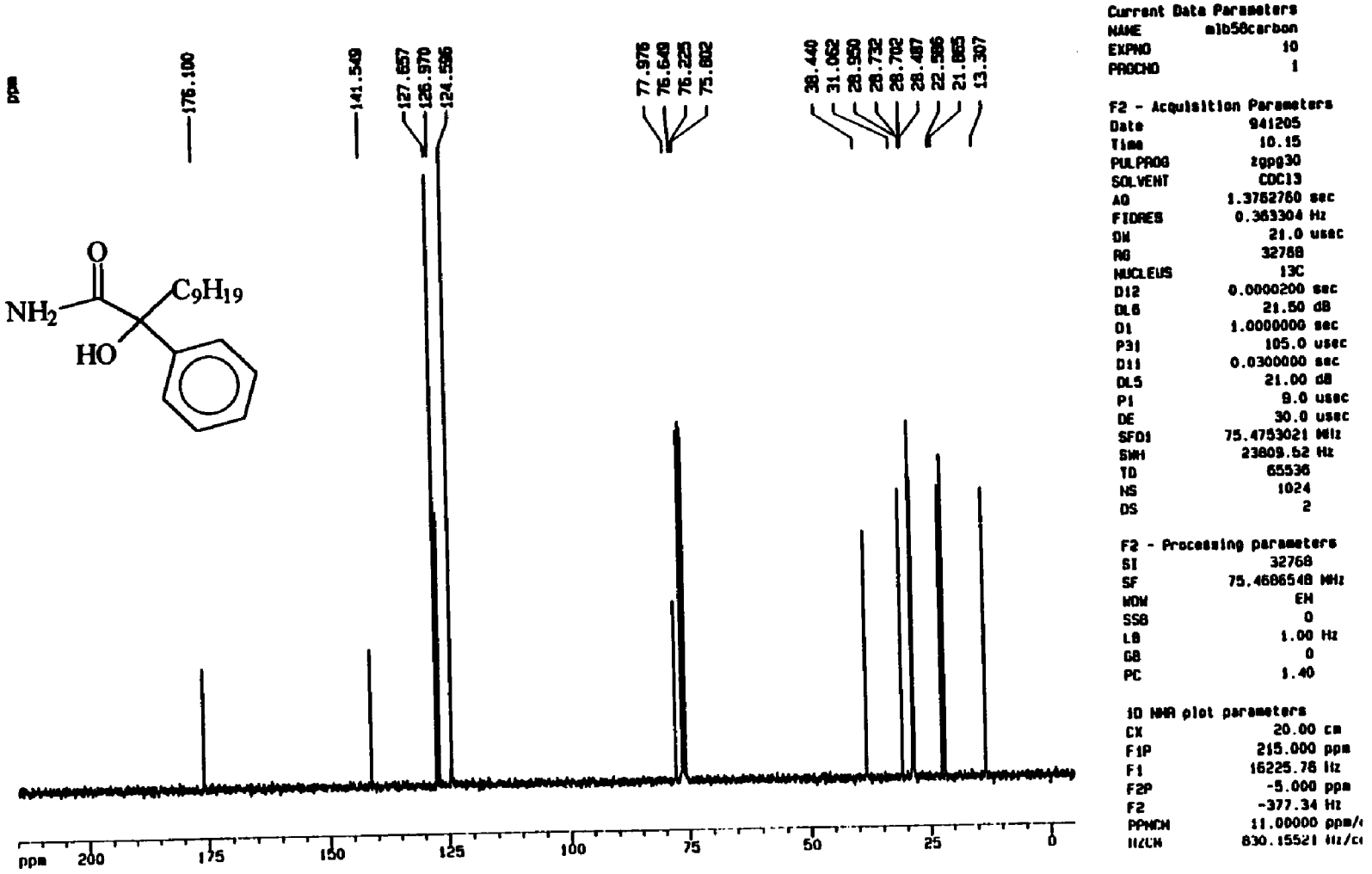

Figure 20. ^{13}C Spectrum (75 MHz) of Compound **12** ($CDCl_3$).

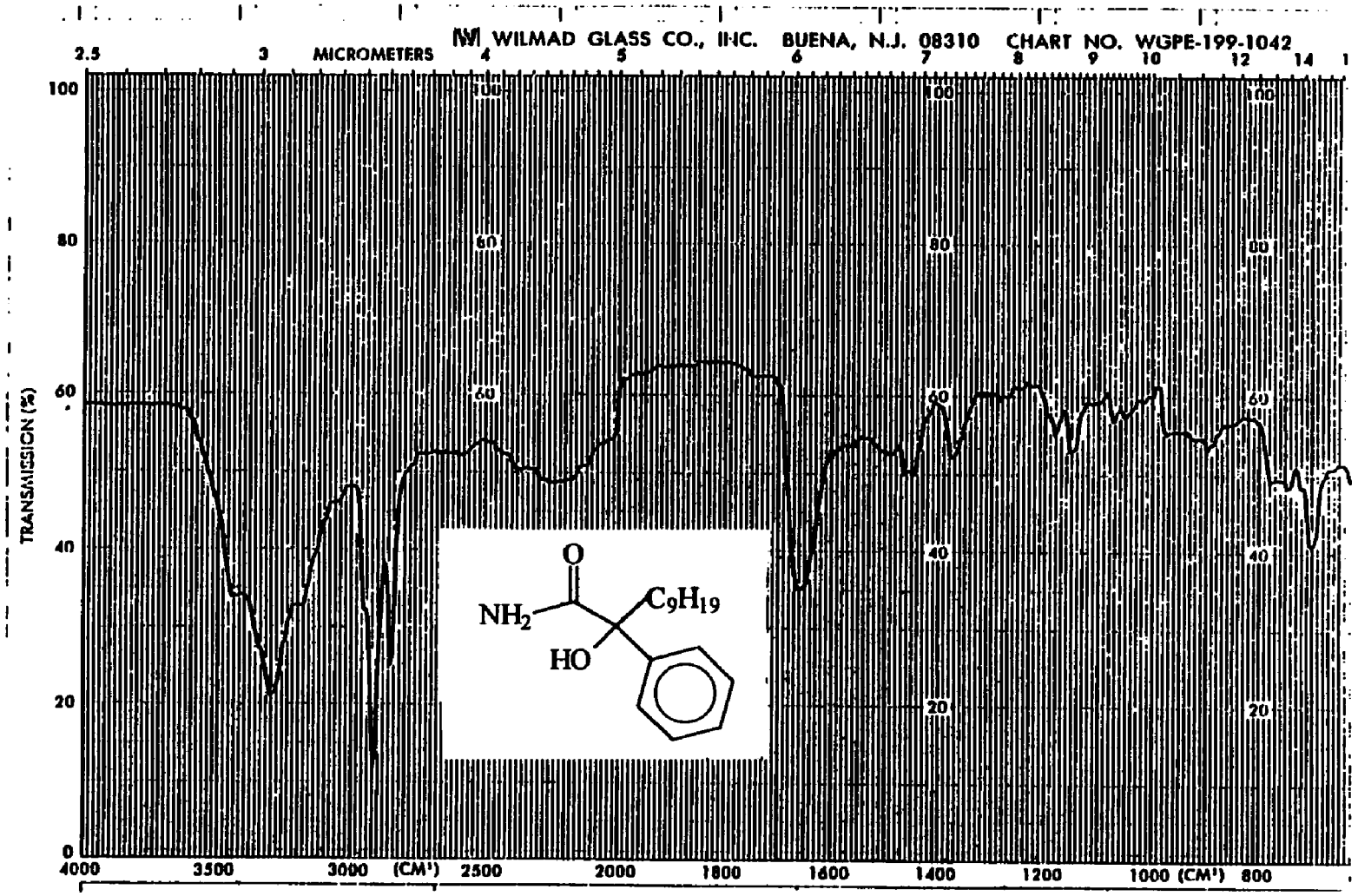

Figure 21. IR Spectrum of Compound 12 (KBr).

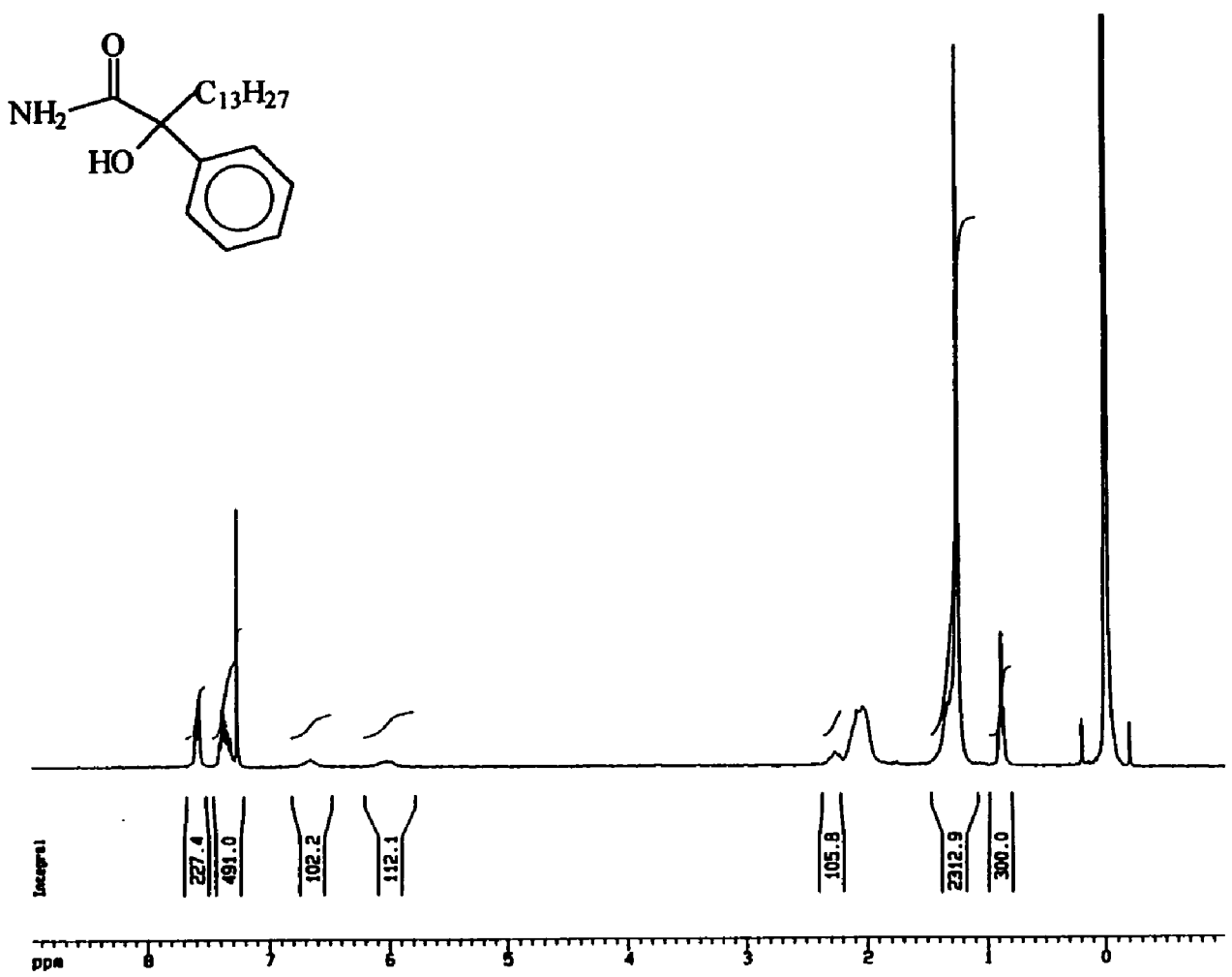


```
Current Data Parameters
NAME        mlb-13amide
EXPNO                30
PROCNO                1

F2 - Acquisition Parameters
Date             950529
Time              19.01
PULPROG           zg30
SOLVENT           CDCl3
AQ          2.6542280 sec
FIDRES      0.188360 Hz
DW               81.0 usec
RG                4096
NUCLEUS             1H
D1          1.0000000 sec
P1                8.0 usec
DE              115.7 usec
SFO1       300.1351620 MHz
SWH        6172.84 Hz
TD               32768
NS                  64
DS                   2

F2 - Processing parameters
SI               16384
SF         300.1333855 MHz
WDW                 EM
SSB                  0
LB            0.30 Hz
GB                   0
PC                1.00

1D NMR plot parameters
CX              20.00 cm
F1P             8.978 ppm
F1              2694.74 Hz
F2P             -0.984 ppm
F2              -295.26 Hz
PPMCM           0.49811 ppm/cm
HZCM          149.50014 Hz/cm
```

Figure 22. ^{1}H NMR Spectrum (300 MHz) of Compound 13 ($CDCl_3$).

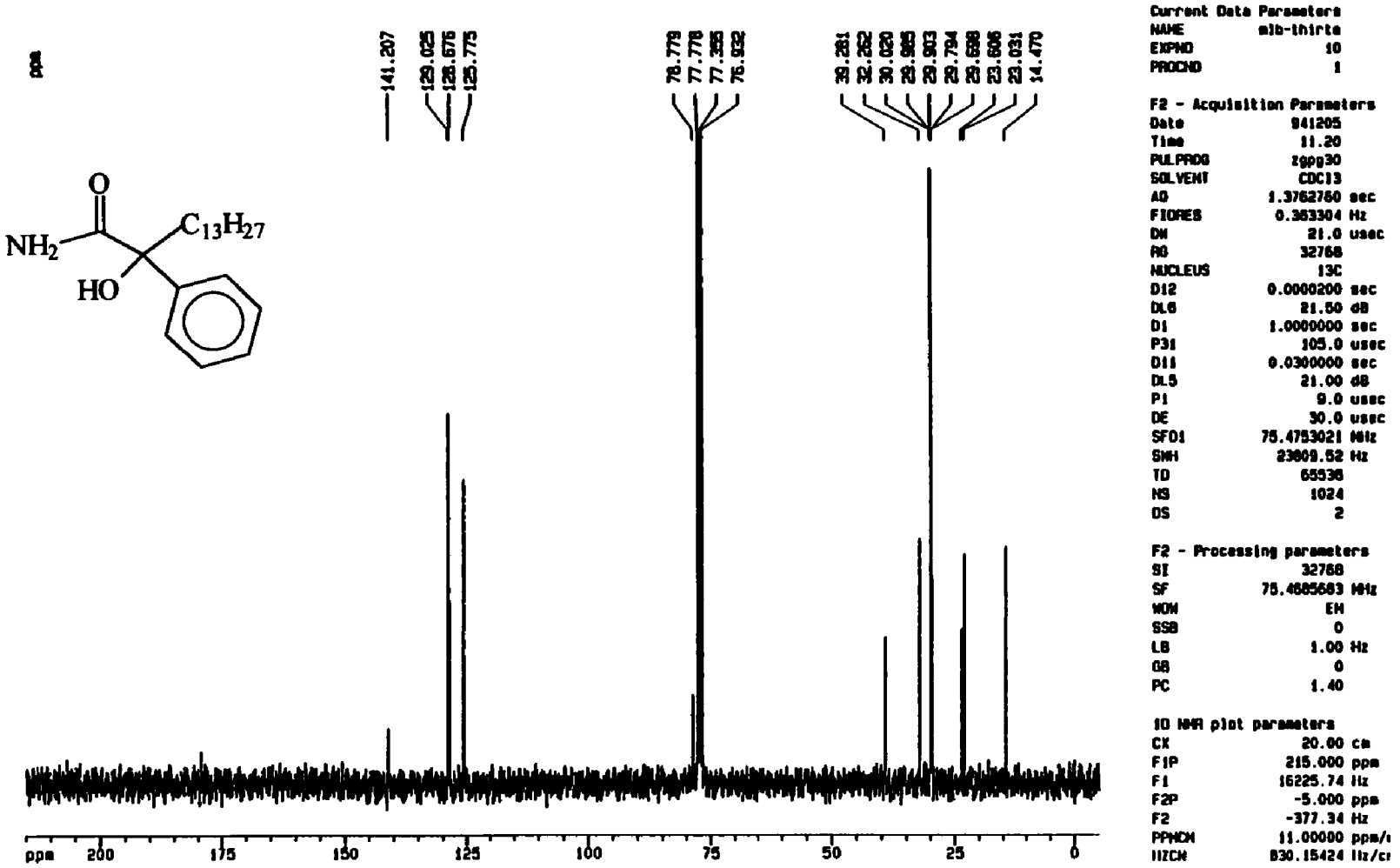

Figure 23. ^{13}C Spectrum (75 MHz) of Compound **13** ($CDCl_3$).

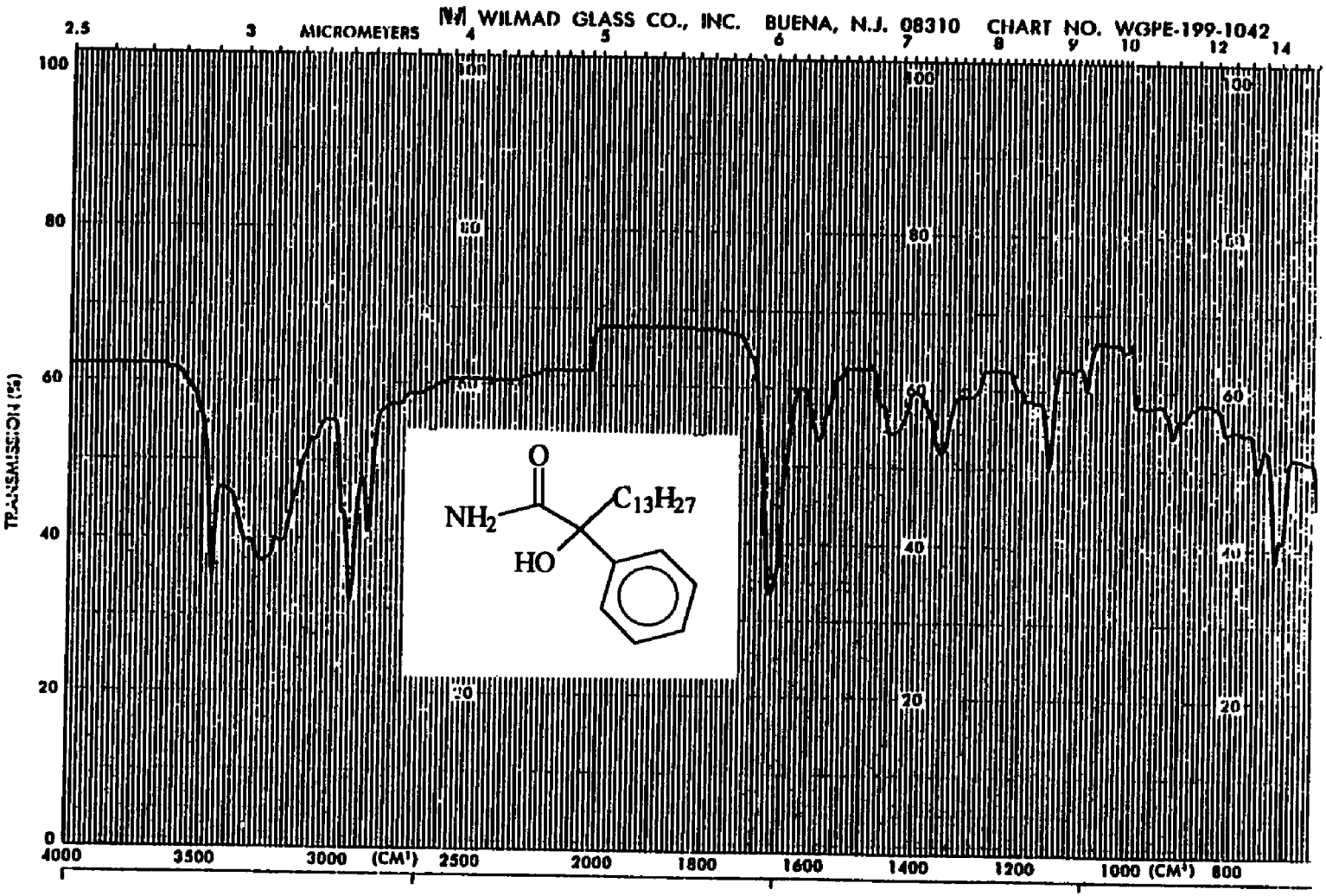

Figure 24. IR Spectrum of Compound 13 (KBr).

GRADUATE SCHOOL
UNIVERSITY OF ALABAMA AT BIRMINGHAM
DISSERTATION APPROVAL FORM

Name of Candidate Milton Lang Brown

Major Subject Organic Chemistry

Title of Dissertation Design of New Anticonvulsant Drugs. Part I: Synthesis and Computer Modeling of Sodium Channel-Directed Hydantoins. Part II: SAR Studies on α-Phenyllactams

Dissertation Committee:

Wayne J. Brouillette, Chairman

Samuel J. Christian

Jerry B. Brown

Donald D. Muccio

Donald E. Kiely

Director of Graduate Program

Dean, UAB Graduate School

Date 06/19/95